THE ROLE OF ENDOTHELIN-2 IN OVULATION

BY

JOSEPH A. CACIOPPO

DISSERTATION

Submitted in partial fulfillment of the requirements
for the degree of Doctor of Philosophy in VMS - Comparative Biosciences
in the Graduate College of the
University of Illinois at Urbana-Champaign, 2015

Urbana, Illinois

Doctoral Committee:

Associate Professor CheMyong J. Ko, Chair and Director of Research
Professor Jodi A. Flaws
Assistant Professor Megan M. Mahoney
Associate Professor Lori T. Raetzman
Professor Mark A. Mitchell

ABSTRACT

During ovulation, the oocyte and associated cumulus cells are expelled from the ovary and travel to the ampulla of the oviduct where fertilization occurs. Concurrently, granulosa and theca cells of an ovulating follicle luteinize and form lutein cells of the highly vascular corpus luteum, which secrete progesterone for pregnancy maintenance. Just prior to ovulation, the gene endothelin-2 (*Edn2*) is highly yet transiently expressed for a two-hour window. Mature endothelin-2 protein (EDN2) is a 21 amino acid peptide that is classically described as a potent vasoconstrictor. EDN2 is produced exclusively by the granulosa cells of mature follicles, and is an important factor in ovulation; mice that are pharmacologically treated to block action of the two endothelin receptors ovulate fewer oocytes and form fewer corpora lutea. Similar effects are seen in mice that globally lack *Edn2*, though they also expire at a young age. While it is clear that EDN2 plays a vital role in ovulation, the exact role for EDN2 has yet to be elucidated. Previous work suggests that EDN2 may cause contraction of mature follicles during rupture, but may also be involved in the critical processes of angiogenesis and leukocyte migration. To understand the pattern of expression, an Edn2-iCre mouse was generated and *Edn2* expression was characterized throughout the body; *Edn2* has widespread expression, particularly throughout the skin and ovary, with additional punctate expression in the GI tract, uterus, brain, kidney, and pituitary. This mouse model will be a useful tool for examining EDN2 signaling targets. Next, to address the role of EDN2 in ovarian contraction, the effect of EDN2 on ovaries from cats, dogs, and chickens was compared; all species' ovaries exhibit a strong and sustained contraction relative to the amount of smooth muscle present in the ovary. Thus EDN2 has an evolutionarily conserved contractile response. To further characterize EDN2 action in the ovary, *Edn2* was removed from either the whole ovary, or only the granulosa cells using a novel Esr2-iCre model. In each model, loss of EDN2 prevents follicle rupture but not folliculogenesis or corpus luteum formation. RT-PCR revealed that expression of genes critical in angiogenesis and leukocyte action are not modified by *Edn2*-ablation, implying no significant involvement of EDN2 in these ovulatory biological processes. To determine whether endothelin receptor A (*Ednra*, EDNRA, ET_A) mediates EDN2 contractile action during ovulation, a conditional gene knockout approach was employed to selectively ablate *Ednra* in smooth muscle cells through a tamoxifen-inducible Cre recombinase system. However, all mice including wild type controls treated with tamoxifen had severely

impaired ovulation; while ovulation occurred, the role of EDNRA cannot yet be determined. Alternatively, available data indicate that granulosa cell-specific loss of *Ednra* causes subfertility, indicating that EDN2 likely exerts an effect through EDNRA receptors on granulosa cells. Lastly, temporal regulation of *Edn2* expression by progesterone receptor (PGR) was confirmed using PGR-knockout mice. Overall, it is proposed based on results herein that EDN2 targets EDNRA to induce periovulatory contraction as a conserved mechanism leading to follicle rupture and subsequent corpus luteum formation, and that this action is under regulation by PGR. Therefore, EDN2 is critical for normal ovulation and fecundity.

To my Mother, Father, Brother, and Sister

ACKNOWLEDGEMENTS

This work would not have been possible without the generous support of a multitude of people throughout my time at the University of Illinois at Urbana-Champaign, to whom I am very grateful.

I first offer my most sincere thanks to my research advisor, mentor, and friend, Dr. Jay Ko. I owe him a great debt for his belief in me and the investment of his time and energy for the past years. Dr. Ko has been a patient guide that has continually offered new and difficult challenges to force me to improve throughout my academic journey, and I am grateful for his focus on my growth as a scientist and as a person. I also offer my appreciation for the members of my doctoral committee, Dr. Jodi Flaws, Dr. Megan Mahoney, Dr. Lori Raetzman, and Dr. Mark Mitchell, for the guidance, support, and motivation that they have provided. I have been beyond fortunate in having a solid foundation upon which to institute my academic career.

I am equally thankful to all those individuals that I have had the opportunity to interact with and learn from while at U of I. The members of the Ko Laboratory, Patrick Lin, Dr. Arnon Gal, Dr. Yongbum Koo, Dr. Kee Jun Kim, Dr. Jongki Cho, Dr. Songwook Oh, Sarah Osmulski, and Stephanie Martynenko, have been instrumental in instilling scientific methodology and providing technical training, support, unique perspectives, and friendship for my growth. I am especially indebted to Patrick Lin for his assistance, his limitless energy, and his boundless patience, and above all for being a noble role model deserving of the utmost respect. I am also grateful for my many colleagues in the Comparative Biosciences Department, particularly Dr. Patrick Hannon, Dr. Juan Davila, Daniel McDougle, Dr. Levent Dirikolu, Dr. Matt Allender, Dr. Jing Yang, Karen Doty, Dr. Leslie McNeil, Shreya Patel, Changqing Zhou, Dr. Carrol Bunick, Dr. Dave Bunick, Todd Blazaitis, Dr. Val Beasley, and Dr. Duncan Ferguson, for generating a dynamic and educational work environment. I also offer my gratitude to my classmates and colleagues in the College of Veterinary Medicine, Daniel Loper, Joshua Good, Catherine Foreman, Natalie Rupp, the classes of 2015 and 2017 for encouraging a fun and social environment and providing a tether to Veterinary Medicine, and Nikki Hausmann and Dr. Lois Hoyer for their watchful oversight, support, and dedication to the Veterinary Medical Scholars Program.

I am also thankful for the previous influential mentors that I have had, and for the views and values that they have instilled. I am thankful to Dr. Alex Augustyn and Tom Wirth for helping me choose my educational path, and to Fred Dennis for introducing us. I would also like to thank my previous advisors, Dr. Jason Weckstein, Dr. John Bates, Dr. Stephen Pruett-Jones, and Dr. Jason Bruck, who have all served as exemplary role models and who I hope to emulate in my future. I am also thankful to Dr. Eric Larsen and Dr. Petra Sierwald for first providing me the chance to help educate others within biology and for their dedication to teaching and sharing knowledge. The quote below is for them and articulates an idea I hope to never let slip from my mind and appreciation.

Finally, I am most grateful to my family and closest friends for their unwavering support throughout this adventure, without which I would neither be able to achieve my goals nor rise from my failings. I am grateful to my mother Dawn, my father Anthony, my brother Michael, my sister Gina, my grandmothers Lynn and Barb, and to Adam, for encouraging me to pursue my best while caring and providing for me when I could not provide for myself. My highest gratitude is to Dr. Heather Honious for her loving inspiration, ceaseless motivation, and interminable support, without whom I would never have completed this undertaking and to whom I am forever indebted. Thank you.

"There is a simple grandeur in this view of life with its powers of growth, assimilation, and reproduction, being originally breathed into matter under one or a few forms, and that whilst this our planet has gone circling on according to fixed laws, and land and water, in a cycle of changes, have gone on replacing each other, that from so simple an origin, through the process of gradual selection of infinitesimal changes, endless forms most beautiful and most wonderful have been evolved."

-Charles Darwin, 1842, unpublished[1]

TABLE OF CONTENTS

LIST OF TABLES AND FIGURES

Chapter 2

Chapter 3

Chapter 4

Chapter 5

Chapter 6

Chapter 7

Chapter 8

LIST OF ABBREVIATIONS

AMHR2	Anti-Mullerian Hormone Receptor Type 2
ANOVA	Analysis of Variance
AREG	Amphiregulin
ARNT	Alpha-Aryl Hydrocarbon Nuclear Translocator
AU	Arbitrary Units
BAC	Bacterial Artificial Chromosome
BCL6	B Cell Lymphoma 6 Protein
CBFβ	Core Binding Factor-beta
CFD	Compliment Factor D
ChIP	Chromatin Immunoprecipitation
CL	Corpus Luteum
COC	Cumulus Oocyte Complex
Cre	Cre Recombinase
CRLZ1	Charged Amino Acid Rich Leucine Zipper 1
CTCF	CCCTC-binding Factor (zinc finger protein)
Cyp19	Cytochrome P450 Family 19 Subfamily A Polypeptide 1; Aromatase
DAVID	Database for Annotation Visualization and Integrated Discovery
E2	Estrogen (17β-estradiol)
EBF1	Early B-Cell Factor 1
ECE-1	Endothelin Converting Enzyme 1
ECE-2	Endothelin Converting Enzyme 2
EDC	Endocrine Disrupting Chemical
EDN1/ET-1	Endothelin-1
EDN2/ET-2	Endothelin-2
Edn2KO	Endothelin-2 Knockout (global)
EDN3/ET-3	Endothelin-3
EDNRA/ET_A/ETa	Endothelin Receptor A
EDNRB/ET_B/ETb	Endothelin Receptor B
EGR1	Early Growth Response 1
EIA	Enzyme Immunoassay
ELISA	Enzyme-Linked Immunosorbent Assay
ENCODE	Encyclopedia of DNA Elements Consortium
ESR1/ERα	Estrogen Receptor α
ESR2/ERβ	Estrogen Receptor β
F3	Coagulation Factor 3
Flox	Flanked by LoxP sites
FLP	Flippase
FRT	Flippase Recognition Target
FSH	Follicle Stimulating Hormone

GFP	Green Fluorescent Protein
GnRH	Gonadotropin Releasing Hormone
GPCRs	G-Coupled Protein Receptors
HAT	Histone Acetyltransferase
hCG	Human Chorionic Gonadotropin
HDAC	Histone Deacetylase
HIF1α	Hypoxia Inducible Factor 1α
HIF1β	Hypoxia Inducible Factor 1β
HIFs	Hypoxia Inducible Factors
i.p.	Intraperitoneal
i.v.	Intravenous
iCre	Codon-improved Cre Recombinase
IL6	Interleukin 6
IVF	In Vitro Fertilization
JUNB	Jun B Proto-oncogene
K+PSS	High Potassium Physiological Saline Solution
KO	Knockout
KOT	Kidney Ovary Transplantation
L19/RPL19	Ribosomal Protein 60S Subunit L19
LacZ	Beta-galactosidase gene of the Lac operon
LC/MS	Liquid Chromatography / Mass Spectroscopy
LH	Luteinizing Hormone
LPM	Liters Per Minute
MET	Motif Enrichment Tool
MMP2	Matrix Metalloproteinase 2
MMP7	Matrix Metalloproteinase 7
MMP9	Matrix Metalloproteinase 9
MMPs	Matrix Metalloproteinases
mN	milliNewton
mOGED	Mouse Ovarian Gene Expression Database
NCOR	Nuclear receptor corepressor
Neo	Neomycin Cassette
NFKB1	Nuclear factor of Kappa Light Polypeptide gene Enhancer in B-cells 1
OVX	Ovariectomized; gonadectomized
P4	Progesterone
PBS	Phosphate Buffered Saline
PCOS	Polycystic Ovary Syndrome
PCR	Polymerase Chain Reaction
PECAM1/CD31	Platelet Endothelial Cell Adhesion Molecule 1
PFA	Paraformaldehyde
PGF	Placental Growth Factor

PGR	Progesterone Receptor
PI3K	Phosphoinositide 3-Kinase
PMSG/eCG	Pregnant Mare Serum Gonadotropin; Equine Chorionic Gonadotropin
PND	Post-Natal Day
polyA, pA	Polyadenylation Sequence
PRKO	Progesterone Receptor Knockout
PSS	Physiological Saline Solution
PTGS1/COX-1	Prostaglandin Endoperoxide Synthase 1
PTGS2/COX-2	Prostaglandin Endoperoxide Synthase 2
qPCR	Quantitative PCR
RFP	Red Fluorescent Protein
ROCCs	Receptor-operated Calcium Channels
rOGED	Rat Ovarian Gene Expression Database
RPL19/L19	Ribosomal Protein 60S Subunit L19
RT-PCR	Reverse Transcription PCR
RUNX1	Runt-Related Transcription Factor 1
SEM	Standard Error of the Mean
SMA	Smooth Muscle Actin
SMRT	Silencing Mediator of Retinoid and Thyroid hormone receptors
SP1	Sp1 Transcription Factor
SPP1/OPN	Secreted Phosphoprotein 1
STDEV	Standard Deviation
TAM	Tamoxifen
TCFCP2l1	Transcription factor CP2-like 1
TESS	Transcriptional Element Search System
TEZO	Tezosentan
TFAP2A	Transcription Factor AP-2 alpha
TIMP-1	Tissue Inhibitors of MMP-1
TIMPs	Tissue Inhibitors of MMPs
TLX1_NFIC	T-cell Leukemia Homeobox 1 - Nuclear Factor 1/c (CCAAT-binding transcription factor) Complex
VEGF(A)	Vascular Endothelial Growth factor (A), also referred to as VEGF
VEGFR1/FLT1	VEGF Receptor 1
VEGFR2/FLK1	VEGF Receptor 2
VISTA	Visual Tools for Alignments
VOCCs	Voltage-Operated Calcium Channels
WNT2	Wingless-related Murine Mammary Tumor Virus Integration Site 2
ZFP423	Zinc Finger Protein 423
ZP3	Zona Pellucida Protein 3

CHAPTER 1: OVERVIEW

Ovulation is the fundamental biological process in vertebrates during which the unfertilized oocyte and associated cells of the cumulus oocyte complex are expelled from the ovary in order to enter the oviduct for fertilization by the sperm and eventual transport to the uterus (or shell gland). In humans, it is both a necessary step in the establishment of pregnancy and also allows for corpora lutea (CL) formation, which is critical for pregnancy maintenance. Though the global population continues to rise alarmingly fast, there is now an increasing rate of infertility in the developed world that lacks a singular causal explanation. Infertility is now the single most common reason to see a doctor in multiple countries, and there is a growing number of infertility clinics worldwide[2]. Additionally, 1-3% of couples experience recurrent miscarriage with three or more consecutive pregnancy losses, and the majority of these cases also go undiagnosed[3,4]. In diagnosed infertility cases, ovulatory disorders account for about 30% of female infertility[5], and are thus a major contributor to millions of cases of infertility each year. Understanding the mechanisms central to ovulation will help alleviate growing issues within infertility and improve treatment procedures used through assisted reproductive technologies, and may also lead to new safer or more economical contraceptive techniques.

This dissertation focuses on the role of the protein endothelin-2 (EDN2) in ovulation. EDN2 is a vasoconstrictive agent produced in ovarian granulosa cells of mature follicles just prior to ovulation[6-8]. Elucidating the role of EDN2 will further identify pathways and targets for use in treating infertility and improving ovulation rates during assisted reproduction.

This dissertation is divided into a total of nine chapters, with all references listed after the final chapter. Figures and tables are located at the end of individual chapters that they are referenced in. Chapter 2 provides a brief background on current issues in female reproduction, a brief summary of the female reproductive system and species differences associated with it, a history of the identification and study of endothelin-2 relative to reproduction, and the specific aims and hypotheses of this work. Chapters 3-8 are data chapters that each address a specific aim; each is formatted as an individual manuscript, except that figures and tables with associated legends are listed at the end of the chapter. Chapter 3, the only chapter published at the time of dissertation composition, discusses the generation of an Edn2-iCre mouse model and identification of cells and cell lineages of *Edn2* expression, and has been published in the journal *Genesis* in

2015 (PMID 25604013). Chapter 4 explores the contractile properties of ovaries in response to EDN2 peptide in dogs, cats, and chickens as well as smooth muscle distribution to demonstrate that EDN2 presence causes ovarian contraction across vertebrate species. Chapter 5 describes the generation of a new Esr2-iCre mouse model that has consistent and robust iCre expression in the granulosa cells. Chapter 6 describes the resulting phenotype of ablating *Edn2* in the whole ovary or in the granulosa cells using the model described in Chapter 5 and explores the intraovarian mechanism by which EDN2 modulates ovulation. Chapter 7 describes the use of a mouse model where endothelin receptor A is lost in smooth muscle cells in an inducible manner and the effect this has upon ovulation. Chapter 8 briefly explores the regulation of *Edn2* expression by progesterone receptor and hypoxia, and generates a hypothesis for future study of potential *Edn2* regulation by RUNX1. Lastly, Chapter 9 provides a brief summary of data presented in this work, conclusions that can be drawn those data, and future directions for study of EDN2.

It must be noted that this dissertation deals exclusively with animal models, and nearly exclusively with mouse models, for practical considerations to investigate the fundamentals of human ovulation. The findings herein are believed to be salient with human physiology and genetics given that humans and mice share a common ancestor only 80 million years ago[9], while both ovulation and the endothelin system are far older. Indeed, humans and mice share approximately 75% percent of their genome[10], with even greater homology among the protein coding regions of approximately 85%, and about 99% of mouse genes have homologues or analogues in humans[11]. As a cautionary point, it has been demonstrated that despite genetic similarity, physiological responses between humans and mice may differ greatly in the specific genes activated[10]. However, the final active form of endothelin-2 differs by a single amino acid between species and each isoform shows the same activity across species[12,13]. Given such high conservation across evolutionary time and retained responses in tissues, the following information is presented under the operating notion that EDN2 acts homologously between humans and mice[14], that the mechanisms of ovulation are also highly conserved, and that it may be logically upheld (pending further contradictory evidence) that findings in one species directly translate to the other for direct application in assisted reproductive technologies and infertility treatment. Greater elaboration on the evolution of the endothelin system and its conserved role in mammals leading to this governing postulate is located in the following chapter.

CHAPTER 2: INTRODUCTION AND REVIEW OF RELEVANT LITERATURE

Contemporary concerns in reproduction: population growth, contraceptives, and infertility

Current issues within reproductive study are centered about two opposite yet related issues: methods to decrease rates of pregnancy achievement in the face of the rapidly rising world population, and treatments for couples that have been unsuccessful in achieving or maintaining pregnancy by natural means. Currently, the world population is at about 7.3 billion people, an increase in global population by 300 million (the approximate size of the US population) since October, 2011[15]. It has been estimated that the carrying capacity of the world, the maximum human population that can be maintained by current food production efficiency and distribution, is about 9 billion people, though estimates range from 5 billion to 15 billion[15-21]. The population is expected to reach this level by 2050; increases in the human population beyond this point are predicted to result in increased starvation and mortality, and, as a succinct understatement, a decrease in the average quality of life[22,23]. Indeed, human population-driven changes are becoming readily apparent in the climate itself[23-27] as well as the total amount of animals[28] and species[29] present. Reduction in the number of human births per year is a necessity, and can only be achieved through proper contraceptive education and use throughout. Development of new contraceptive techniques that are cheaper and safer or have fewer side effects than conventional estrogen and progesterone birth control pills, and are more culturally acceptable than condoms would greatly aid in the struggle against the increasing world population. Thus new contraceptive targets must be designated through scientific investigation of the human reproductive process, and subsequently developed and tested.

On the other end of the spectrum, for largely inexplicable reasons, the developed world is facing an increasing rate of widespread infertility. This developing-world trend toward low fertility in each gender may be partially attributed to the socioeconomic status, career demands in women, and/or improvements in contraception[30]. Though it does little to offset global population growth, infertility is now the single most common reason to see an OB/GYN specialist in several countries, and there is a trend towards a worldwide increase in infertility clinics[2,31]. Consequently, the use of assisted reproductive technologies (ART)[30,32-34] has increased as well. It has been estimated that 15-20% of all clinical pregnancies in the US end in miscarriage[4], and this percentage is expected to increase. Most instances of infertility are idiopathic and undiagnosed. A recent register linkage study demonstrates that the age of a mother at conception is a major risk factor for miscarriage[35], and risk of fetal loss increases after 35 years of age[35-37]. Though increasing age during childbirth

is one possible contribution to infertility epidemic, age itself is not a direct causative agent. Within infertility, 1-3% of couples experience recurrent miscarriage (RM), with three or more consecutive pregnancy losses; the majority of cases of RM are also undiagnosed[3,4].

In diagnosed cases, ovulatory disorders account for about 30% of female infertility[5]. Ovulation is the event in which a mature oocyte, the female germ cell, is released from its follicle in the ovary and enters the ampulla of the oviduct where fertilization may then occur. Disorders may be caused by failure of follicles to be maintained, to grow and develop in response to gonadotropic signals, to produce or respond to normal ovarian hormones, to undergo cumulus oocyte complex expansion, to undergo luteinization and produce progesterone, or to rupture from the ovary and allow the oocyte entrance to the oviduct. Changes to these functions may be caused by cancer[38-40], infection, or cysts[41] within the ovary itself, by hormonal imbalances of ovary-derived hormones caused by either primary or secondary endocrine signaling disorders[42-44] such as polycystic ovarian syndrome (PCOS)[45-48], by autoimmune diseases that target the ovary[49-51], or by exposure to endocrine disrupting chemicals (EDCs) that modify hormonal or genetic signals[52-56] within the reproductive signaling axis, to name a select few causes. Thus the ovary is one particular area that may be studied to understand the genetic and molecular basis leading to a large percentage of infertility cases. An increased knowledge of the basic mechanisms of ovulation may also lead to creation of improved female contraceptives and provide greater hope for slowing and eventually halting global population growth.

The female reproductive system: an essential overview of ovulation

Understanding ovulatory function and disorders arising from malfunction requires a grasp of the female reproductive system as a whole, as multiple organs work in a synchronized temporal manner to stimulate ovulation and allow for fertilization and pregnancy. Though it is not possible to provide an in-depth review of multiple systems, a brief overview is possible with a particular focus on ovulation itself.

The female reproductive system directly involves the ovaries, oviducts, uterus, cervix, vagina, external genitalia[57], and also requires signaling and cellular interplay with the brain, pituitary gland, and spleen[58]. Of these, the brain, pituitary, and ovary are the primary components in reproduction leading to ovulation and fertilization, with more recent evidence also including the spleen[58] (Figure 2.1A). The ovary undergoes predictable and repeated changes as women or female animals go through their respective reproductive cycles. The primary function of the ovary is to maintain the germ cells (oocytes, egg cells), to prepare them for fertilization, and to generate hormones necessary for germ cell growth and also for pregnancy maintenance (in most species). Germ cells in the ovary are organized into follicles, which grow and develop prior to ovulation. Follicles within a healthy and mature ovary may be morphologically and functionally classified as primordial, primary, secondary, antral, or Graafian (periovulatory)[59]; follicles sequentially develop in this order leading up to ovulation. Graafian follicles are the largest and most mature follicles, and contain an oocyte surrounded by a zona pellucida and a layer of cumulus granulosa cells[60-62] (Figure 2.1B). Together, these make up the cumulus oocyte complex (COC), which is released during follicle rupture into oviduct where fertilization occurs. The COC is surrounded by antral fluid and is contained within the wall of the follicle, which consists of the inner mural granulosa cell layer and outer theca cell layers. The theca cells may be further divided into the theca interna and the theca externa cells; prior to ovulation, vasculature is present in the theca cell layer but does not pass the basement membrane between the theca and granulosa cell layers until follicles are mature and near ovulation[63]. Both the granulosa cells and the theca interna cells are steroidogenic[64,65], and produce estrogen and testosterone, respectively; however, the theca externa cells are contractile, possess smooth muscle actin, and retain a shape similar to that of a fibrocyte/fibroblast[66].

Many events leading to ovulation and follicle rupture are controlled by two hormones, follicles stimulating hormone (FSH) and luteinizing hormone (LH), which are secreted from the

anterior pituitary under the influence of gonadotropin releasing hormone (GnRH) from the hypothalamus of the brain via the hypophyseal portal blood system[59]. GnRH is in turn regulated by neuronal stimuli such as kisspeptin and is released in a pulsatile fashion, where low frequency pulses stimulate a slight increase in FSH to enhance follicle growth, and high frequency pulses lead to a sharp rise in LH (the LH surge)[67]. The LH surge is necessary for ovulation and formation of the corpus luteum (plural corpora lutea, CL), which develops in place of the Graafian follicle after ovulation occurs and secretes progesterone to maintain pregnancy[68]. The ovary has a concurrent necessary role in signaling feedback during these processes by producing molecules such as activins, inhibins, androgens, and estrogens[69,70]. In particular, estrogen is produced by the granulosa cells of developing follicles starting during the secondary follicle stage as aromatase expression becomes active, which converts testosterone from the theca interna cells into estrogen[71-73]. Estrogen diffuses from the granulosa cells into the bloodstream and travels to the brain, where it exerts negative feedback upon GnRH production until a critical threshold is reached, after which it instead exerts positive feedback to increase the frequency of GnRH pulses and cause the LH surge, leading to ovulation[74,75].

The CL develops from the cells of a follicle following the release of an oocyte during ovulation[76,77]; theca and granulosa cells luteinize into the small and large luteal cells, respectively, and endothelial cells (ECs) migrate into the developing CL to form new vessels via angiogenesis[78-82]. The CL is an organ of prolific angiogenesis on a dynamic timescale, as vessels invade to deliver progesterone (P4) precursors and carry P4 out to the body[83,84]. This angiogenesis requires local production of vascular endothelial growth factor (VEGF). Luteinizing granulosa cells secrete VEGF, activating two VEGF receptors (VEGFR-1 and -2) that are localized to luteal ECs and steroidogenic cells[85-87]. VEGF receptor activates endothelial cells lining vessels and causes proliferation[88,89]. Other factors, such as hypoxia, have been identified as playing a role in inducing VEGF in luteinizing granulosa cells[90]. Angiogenesis in CL formation proceeds after VEGF induction with matrix metalloproteinase (MMP)-mediated dissolution of the follicular basement membrane, sprouting of new vessels with proliferating ECs, and eventual vessel anastomosis that is mediated by macrophages through the surface proteins TIE2 and NRP1[91]. Tissue inhibitors of metalloproteinases (TIMPs) are highly expressed in the ovary just after the LH surge[92-96]. TIMPs are released in large quantities during ovulation from the granulosa cells and subsequent lutein cells [97-99], and are also produced in the growing CL[97].

Until the mid-1960s, it was thought that an increase in intrafollicular pressure was the driving force for follicle rupture[100]. However, artificially increasing pressure by saline injection is insufficient to induce follicle rupture[101,102] and more accurate measurements of follicle pressure report that there is not much change during ovulation[100]. It is now known that a decrease in follicle wall strength is necessary during ovulation[103-105]; this change in tension is caused by proteolytic enzymes such as matrix metalloproteinases (MMPs) and the plasminogen system[106]. Both ovarian cells and leukocytes, which enter through circulation, secrete proteases into the ovary. MMP-2 and MMP-9 have been previously implicated in degradation of the follicle wall during ovulation[107,108]. Additionally, a decrease in activity of TIMPs has also been correlated to ovulation, specifically of TIMP-1[109,110]. Ovarian modulation of TIMPs and MMPs may occur through leukocytes, which double in the ovary prior to ovulation in the rodent while decreasing by a similar amount in the spleen[58]. Macrophages, dendritic cells, and lymphocytes are all localized to the Graafian follicle during ovulation, and dendritic cells in particular have been reported as necessary for normal ovulation[103,111]. Additionally, other recent physiological studies have implicated contraction of the follicle wall, specifically of the theca externa layer, as a contributing final factor in follicle rupture[6,66]. It is this contribution to rupture by ovarian contraction upon which this dissertation is focused. A summary of the molecular pathways leading to and required for ovulation has been recently generated by Dr. J.S. Richards (2010)[67,112]. These pathways include interactions between key reproductive hormones and their receptors as well as multiple downstream genes and transcription factors (Figure 2.2). Thus ovulation is a multi-faceted process with many genetic interactions contributing to several key physiological processes including leukocyte invasion and weakening of the follicle wall, and potentially an increase in ovarian tension as well.

Specifics of mouse reproduction

Unlike humans, rodents do not go through a menstrual cycle and do not repeatedly shed uterine lining in preparation for implantation. Instead, mice go through an estrous cycle. After reaching puberty at approximately 35 days of age, though this varies highly by strain used, the vaginal tract opens (vaginal introitus) in response to elevated estrogen levels[113]. Mice then go through a 4-5 day long, light and nutrient-dependent cycle that may be divided into four distinct phases: diestrus, estrus, metestrus, and proestrus[114]. These may again be subdivided into as many as 13 different cycle periods, although this extensive subdivison is not routinely considered. The stage of the estrous cycle can be established by performing vaginal cytology[115]; the cells lining the vagina vary in appearance under different hormonal conditions: rounded and nucleate during proestrus, cornified and anucleate during estrus, cornified and anucleate with some leukocytes during metestrus, and predominantly leukocytes during diestrus[116]. Changes in estrogen concentration correspond to cyclic changes in the estrous cycle. Estrogen is highest in proestrus (10.5pg/mL), and decreases through estrus (8.5pg/mL) to a low of about 7.0pg/mL during metestrus, before rising slightly again during diestrus (8.0pg/mL) as follicles mature[116]. Mice of normal reproductive age show relatively high variability in estrous cycle length compared to other model species[117], such as rats[118]. Proestrus marks the period of follicle growth in mice, whereas estrus begins with the ovulation of fully mature oocytes. Metestrus marks the end of receptivity, the closure of vagina, and movement of the egg through the oviduct. After metestrus, mice that are not pregnant enter diestrus where unfertilized eggs are eliminated and new follicles begin to be selected for potential growth to ovulation. Mice may also enter a pseudopregnancy period after metestrus that may last for 1-2 weeks after sterile copulation owing to prolactin signaling[119].

Mice are spontaneous ovulators, with ovulation occurring during estrus between 12 and 14 hours after the LH surge[6]. Ovulation in the mouse may not occur every estrous cycle, particularly in young virgin females after vaginal introitus. The gonadotropins LH and FSH may be mimicked by administration of equine chorionic gonadotropin (eCG), which is also known as pregnant mare serum gonadotropin (PMSG), as an FSH analogue and human chorionic gonadotrope (hCG) as an LH analogue in mice to control timing of ovulation[6]. Injections of PMSG followed by hCG are normally done at 48 hour intervals with 5 international units of each (5 I.U.), with ovulation occurring 12-14 hours following hCG injection (Figure 2.3A). Multiple corpora lutea form in the mouse ovary after ovulation, and persist for 2-4 estrous cycles (up to three weeks). Though an

average of 8 follicles mature to the antral/Graafian stage per mouse ovary (Figure 2.3B), only about half of these are ovulated, with the rest undergoing atresia of the oocyte[119]. Ovulated oocytes travel through the oviduct to the ampulla where fertilization occurs (Figure 2.3C); this passage takes 2-3 days, with uterine implantation occurring on day 4[120]. In the ovary, the lifespan of the corpora lutea modify the level of progesterone in the mouse ovary relative to humans: murine progesterone is lowest during diestrus, is approximately four times this during metestrus, is 7.5 times higher at proestrus than diestrus, and is eight times higher during estrus than diestrus[121,122]. Thus progesterone rises prior to ovulation in the mouse estrous cycle unlike in menstrual species. Also, interestingly, the lifespan of the corpora lutea is under regulation by prolactin in mice, as opposed by prostaglandins in humans[123]. Prolactin secretion is sensitive to prostaglandins and LH, and will increase after copulation. Prolactin is necessary for angiogenesis to occur during functional CL formation[124]. After successful mating, pregnancy lasts between 19 and 23 days, though it is best approximated by 21 days in C57B/6 mice. Mice may become pregnant while nursing one litter and may give birth one gestation period after parturition.

Species differences during ovulation: domestic cats, dogs, and chickens

Though rodents are important tools for understanding key processes that cannot be directly manipulated in humans and human tissues, it is important to validate findings across multiple species when possible. Though not all processes are directly conserved across evolution, retention of signaling pathways in highly divergent species lends great evidence for similar mechanistic retention in humans as well. Three readily available species for reproductive study include the domestic cat, the domestic dog, and the domestic chicken.

Cats normally have an abundance of different follicle populations, cycle repeatedly through the majority of the year, provide a readily available tissue pool from local routine veterinary spays (ovariohysterectomy)[125], and are important to study reproductively given the over-population issues that currently plague veterinary medicine[126]. Additionally, cats have been previously studied in response to superovulation protocol and CL formation, and new knowledge of the factors necessary for ovulation and luteal maintenance may importantly impact the currently low success rate for IVF among the 36 (of 37)[125] endangered felid species. Cats enter puberty between 6 and 9 months depending on breed, light cycle, and nutrition, but there are reports that pregnancies can begin as early as 4 or 5 months. Cats are induced ovulators, and if not bred they will cycle in heat every 2-3 weeks, with estrus lasting an average of 6 days[127-131]. Coital stimulation during mating triggers hypothalamic GnRH release, causing the LH surge within approximately 20 minutes of mating[132,133]. Ovulation is reported to occur 24-56 hours after mating, though few studies have looked specifically at the time of follicle rupture. Results vary from a range of 24-36 hours to 22-56 hours and few studies used precise measures to determine ovulation timing[134,135]. As in other mammals, CL formation begins at the time of ovulation, but luteal cells do not reach their maximum size in the cat until 12-16 days later. Progesterone (P4) rises above a basal level (<1ng/mL) in 2-4 days after mating[136-138], and peaks 21 days after mating in both pregnant and pseudopregnant cats[129,137]. CL become histologically visible 2-3 days after ovulation[129]. Multiple studies have reported good efficacy in superovulating cats. In a study by Chatdarong *et al*. (2007), treatment with 100IU human chorionic gonadotropin (hCG) after estrus induced ovulation in 95% of cats[139]. An equal dose of pregnant mare serum gonadotropin (PMSG) has been used to bring 95% of cats in estrus when given 3 days earlier[140]. On average, 3-4 oocytes are ovulated per stimulated cat[141]. Similar results are obtained (3.4 oocytes/cat) even when exogenous gonadotropins are given during mid-gestation[127].

Similar to cats, tissue from intact canine females (bitches) is readily available from local pets that routinely undergo veterinary ovariectomy and ovariohysterectomy to prevent undesired pregnancies. Dogs are generally considered monoestral polyovulatory nonseasonal spontaneously ovulating species[142]. Like cats and mice, dogs go through an estrous cycle, though there is a long period of anestrus between follicular phases. Generally, dogs go through a 2-3 week long 'heat' cycle, consisting of proestrus and a 5 day estrous period with ovulation occurring on day 1 of estrus. Dogs then go through a mandatory luteal phase of approximately 64 days if pregnancy does not occur, whereas pregnancy is 65 days on average[143]. Following the luteal phase or pregnancy, bitches enter a highly variable anestrous cycle that ranges from 5-12 months in length. The end of anestrus in the dog is not yet well understood, and may depend on interplay between photocycle, pheromones, and an endogenous circannual cycle in the brain[143]. Interestingly in bitches, blood progesterone concentrations increase prior to ovulation and the LH surge. Serum progesterone is approximately 2ng/mL at the time of ovulation; this is caused by the occurrence of preovulatory luteinization[144]. Also, oocytes are ovulated in the immature diploid stage and complete maturation in the oviduct prior to fertilization[142,145]. Ovulated oocytes are 5-7mm in diameter. Implantation occurs after 2.5-3.0 weeks after ovulation[146]. Beyond the early increase in progesterone, which may be used as a clinical marker to determine timing of breeding, ovulation is similar to other mammalian species and is dependent upon FSH, LH, estrogen, and progesterone signaling[147,148]. Both dogs and cats have a similar follicular structure to mice and humans[149].

Laying hens have a relative unique ovulatory system compared to mammals. In hens, only the left ovary is present, and ovulation occurs daily at approximately 24 hour intervals. Hens are light sensitive, and eggs are laid 9-10 hours after the onset of darkness; the time of lay from darkness onset increases until the lay is ~20 hours after darkness onset and at this point the hen may miss a day of ovulation to 'reset'[150]. The ovary physically resembles a 'bunch of a grapes' where preovulatory follicles are arranged in a hierarchy, with size being indicative of the next follicle to ovulate[151]. The leading, or F1 follicle, consists of an oocyte, granulosa cell layer, theca cell layer, and blood vessels[152,153]. However, the granulosa cells of mature follicles are a single avascular cell layer, and the theca cell layer has high contractile potential. Ovulation occurs at a break in the follicle called the stigma that can be recognized by the lack of vessels more than 48 hours prior to ovulation[154]. Unlike mammals, progesterone is the principal steroidogenic endpoint of the growing follicle and is produced by the granulosa cell layers, particularly of the F1 and F2

follicles. Alternatively, estradiol is secreted by the theca layer of the smaller follicles and estradiol production decreases over 10-fold in the 5 days leading up to ovulation in the follicle[155]. Thus aromatase is active in the theca layer, not the granulosa layer as in mammals. Further, it is progesterone produced by the granulosa cells that induces the LH surge to cause ovulation; LH peaks 3-6 hours prior to ovulation[150] and progesterone peaks at 8 hours prior to ovulation[156,157]. Estradiol does not stimulate LH release in the laying hen[150], though it does stimulate progesterone receptor upregulation in the hypothalamus and pituitary. Treatment of hens prior to ovulation with tamoxifen, a dual estrogen receptor antagonist, does not prevent ovulation, though long term treatment does as estradiol is necessary for basal LH secretion. The chicken is an important ovulatory model owing to the large follicle size, which easily allows examination of cells of ovulatory follicles compared to non-ovulatory F2 follicles within the same animals. Chickens are also easy to time ovulation in and do not require exogenous gonadotropins to induce ovulation. Their quick time to maturity, daily ovulation schedule, and potential use as a comparable non-mammalian out-group to other species make them an excellent, and often under-utilized, model reproductive species.

Previous investigations into the role of ovarian contraction during ovulation

Within the ovary, there is a network of smooth muscle cells that is conserved across species. This network is composed of both the cells surrounding the arteries and arterioles of the ovary that control vascular tension, and also the theca externa of mature follicles (Figure 2.3D,E). Consequently, the topic of contraction as a mediator of ovulation has long been debated and was a particularly active area of research in the 1970s and early 1980s[158-165]. This is discussed in further detail in Chapters 4 and 7. It is well established that ovaries have high contractile potential and even respond outside the body to exogenous agents[66]. Despite the presence of autonomic nerves in the ovary and the production of contractile agents such as prostaglandins, no definitive ligand or neurologic signal has been identified as a physiological trigger for ovarian contraction. This, in addition to inconsistent reports on changes in follicular pressure and seminal work showing that increasing intrafollicular pressure does not cause ovulation[101,166-168], resulted in a shift away from the focus on contraction for many years. It is now well known that collagenase and proteinase activity are required for ovulation, and it is widely believed that weakening of the follicular wall is one of the most critical ovulatory events[70,112].

Recently, a return to the idea of ovarian contraction has been suggested by Matousek *et al*. (2001)[100], who demonstrated that there are mild and short-term increases in follicular pressure in the rat ovary just prior to ovulation. Related to this, a unique continuous imaging method by Dahm-Kahler *et al*. (2006) of *in vivo* rabbit ovulation showed that blood flow ceases in the apex of an ovulating follicle three minutes before ovulation and the follicle protrudes from the ovarian surface. This is rapidly followed by rupture: fluid first leaks from the apex, followed within 10 seconds by granulosa cell extrusion. Though rupture occurs rapidly and the entire follicle is removed from contact with the stroma, follicles remain attached to the surface of the ovary for over an hour and a half[169], which may imply that there is an initial 'pushing' force from within the ovary prior to sufficient dissolution of the extracellular matrix to fully free the follicle from the ovary. The cessation of blood flow in the follicle apex is also of interest, as this would require a highly local vasoconstrictor or clotting agent to be very rapidly produced, or previously produced and sequestered from the blood supply, until just prior to ovulation lest the follicle and oocyte become oxygen and nutrient starved. More recent work[6,170,171] suggests that contraction plays an important role in the ability for a follicle to rupture from the surface of the ovary. However, definitive proof for a ligand or signal for ovarian contraction induction *in vivo* remains elusive.

New tools for genetic investigation in ovulation: the Cre/LoxP system

The Cre-LoxP recombination system has been widely used in bacterial and whole animal studies to mediate tissue specific gene ablation. The removal or modification of individual genes or portions thereof has been a powerful tool in molecular biology, and allows *in vivo* examination of the roles of various ligands, receptors, enzymes, cell types, etc. that could not have been individually characterized previously. It is common to explore the role of a particular target by removing it from a cell or animal and then observing the resulting phenotypes. The next stage in such exploration, after validation of target loss, is to the phenotypes that are likely influenced by removal of the original target.

The enzyme Cre recombinase, originally isolated from the P1 bacteriophage, belongs to the integrase family of site-specific recombinases[172]. It is a 38kD protein that catalyzes recombination of DNA sequences between specific sites (LoxP sites) within a DNA molecule[173]. A LoxP site is a 34 basepair stretch of DNA consisting of a core spacer sequence of 8 basepairs with two 13 basepair palindromic flanking sequences. A LoxP sequence is recognized by its unique sequence: ATAACTTCGTATAGCATACATTATACGAAGTTAT (spacer sequence is underlined). When a portion of DNA within a cell has a LoxP sequence on each side of it, it is flanked on each side by LoxP, and hence is "floxed." Thus DNA with a floxed gene has two LoxP sequences within a portion of a specific gene. Two LoxP sequences in one DNA stretch, when oriented in the opposite direction, mediate inversion of that DNA sequence. When LoxP sequences have the same directionality, the DNA between them will be excised instead of inverted, leaving only a single LoxP behind the now-joined regions of DNA. Also, if LoxP sites are found on two different chromosomes, Cre recombinase may mediate chromosomal translocations[174]. LoxP sites can be introduced into genomic loci of interest by homologous recombination coupled with chemically or electrically-induced transfection. Most commonly, LoxP sites are inserted into the genome in the same directional orientation. In mammals, this is most commonly done in C57BL/6 mice, though it has also been done in other inbred mouse strains such as 129. It is also a common practice in some immortalized laboratory-specific cell lines. Thus activity by Cre recombinase will generally recognize those two LoxP sites and will excise the DNA stretch between them in conventional transgenic mouse biology.

Coupled with the ability to remove a floxed sequence of DNA, Cre recombinase may be expressed throughout all of the cells of a mouse or only in specific cells. Generally, the DNA

coding for Cre protein is placed after the promoter for a specific gene that is active in only one or a few cell or tissue types, or after a promoter that is only active at a particular stage of development, or both. For targeting specific cells, this requires prior knowledge of the promoter being used. However, it is conversely possible to place Cre recombinase after the promoter of a gene of interest and to then use Cre activity to characterize cells and times when that promoter, and hence the original gene, becomes active[174]. The Cre/LoxP system has been utilized to 'turn on' genes for characterization purposes, usually by interposing a floxed polyadenylation (polyA) sequence (which will cause transcriptional arrest) within a gene of interest. Cre activity removes the polyadenylation sequence, allowing that gene to then become active. Two common reporter lines utilize this conditional on-switch technology coupled with expression of genes not normally present in the mouse genome that can be easily detected or visualized. ROSA26 mice[175] express beta galactosidase in cells that are positive for Cre expression; beta galactosidase can be detected by x-gal staining, wherein cells that produce beta galactosidase will induce a blue color change in an x-gal substrate of galactose linked to indole[176]. One potential issue with this system is the action of endogenous beta galactosidase or similar enzymatic activity in WT mice, such as in the gut or kidney cortex, which may confound the blue signal. A second approach uses mice where a jellyfish-derived fluorescent protein is preceded by a floxed transcription arrest sequence; these mice demonstrate fluorescence of a particular wavelength only in cells where Cre recombinase is active[177], which has been characterized as a more accurate method for Cre activity observation. Several other recent Cre/LoxP approaches have utilized synthetic genes with floxed transcriptional arrest sites to add voltage or calcium-dependent channels linked to fluorescent reporters for real-time imaging of cell signaling[178-180], to add specific toxin receptors to only membranes of desired cells prior to toxin exposure allowing for cell- and time-specific *in vivo* cell death[181,182], or to color-code numerous identical cells within a particular tissue (usually brains) to trace their unique sites of interaction[183-185].

The ability of Cre recombinase to remove a target floxed DNA sequence is limited by the distance between the two recombination sites[186], by genomic position and local interaction with other DNA sequences or protein molecules, by what cell type Cre recombinase is expressed in, and by the level of Cre recombinase expression in the target cell population[172,187]. This may mean that not all floxed DNA sites are successfully removed in a tissue *in vivo*, and thus not all Cre systems demonstrate 100% successful recombination[188]. To enhance the level of Cre

recombination in mammalian systems, because Cre is originally derived from a prokaryotic source and its codon usage is not optimal for eukaryotes and it has an excessive amount of CpG dinucleotides which may induce genetic silencing, a codon-improved version of Cre recombinase (iCre) that is optimized for mammals was generated in 2001[172]. The newer transgenic mice that utilize iCre have a generally higher success rate in gene ablation than traditional Cre mice.

Another limitation of Cre (or iCre) recombinase is that it is active in a cell whenever its added promoter is active, and promoter activity may be very different in developing animals (mice) from adults. Many attempts to remove floxed genes to study their function in adult mice have resulted in embryonic death from unperceived early or additional gene functions[189,190]. To overcome this hurdle, mice that have inducible Cre recombinase have been generated. In these animals, Cre is only transcribed when a particular cofactor is present that is not normally produced in the transgenic mice. Cre activity may occur globally when that particular factor is present, or it may be limited by activity of a specific promoter to a particular cell type. Examples include doxycycline-dependent global Cre recombinase expression[191], RU486-induced Cre expression in the salivary glands[192], and smooth-muscle cell specific Cre expression in the presence of tamoxifen[193]. Many transgenic mouse lines are now available for commercial purchase from Jackson Laboratory (Bar Harbor, Maine).

In addition to Cre recombinase, other recombinase systems have also been identified, and may be utilized for similar purposes. Flippase (FLP) recombinase and flippase recognition target (FRT) sites were originally identified in yeast and, after modification for successful activity at mammalian body temperatures, are also commonly utilized[194]. Most importantly, FLP recombinase may be coupled with Cre recombinase systems to allow modification of a gene, *in vivo* or *in vitro*, when a LoxP site is also present and modification of the floxed DNA is undesirable. FLP technology is now normally used for insertion of Cre recombinase and LoxP sites into genomic constructs with drug-dependent targeting vectors. Drug-resistance sequences can then be later removed without modifying the desired Cre or LoxP insertions[174].

A new and growing-in-popularity transgenic technology, the CRISPR-Cas9 system (clustered regularly interspersed short palindromic repeat-Cas9 system), can also be used to generate and modify gene presence or function *in vitro* or *in vivo*[195]. The CRISPR system utilizes microbial nucleases to modify genomic DNA. The Cas9 protein can be targeted to specific DNA sites using a custom RNA guide[196]. One key advantage of CRISPR is that multiple RNA sequences

can be used at the same time, allowing for multiple modifications within the same cell. However, Cas9 may itself also be modified by fusion to modular functional effector domains, essentially allowing for any known enzymatic modification to be targeted to a specific DNA site(s) concurrently[196]. This process can be further controlled with genome and epi-genome modifying elements under inducible control systems[197]. It is likely that future transgenic mouse studies will utilize CRISPR systems for Cre or FLP recombinase insertion, for direct stem cell modifications, or for *in vivo* modification in place of the Cre/LoxP system.

The evolution of new tools, such as the Cre/LoxP system and CRISPR-Cas9 system, fueled an increased interest in the genetic and molecular mechanisms governing female reproduction, and ovulation in particular, over the past decade. The application of emerging tools allowed scientists to search for new molecules beyond classic hormones and cell signaling mediators with the hope of improving both contraceptive methods and infertility treatments.

The search for the genetic mechanisms of ovulation: identification of endothelin-2

To identify new molecular mediators of ovulation and CL formation, microarrays were previously generated examining gene expression at different time points throughout the ovary in rat and mouse models by multiple labs in the mid-2000s[6,7,198]. Ovaries were collected from gonadotropin-stimulated rodents and collected at various time points before and after ovulation; these data were also used to create ovarian gene data bases, rOGED and mOGED[199] and the Ovarian Kaleidoscope Database. The rOGED database is publicly accessable, as is the Ovarian Kaleidoscope Database. Two separate labs, the Ko Lab and the Bagchi Lab, independently published on increased expression of the endothelin-2 (*Edn2*) gene in 2006. The Ko Lab identified *Edn2* through the rOGED, while the Bagchi Lab identified *Edn2* after microarray in progesterone receptor knockout (PRKO, PgrKO) mice. EDN2, the final protein product of the *Edn2* gene, is a 21-amino acid peptide with two internal sulfide bonds. Interestingly, expression of the *Edn2* gene increases several thousand fold in approximately a two hour window, hCG11-12 hours, that occurs after the LH surge (hCG0) and just before the average time of rodent ovulation (hCG12-14)[6,7,14,200]. This has been previously indepenently confirmed by multiple groups.

In the rat, *Edn2* mRNA is increased specifically in the granulosa cells (Figure 2.4A). The Ovarian Kaleidoscope Database from Stanford University confirms this level of increased expression in the ovary as a whole (Figure 2.4B)[198], as do data from the rOGED (Figure 2.4C)[199] and the mOGED (Figure 2.4D) databases. When Graafian (periovulatory) follicles were collected and fixed from rats, *in situ* hybridization confirmed *Edn2* transcription occurs in the granulosa cells of mature follicles[6,7] (Figure 2.4E), but not in other local immature follicles or corpora lutea. This induction was absent in mice lacking the progesterone receptor gene[7]. Mice that lack the progesterone gene fail to ovulate[7,201]. Similarly, in rats and mice that are treated with an antagonist for the receptors of EDN2 during ovulation, the number of oocytes released from the ovary are significantly reduced[6]. In 2006, EDN2 was best known as a potent vasoconstrictor[202,203]. This raised significant questions about the mechanism of its action within the ovary, and also helped expand the field of endothelin study into its present day form[204].

Overview of the endothelin system

EDN2 has two similar isoforms, coded by separate genes: *edn1* and *edn3*. EDN1 is the most commonly studied endothelin. Endothelins were originally discovered in 1988; EDN1 was isolated from porcine aortic endothelial cells, hence their name[12]. EDN1 and EDN2 differ by only two amino acids in their final form, while EDN1 and EDN3 differ by 6 amino acids, as do EDN2 and EDN3 (Figure 2.5A). Current antibodies commercially available (583151, Cayman Chemical Company, and ab2793, Abcam) have 100% affinity for all three active endothelins, as well as their big form and their prepro forms[205-207] owing to the high similarity between peptide forms. Other available antibodies have no data listed on specificity (ab117757 Abcam, sc-21625, Santa Cruz). This is an important consideration in clinical vascular pathologies, where endothelin measurement is done by ELISA in hypertensive cases, though this is usually only interpreted as an increase in EDN1 presence[14].

Endothelins are first synthesized as inactive 212 amino acid-long precursors in the cytoplasm known as prepro-endothlins; they are then cleaved by peptidases such as furin-like endopeptidase or chymotrypsin into a 39 amino acid form known as big endothelins; lastly, they are converted to their 21 amino acid active form by one of two endothelin converting enzymes (ECE-1 and ECE-2, encoded by the *ece-1* and *ece-2* genes)[208] (Figure 2.5B). ECE-1 is a zinc-dependent type II membrane protein with an active domain in the ectodomain[209]; ECE-2 is a membrane-bound protein with similar metalloproteinase-like activity but is localized to an intracellular compartment[210] and functions optimally at lower pH[211].

All endothelins exert their actions through two G-protein coupled receptors (GPCRs), EDNRA and EDNRB, which are produced by the *Ednra* and *Ednrb* genes, respectively[212-214]. EDN3 has different receptor affinites from EDN1 and EDN2 and has a higher affinity for EDNRB. EDN1 and EDN2 have equal receptor affinities to each other[214-216], yet are produced in a very different manner. EDN1 is constitutively expressed in low amounts in the endothelial cells of the vasculature and is necessary for maintaining cardiovascular tonicity, while EDN2 appears to be produced in higher amounts but is temporally and transcriptionally limited[208,217]. Endothelin receptors are found in a wide range of cells throughout the body, but are classically best characterized as present on smooth muscle cells about the vasculature to receive signaling from endothelial cells via EDN1 to cause arteriolar contraction.

The genes encoding endothelins are specific to vertebrates[218], although ciliates and cnidarians have demonstrated chemotactic behavior[219] and muscle contractions[220], respectively, in response to EDN1. Endothelin ligands have gone through two or three rounds of genomic duplication and subsequent evolution to arrive in their present distribution. Vertebrate ancestors possessed only a single endothelin gene (*edn1*) that underwent two rounds of duplication prior to the common teleost fish ancestor; therefore, at one point in evolutionary history, four endothelins were present, EDN1, EDN2, EDN3, and EDN4. This is true today in cartilaginous fishes, the spotted gar, and the coelacanth[218]. An additional duplication of *Edn2* and *Edn3* has also occurred in some fish, such as the zebrafish (*Danio rerio*), so that these animals actually have six endothelin ligands. In tetrapods, in addition to not having this final duplication, the *Edn4* gene was lost. Thus, to the best of present knowledge, all mammals, birds, amphibians, and reptiles possess *Edn1*, *Edn2*, and *Edn3*, but not *Edn4* or any duplications of any other endothelin ligand gene[218,221]. However, these genes are individually very important, as a rodent model of global *Edn1* loss is embryonically lethal[222], *Edn2* loss is lethal after birth and prior to reproductive age owing to starvation[223], and *Edn3* loss results in postnatal lethal aganglionic megacolon with white spotting as a result of abnormal neural crest cell migration[224,225]. A homologous phenotype is also seen in lethal white foal syndrome.

Endothelin receptors are similarly found in all chordates[218]. By examining approximately 30 different species' genomes, Braasch *et al.* (2014)[221] showed that early jawless vertebrates possessed only one endothelin receptor gene similar to *Ednra*. However, early bony vertebrates such as sharks possess three different endothelin receptor genes, which correlate to two early genomic duplication events[218]. Thus *Ednrb* arose from a duplication of *Ednra*, and *Ednrb2* (which is not present in mammals) also arose from a similar duplication. Within telost fish, additional genomic duplications have occurred and many fish such as the Japanese and European eels, which were both recently genomically sequenced, possess six different endothelin receptor genes[226]. More commonly known species, such as zebra fish, had ancestors that lost both copies of the *Ednrb2* gene prior to a duplication event, and now possess four endothelin receptor genes, *Ednra*, *Ednrb*, and their duplicates, but not *Ednrb2*[221]. During the evolution from fish to land dwelling animals, no duplications or gene loss events occurred, such that amphibians, sauropsidans (turtles, lizards, snakes, dinosaurs / birds), and monotremes (playtpi) each have an *Ednra*, an *Ednrb*, and an *Ednrb2* gene[221]. However, therian mammals (placentals and marsupials) lost the *Ednrb2* gene,

and at present the receptors EDNRA and EDNRB are only commonly considered in contemporary biomedical research[221]. The function of the additional ligands and receptors in other vertebrate species remains largely unexplored, excepting the defined role of EDN1 as a potent vasoconstrictor produced by the endothelial cells in many species. Global loss of *Ednra* is lethal owing to cardiac and cranial malformations[227], while global loss of *Ednrb* is similar to global loss of *Edn3* resulting in postnatal lethality by colonic aganglionosis with white spotting[224]. Overall, in understanding the roles for endothelin expression, knowledge of endothelin evolution may be a useful framework for evaluating highly conserved roles.

In mammals, demonstrated largely via rodent studies, endothelin receptor A (EDNRA, also ET_A, ETa) is highly expressed in vascular smooth muscle cells. There it exerts its effects through coupling to $G_{q/11}$ proteins and $G_{12/13}$ proteins (Figure 2.6A). The $G_{q/11}$ pathway, which stimulates phospholipase C-beta to induce inositol (PI_3) production resulting in opening of store-operated calcium channels and receptor-operated calcium channels (SOCCs and ROCCs), as well as the $G_{12/13}$ pathway, which induces the Rho-kinase (ROCK) pathway and phosphorylation of myosin phosphatase, each result in vasoconstriction through phosphorylation of calcium-dependent myosin light chain kinase and phosphorylation of myosin phosphatase. Summarily, EDNRA induces an increase in intracellular calcium concentration that induces vasoconstriction and cell proliferation through store-operated and receptor operated calcium channels[208].

Endothelin receptor B (EDNRB, ET_B, ETb) generally has the opposite actions of EDNRA and is believed to act as a mediator for endothelin ligand clearance and EDNRA attenuation by release of vasoconstrictors. Release of the G-protein heterotrimer by ligand binding to EDNRB similarly results in an increase in intracellular calcium via phospholipase C-beta (Figure 2.6B), but this instead activates calcium-dependent nitric oxide (NO) synthase (eNOS) and calcium-dependent prostaglandin endoperoxide synthase (*Ptgs2*, also *Cox-2*) expression in the vasculature. NO acts directly as a vasodilator and PTGS2 synthesizes prostaglandins that then act as vasodilators. EDNRB binding and heterotrimer release further stimulate NO production via Akt (a serine/threonine kinase) signaling. Also, after ligand binding, EDNRB is trafficked via endocytosis to the endosome for degradation, thus clearing endothelin ligands from circulation[208]. Thus EDNRB acts in an opposite manner from EDNRA to cause calcium-dependent vasodilation and increased NO and prostaglandin synthesis.

Calcium-dependent signaling is important for nearly every cell and triggers a variety of intracellular processes depending on the tissue type. SOCC and ROCC activation in smooth muscle cells are each triggered by phospholipase C-beta activation via EDNRA and EDNRB to cause secondary inositol (IP_3) signaling. IP_3-mediated calcium release, either by SOCC or ROCC activation, occurs through specific transient receptor potential-canonical (TRPC) channels (Figure 2.6C). In cells receiving endothelin signaling, it is known that TRPC1, TRPC3, TRPC6, and TRPC7 are active to induce calcium-mediated signaling; all of these studies were performed on smooth muscle cells or cardiomyocytes. Interestingly, TRPC1, TRPC3, and TRP6 are also activated by alpha-adrenergic receptors, angiotensin receptors, and purinergic receptors[208]. Together, these data imply that endothelin receptor signaling is similar to multiple other forms of membrane receptor signaling, and instead it is the cell type that dictates the action of endothelin ligand binding. This is classically seen where EDNRB clears endothelin ligand from circulation in endothelial cells, while EDNRA induces contraction through a similar signaling pathway.

Therefore, to understand the role of endothelins in the ovary, and EDN2 in particular, it is necessary to understand the location of each receptor type. This is complicated by the lack of available antibodies to localize receptors in mouse models. However, immunohistochemistry using anti-human endothelin receptor antibodies has successfully demonstrated where in the ovary EDNRA and EDNRB are located[14], which has also been confirmed by northern blotting and *in situ* hybridization in the rat[228,229]. In the human ovary, in women undergoing gonadotropin stimulation for IVF owing to male factors or oviduct complications, EDRNA is localized to the smooth muscle cells of the theca externa, the theca interna, and the granulosa cells, while EDNRB is confined to the theca interna[14]. The localization of ovarian receptor expression, and a basic background of the endothelin system, are useful for interpreting the results of previous investigations into the role of EDN2 in the ovary.

Previous study of endothelin-2 in ovulation

Findings from past investigations clearly indicate that EDN2 plays a role in oocyte release, and may act as a direct trigger in follicle rupture[6] by causing contraction of the myoid cells of the theca externa. This has been studied in both rodents and humans[14]. It is well agreed that EDN2 is produced by granulosa cells during ovulation, specifically from hCG11 – hCG12 hours[7]. EDN2 accumulates in follicular fluid[230-232] where it is in direct contact with granulosa cells, though it is debated if EDN2 may influence other target cells such as the theca interna, theca externa, or vascular tissues. The mechanism of EDN2 to enhance follicular rupture during ovulation has not yet been determined. Pharmacological treatment with an endothelin dual-receptor antagonist drug also results in fewer oocytes released when injection occurs just prior ovulation in rodent models[6]. Work by Ko *et al.* (2006) shows that EDN2 induces contraction in strips of ovarian tissue *ex vivo*. This phenomenon also occurs when ovarian tissues are treated *ex vivo* with other vasoconstrictive agents such as norepinephrine[66], or even with depolarizing agents such as potassium chloride. Using drugs that are more or less specific for antagonization of one endothelin receptor, several studies have suggested that EDNRA is responsible for ovarian contraction. However, pharmacology studies are imperfect in that nearly all 'specific' drugs have some binding affinity for related receptors and can activate or block both at high concentrations. The original data by Palanisamy *et al.* (2006) oppositely suggest that EDN2 acts through EDNRB[7], based on immunohistochemical localization of EDNRB coupled with receptor-specific antagonization thereof. This study by Palanisamy *et al.* utilized JKC-301 (10mg/kg) to inhibit EDNRA and BQ788 (10mg/kg) to inhibit EDNRB (n=4), and, though the study concluded that BQ788 inhibited ovulation, the data reveal a decrease in ovulation from either treatment when drugs were given at hCG6 hours.

To determine which endothelin receptor is involved in endothelin signaling during ovulation, recent work by Bridges *et al*. (2010) examined the effect of EDNRA antagonization by BQ123 (10mg/kg) versus EDNRB antagonization by BQ788 (10mg/kg) in the rat ovary (n=5-7) and the mouse ovary (n=4-5), and instead found that neither antagonist at these concentrations, the same used by Palanisamy *et al*., or when directly injected into the ovary, had any effect on the number of oocytes ovulated[170]. However, BQ123 did significantly decrease ovarian contraction *ex vivo*. These data suggest that contraction at least occurs through EDNRA, but effect on follicle rupture remains inconclusive.

In contrast to pharmacological agent injection, a proposed 'cleaner' approach to studying ligand-receptor interaction utilizes transgenic mice which may lose a specific receptor throughout the whole body or in a particular tissue via the Cre/LoxP system. To overcome issues using global endothelin receptor knockout mice, which have lethal mutations, an EDNRB-rescued mouse line was created where EDNRB is only present in adrenergic cells (ovarian loss confirmed by RT-PCR)[233]. These mice were reported to give birth to larger litters than normal, although the average litter size of 7-8 pups in the EDNRB-rescued mice is not different from the reported litter size in C57BL/6 mice on which they were generated. The control group in that specific 2012 study, surprisingly, gave birth to only an average of 5-6 pups. A low but consistent number of pups born to controls may indicate a confounding issue in the study, such as animal husbandry, mouse obesity, or poor neonatal nursing, or loss of EDNRB may indeed cause hyperfecundity. This work by Cho *et al.* (2012) did not examine the number of oocytes ovulated, but instead used the number and size of corpora lutea as a proxy for ovulations that had occurred. The number of corpora lutea (CL) were greater in rescued mice; however, ovaries were collected at 10-11 weeks of age[233], and as CL persist for multiple rounds of ovulation, this number may instead be indicative of earlier onset of puberty or longer CL lifespan. The former may be particularly likely if the 'treatment' group of mice were from a different litter than controls. Data from the same author in a poster presentation the previous year indicate that dual endothelin receptor antagonism does prolong CL lifespan, though these data were never published in a peer-reviewed journal. Thus, counting CL may be taken as a proxy for the ability ovulate, but it should be done with caution and consideration to the respect of the animals' age in the study. Overall, these data suggest that EDNRA, and not EDNRB (as knockout animals are normally or hyper-fertile), has a direct influence on ovulation, and particularly on ovarian contraction. This matches well with literature from other tissues, which suggest EDNRA is the primary mediator of endothelin ligand effects, while EDNRB acts to clear endothelins over time and has directly opposing effects to EDNRA, at least in the vasculature[200,233]. Further, this study suggests that EDN2, or its receptors, may influence the number of CL or their lifespan. The particular cell types involved in ovarian-EDN2 interaction remain unknown, as EDNRA is present in the theca cells, the granulosa cells, and the vascular smooth muscle cells[14].

The physiological actions of EDN2 in the ovary remain up for debate. Although studies performed *ex vivo* suggest EDNRA mediates contraction to cause rupture, further confirmation of this hypothesis is yet needed. In the hope of examining the role EDN2 on a whole-body level, a

global *Edn2* knockout mouse (Edn2KO) was created and extensively characterized by Chang *et al.* (2013)[223]. This mouse was generated by inserting a neomycin cassette into exon 2 (Figure 2.7A), the exon containing the active EDN2 protein sequence. Their work concluded that EDN2 is necessary for thermoregulation, to prevent emphysema, and to prevent starvation; mice with the neomycin cassette insertion expired at 24 days of age on average[223]. These mice were smaller with smaller reproductive tracts and ovaries (Figure 2.7B,C). As normal mice respond to gonadotropins by 22 days of age, the effect of global EDN2 ablation on ovulation was examined using these mice as a loss of function model[171].

In a study by Cacioppo *et al*. (2014), ovaries collected from five to seven week old Edn2KO mice and Edn2+/- littermates (n=5) were serially sectioned and stained. All ovaries contained follicles of various stages, but no CL were seen in the Edn2KO ovaries[171] (Figure 2.7D). Some Edn2KO ovaries had prominent congested blood vessels. Importantly, when Edn2KO mice were superovulated and oocytes were collected at hCG16 or hCG24 hours, Edn2KO mice did not ovulate more than one oocyte in three of four superovulation trials. This supports previous findings that EDN2 is necessary for oocyte release. Two Edn2KO mice did ovulate in this study, but no structurally identifiable CL were found in the ovaries. Instead, ovaries contained multiple large follicles. Some of these did not contain oocytes, and all failed to stain for P450scc, αSMA, or CD31[171], and lacked consistent signs of angiogenesis and luteinization[234-237]. Lack of functional CL formation was further confirmed by significantly lower circulating progesterone levels in Edn2KO mice (5.1 ng/ml in WT *vs* 1.2 ng/ml). Replacement of EDN2 peptide into periovulatory Edn2KO ovaries was tested by giving a single injection of 20pmols of EDN2 peptide in 4uL PBS into one ovary of WT and Edn2KO mice at hCG11 hours. Mice were sacrificed at hCG16 hours (Figure 2.7E). Although no significant differences were observed, all Edn2KO ovaries (n=3) that received EDN2 supplementation ovulated whereas only one vehicle injected ovary did (avg 8.3 vs 2.0, p=0.127)[171]. Use of injection technique was also demonstrated to decrease the number of oocytes ovulated in WT mice, additionally suggesting that this trend could represent restoration of ovulation by *in vivo* EDN2 injection. Overall, this study demonstrated that Edn2KO mice have major ovulatory defects in regard to oocyte release and CL formation.

If findings in Edn2KO mice result from ovarian genetic defects alone and not the overall unhealthiness of the model, then pharmacological endothelin receptor antagonism should cause similar defects in CL formation in WT mice, if antagonization occurs after ovulation and before

CL formation is complete[6]. In unpublished data by Cho *et al.* (2012), the antagonist drug tezosentan was injected into 24 day old mice every two hours from hCG12 to hCG22 hours (5 mg/kg body weight). Injections were given at 2 hour intervals to maintain the antagonism throughout the early phase of CL formation, as the half-life of tezosentan is about 2 hours *in vivo*[238-240]. Mice lacking oocytes in their oviducts were determined to have not ovulated and their ovarian tissue was not considered in subsequent analyses. In mice that ovulated, 5/5 failed to form CL and instead had large follicles present. Therefore, these initial data suggest that EDN2 may play a role in CL formation as well as follicle rupture, though global receptor effects must be considered.

The time of *Edn2* expression coincides with both ovulation of mature follicles and the initial transformation process to form CL[241,242]. CL formation and ovulation are intimately coupled events, and it is rare that one occurs without the other, though this does happen in global progesterone receptor knockout mice after gonadotropin stimulation[7,243,244]. In the newly forming CL, an extensive capillary network serves as a supply route for oxygen and steroid hormones precursors, as well as a route for secreting progesterone in preparation for potential implantation and pregnancy maintenance[83,84]. Vascular endothelial growth factor (VEGF) plays a central role in CL angiogenesis by activating endothelial cells and causing proliferation[88,8985,86]. It is also well established that hypoxia plays a critical role in inducing VEGF in luteinizing granulosa cells[90], and therefore in angiogenesis[245]. Klipper *et al.* (2010) recently showed that EDN2 also directly induces VEGF in granulosa cells of the bovine ovary[246]. It is noteworthy that a hypoxia inducing factor-1 (HIF-1) binding sequence in the proximal promoter region of the *Edn2* gene is involved in the induction of *Edn2* expression under hypoxic conditions based on luciferase assay[247]. It is possible that the hypoxic effect on VEGF expression and angiogenesis, and therefore CL formation, is achieved by *Edn2* induction via HIF-1. Multiple sources indicate HIFs as upregulating *Edn2* expression[246,248-253] and being involved in CL formation[90,245,246,254].

Angiogenesis in CL formation continues after VEGF induction with MMP-mediated dissolution of the BM, sprouting of new vessels with proliferating endothelial cells, and eventual vessel anastomosis that is mediated by macrophages[91]. MMP-2 and MMP-9 are known to be significantly elevated in malignant ovarian tumors[255], and at the time of ovulation and luteal formation MMP-2 is elevated in the rat[256-259], while MMP-9 is elevated during ovulation in the mouse[97,244]. Though both MMP-2 and MMP-9 are known to be important collagenases for dissolution of the follicle wall, they are likely involved in CL formation as well. TIMPs are highly

expressed in the ovary after the LH surge[92-96]. In particular, TIMP-1 mRNA is upregulated 10-fold after the LH surge[260], is released in large quantities during ovulation from the granulosa cells and subsequent lutein cells [97-99], and is highly produced in the growing CL[97]. EDN2 may furthermore antagonize TIMP-1 expression as well, as excessive TIMP-1 is associated with fewer CL, zygotes, and follicles[261,262]. Importantly, Rattner *et al*. (2013) recently demonstrated that EDN2 in the retina activates endothelial cells into tip cells, which are normally present in the growing vascular plexus[263]. EDN2 acts there through EDNRA, and local elimination of EDNRB sensitizes the tissue to the effects EDN2. Together, it is possible that EDN2 may influence vascular formation just after ovulation in the CL, which has been otherwise untested. However, EDN1 is thought to act as a luteolytic, and given their similar receptor affinity, it would be hypothesized that EDN2 would have similar action[264-266]. Thus the potential influence of EDN2 on CL formation and vascularity remains an area of speculation and contention[200].

Although Edn2KO mice generated by Chang *et al.* have been used to analyze the role of EDN2 in ovulation and CL formation, poor systemic health as a confounding factor makes these an undesirable model, and this mouse line is no longer available. Nutritional deficiencies can compromise all aspects of the reproductive axis, including gonadotropin responsiveness[267]. Thus, use of a global Edn2KO mouse model alone is insufficient to explore the effects EDN2 on ovulation, and newer molecular and transgenic tools are required to further investigate EDN2.

In summary regarding EDN2 in the ovary, it has been observed and established that *Edn2* is expressed in a two hour window just prior to ovulation in the granulosa cells of Graafian follicles of mice and rats, and at a related time in cows and humans. Endothelin receptors, A and B, normally mediate EDN2 action; without EDN2, follicle rupture and CL formation are impaired. Dual endothelin receptor antagonization with tezosentan results in similar ovulation and CL formation deficits. EDNRA or EDNRB-specific antagonization has been a topic of debate, but the majority of pharmacological evidence suggest that EDN2 acts via EDNRA to influence ovulation. This is supported most strongly by examination of *Ednrb*-knockout mice, which demonstrate normal fertility and possibly increase fertility as well. EDN2 is a potent vasoconstrictive agent and induces ovarian contraction when administered *ex vivo*, though this can be attenuated by endothelin receptor blockade. EDN2 is thought to act as a localized inducer of contraction in the smooth muscle cells of the ovary to cause follicle rupture after weakening of the follicular wall.

Expression of *Edn2* is thought to be induced by hypoxia and/or progesterone receptor, though the latter is also a topic of debate with a single publication in support and a second against.

These observations raise several key questions: What is the distribution of endothelin-2 in the developing ovary, the mature ovary, the remainder of the reproductive system, and throughout the body, and do these latter data increase understanding of endothelin-2 signaling during ovulation? What is the specific mechanistic role of EDN2 during ovulation? Is it limited to the ovary, to the granulosa cells or the stroma, or does it require signaling in other organs? What is the effect of EDN2 loss only in the ovary? How is EDN2 related to corpus luteum formation? Does EDN2 have an effect on leukocyte invasion? What receptor(s) does EDN2 act through? Where are they located? What signaling cascade is EDN2 downstream of following the LH surge? How is *Edn2* transcription controlled? Is EDN2 signaling necessary for ovulation in normal ovulation in species other than rodents? Though it is not possible to address all portions of these essential inquires, this work aims to generate new knowledge through the testing of disprovable hypotheses focused on the above questions.

The aims of the dissertation

To advance understanding of the roles and mechanism of EDN2 action during ovulation, during corpus luteum formation, and throughout the body in general, as well as to generate novel and innovative transgenic mouse tools that may be widely used for the of endothelins, reproductive signaling, and beyond, the following aims were created and are achieved through this dissertation:

Aim 1: To generate a transgenic mouse to characterize global *Edn2* expression

1a. Construct a transgenic BAC vector and screen Edn2-iCre founder mice for gene transfer

1b. Demonstrate that Cre recombinase mimics *Edn2* expression *in vivo* in gonadotropin-stimulated mice

1c. Characterize *Edn2* expression in adult tissues, previously reported and novel

1d. Characterize *Edn2* expression during development in mouse embryos and pups

Aim 2: To analyze conserved ovarian contraction in response to EDN2 in three domestic vertebrates: the cat, dog, and chicken

2a. Determine if smooth muscle arrangement about mature follicles in the ovary is conserved across species

2b. Investigate the expression patterns of all genes of the endothelin system in the ovary

2c. Quantify and compare ovarian contraction *ex vivo* in response to EDN2 treatment

2d. Determine if ovarian *Edn2* expression occurs naturally during ovulation in the hen

Aim 3: To determine the significance of ovarian *Edn2* expression in ovulation

3a. Generate and characterize a novel estrogen receptor beta (*Esr2*)-iCre knock-in mouse line for the successful ablation of mRNA expression within ovarian granulosa cells

3b. Generate novel whole-ovary and granulosa cell-specific *Edn2*-knockout mice

3c. Characterize ovulatory ability, CL function, and fertility relative to *Edn2* expression

3d. Quantify potential EDN2 downstream transcriptional changes during ovulation

3e. Determine if global adrenergic activation during ovulation can restore normal oocyte release to an EDN2 deficient ovary

Aim 4: To analyze the role of EDNRA in ovarian contractile cells in ovulation

4a. Characterize the effect of myoid cell-specific EDNRA loss on ovulation, corpus luteum formation, and progesterone synthesis

4b. Determine the effect of loss of function of EDNRA on total ovarian contractility in response to EDN2 and an EDNRA antagonist

4c. Quantify ovulatory capacity, corpus luteum formation, and progesterone synthesis in an ovary-specific deletion of *Ednra* from contractile cells

FIGURES

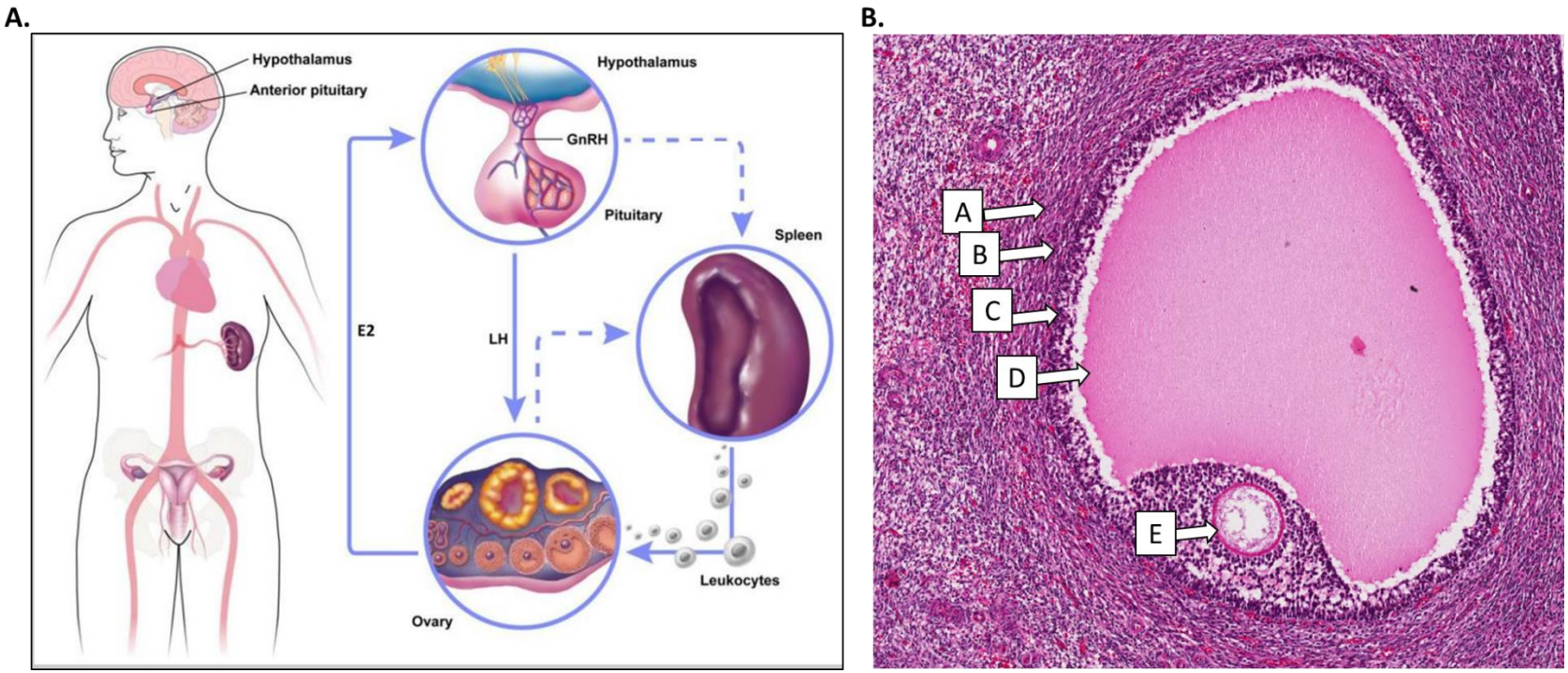

Figure 2.1. The female reproductive axis and the Graafian follicle in ovulation. A. Following follicle growth to the antral stage and the generation of estrogen by granulosa cells, the preovulatory rise of E2 (estradiol) of a critical threshold stimulates release of LH into the bloodstream from the pituitary via increased pulsatile GnRH release from the hypothalamus. Then LH triggers leukocyte release from the spleen into the bloodstream and subsequently into the ovary in response to cytokines and chemokines that act as leukocyte attractants. MMPs and other proteinases weaken the follicular wall making rupture possible; smooth muscle contraction by the ovary may also allow for follicle rupture. Following ovulation, a corpus luteum is formed from luteinized cells and secretes progesterone to maintain pregnancy. CL angiogenesis is dependent upon prolactin, VEGF, MMPs, and leukocytes. **B.** The Graafian follicle just prior to ovulation is composed of A) an outside theca externa layer of contractile cells, B) a layer of theca interna cells producing testosterone, C) a layer of avascular granulosa cells that produce estrogen and respond to progesterone receptor, D) antral fluid, and E) the oocyte itself surrounded by the zona pellucida. This is a cat Graafian follicle with hematoxylin and eosin staining. Image 1A is modified with permission from Oakley *et al*. 2011[58].

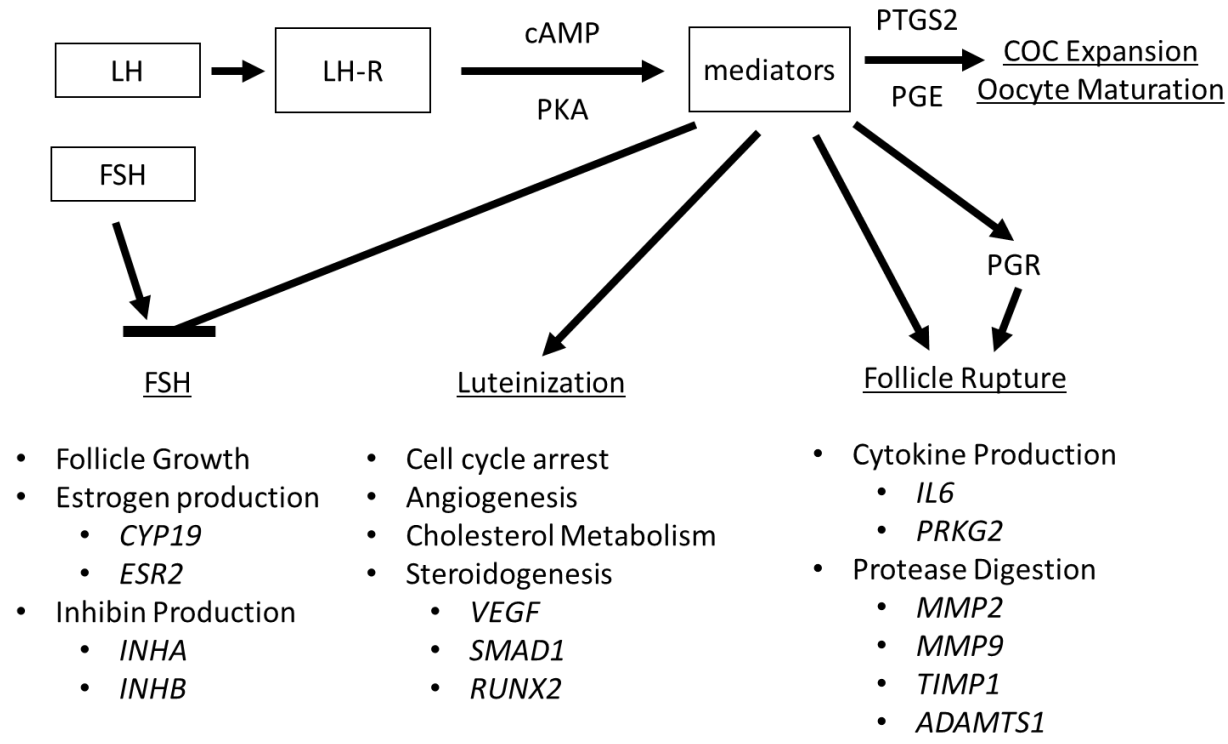

Figure 2.2. Molecular pathways to ovulation, luteinization, and CL formation. LH induces ovulation, COC expansion, oocyte maturation, and luteinization in Graafian follicles. These events are mediated by LH activation of the PKA pathway, which induces the expression of multiple mediators such as EGF-like factors. These mediators in turn activate signaling cascades and specific transcription factors to affect ovulation and luteinization. The specific functions of multiple known mediators in ovulation and luteinization remain to be defined. Additionally, oocyte-derived factors affect cumulus cell and granulosa cell functions in a gradient-dependent manner. PGR is involved downstream of LH-R in follicle rupture. Other events involved in ovulation and selected associated genes are listed. This image is adapted with permission from a review by Dr. JoAnne S. Richards, 2010[67].

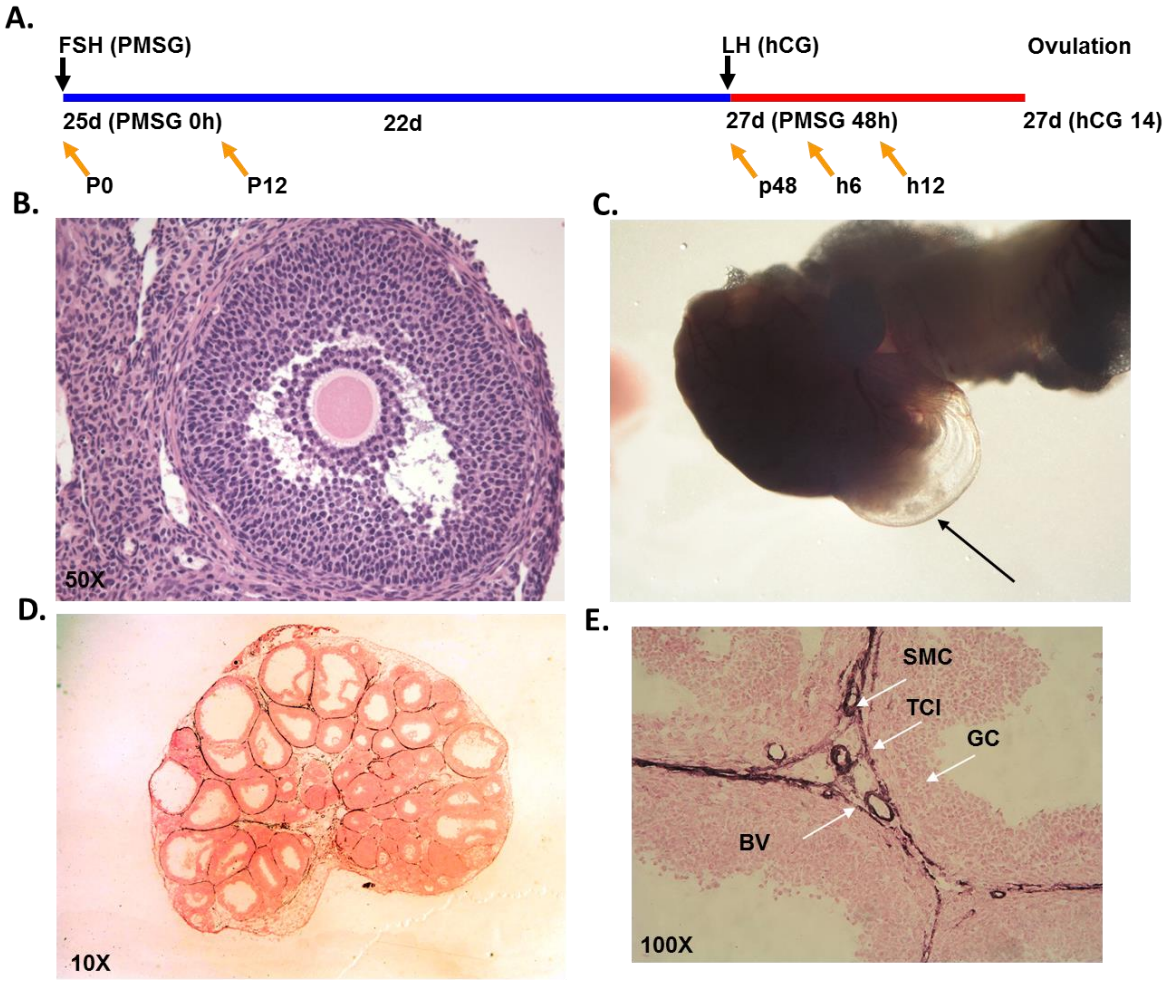

Figure 2.3. Induced mouse ovulation and smooth muscle about Graafian follicles. A. Timeline for gonadotropin injection to induce ovulation at 12-14 hours after hCG injection in 25 day old immature mice. **B.** A murine antral follicle prior to ovulation. **C.** Expansion of the ampulla after ovulation (hCG24 hours); oocytes are indicated by the arrow. **D,E.** Immunohistochemical staining for smooth muscle actin in the rat ovary at low and high magnification. White arrows indicate structures: SMC: Smooth muscle, BV: blood vessel: TCl: theca cell layer; GC: granulosa cells. Figures D and E adapted with permission from Ko *et al.* 2006[6].

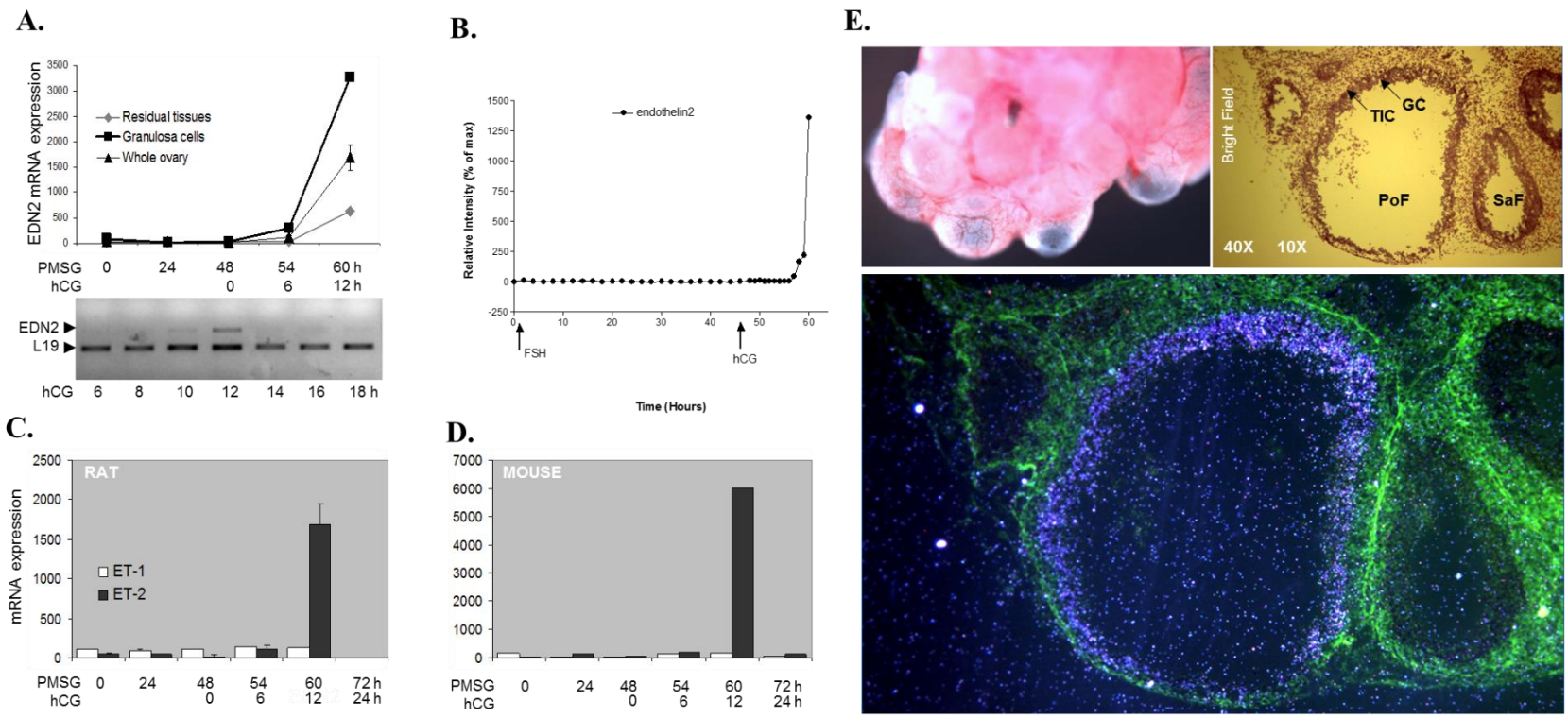

Figure 2.4. *Edn2* mRNA expression in the rat and mouse ovary treated for superovulation. A. *Edn2* mRNA expression in the rat ovary, granulosa cells, and residual tissues after superovulation. This graph was generated by rOGED[199]. The residual ovarian tissues represent mostly theca-interstitial cells. Error bars are difference of two independent experiments. At bottom, an RT-PCR analysis of *Edn2* mRNA expression during the periovulatory period where *Edn2* expression was evident only at hCG 12 hours and *Rpl19* was used as an internal control. **B.** Confirmation of *Edn2* expression in the rat ovary by the Ovarian Kaleidoscope Project[198,268]. **C,D.** Comparison of *Edn2* expression to *Edn1* expression in the rat and mouse (respectively) during and after ovulation. **E.** External view of rat periovulatory follicles at hCG 12 hours, i*n situ* hybridization localization of *Edn2* mRNA in the granulosa cells of Graafian follicles, and confirmatory *Edn2* mRNA localization (*blue*) by brightfield microscopy. No *Edn2* mRNA expression was detected at non-periovulatory stages of follicular development[7]. GC, Granulosa cell layer; TIC, theca-interstitial cells; PoF, periovulatory follicle; SaF, small antral follicle. These data adapted and modified with permission from Ko *et al*. 2006[6].

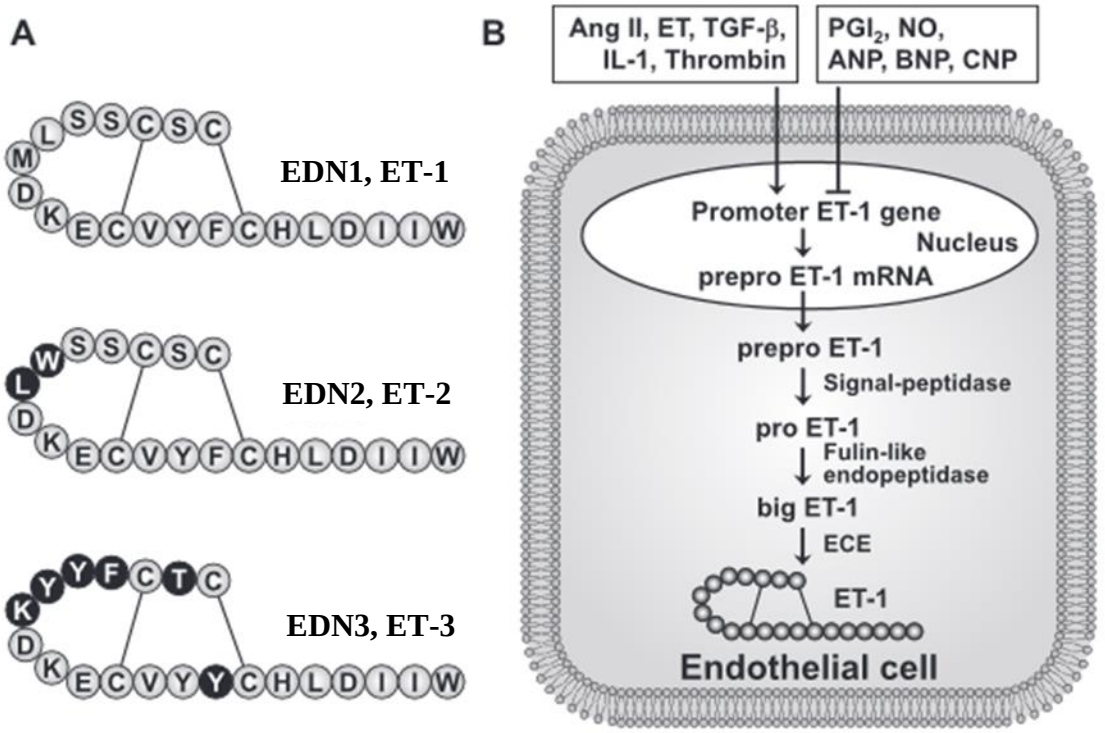

Figure 2.5. Endothelins and their synthesis. A. Amino acid sequences of the three endothelin isoforms where EDN2 and EDN3 differ by 2 and 6 amino acids, respectively, from EDN1, which are indicated by closed circles. **B.** Synthesis and basic regulation of endothelin-1 as a model for endothelins, which are produced first as a prepro form, cleaved to a pro form, then a big form, and final to a 21 amino acid active form by an endothelin converting enzyme (ECE). This figure is adapted and modified with permission from Horinouchi *et al.* 2013[208].

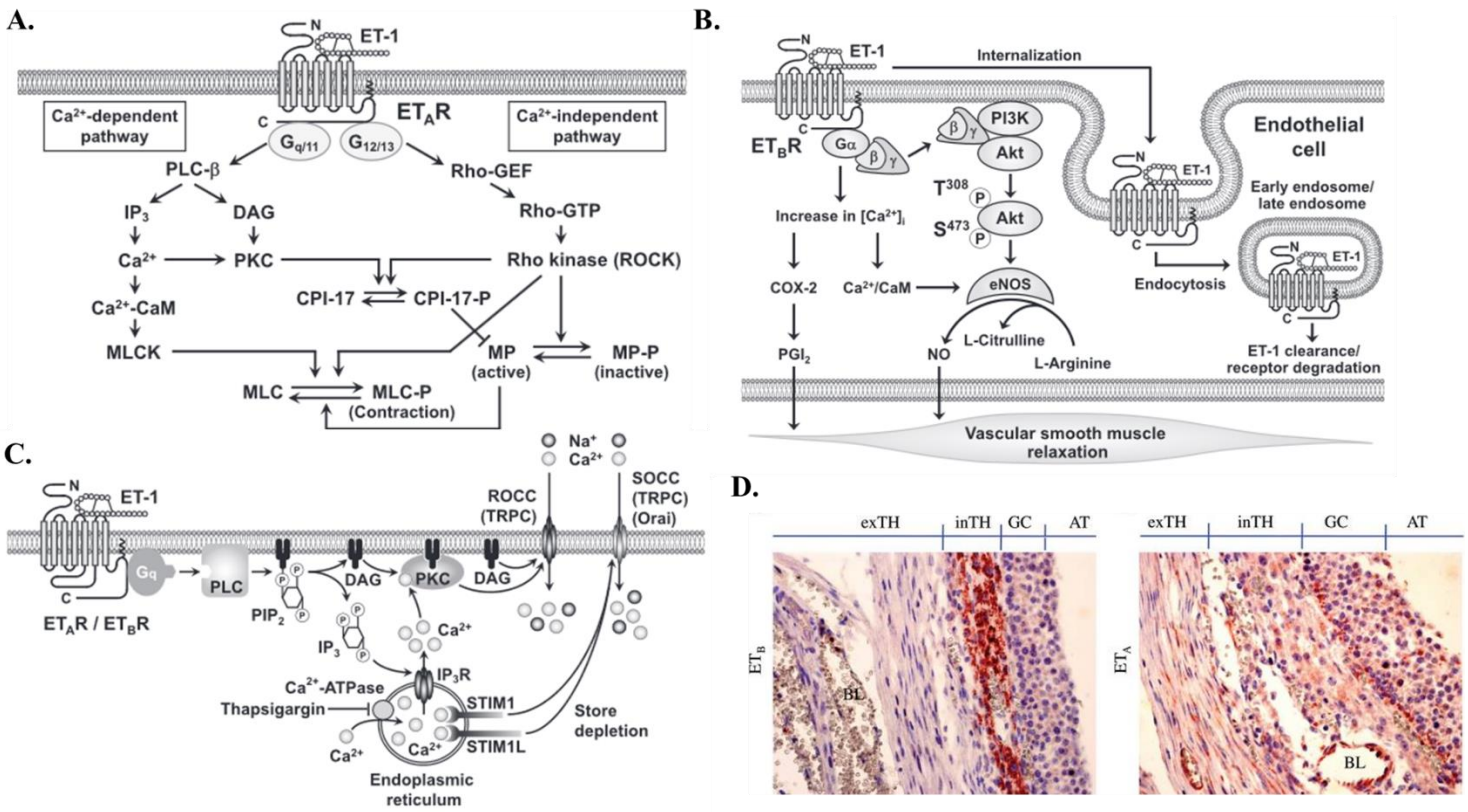

Figure 2.6. Endothelin receptor pathways, signaling mechanism, and localization. A. Stimulation of EDNRA (ET_A) can increase vascular smooth muscle tone via a Gq/G11 protein–mediated, Ca2+- dependent activation of MLCK and via G12/13 protein–mediated, Ca2+-independent inhibition of myosin phosphatase (MLCP) through the Rho kinase pathway. **B.** EDNRB (ET_B) can regulate tone by release of vasodilators, NO and PGI2, and via clearance of EDN2 to prevent EDN2 from excessively stimulating EDNRA expressed in vascular smooth muscle cells. **C.** Molecular mechanisms underlying G protein–coupled receptor-mediated Ca2+ mobilization. **D.** Localization of αSMA, EDNRA, and EDNRB protein in large antral follicle. Note that *Ednrb* expression is specific to theca interna, whereas *Ednra* expression is seen in the GC, theca interna and theca externa where αSMA staining is most intense. PLC-*b*, phospholipase C-*b*; IP3, inositol 1,4,5-trisphosphate; DAG, diacylglycerol; PKC, protein kinase C; CaM, calmodulin; MLCK, myosin light chain kinase; MLC, myosin light chain; MLC-P, phosphorylated MLC; CPI-17, PKC-potentiated inhibitor protein of 17 kDa; CPI-17-P, phosphorylated CPI-17; MP, myosin phosphatase; MP-P, phosphorylated MP; Rho-GEF, Rho-guanine nucleotide exchange factor; Rho-GTP, GTPbound Rho, COX-2, cyclooxygenase-2; PGI2, prostaglandin I2 (prostacyclin); CaM, calmodulin; PI3K, phosphoinositide 3-kinase; eNOS, endothelial nitric oxide synthase; NO, nitric oxide, inTH, theca interna; exTH, theca externa; BL, blood vessel; AT, antrum. These images are reproduced with permission from Choi *et al*. 2011 (A,B,C) and Horinouchi *et al*. 2013 (D).

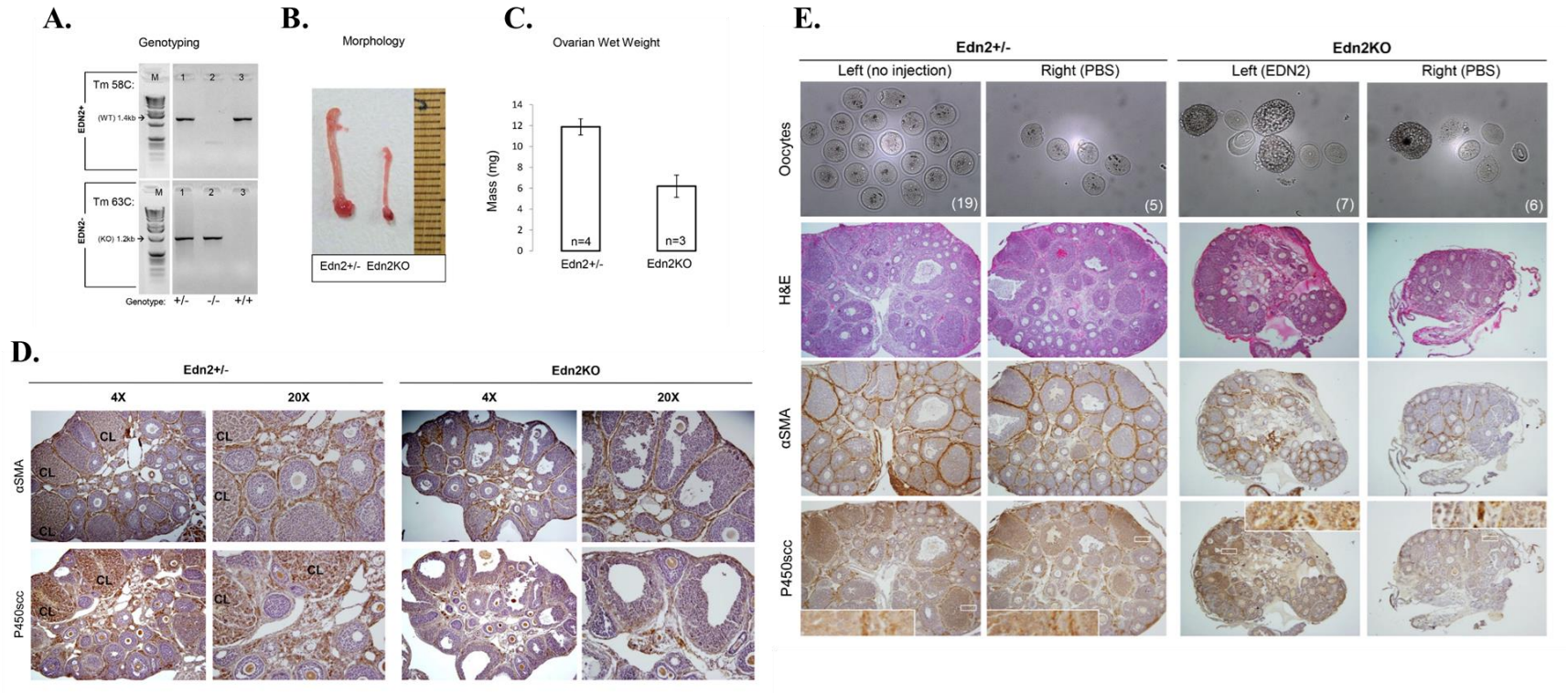

Figure 2.7. Global Edn2KO mice fail to ovulate or form corpora lutea. A. Confirmation of Edn2KO mouse genotype. **B,C.** Edn2KO mice are smaller with smaller reproductive tracts when collected after superovulation treatment. Low n-values result from the majority of mice expiring prior to weaning. **D.** Edn2KO mice fail to form corpora lutea compared to age-matched siblings, but instead have multiple antral/Graafian follicles present. Follicles lack P450scc and SMA staining. E. Replacement with EDN2 allows some Edn2KO mice to ovulate more oocytes and form CL that stain positively for P450scc. These data are reproduced with permission from Cacioppo *et al.* 2014[171].

CHAPTER 3: GENERATION AND CHARACTERIZATION OF AN ENDOTHELIN-2 ICRE MOUSE

Joseph Cacioppo[1], Yongbum Koo[1,2], Po-Ching Patrick Lin[1], Arnon Gal[1], and CheMyong Ko[1]*

[1]Comparative Biosciences, College of Veterinary Medicine, University of Illinois, Urbana-Campaign, IL 61802, USA
[2]School of Biological Sciences, Inje University, Gimhae, South Korea.

*Corresponding author
CheMyong Ko, Ph.D.
Department of Comparative Biosciences
College of Veterinary Medicine
University of Illinois at Urbana-Champaign
3806 VMBSB, MC-002
2001 South Lincoln Avenue
Urbana, IL 61802, USA
217-333-9362 (office), 217-244-1652 (fax)
jayko@illinois.edu

This work was supported by NIH (HD052694 and HD071875 to CK).

Running Title: Edn2-iCre Transgenic Mouse Model
Key Words: Endothelin-2, Cre recombinase, Transgenic, Ovary, BAC Clone

The work presented in this chapter has been published and is modified here with permission from the author:
Genesis. 2015. 53(2): 245-256. PMID 25604013.

ABSTRACT

A novel transgenic mouse line that expresses codon-improved Cre recombinase (iCre) under regulation of the endothelin-2 gene (*Edn2*) promoter was developed for the conditional deletion of genes in endothelin-2 lineage cells and for the spatial and temporal localization of endothelin-2 expression. Endothelin-2 (EDN2, ET-2, previously VIC) is a transcriptionally regulated 21 amino acid peptide implicated in vascular homeostasis, and more recently in female reproduction, gastrointestinal function, immunology, and cancer pathogenesis that acts through membrane receptors and G-protein signaling. A cassette (Edn2-iCre) was constructed that contained iCre, a polyadenylation sequence, and a neomycin selection marker in front of the endogenous start codon of the *Edn2* gene in a mouse genome BAC clone. The cassette was introduced into the C57BL/6 genome by pronuclear injection, and two lines of Edn2-iCre positive mice were produced. The Edn2-iCre mice were bred with ROSA26-lacZ and Ai9 reporter mice to visualize areas of functional iCre expression. Strong expression was seen in the periovulatory ovary, stomach and small intestine, and colon. Uniquely, punctate expression in the corneal epithelium, the liver, the lung, the pituitary, the uterus, and the heart is reported. In the embryo, expression is localized in developing hair follicles and the dermis. Therefore, Edn2-iCre mice will serve as a novel line for conditional gene deletion in these tissues.

INTRODUCTION

The endothelin system is made of three 21 amino acid peptides (EDN1, EDN2, EDN3), two receptors (EDNRA and EDNRB), and several activating peptidases including ECE-1 and ECE-2. The system is highly conserved throughout mammals, and within vertebrates as a whole[221]. Though EDN2 (also seen as ET-2, previously vasoactive intestinal contractor VIC) differs from EDN1 by two amino acids and has the same receptor affinities, and differs from EDN3 by six amino acids and has the same affinity to EDNRB, there now exists a substantial body of evidence suggesting that EDN2 acts through unique regulation and synthesis from its familial isoforms[217]. Previously, approaches using Cre/LoxP-mediated recombination have demonstrated the importance of EDN1, EDN3, ENDRA, and EDNRB in mice, though with phenotypes unique from newly generated EDN2 deficient mice. It is now apparent that EDN2 has a unique role within the endothelin system in female reproduction[200], and there is also strong evidence that it is involved in gastrointestinal function[223,269], immune cell function[270], heart failure[271], and various cancers[217]. It has been previously demonstrated that *Edn2* is expressed at low levels in the cerebellum, cerebrum, and lung; that it is more highly expressed in the testes and stomach, and it is particularly highly expressed in the intestines, ovary, and uterus[272,273]. Embryonic expression begins by embryonic day 15 (e15) and persists until at least e17[223,273]. Global loss of *Edn2* is lethal, wherein mice expire around three weeks of age from internal starvation, hypothermia, and emphysema[223] and also exhibit ovulatory defects[171], thus demonstrating a critical functional role in the brain, lungs, GI tract, and ovary. Although a floxed *Edn2* mouse became recently available to selectively ablate *Edn2*[263], no tool has yet been available to remove genes in those cells with *Edn2* expression. Thus the aim of this project was to generate a novel mouse model that expresses codon-improved Cre recombinase (iCre) driven by the natural promoter for the *Edn2* gene. Two lines of Edn2-iCre mice were produced and the sites of functional iCre expression and, presumably, localization of endogenous *Edn2* expression was determined using two lines of reporter mice: ROSA26-lacZ[175] and Ai9[177].

METHODS

Ethics Statement

This study was carried out in tight accordance with the recommendations in the Guide for the Care and Use of Laboratory Animals of the National Institutes of Health. Animal protocol was approved by the University of Illinois Animal Care and Use Committee (Protocol: 11184), and all efforts were made to minimize animal suffering. Animal models generated in this study will be made readily available to the research community.

Construction of the iCre-polyA-FRT-neo-FRT cassette

E. coli SW105, pL253, pL451, and pICGN21 were obtained from Frederick National Laboratory for Cancer Research (Frederick, MD). An iCre-polyA-FRT-neo-FRT cassette was constructed by cloning the following DNA fragments between HindIII restriction site and AatII restriction site of pGEM7Zf(+) (Promega, Madison, WI): HindIII-EcoR1 fragment (1100 bp) containing the coding region of the codon-improved Cre recombinase (iCre) from pBluescript KS(+)-iCre, EcoRI-KnpI fragment (283 bp) containing SV40 late polyadenylation signal sequence from pCS2+MT, KpnI-SfiI fragment(1500 bp) containing FRT-neo-FRT from pICGN21 and Sfi1/AatII adaptor sequence (5'-CGGCCCTGATCAGTGCTAGCGACGT-3' annealed with 5'-CGCTAGCACTGATCAGGGCCGCCT-3').

Insertion of iCre-polyA-FRT-neo-FRT cassette into the Edn2 BAC clone

The iCre-pA-FRT-neo-FRT cassette was inserted into exon 1 of the *Edn2* gene of the BAC clone (ID RP23-98J9) that was purchased from Invitrogen (Carlsbad, CA). Recombineering was performed according to protocols provided by Frederick National Laboratory for Cancer Research[274-276]. Briefly, the iCre-polyA-FRT-neo-FRT cassette was inserted in front of the ATG initiation codon in the BAC plasmid[277]. A homology arm (upstream from ATG) was amplified using primer pairs (5'-ACGCGTTCCTGAAGGTGTTGCAGAGAA-3', 5'-AAGCTTAGCAGCAGCGGCAGAGTG-3') and cloned between the Mlu1 site and the HindIII site upstream of iCre-polyA-FRT-neo-FRT cassette. Another homology arm downstream from ATG was amplified using primer pairs (5'-GGCCGAGGCGGCCATGGTCTCCGCCTGGTGTT-3', 5'-GACGTCCCTTGGTGTTCAGGAACCAC-3') and cloned the between SfiI site and the

AatII site after the cassette. The cassette with the two homologies was cut with MluI and AatII and gel purified. Approximately 15ng of the gel-purified cassette was electroporated into red-induced E.coli SW105 carrying the BAC clone. The recombinants were selected on LB agar plates supplemented with kanamycin (25 mg/ml). The selected bacterial cells were then treated with arabinose (0.1%) for one hour to delete FRT-neo-FRT from the BAC. The recombinant BAC plasmid purification, plasmid integrity test, and pronuclear microinjection were performed at the Transgenic Animal Model Core of University of Michigan. Fertilized eggs from C57BL/6 mice were microinjected with the BAC plasmid and implanted into pseudopregnant foster mothers (C57BL/6). Genomic DNA was extracted from the tails of 69 offspring from the pseudopregnant mothers. The presence of iCre was determined by PCR using the following primer pairs: Cre-F (5′-TCTGATGAAGTCAGGAAGAACC-3′) and Cre-R (5′-GAGATGTCCTTCACTCTGAATC-3′)[278].

RT-PCR

Of those offspring that had correct construct insertions, founder lines #9 and #12 were used for further evaluation for ovarian *Edn2* expression. It is known *Edn2* is induced during ovulation; thus female 28-day old pre-pubertal Edn2-iCre mice of these lines and control WT mice were injected in the intra-peritoneal cavity with 5 IU of pregnant mare serum gonadotropin (PMSG) at 25 days old to induce follicle development, and then 48 h later with 5 IU of human chorionic gonadotropin (hCG) to induce ovulation. Mice ovulate 12-14 hours after hCG injection, and ovaries were collected at 0, 6, 12, 16, and 24 hours after hCG injection (n=5). Animals were euthanized by CO_2 asphyxiation and cervical luxation, ovaries were removed, and homogenized in Trizol solution (Life Technologies, Grand Island, NY) for RNA extraction. RNA was purified with an RNeasy kit (Qiagen, Germantown, MD), and cDNA was generated using a reverse transcription superscript VILO synthesis kit (Invitrogen). For RT-PCR, *iCre* was amplified using the above primer set; *Edn2* was amplified with (5'-CTCCTGGCTTGACAAGGAATG-3') and (5'-GCTGTCTGTCCCGCAGTGTT-3'), and *Rpl19* was amplified as a control housekeeping gene with (5'-CCTGAAGGTCAAAGGGAATGTG-3') and (5'-GTCTGCCTTCAGCTTGTGGAT-3'). PCR products were visualized on an agarose gel; band intensity was analyzed using ImageJ software (NIH, Bethesda, MD) for relative intensity.

Visualization of Transgene Expression

Animals were bred with B6;129S4-*Gt*^{279}*26Sor*^{tm1Sor}/J (ROSA26-lacZ) reporter mice to visualize *Edn2*-expressing tissues by X-gal staining[175]. Mice were euthanized by CO_2 asphyxiation; perfused intracardially with cold PBS solution and then a 4% paraformaldehyde (PFA) solution to assist in fixation. Tissues were then collected and washed 2 times with cold PBS; large and lipid-dense tissues (brain, liver, lungs, heart, stomach, kidney, tubular organs) were cut into sections with a scalpel to allow better fixative penetration. Tissues were placed in 4% PFA on ice for 1 hour. They were then washed twice with PBS and placed into individual vials with X-gal stain solution (Millipore, Billerica, MA), diluted 1:40 according to the manufacturer's instructions. Tissues were incubated in the dark in at 4^{o}C on a shaker for 24-48 hours, washed 3 times with PBS, incubated in the dark at room temperature for 1 hour with X-gal holding solution, and then fixed overnight in 4% PFA at 4C. Embryos were similarly fixed and stained. Gross images of tissues were taken of tissues following this final fixation. Tissues were then dehydrated, embedded in paraffin blocks, and sectioned by microtome at 5um thickness. Background staining was performed with nuclear fast red (Fisher Scientific, Pittsburg, PA) and images were taken with an Olympus BX51 microscope. The Edn2-iCre animals were also bred with B6;129S6-*Gt*^{279}*26Sor*$^{tm9(CAG\text{-}tdTomato)Hze}$/J (Ai9) reporter mice[177]. Gross images were taken immediately after euthanasia under a Zeiss SV11 fluorescent microscope. Tissues were fixed overnight, embedded, and serially sectioned at 5uM; one section was used for fluorescence visualization and an adjacent slide was stained with hematoxylin and eosin (Thermo Scientific, Kalamazoo, MI).

RESULTS AND DISCUSSION

Little is known of the regulation of *Edn2*, both from the transcriptional and peptide conversion perspectives. Although *Edn1* has been shown to be largely transcriptionally regulated through cis-acting promoter elements, and *Edn2* was thought to have similar regulation, it has been shown previously to be regulated by transcription factors such as epidermal growth factor, TNF-α, forskolin, HIF1-α, and pituitary gonadotropins within the reproductive system[7,200]. Hence a strategy that encompassed all potentially involved regulatory DNA regions was mandated to ensure correct mimicry of *Edn2* expression by Cre recombinase.

To this end, a bacterial artificial chromosome (BAC) clone that contained the entire *Edn2* gene and neighboring sequences as the vector for iCre insertion was used (Figure 3.1). A cassette containing iCre, a polyadenylation sequence, and a neomycin selection marker was inserted in front of the ATG start codon of the *Edn2* gene (Figure 3.1). Following removal of the neomycin selection marker by FLP-mediated recombination, the entire 200Kbp vector was inserted into the C57BL/6 genome by pronuclear injection. Sixty-nine pups were produced, of which 12 contained the Edn2-iCre vector in their genome (Figure 3.1). Two of these 12 Edn2-iCre positive mice, Edn2-iCre#9 and Edn2-iCre#12, showed no health issues or major fertility defects and were chosen for follow-up characterization of iCre expression. To validate that iCre expression mimics *Edn2* expression in Edn2-iCre mice, the ovaries were examined from 28 day old mice following gonadotropin stimulation to induce ovulation. Expression of *Edn2* specifically occurs between 11 and 12 hours after hCG injection[6,7], and it was expected iCre expression would be limited to this time frame. Ovaries were examined at 0, 6, 12, 16, and 24 hours after hCG injection for iCre RNA in wild type (WT) mice and the two founder lines of transgenic mice. As expected, both founder lines demonstrated iCre expression only 12 hours after hCG injection concurrent with their own and WT *Edn2* expression (Figure 3.2). The gene *Rpl19*, encoding murine ribosomal 60S protein L19, as chosen as an internal control based on previous publications[280,281]. From these data, it may be concluded that iCre expression mimics *Edn2* temporally in the ovary, and that in addition to removing floxed genes at the times and locations of *Edn2* expression, Edn2-iCre tissues can also be used to localize *Edn2* expression sites.

To typify expression, transgenic mice were crossed with ROSA26-lacZ reporter mice, which express β-galactosidase under a universal promoter with a floxed stop codon[175]. Both founder lines demonstrated similar staining patterns with X-gal. Of these, Edn2-iCre#9 was further

characterized for localization of *Edn2* expression. This line was chosen because it provided an average number of healthy pups per litter for C57BL/6 mice, approximately eight, while line Edn2-iCre#12 averaged only four pups per litter. All results described below, using either reporter mouse, are from this single founder line; other lines were euthanized and frozen sperm was stored for potential restoration of the line if necessary. Of note, positive staining marks cells that are expressing or have expressed *Edn2*, or are descended from cells that have expressed *Edn2*. No phenotypes are associated with homozygosity for the transgene insertion in these animals.

Pregnant mice were sacrificed and embryos of varying days of development were analyzed by X-gal staining. Positive staining was not present prior to day e12.5 (Figure 3.3), though placental tissue stained positively past day e8.5 including the umbilicus (data not shown). By day e13.5, faint positive staining was visible in the skin of the embryos; staining was present in a punctate pattern throughout the skin by day e15.5, and was readily apparent in the sinusoid hair follicles of the rostrum (whiskers). This skin staining consistently was present in the outer layer of cells of the developing dermis. Staining was also present on the surface of the digits of fore and hind limbs, the dorsum, and the tail. By day e17.5 near parturition, staining had expanded throughout the skin of the ventrum and was consistently present in the skin surrounding areas of the eye, mouth, and ear openings, and between digits (Figure 3.3). Staining eventually expands throughout the entirety of the skin by puberty. It is interesting to note early staining presence in those areas that must undergo early keratinization for function in neonates[282], though these areas coincide with those of hair follicle development. This timing of expression is consistent with earlier findings that concluded EDN2 is important for normal embryonic development[283,284].

Twenty-eight day old healthy mice were sacrificed and individual organs previously implicated to be involved in EDN2 signaling were stained with X-gal to localize *Edn2* expression. In the majority of the organs examined, staining revealed a punctate pattern (Figure 3.4). Brains demonstrated intense staining around the olfactory bulb, although individual neurons stained positively throughout the cerebrum and cerebellum (cerebellum histology pictured). Heart staining revealed that the majority of the epicardium expressed *Edn2*, though only a few scattered cardiomyocytes and endothelial cells stained positively in a seemingly random arrangement, complimenting previous findings[285,286]. A similar stippled pattern was visualized in the lung throughout the pneumocytes of the parenchyma and the respiratory epithelium. In the kidney, staining was present in only some renal corpuscles and tubules, although staining was limited to

the cortex and not present in the medulla. However, cells expressing iCre in the kidney may become more prevalent during renal stress or disease[287,288]. Interestingly, the entirety of the epidermis stained positively, as well as the cells surrounding the hair follicles and the inner root sheath of the follicles themselves. Beyond hair follicles[289], this is a novel area of EDN2 expression, and presents a potential unique application for future gene removal. In the gastrointestinal tract, cross-sectional staining was limited to individual villi or to individual tubular glands, and was also present in patches on the exterior surface, which may be a reflection of the enteric nervous system as endothelins are known to be involved in neural crest cell migration[290]. Ovarian staining was highly prevalent, present throughout the organ stroma, capsule, and small follicles, in addition to large follicles and corpora lutea as previously reported[6,7]. Punctate staining was present in the epithelium of the oviduct, while individual myofibers of uterine myometrium stained to create a stippled appearance.

X-gal staining may occur as a false positive in adult tissues through endogenous beta-galactosidase activity[176,291], and may additionally create 'edge-effect' artifact staining on any tissue. Although the majority of tissues of interest showed little or no negative staining in mice lacking the Edn2-iCre mutation, false positive staining was present in the gross view of the kidney, GI tract, portions of the uterus, and exterior of the skin (Figure 3.5) though little staining was present histologically. Additional false positive staining was present in the bone, adrenal, tarsal gland, and liver tissue (not pictured), though decreasing incubation temperature significantly reduced gross background x-gal staining. Similarly, control embryos showed no x-gal staining at any age except for slight edge-effect staining of the skin which does also not appear histologically (Figure 3.5).

To verify the sites observed as positive for X-gal staining and to identify other novel sites of *Edn2* expression, Edn2-iCre mice were crossed with Ai9 reporter mice that produce red fluorescent protein in cells with functional iCre expression. Tissues from 28 day old males and females were visualized grossly under fluorescent light during dissection, and histological images were compared with H&E staining (Figure 3.6). Of interest, fluorescence was seen in the anterior and intermediate pituitary, the cornea and photocells of the eye, the detrusor muscle of the bladder, the male coagulation gland (anterior prostate), and the interstitium of the testes. The majority of expression appears in a punctate manner, excluding the epidermis, ovary, testicular interstitium, and coagulation gland. These areas are potential key areas for the utilization of the Edn2-iCre

transgenic mouse outside of localization of *Edn2* expression and removal of potential downstream endothelin target genes. Eye expression is particularly interesting, given recent work by Rattner *et al*. showing that EDN2 can override VEGF signaling to inhibit retinal angiogenesis[263]. Expression of *Edn2* may act in the cornea and retina continually to inhibit angiogenesis, whereas loss of *Edn2* could eventually lead to vascularization and visual impairment. A summary of fluorescence observed grossly and histologically is listed in Table 3.1. No fluorescence was observed in control tissues.

ACKNOWLEDGEMENTS

The authors thank Dr. Lori Raetzman for technical advice on the use of reporter mice, Dr. Jing Yang for the pCS2+M2 plasmid, and Karen Doty and David Ko for histological assistance.

TABLES

Table 3.1. Summary of Edn2-iCre expression in multiple adult organs. Expression determined by localization of red fluorescence after crossing with an Ai9 reporter mouse line. WT tissues were used as controls (no fluorescence observed). Table continued on multiple pages.

Tissue	Relative Fluorescence	Notes	Relevant Previous Literature
Adrenal	+++	Punctate fluorescence throughout adrenal cortex; little to none in medulla	[292]
Aorta	+	Very limited punctate fluorescence in tunica media in smooth muscle cells	[12,293-295]
Bladder	+	Punctate fluorescence in smooth muscle cells of detrusor muscle, not in epithelium	-
Blood (circulating)	-	No fluorescence seen (in all RBC and WBCs observed)	[250,270]
Bone (femur)	-	No fluorescence seen in osteocytes or bone marrow	[296]
Brain	+	Mild fluorescence throughout cortex and cerebellum, extremely limited, 1-2 / 100 neurons. More intense in hypothalamus and optic chiasm. Greatest fluorescence in olfactory bulb.	[297,298]
Coagulation gland (anterior prostate)	+++	Fluorescence seen in all secretory cells	-
Colon	+++	Punctate fluorescence throughout mucosa; cells of mucosa will either all fluoresce or not within one tubular gland (all or none expression by gland); not present in submucosa or muscularis; punctate pattern seen in mesothelial cells of serosa.	[223,299,300]
Duodenum	+++	Fluorescence in groups of epithelial cells of individual villi with punctate expression of some submucosal glands; punctate serosal fluorescence present.	[223,269,301]
Epididymis	±	0-1 cells/100 of epithelial cells in lumen of epididymis	-
Esophagus	-	No fluorescence visualized	-
Eye	+	Punctate / striped fluorescence in most outer cellular layer of corneal epithelium; fluorescence in photocell layer with fluorescence extending through all retinal layers in striped pattern in limited areas of retina approx. 0-1 per section, fluorescence in tarsal gland, no fluorescence in lens or iris	[263,302,303]
Heart	+	Punctate fluorescence in cardiomyocytes (2-5/100) and the majority of epicardial cells	[284-286,304,305]
Ileum	+++	Fluorescence seen in villi similar to duodenum - punctate in groups of cells and often near crypts, fluorescence in individual cells within peyer's patches (1-2/100), fluorescence in serosa cell layer in patches	[223,306,307]

Table 3.1. Continued from previous page.

Jejunum	+++	Punctate fluorescence seen in villi and serosa similar to duodenum, ileum; may not extend entire villi if fluorescence seen in crypt	[223]
Kidney	+	Limited punctate fluorescence in a few individual cells of corpuscle or proximal tubules, entirely limited to cortex	[308-310]
Liver	+	Punctate fluorescence seen in parenchyma, limited to cells appearing stellate	[311]
Lung	+	Moderate punctate fluorescence in respiratory epithelium; limited in alveoli/pneumocytes (0-1/100)	[223,284,312]
Mouth / oral cavity	+	No fluorescence in teeth, present on entirety of gingival surface	-
Nerve (thoracic vagus)	-	No fluorescence visualized	[313]
Ovary	+++	Fluorescence seen encompassing all of ovarian capsule, majority of cells of stroma, corpora lutea, and granulosa cells; not seen in oocytes	[6,7,171,246,284]
Oviduct	+++	Punctate fluorescence pattern in epithelium; more prevalent fluorescence in epithelium of isthmus	[314,315]
Pancreas	+	Seemingly random punctate fluorescence throughout parenchyma, 2-5 cells/100	-
Penis	+	Seen in all cells of transitional epithelium of urethra and in the skin surrounding the prepuce	-
Pituitary	+	Punctate pattern throughout anterior and intermediate pituitary; not present in posterior pituitary	[298]
Preputial gland	+++	Fluorescence seen in the majority of acini in both basal and secretory cells	-
Rostrum	+	Visible in epidermis, in inner layer of dermal root sheath of large sinusoid hair follicles	-
Salivary gland	+	Punctate pattern present through some cells of acini; more prevalent in mucous than serous glands	[316,317]
Seminal vesicle	-	No fluorescence visualized	-
Skeletal muscle	-	No fluorescence visualized	-
Skin	+++	Visible throughout epidermis, extending into hair follicles	[289,318]
Testes	+	Interstitial cells, potentially including Leydig cells; not seen within seminiferous tubules	[319]
Uterus	+	Seen in some smooth muscle cells of the myometrium throughout the uterus in a banded pattern (Figure 3.4)	[320,321]

FIGURES

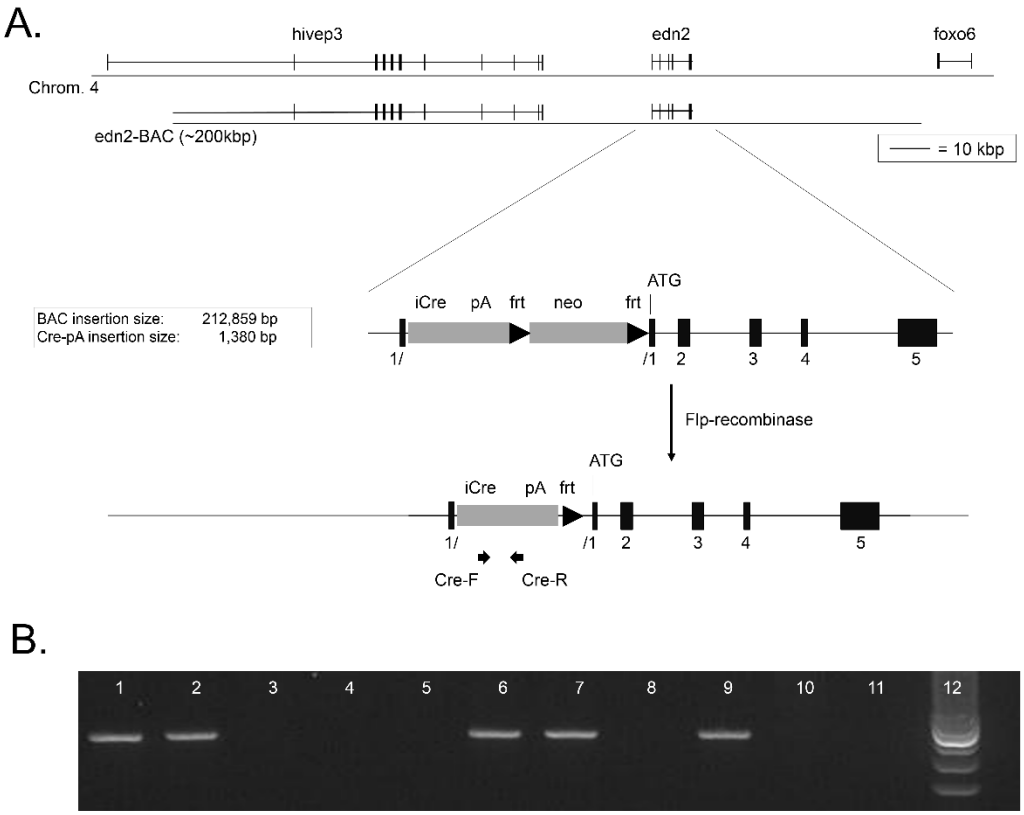

Figure 3.1. Transgenic vector construct and screening of Edn2-iCre transgenic mouse. A. Schematic diagram of a part of chromosome 4 and the Edn2-iCre BAC transgenic vector. *Edn2* and its neighboring genes are shown. Exons are shown in blue boxes. Positions of PCR primers for screening transgenic mice are indicated by horizontal black arrows. The cassette containing the coding region of iCre, SV40 late polyadenylation signal, and frt-neo-frt cassette was inserted in front of ATG of *Edn2* by homologous recombination. The frt-neo-frt cassette was then deleted by Flp recombinase. **B.** Screening of transgenic mice carrying the transgene *iCre* (a representative gel image). The transgene was inserted into the mouse genome by pronuclear injection to C57B/6 blastocysts. Lanes 1-8: founder mouse template genomic DNA (gDNA) from one litter; Lane 9: iCre sequence positive control; Lane 10: WT gDNA negative control; Lane 11: No template DNA negative control; Lane 12: 100bp ladder (Invitrogen).

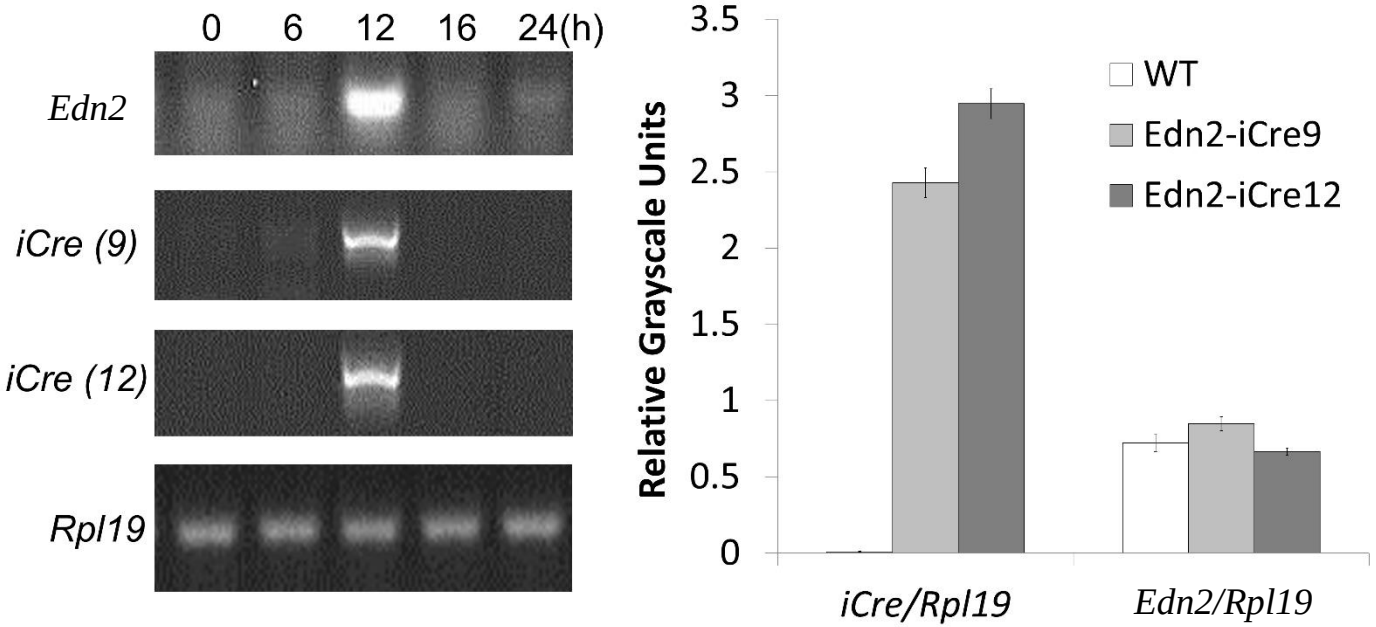

Figure 3.2. Temporal mRNA expression of *Edn2* and *iCre* in the Edn2-iCre mouse ovary. Twenty-five day old Edn2-iCre9 and Edn2-iCre12 mice were injected with PMSG/hCG for superovulation induction. Ovaries were collected at the indicated hours (h) after hCG injection, and mRNA expression levels were measured by semi-quantitative RT-PCR. Shown is a representative image of n=5 mice of each genotype. Note the temporal expression pattern of *Edn2* and *iCre* mRNA. *Rpl19* was used as internal control. Bar graph indicates quantification at 12 hours after hCG administration and was normalized to *Rpl19*. No significant differences were present between groups for *Edn2* expression.

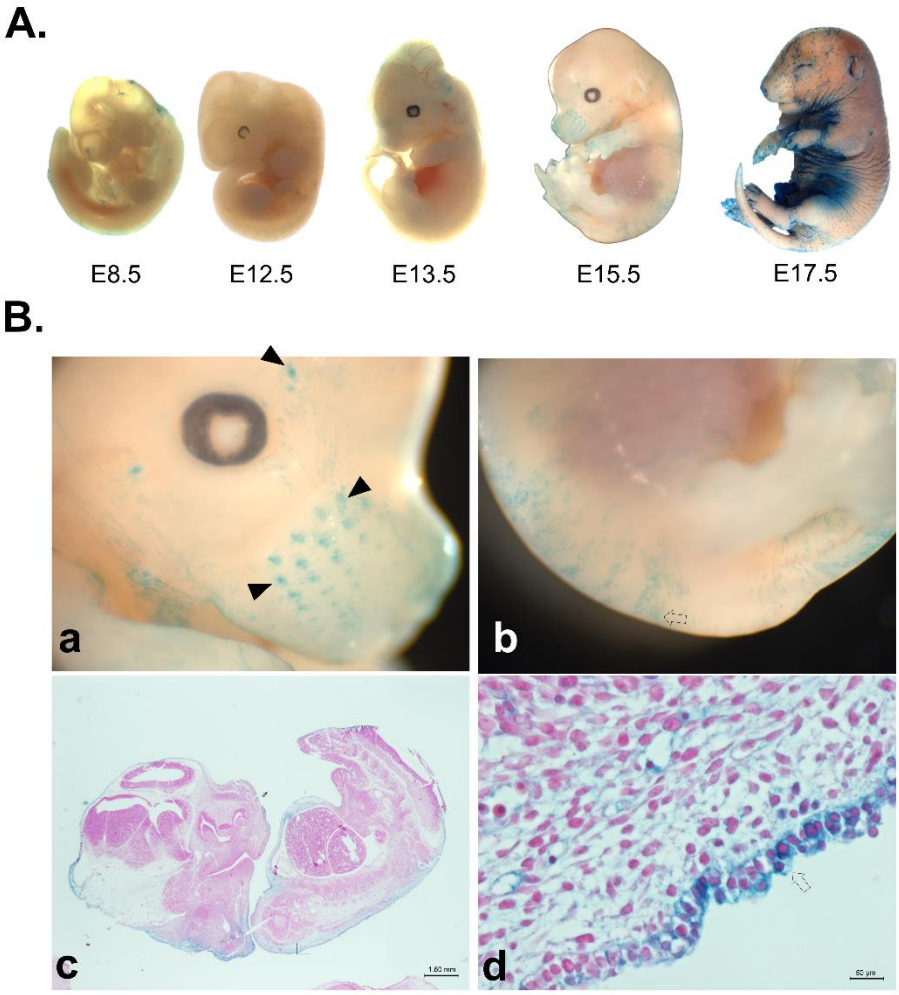

Figure 3.3. X-Gal characterization of Edn2-iCre embryos. A. X-Gal staining detects iCre expression and successful recombination in whole mount embryos of Edn2-iCre mice crossed with ROSA26-lacZ reporter mice. Faint positive staining is consistently observed as early as e12.5 in the skin of the ventrum. It becomes noticeable throughout much of skin in a fragmented pattern by day e15.5. **B.** Higher magnification of dissecting scope images of Edn2-iCre fetuses at approximately embryonic day e15.5 after X-Gal staining. Images show a) rostrum, b) dorsal skin and tail, c) whole-mount histological staining 1.25x, and d) magnified histological staining of skin of embryo 40x. Staining of sinus follicles of rostrum is visible by day e15.5, while wide-spread staining of ventrum begins one to two days later. By day 17.5, staining is also visible at opening of mouth, eyes, and ears, and between digits. Closed arrowheads: sinus hair follicles; open arrows: staining in developing dermis/epidermis.

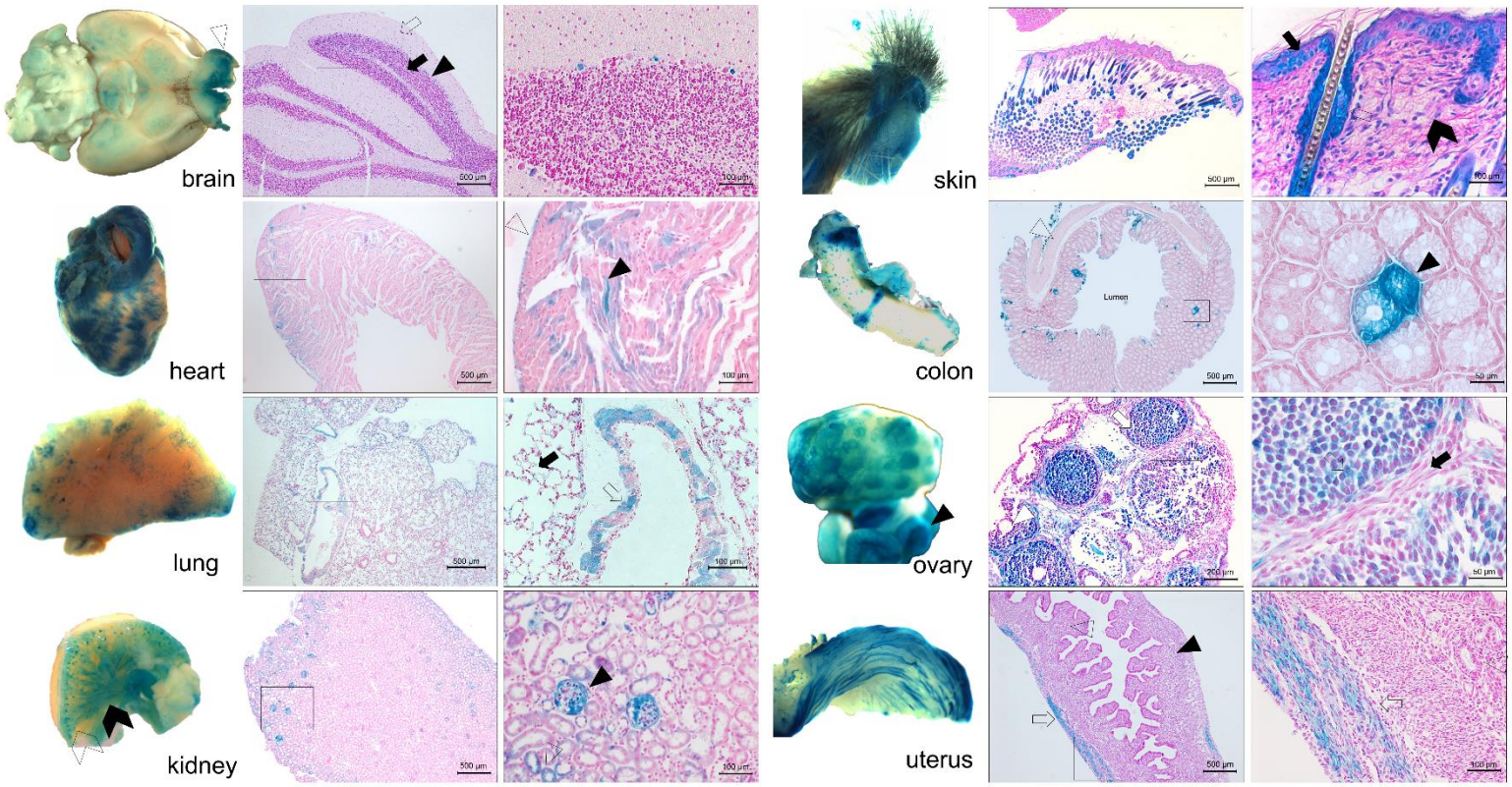

Figure 3.4. Localization of functional iCre expression in adult Edn2-iCre mouse organs. X-Gal staining detects iCre expression and successful recombination in whole organs of Edn2-iCre mice crossed with ROSA26-lacZ reporter mice that have previously been shown to produce EDN2 peptide. Gross images are shown at left and histology images with nuclear fast red background staining are at right. Kidney tissue was bisected, ovary was punctured, and heart and colon were flushed prior to staining. The oviduct is visible in the bottom portion of the gross ovarian image. Symbol labeling is as follows: Brain: open arrowhead: olfactory bulb; open arrow: molecular layer; closed arrow: granule cell layer; solid arrowhead: purkinje cell layer. Heart: open arrowhead: epicardium; closed arrowhead: cardiomyocyte. Lung: solid arrow: pneumocytes of alveoli; open arrow: respiratory epithelium of bronchiole. Kidney: open chevron: cortex; closed chevron: medulla; closed arrowhead: renal corpuscle; open arrowhead: tubules of cortex. Skin: solid arrow: epidermis; open arrow: bulge stem cells; closed chevron: dermis. Colon: open arrowhead: muscularis interna; closed arrowhead: goblet cells of longitudinal mucosal fold. Ovary: closed arrowhead: oviduct; open arrowhead: oocyte of secondary follicle; open arrow: secondary follicle granulosa cells; closed arrow: theca cell layer and stromal cells. Uterus: solid arrowhead: endometrium; open arrowhead: uterine glands; open arrow: smooth muscle cells of myometrium.

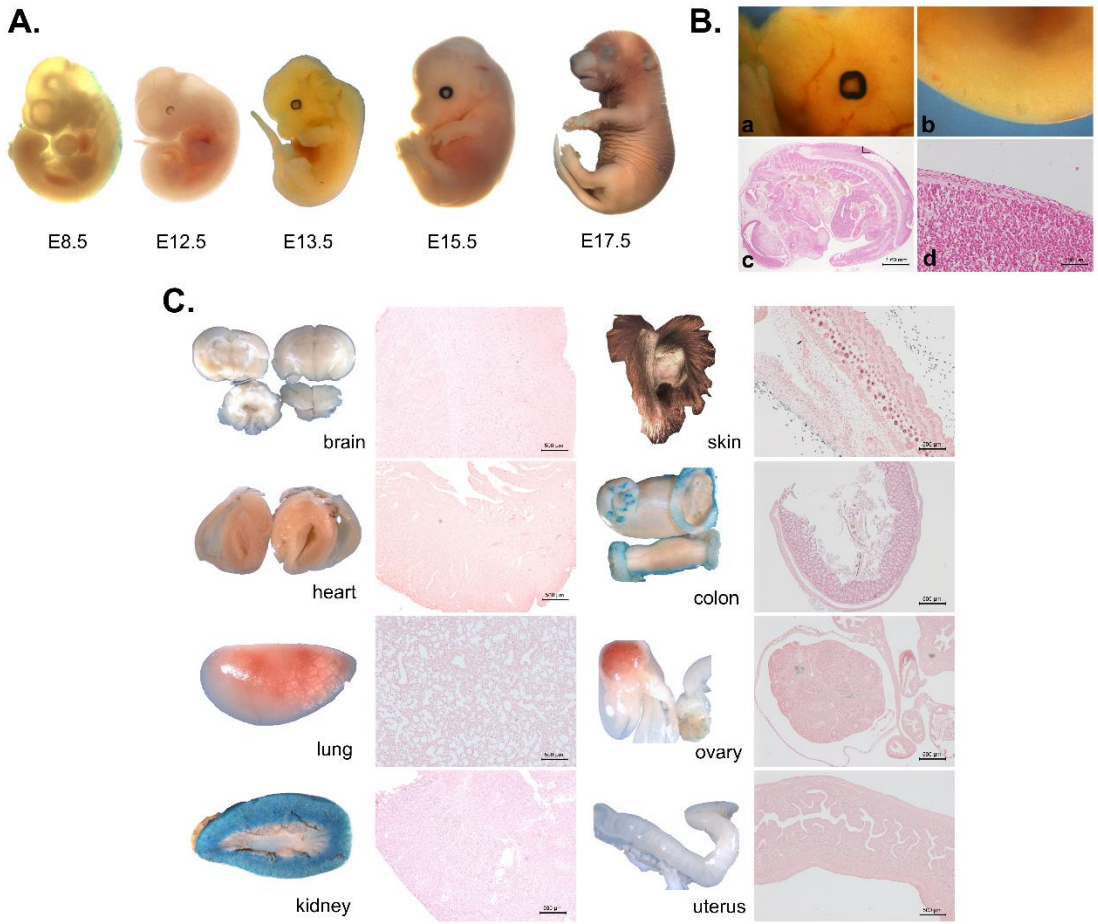

Figure 3.5. Visualization of false positive x-gal staining in embryos and adult tissues. X-Gal staining detects false-positive beta-galactosidase activity or edge-effect staining in **A,B.** whole embryos or **C.** whole organs of control mice crossed with ROSA26-lacZ reporter mice. For embryos in **A.**, higher magnification of dissecting scope images of Edn2-iCre fetuses at approximately embryonic day 15.5 are shown in **B.** Images show a) rostrum, b) dorsal skin, c) whole-mount histological staining 1.25x, and d) magnified histological staining of skin of embryo 40x. For adult tissues **C.**, gross images are shown at left and histology images with nuclear fast red background staining are at right. Brain, heart, and kidney tissue were bisected, ovary was punctured, and colon was flushed prior to staining. The oviduct and uterus are visible in the gross ovarian image. Note the light staining on the edges of the embryos, the brain, lung, and uterus. Additionally, there is staining throughout the cortex of the kidney and visible histological staining on the hair from the skin section and in the lumen of the colon.

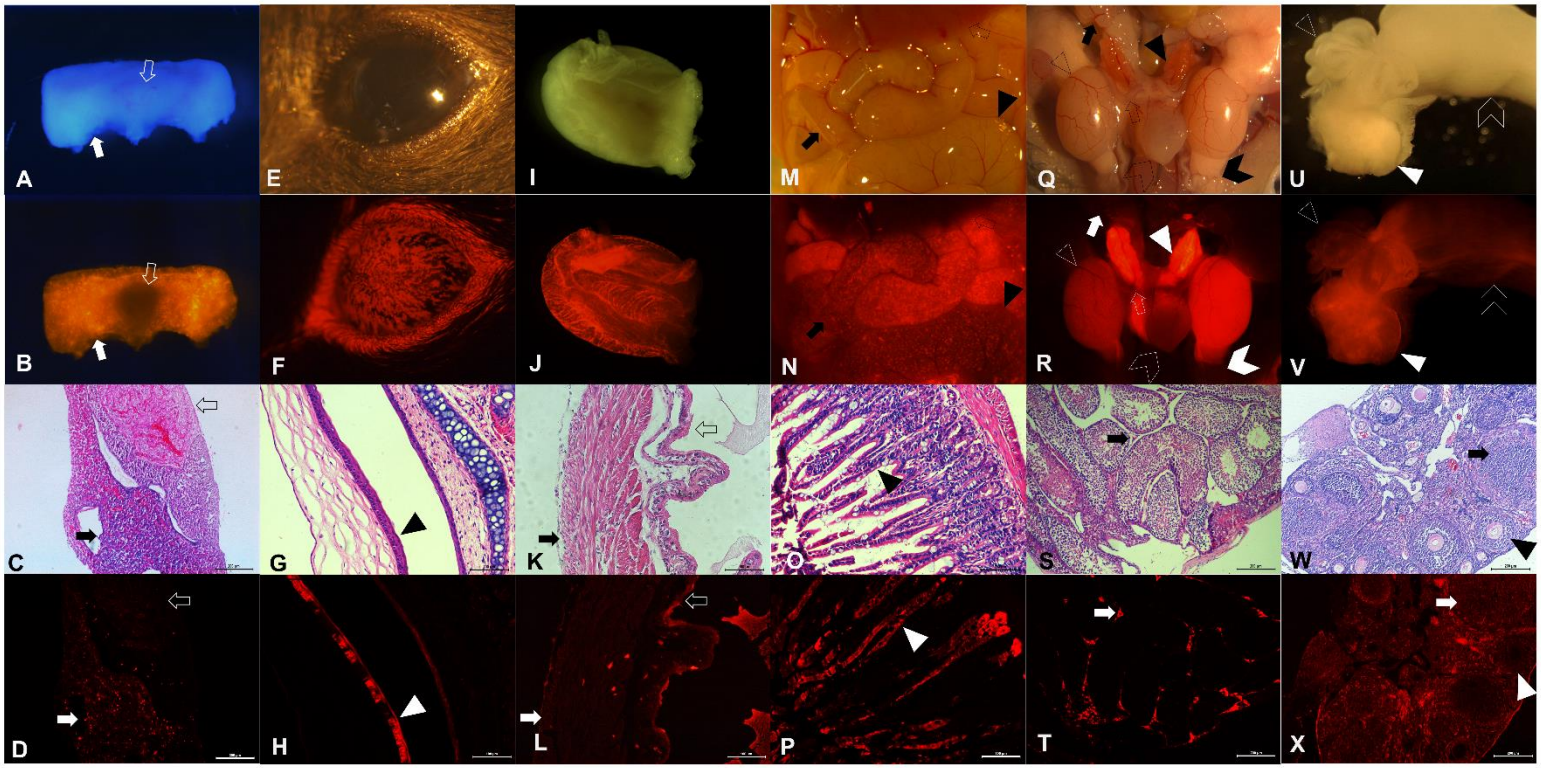

Figure 3.6. Localization of iCre expression by red fluorescence in adult Edn2-iCre mouse organs. Edn2-iCre mice were crossed with Ai9 reporter mice for rapid visualization. Fluorescence intensity at low magnification (row 2) correlates with the number of Edn2-iCre-expressing cells. Red fluorescence indicates areas of cell lineage expression of iCre (row 4). Top rows: gross images and fluorescence comparison. Bottom rows: histological images and fluorescence comparison. **A-D**: pituitary (female, PND28); **E-F**: Eye; **G-H**: Cornea of eye; **I-L**: Bladder (detrusor muscle); **M-N**: Gastrointestinal tract; **O-P**: Jejunum; **Q-R**: Male reproductive organs; **S-T**: Seminiferous tubules; **U-V**: Female reproductive organs; **W-X**: Ovary. Symbols are used to mark specific organs or cell types. Image A, B, C, D: solid arrow: anterior pituitary (adenohypophesis); open arrow: posterior pituitary (neurohypophysis). Image G, H: Solid arrowhead: corneal epithelium (anterior epithelium, outside of eye). Image K,L: solid arrow: smooth muscle cells of detrusor muscle (3 layers); open arrow: transitional epithelium of bladder facing lumen. Image M,N: Solid arrow: small intestines; open arrow: liver; solid arrowhead: large intestines. Image O,P: Solid arrow head: luminal epithelium of jejunum. Image Q, R: solid arrow: seminal vesicle; open arrow: ductus (vas) deferens; solid arrowhead: coagulation gland (anterior prostate); open arrowhead: testis; solid chevron: epididymis; open chevron: bladder. Image S, T: solid arrow: interstitial cells of testes. Image U, V: Solid arrowhead: ovary; open arrowhead: oviduct; open chevron: uterus. Image W, X: Solid arrowhead: secondary follicle; solid arrow: antral follicle.

CHAPTER 4: OVARIAN CONTRACTION BY ENDOTHELIN-2/RECEPTOR SYSTEM IS CONSERVED IN DOMESTIC VERTEBRATES

Joseph Cacioppo[1], Arnon Gal[1], Patrick Lin[1], Jongki Cho[1,2], Janice Bahr[3], and CheMyong Ko[1]*

[1]Comparative Biosciences, College of Veterinary Medicine, University of Illinois, Urbana-Champaign, IL 61802 USA
[2]College of Veterinary Medicine, Research Institute of Veterinary Medicine, Chungnam National University, Daejon, South Korea
[3]Department of Animal Sciences, College of Agricultural, Consumer and Environmental Sciences, University of Illinois, Urbana-Champaign, IL 61802 USA

*Corresponding author
CheMyong Ko, Ph.D.
Department of Comparative Biosciences
College of Veterinary Medicine
University of Illinois at Urbana-Champaign
3806 VMBSB, MC-002
2001 South Lincoln Avenue
Urbana, IL 61802, USA
217-333-9362 (office), 217-244-1652 (fax)
jayko@illinois.edu

This work was supported by NIH (R01HD052694 to CK).

ABSTRACT

The peptide endothelin-2 (EDN2) is transiently produced in the granulosa cells of rodent and human periovulatory ovaries immediately prior to ovulation. *Ex vivo* experiments showed that, upon treatment of EDN2, the rodent ovary rapidly contracts, while when the endothelin receptor pathway is antagonized *in vivo*, ovulation is inhibited. Human and rodent ovaries possess a layer of contractile smooth muscle-like cells in the theca externa of developing follicles. In addition, ovaries have been documented to spontaneously contract *ex vivo*. However, the significance of this contraction and its relevance to the role of EDN2 in regulation of ovulation remain to be determined. Here the effect of EDN2 on the characteristics of contraction in feline, canine, and chicken ovaries was investigated. Immunohistochemical staining for smooth muscle actin was present in the theca layer of feline and chicken follicles as well as the vessels, but only in the arteries and arterioles of canine ovaries. RT-PCR showed that both mammalian ovaries express mRNA for *Edn1*, *Edn2*, *Edn3*, both isotypes of endothelin receptors (*Ednra* and *Ednrb*), and endothelin converting enzymes 1 and 2 (*Ece-1* and *Ece-2*), though chickens only express *Ednrb* in F1 and F2 follicles. Feline ovaries exhibited a period of strong and sustained contraction when treated with 50 nM EDN2. When treated with the dual endothelin receptor antagonist tezosentan, contraction was reduced in a dose-dependent manner. A similar contractile in response to EDN2 was observed in the theca layer of chicken periovulatory follicles. However, canine ovaries demonstrated a significantly lower contractile response to EDN2 (0.11±0.07mN) than feline ovaries (2.48±0.40mN) or the chicken theca layer (2.04±0.85mN, p=0.038). Taken together, this study demonstrates that EDN2 produces a strong contraction in the ovaries of two novel species and that this contraction can be localized to the theca layer of the chicken follicle.

INTRODUCTION

The protein endothelin-2 (EDN2, product of the gene *Edn2*) is expressed in the mouse, rat, bovine, and human ovaries near or at the time of ovulation following stimulation with injectable gonadotropins[6,7,12,217,246]. Expression is limited to granulosa cells in rodent and bovine ovaries. EDN2 is part of the endothelin system, which in therian mammals consists of three ligands, endothelin-1, -2, and -3 (*Edn1*, *Edn2*, *Edn3*); two receptors, endothelin receptor A (*Ednra*) and endothelin receptor B (*Ednrb*), and two enzymes, endothelin converting enzyme-1 and -2 (E*ce-1*, *Ece-2*)[218,221]. Endothelins are produced in a prepro-form, are cleaved by converting enzymes upon exiting the secreting cell, and bind to their membrane-bound GPCRs. In birds, reptiles, amphibians, and other descendants of lobefinned fish, the endothelin receptor B2 (*Ednrb2*) is also present[221]. In all vertebrates, the endothelin system is highly conserved, though there are some differences in ligand and receptor number[221,322].

Pharmacological inhibition of endothelin receptors during ovulation has been shown to decrease ovulatory capacity[6,170,171,314]; this is believed to occur through inhibition of a contractile mechanism through EDNRA, as endothelins are well characterized to induce smooth muscle contraction. Exposure to EDN2 induces contraction in rodent ovaries *ex vivo*, while exposure to a dual-receptor antagonist drug decreases the contractile response, as measured on a custom analog myograph system[6]. It has been previously proposed that EDN2 induces contraction of the smooth muscle of the theca externa layer[323], which surrounds mature follicles, at the time of ovulation as a final trigger for follicular expulsion[6]. As fertility drops sharply when endothelin signaling is blocked, study of the endothelin system may generate useful targets to improve assisted reproductive technologies or to act as novel nonhormonal contraceptives[324,325].

Considering the highly conserved sequence of EDN2 (Figure 4.1) and previous observations of periovulatory expression in humans and several model species, it is hypothesized that EDN2, or antagonists of its receptors, causes a similar contractile response in multiple vertebrate species' ovaries. The aims of this study were to 1) use a myograph system as a novel, commercially available digital tool for the study of ovarian contraction, frequency, and amplitude, and 2) to demonstrate that the ovaries of multiple new species express components of the endothelin system and respond in a similar manner to exposure to EDN2 peptide *ex vivo*. A DMT myograph system (DMT-USA, Ann Arbor, MI) was chosen as a commercially available digital machine that was highly sensitive (mN range) and took frequent readings at least 10x/ second,

could be modified to either pin or tie tissue to the arm of the transducer, and allowed for temperature, oxygen, and pH maintenance to keep tissues alive for multiple hours[326-329]. To accomplish our second aim, domestic cat ovaries which were readily available from local ovariohysterectomy procedures were first examined. Reproductive tissues from domestic dogs and chickens that were similarly available were then used for comparison.

Ovulatory regulation and timing varies by considerable degrees between these three species. Each experiences the growth of an oocyte and its surrounding cells into a large follicle prior to ovulation through pituitary gonadotropin stimulation[330]. However the timing of this event varies by the animal's lifestyle and survival strategy. Cats are seasonal polyestrous breeders, while dogs are generally considered to be seasonal monoestrous breeders. Though each species is dependent upon photostimulation for estrous cyclicity, nonferal individuals with access to indoor lighting generally cycle year-round[74]. The average queen cycle transverses a 2 day proestrus, a highly variable 6 day estrus, a return to proestrus if no mating occurs or a potential 2-3 week inter-estrus period, a 7 week pseudopregnancy if nonfertile ovulation occurs, and a possible 2-3 month anestrus period[134]. The average dog cycle moves between a 9 day proestrus, a 9 day estrus, a 2 month diestrus with a pseudopregnancy, and a 5 month anestrus, though there is considerable breed and individual variation, as well as other environmental factors such as nutrition and male presence[331]. Both queens and bitches can ovulate multiple mature follicles in one cycle.

Alternatively, the laying hen (as opposed to broiler strains) ovideposits a single egg nearly each day at a 24 hour interval. Unlike cats and dogs, the hen ovary contains a hierarchy of growing follicles that gradually progress towards maturity, with less atresia occurring[151]. The hen also possesses only a functional left ovary upon reaching maturity. The mature follicles of all three species, though quite variable in size, each possess common granulosa and theca steroidogenic layers. The contractile potential of the cat ovary and chicken follicle have been previously characterized, and each is known to possess smooth muscle in the theca externa layer[144,154,161,332,333]. Dogs, like cats and hens, are known to possess cholinergic nerves in the ovary, but no data presently exists on smooth muscle presence or contractility. The theca layers of all three species also contain small arterioles that are encircled by smooth muscle, which invade the granulosa cells during ovulation and luteinization. Though female tract contractions are known to be important for fertility, the majority of previous studies have focused on the uterus and sperm transport. Here it was hypothesized that EDN2 causes significant ovarian or follicular contractions

in multiple species, and that these tissues express some or all of the components of the Endothelin system. This was tested by localizing the smooth muscle within each tissue, by performing RT-PCR for endothelin genes, and by treating feline ovaries, canine ovaries, and chicken theca cells with EDN2 and endothelin receptor antagonists and quantifying their tensile response.

MATERIALS AND METHODS

Ethics Statement

This study was carried out in tight accordance with the recommendations in the Guide for the Care and Use of Laboratory Animals of the National Institutes of Health. Animal protocol was approved by the University of Illinois Animal Care and Use Committee (Protocols: 12164 and 14205), and all efforts were made to minimize animal suffering.

Animals

Feline reproductive tissues were collected following routine spay procedures from October 2012 to May 2013 at the University of Illinois at Urbana-Champaign College of Veterinary Medicine through the junior surgery program for student training. Cats ranged in age from 8 months to 3 years old and in weight from 2.1 – 3.1 kg; ages were estimated by dental health when no date of birth was available. Following a physical exam, healthy cats were pre-medicated with dexmedetomidine 0.008mg/kg, ketamine 5mg/kg, and morphine 0.1mg/kg by IV injection about 30 minutes prior to spay surgery. At the start of surgery, anesthetic induction was performed by IV propofol 4mg/kg and maintained by inhaled isoflurane 1% for the duration of surgery. After the abdominal cavity was opened and reproductive tract exteriorized, both ovarian arteries anterior to the ovaries and the uterine body posterior to its bifurcation were ligated, cut by scalpel, and the entire tract was removed from the body and transported out of the surgical suite. Canine tissues were collected in the same manner as feline tissues from the junior surgery program, though dogs received atropine (0.04mg/kg) instead of ketamine. Dog weights ranged from 5.8-19.7kg, and age estimates ranged from 12 weeks to 2 years. Chicken ovaries were collected immediately following humane euthanasia from the Animal Sciences Department at the University of Illinois at Urbana-Champaign. All chickens were layers of 10-14 months of age and average weight of 1.50kg, and had a history of laying eggs reliably for at least three days. Chickens were sacrificed one hour before the estimated time of ovulation as observed the previous day, which was based on time of oviposition. Theca and granulosa cell layers were isolated as previously described by Gilbert *et al*. 1977[334].

Histology and Immunohistochemistry

Feline, canine, and chicken ovaries were fixed for 48 hours in a 4% paraformaldehyde solution following removal. Tissues were then embedded in paraffin and sectioned at 7 μm, mounted on charged glass slides, deparaffinized, and rehydrated. Tissues were then either stained with hematoxylin (Harris*)* and eosin (Surgipath*)* for cellular visualization, or were processed for immunohistochemistry to localize contractile cells. Antigen retrieval was done with X1 Citrate Buffer pH 6.0 for 60 minutes in a vegetable steamer, rinsed under deionized water for 5 minutes, loaded onto a Shandon-Sequenza system (Thermo Scientific, Kalamazoo, MI), and washed with PBS to remove bubbles. Tissues were then blocked with 5% rabbit serum for 30 minutes, treated with the primary polyclonal antibody rabbit anti-mouse smooth muscle actin (SMA), Abcam ab5694, or Dako (Carpintera, CA) negative control rabbit immunoglobulin fraction (15g/L normalized in PBST to the SMA concentrate), washed twice with PBST, treated with fresh Avidin Biotin complex solution for 20 minutes at room temperature, washed twice with PBS, and incubated with Nova Red for 2 min at room temperature, prior to hematoxylin counterstaining. Murine ovaries, bladder, and uteri were concurrently stained as positive controls (data not shown).

Gene Expression

To assessment whether or not the genes in the endothelin system of the cat were being transcribed within the ovary, five ovaries (estrous stage unknown) from five cats ranging in age from 8 months to three years were analyzed by semi-quantitative PCR. Whole ovaries were removed at the time of spay and frozen immediately in liquid nitrogen. They were stored in a -80 freezer until analysis. Whole ovaries were ground by mortar and pestle; RNA was extracted by Trizol® solution (Ambion, Carlsbad, CA), washed twice with ethanol, and then purified with a Qiagen RNA-Easy Kit (Valencia, CA). RNA was analyzed by a Nanodrop machine (Thermo Scientific) for quantity and quality. Complementary DNA was then generated by M-MLV Reverse Transcriptase using random primers. Template RNA quantities were normalized to 1.0μg/μL prior to reverse transcription. 1.0μL of resulting cDNA from each ovary was used as template with 15μL Taq Platinum (Invitrogen) and 0.3μL of each primer per PCR reaction for a total reaction volume of 16.6μL; reactions were cycled 30x for 94C for 1:00 min, 59C for 1:00, and 72C for 1:30. Amplified DNA (3.0 μL) was visualized on a 2.0% agarose gel and was quantified using ImageJ freeware (NIH, Bethesda, MD) to measure peak pixel grayscale levels within the defined areas of

the bands. Preliminary PCR reactions were used to optimize the cycle number; *Rpl19 (L19)*, which encodes a portion of the cytoplasmic ribosomal protein 60S subunit, was used an internal control housekeeping gene. This was repeated for canine ovarian samples from five dogs age estimated 16 weeks to 2 years, unstaged. For chickens, RT-PCR was performed on F1 follicles one hour prior to the time of ovulation as above and compared to RNA extraction from F2 follicles from 6 birds. F1 follicles were collected at one hour prior to the time of ovulation, which was estimated through repeated observations of oviposition for four consecutive days. Primer sequences are listed in Table 4.1.

Ovary Mounting

Ovaries used for tension analysis were placed into a 4°C physiological saline solution (PSS) in the surgical suite and transported to the laboratory, where a wire myograph system (Tissue Bath System 620M, Danish Myo Technology, DMT-USA Inc., Ann Arbor, MI) was located. Half-ovaries were used for removal of large ovarian vessels, and pin mounting was chosen to minimize tissue damage and increase mounting speed. Sectioning was done with a scalpel on the axis perpendicular to the hilus, on the axis that runs the length of the kidney-bean shape of the ovary (Figure 4.2). The half ovary that did not contain the hilus region was then placed into fresh 6mL of 4C PSS in the test chamber of the myograph and was punctured on each end by one of the 4mm mounting pins on each arm of the myograph. The myograph was then turned on, to gradually heat the PSS to 38.5°C while also slowly bubbling a mixture of 50% oxygen, 45% nitrogen, and 5% carbon dioxide through the chamber. Meanwhile, fresh PSS and a 60mM K+ in PSS (K+PSS) were placed into a water bath to also reach a physiological temperature. Two ovaries were processed at the same time for each set of experiments. Ovarian tensile measurements were recorded via LabChart software (ADInstruments, Colorado Springs, CO). After about 20 minutes when the test chamber containing the ovary had reached the appropriate temperature, the PSS solution was removed and fresh, warm PSS buffer was added. The system was then zeroed.

Tension was next applied to the half ovary over the following 20 minutes to a tension of 3mN. The knob controlling pin width was lightly turned at approximately one minute intervals to maintain 3mN of tension as the tissue was stretched. Optimal tension-contraction response in feline ovaries occurred with ~3mN of passive tension applied per half ovary. Lastly, a ‘wake-up’ protocol was used to finish the equilibration: K+PSS was applied to the stretched ovary, and was removed

3 minutes later. The ovary was then washed 4 times over 5 minutes with PSS, and allowed to sit for 5 more minutes. This procedure was repeated twice. The PSS was then replaced a final time and the contractile experiment began. Canine ovaries were mounted similar to feline ovaries with bisection to exclude the ovarian pole. Chicken theca layers were also mounted similarly, though a passive tension of 1mN was used instead of three; reported contraction values were not modified to account for this. Pins were passed through each end of the strip of the theca cells.

Pilot studies in mice indicate that ovaries remain alive and responsive in this system for up to eight hours; ovaries are largely similar to in vivo ovaries, with similar expression of genes at the time of ovulation after gonadotropin stimulation (data not shown). However, follicle rupture and ovulation itself is inhibited, likely by lack of blood flow through ovaries.

Ovarian Tensile Analysis

To determine if feline ovaries contract in response to EDN2 agonization, ovaries were first allowed to sit in fresh PSS at a physiological temperature and pH with supplied oxygen and CO_2 for five minutes to generate a baseline tensile measurement, the average tension in mN during this treatment. For ovaries that demonstrated cyclical contractions during this period, baseline measurements were averages of the trough tension for five troughs between peaks. Next, K+PSS solution was applied a 3rd time for a duration of 5 minutes. This served as a reference point for the relative contractility of that ovary to account for variation in mounting, ovary size, and ovary health. Any ovary that failed to demonstrate contraction in response to K+PSS was discarded. K+PSS was then removed with four PSS washes at 1 min intervals, and the ovary was allowed to equilibrate for 5 additional minutes.

Next, recombinant human endothelin-2 purified peptide (American Peptide Co, Sunnyvale, CA) was added to the PSS solution of the chamber to generate a 50nM solution. After 20 min, without changing the buffer solution or removing the ligand, the dual-endothelin receptor antagonist drug tezosentan was added to a concentration of 140nM and left for 20 minutes. These concentrations were calculated from preliminary titration experiments. Tensile measurements represent the difference from resting measurement (the average of 5 minutes prior to the final K+PSS addition) to either average K+ contraction (the average of minutes 2:00-5:00 after the K+PSS addition at 0:00) or average EDN2 contraction (the average of the 5 minutes prior to tezosentan administration for EDN2-induced contraction). The average of the final 5 minutes of

the experiment was subtracted from peak EDN2-induced tension to calculate the change after tezosentan addition (recorded as a positive, not a negative, number). All measurements were made in mN, and were later converted to arbitrary units (AU) for relative comparison by dividing each by the contractile response to K+PSS for that ovary. Titrations of EDN2 or tezosentan to determine minimum concentrations for optimum effect were made as above, except varying doses of each were added in 20 minute intervals without washing away previous buffer solution to those ovaries. Canine and chicken tension analyses were performed similarly.

Statistical Analysis

Data analyses were performed using statistical software (SPSS, Inc., released 2009, PASW Statistics for Windows, Version 18.0, Chicago, IL). All normally distributed continuous data were analyzed with parametric tests (student's t-test and ANOVA) and a Bonferroni *post hoc* test for variance between groups. All non-normally distributed continuous data, solely the data for absolute K+PSS induced tension in mN, were transformed by log function to a normal distribution. Ordinal data were analyzed with nonparametric tests (Mann-Whitney and Kruskal Wallis). Normally distributed data are presented as mean and standard error of the mean, whereas non-normally distributed data are presented as median and range. For all analyses the alpha value was set to 0.05.

RESULTS

Cat and hen ovaries possess smooth muscle encircling mature follicles in the theca externa

It has been previously documented that the ovaries of cats possess a large amount of smooth muscle tissue, which is comparable to that of the human ovary. Using immunohistochemistry to localize smooth muscle actin, it was demonstrated and confirmed that the follicles of feline ovary possess a layer of smooth muscle around them after reaching the antral stage (Figure 4.3). The majority of feline ovaries possess follicles of all stages, including primordial, primary, secondary, antral, and Grafiaan. The theca externa layer contains the smooth muscle actin-expressing cells and continues around the circumference, approximately 3-5 cells thick, of mature follicles. Additional staining is seen in vasculature throughout the ovary. Similar smooth muscle localization around peri-ovulatory follicles was likewise observed in the chicken ovary (Figure 4.3). However, canine ovaries did not demonstrate positive staining in the theca externa layer, only in the vessels of the ovary. This is a unique and surprising finding given the smooth muscle network that is present about follicles in mice, rats, humans, cats, and chickens.

Feline, canine, and chicken ovaries express components of the endothelin system

Total RNA was extracted from the ovaries of cats (n=5), dogs (n=7), and the F1 and F2 follicles of chickens (n=6); RNA was purified, complimentary DNA was generated using reverse transcription, and semi-quantitative PCR was performed to determine if ovaries express the components of the endothelin system at various points in the cycle. Canine and feline ovaries demonstrated expression for *Edn1*, *Edn2*, *Ednra*, *Ednrb*, *Ece-1*, and *Ece-2* (Figure 4.4). Only feline ovaries, not canine ovaries or chicken follicles, expressed detectable amounts of *Edn3*. Chicken follicles, F1 and F2, expressed only *Ednrb*. There was no difference in gene expression between chicken follicles of different ages. Expression of all three ligands and *Ednrb* were low in feline ovaries, and expression of *Edn2* and *Ece-2* were low in canine ovaries. It should be noted that differences in expression level cannot be compared between genes owing to different primer binding affinities and amplicon lengths, nor are these representative of a mature follicle but of an average unstaged ovary as a whole, excepting the chicken periovulatory F1 follicle when compared to the developing F2 follicle.

Ovaries respond strongly to a 50nM EDN2 solution

A passive tension was applied to each ovary relative to the starting mounting tension. To determine what concentration of EDN2 causes ovaries to contract, a set of titration experiments was performed in which, following the K+PSS wake-up protocol, increasing doses of EDN2 were added in 20 minute intervals to ovaries. An increase in tension in response to EDN2 treatment reached a maximum response between the concentrations of 5 and 50 nM EDN2 in the K+PSS solution (Figure 4.5). 50nM was chosen as the minimal concentration of EDN2 to induce sustained contraction in ovaries in further studies. In a similar manner, after adding 50nM EDN2 to the PSS solution, tezosentan was added in a stepwise manner. 14.0-140nM tezosentan was the range of minimal concentration that maximally decreased contraction caused by EDN2 ligand (Figure 4.5).

Feline ovaries contract in response to EDN2

To measure the average contractile response to 50nM of EDN2, feline half-ovaries received wake-up protocol, were dosed with K+PSS to provide a comparable baseline tension measurement change, and then received 50nM EDN2, followed by 140nM tezosentan to determine if tensile change was specifically occurring through endothelin receptors (Figure 4.6). The average absolute changes in tension in the feline ovary were as follows: K+PSS: 0.80±0.17mN, EDN2: 2.48±0.40mN, and tezosentan: -1.68±0.26mN. Relative changes in tension, normalized to K+PSS where the change from K+PSS = 1.00, were EDN2: 3.65±0.44AU and tezosentan -2.72±0.50AU (Figure 4.7). Spontaneous contraction was observed in 30.7% feline ovaries after mounting and passive tension were applied. Relative to the baseline tension of these ovaries, recorded as the average trough amplitude between contractions, these ovaries spontaneously contracted with amplitude of 4.08 ± 2.45mN, duration of 22.2 ± 6.4sec, and a time of 60.9 ± 20.2sec between contractions. These contractions continued after EDN2 treatment, but contraction amplitude was reduced (1.25 ± 0.95mN) as was the time between contractions (13.8 ± 6.5sec) for all ovaries. The duration between contractions after EDN2 treatment was not significantly different (20.13 ± 4.66sec, p=0.240).

Canine ovaries and chicken follicular theca layers contract in response to EDN2

To measure average contractile responses to the same dose of EDN2 peptide, the same 60mM K+PSS, 50nM EDN2, and 140nM tezosentan application regimen was used on canine half-

ovaries and the theca layer of F1 chicken follicles (Figure 4.6). In canines, the average absolute tensile changes were: K+PSS: 0.26±0.10mN, EDN2: 0.11±0.07mN, and tezosentan -0.08±0.04mN. Relative changes in tension, normalized K+PSS, were: EDN2: 2.83±1.30AU, tezosentan: -0.52±0.44 (Figure 4.7). Chicken theca cells, though comparatively smaller than canine or feline ovaries, demonstrated marked tensile response to the tested stimuli. The average chicken absolute tensile changes were K+PSS: 0.73±0.42mN, EDN2: 2.04±0.85mN, and tezosentan: -0.67±0.10mN. After normalization to K+PSS, the relative contractile response to EDN2 was 3.70±1.23AU and to tezosentan was -1.64±0.76AU (Figure 4.7).

Feline ovaries and chicken theca layers respond similarly to EDN2 and tezosentan

When comparisons were made between the average absolute and relative tensile changes between species, several significant differences were noted (Table 4.2). There was a significant difference between the absolute response to EDN2 peptide between cats and dogs ($p=0.002$), but not between cats and chickens ($p=1.000$) or dogs and chickens ($p=0.081$). This may be accounted for by the low number of chickens used. Similarly, there was a significant difference in the absolute response to tezosentan between cats and dogs ($p<0.001$), but not between cats and chickens ($p=0.127$) or dogs and chickens ($p=0.743$). There was a significant difference in the relative response to tezosentan between cats and dogs ($p=0.024$), but not between cats and chickens ($p=0.905$) or between dogs and chickens ($p=0.970$). No significant differences were observed in the average absolute tensile responses to K+PSS treatment ($p=0.067$) or the relative response to EDN2 peptide ($p=0.747$). P-values close to 0.05 indicate trends towards significant differences that are likely masked by the small sample sizes used here, particularly of the low n-value for chicken follicles tested.

DISCUSSION

The data presented here demonstrate the presence of smooth muscle-expressing cells around the large and peri-ovulatory follicles of ovaries in the cat and chicken but not the dog, the expression and functionality of the components of the endothelin system in those ovaries, and the novel use of a DMT myograph system to record and compare contraction between those tissues when exposed to the peptide EDN2 were demonstrated. To the best of the authors' knowledge, this is also the first quantitation of contraction in a canine ovary. EDN2 concentrations used here are similar to estimations of antral fluid endothelin concentrations based on previous studies in rats and humans[14,335,336]. Though of a lesser degree in the canine ovary, potentially owing to lesser smooth muscle content[333], contraction was demonstrated in all three species, and specifically in the theca layer of chicken follicles. The chicken follicle does not demonstrate a similar rise in *Edn2* expression one hour prior to oviposition as has been previously observed in mouse, rat, and human ovaries after gonadotropin stimulation[6,7,14]. Similar study in cats and dogs remains challenging owing to seasonal monoestrus in the canine and highly variable timing in response to gonadotropins in each species[140,337-342]. Previous comparison of the contractile potential in cats at different stages of the estrous cycle found little difference[161], though spontaneous contractions were also observed throughout various points of the cycle[343]. It is also noted in our data that when adding tezosentan after EDN2 ligand treatment, no ovary completely returned to baseline tension during the time of the experiment, likely owing to prior ligand binding. When tezosentan was added before EDN2 ligands in pilot studies, no contractile response was observed in response to EDN2, as is expected when adding a competitive antagonist drug.

Contraction in the ovary at the time of ovulation remains a controversial issue, and has been well discussed in previous review by L.L. Espey (1978)[66]. Although it has been suggested that this is a final trigger for the expulsion of a follicle[6] from the organ following collagenase digestion of the surface epithelium and basement membrane[112,344], specifically by EDN2[200], it has also been shown that there is not a vast increase in ovarian follicular fluid pressure during ovulation[100,101,345], though there may be increased ovarian contraction frequency at the time of ovulation, as seen previously in rabbits given hCG stimulation[167]. Contractions of the theca wall have also been previously observed in chicken follicles, and hypothesized to promote stigma rupture[332]. Thus it is possible that EDN2 of near-ovulatory and ruptured follicles contributes to increased ovarian tone and, by shortening muscle cell length, increases the frequency of ovarian

contractions, as was trended towards by the spontaneously contracting cat ovaries when receiving EDN2 stimulation. Indeed, contractions of the female reproductive tract have been shown to be essential for normal fertility, while secretions from the male reproductive organs can modify and generally enhance this motion, though previous studies have largely focused on the uterus and sperm transport[346-349].

The widespread expression of the endothelin system is not surprising, particularly the receptors and converting enzymes. Endothelin receptors are known to be expressed in a variety of tissues, and immunohistochemistry has previously demonstrated their presence in multiple components of the ovary[14]. Furthermore, the constitutive expression of *Edn1*, which consequently mandates the expression of each converting enzyme, has been well defined within endothelial cells as well as leukocytes, myofibroblasts, and neuronal stromal cells, which are abundant in the ovary[350]. Endothelin-3 has also been demonstrated to have constitutive expression in the brain, GI and reproductive tracts, lung, spleen, and kidney. Similarly, Uchide *et al*.[273,284] have previously demonstrated that all three ligand isoforms and each mammalian receptor are expressed in similar levels in the murine ovary, though *Edn1* and *Edn3* possess a broader distribution while *Edn2* is more limited. The presence of an amplification product and the variability of its individual intensity are of interest within our study. Particularly, *Edn2* appears to be consistently expressed in these naturally cycling cat and dog ovaries, unlike previous observations in rodents and humans. It is unlikely that, if *Edn2* has only a 2 hour window of expression as in the mouse ovulation model, significant expression would be seen in all ovaries collected, as was observed. The gene *Edn1*, which is believed to constitutively expressed at low levels across mammals, has very little variation between feline ovaries. Thus expression of endothelin components in the ovaries of these species substantiates that receptor expression is conserved among mammals, at least at a low level, though not in birds. Potential inductive factors beyond hypoxia[6] remain a topic of future exploration.

The observed differences between species are likely due to the poor response of canine ovaries to any K+PSS or EDN2 treatment. Lack of significant difference between absolute K+PSS response by ANOVA may be attributed to type II error from the low n-values. Indeed, the average dog ovary exhibited little response to EDN2 peptide and had little response to tezosentan consequently, despite being larger than feline ovaries and much more massive than the theca layer of chicken follicles. Oppositely, the chicken ovary appeared to have a similar contraction in response to EDN2 as feline ovaries, though relatively much smaller in mass. This may suggest that

EDN2 acts to cause contraction in only ovaries that may be preparing or prepared to ovulate, or that endothelin receptors require estrogenic priming prior to contractile signaling. However, as relatively few canine ovaries and chicken follicles were examined, differences not observed may be due to a type II error, and it is instead possible that chicken, canine, and feline ovaries all respond uniquely to EDN2, as the relatively constitutive expression of EDN2 in feline ovaries would suggest. It must also be noted that contractile differences between cats, dogs, and chickens are also dependent upon the amount of blood vessels present, which have been shown to consistently contract in response to EDN2. Though a chicken theca layer possesses some blood vessels[154,351], these are unlikely to be capable of the magnitude of contractile response possible by branches of the ovarian artery in large canine and feline ovaries. It is most parsimonious to state that feline ovaries and chicken theca layers contract in an apparently similar manner in response to EDN2 peptide, whereas canine ovaries demonstrate little absolute response to EDN2, and the cause of these differences is likely attributed to a lack of SMA about the mature canine follicles, as well as fewer follicles. This may also relate to the relative long anestrus in the reproductive cycle of the bitch and infrequent, singular ovulations.

In conclusion, endothelin-2 may play a critical role for successful reproduction across a variety of mammalian species in addition to humans and rodents. EDN2 may function as a final trigger for follicular rupture in ovulation, and/or may act to increase ovarian tone and increase the frequency of ovarian contractions during ovulation. Future work with the endothelin system in feline and canine tissues is merited both as models for human reproduction and in respect to individual animal groups, given the need for feral animal population control[352], the need to improve breeding in endangered species[353], and the need for improved sterilization techniques for household pets[354]. Studies may focus on these species as models of ovulation given the readily available tissues and ease of physiological measurements in contrasts to mouse ovaries, the effects of novel oral endothelin antagonists such as macitentan[324] on ovulation in both species, and further work on the genetics of ovulation in the chicken model given the ease of tissue layer separation, relative RNA availability, and recent advances in transgenic avian production[355].

ACKNOWLEDGEMENTS:

The authors thank Dr. Danielle Merema, Dr. George Robert Weedon, Heather Soder, and the Illinois veterinary classes of 2014-16 for their assistance in collection of tissues, William Hanafin and Clara Lee for chicken oviposition timing, Sarah Osmulski for semiQ-RT-PCR work in the chicken, and Karen Doty for her advice in performing histology and immunohistochemistry.

TABLES

Table 4.1. Primers used for RT-PCR. Continued on multiple pages.

Species	Gene	Primer Name	Sequence 5'-3'	Amplicon size (base pairs)
Feline	*Edn1*	FelisET1_F	TCT TGG GCG CAG AGC TCA GCA C	162
		FelisET1_R	GGA GTG TTG ACC CAG ATG ATG TCC A	
Feline	*Edn2*	FelisET2_F	CAA GGG CCA GGT GGC TGC TG	155
		FelisET2_R	CGG GAG TGT TCA CCC AGA TGA TGT C	
Feline	*Edn3*	FelisET3_F	GGG GAA ATT TAA GGT GGT GAA	112
		FelisET3_R	TCC GGG TGA TAG GTA CTC CTT	
Feline	*Ednra*	FelisETA_F	TAC CAA GAT GTG AAA GAC TGG TGG CTC	148
		FelisETA_R	GTT TAA GGT GTT CAC TGA GGG CAA TTC	
Feline	*Ednrb*	FelisETB_F	CTT GCC GAG GAC TGG CCC TTT G	101
		FelisETB_R	CTT AGA GCA CAT AGA CTC AAC ACA G	
Feline	*Ece-1*	FelisECE1_F	CGC CCC CAG TGT GCC TAA GTG A	205
		FelisECE1_R	AGG TGC TTG ATG ATG GCT TGG TTG TG	
Feline	*Ece-2*	FelisECE2_F	TGT GGG AAC AGT GCC CTG AGC T	279
		FelisECE2_R	ACT CAG CAC CTG GTC CAC AGT G	
Feline	*Rpl19*	FelisL19_F	GCT CAG GCT TCA GAA GAG GCT TGC	100
		FelisL19R	GTT GGC ATT GGC GAT TTC ATT TGT CTC	
Canine	*Edn1*	K9_ET1_F	GGT CCT GGG TGC GGA GCT CA	167
		K9_ET1_R	CAG GAG TGT TGA CCC AGA TGA TGT C	
Canine	*Edn2*	K9_ET2_F	AAG GGC CAG GTG GCC GCT G	154
		K9_ET2_R	CGG GAG TGT TCA CCC AGA TGA TG	
Canine	*Edn3*	K9_ET3_F	ATT GGT ACC TTG CCC CCA GCC T	284
		K9_ET3_R	GAG TGT TGA TCC AGA TGA TGT CCA	
Canine	*Ednra*	K9_ETA_F	CAG AGC AGT TGC CTC CTG GAG T	194
		K9_ETA_R	CAT GAA TTT TGA TGT GGC ATT GAG CAT	
Canine	*Ednrb*	K9_ETB_F	ATC GAG CCG TTG CCT CTT GGA GT	201
		K9_ETB_R	GCA TGA AGG CTG TTT TCT GGG TAG GA	
Canine	*Ece-1*	K9_ECE1_F	ACC CCC CCA GTG TGC CTA AGT G	209
		K9_ECE1_R	AGG AGG TGC TTG ATG ATG GCC TG	
Canine	*Ece-2*	K9_ECE2_F	CAT CCC ACA ACA CCT GCC TCA CA	211
		K9_ECE2_R	AGC AGG TGC TTC AGT ATG GCC TG	
Canine	*Rpl19*	K9_L19_F	GCA GAT ACG AAA ACT GAT CAA AGA TGG	112
		K9_L19_R	CAT ATG CCT GCC CTT CCG GCG	
Chicken	*Edn1*	Gallus_ET1_F	CTC CTG TTC GTC GCT GCT GGA C	162
		Gallus_ET1_R	CTG GCT CCA GCA AGC ATC TCT G	
Chicken	*Edn2*	Gallus_ET2_F	GAC CAA GCG GTG CTC CTG CAA C	140
		Gallus_ET2_R	GCG ATC TCT TGC GCC GTC GT	
Chicken	*Edn3*	Gallus_ET3_F	CTT CCC AGC CTT CAT TTC GGT GC	243
		Gallus_ET3_R	GTT CAC GTG CCC TCA GAA TGG C	

Table 4.1. Continued from previous page:

Chicken	*Ednra*	Gallus_ETA_F	GAA TGG CCC GAA TGC ACT GAT AGC	184
		Gallus_ETA_R	GAC TGT GAT TCC CAC TGA TGC CTT C	
Chicken	*Ednrb*	Gallus_ETB_F	ACA GGG TAC CGA GCA GTT GCT TCT	110
		Gallus_ETB_R	CTT CAG GAA CAG CCA ATA CCA CCG	
Chicken	*Ednrb2*	Gallus_ETB2_F	CTG GGA CCA AGA CCT GTG GGT G	89
		Gallus_ETB2_R	GCC ACC AGT CCT TCA CAT CAC GAT A	
Chicken	*Ece-1*	Gallus_ECE1_F	TGC TGG GGC TCG TCC TGC AGT A	141
		Gallus_ECE1_R	CGC AGG CAT AGC TGA AGA AGT CC TC	
Chicken	*Ece-2*	Gallus_ECE2_F	CTG ACT ACA AGC ATG CCA CAC TGC A	251
		Gallus_ECE2_R	ACC CCA GCA TGG CGG TCT CCT A	
Chicken	*Rpl19*	Gallus_L19_F	TCG GGC ACG ATG CAG GAA GAA CA	142
		Gallus_L19_R	CTG AGA ATC CGC ATC CTC CTC ATC	

Table 4.2. Relative differences in ovarian contraction between species.

	n-value	Abs K+PSS (mN)	Abs EDN2 (mN)	Abs tezo (mN)	Rel K+PSS (AU)	Rel EDN2 (AU)	Rel tezo (AU)
Feline	13	0.80±0.17	2.48±0.40	-1.68±0.26	1.00	3.65±0.44	-2.72±0.50
Canine	7	0.26±0.10	0.11±0.07	-0.08±0.04	1.00	2.83±1.30	-0.52±0.44
Chicken	3	0.73±0.42	2.04±0.85	-0.67±0.10	1.00	3.70±1.23	-1.64±0.76
ANOVA	p=	0.067	**0.002***	**<0.001***		0.747	**0.027***

Abbreviations used: Abs = Absolute, Rel = Relative, tezo = tezosentan, mN=milliNewtons, AU=Arbitrary Units

FIGURES

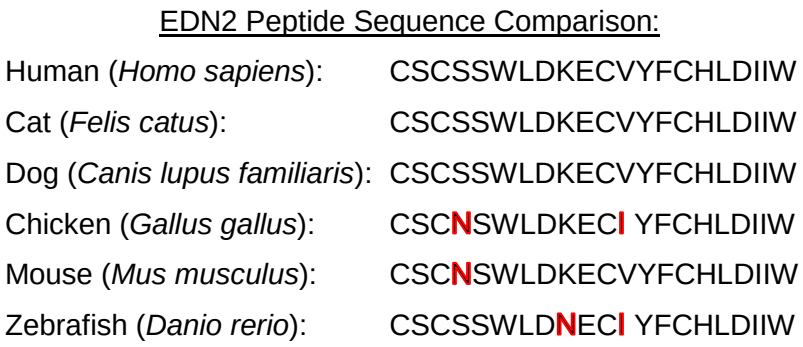

Figure 4.1. Comparison of the biologically active portion of the EDN2 peptide sequence among vertebrates. Differences from the human sequence are highlighted in red. Data were obtained from the National Center for Biotechnology Information, US National Library of Medicine.

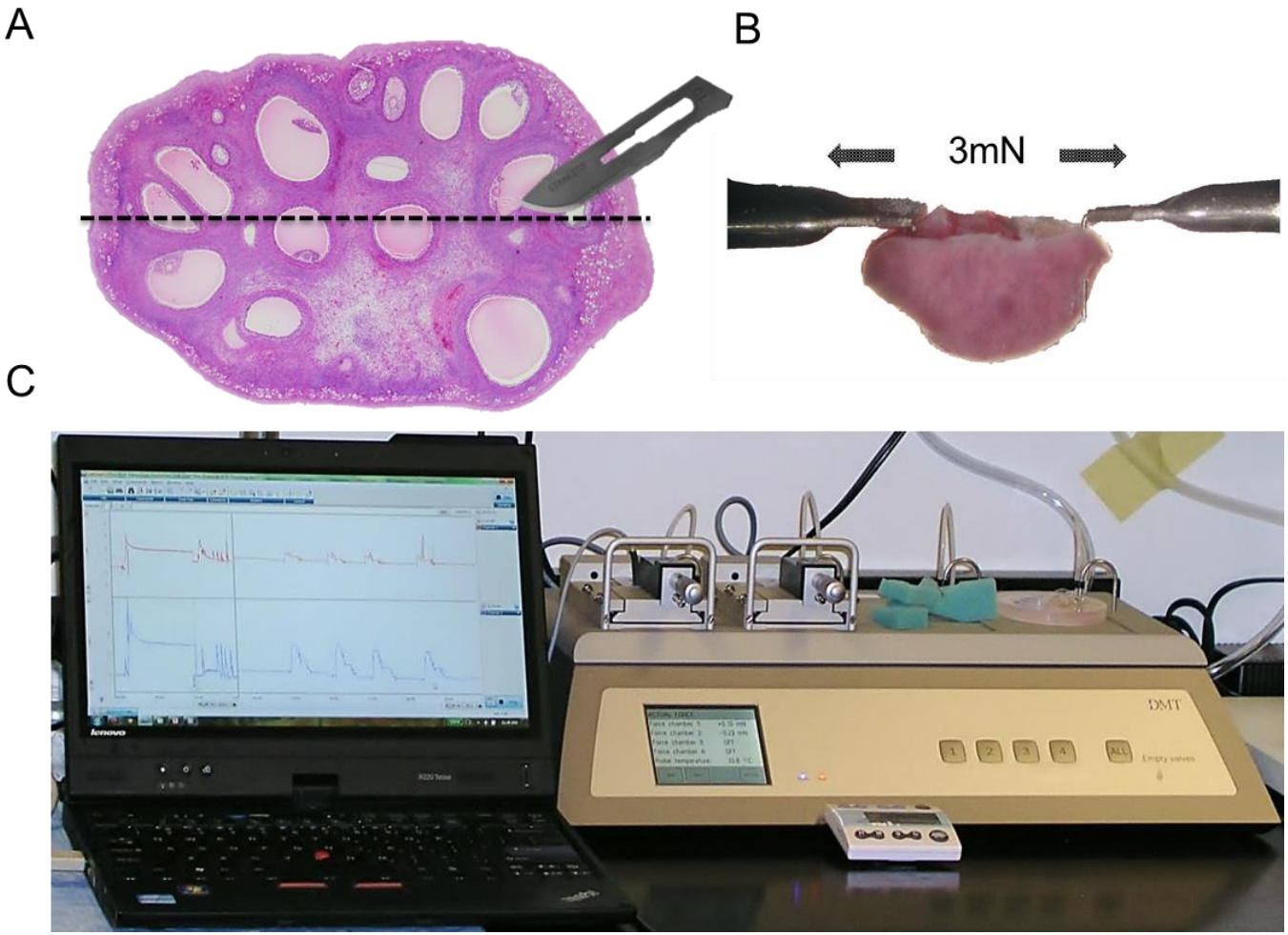

Figure 4.2. Measurement of ovarian contraction. A. Diagrammatic sectioning of a cat ovary for placement onto two 4mm pins of the *DMT* myograph system, which is composed of two chambers with a force transducer to sense tissue tension, a heated base to optimize tissue temperature, and gas and vacuum lines to supply tissues with oxygen and remove solutions. Electrical signals are sent to an amplifier and then to the LabChart™ software on a connected computer. **B.** Image of a bisected feline ovary after mounting. **C.** The DMT myograph system and adjoining LabChart™ Software output with timer.

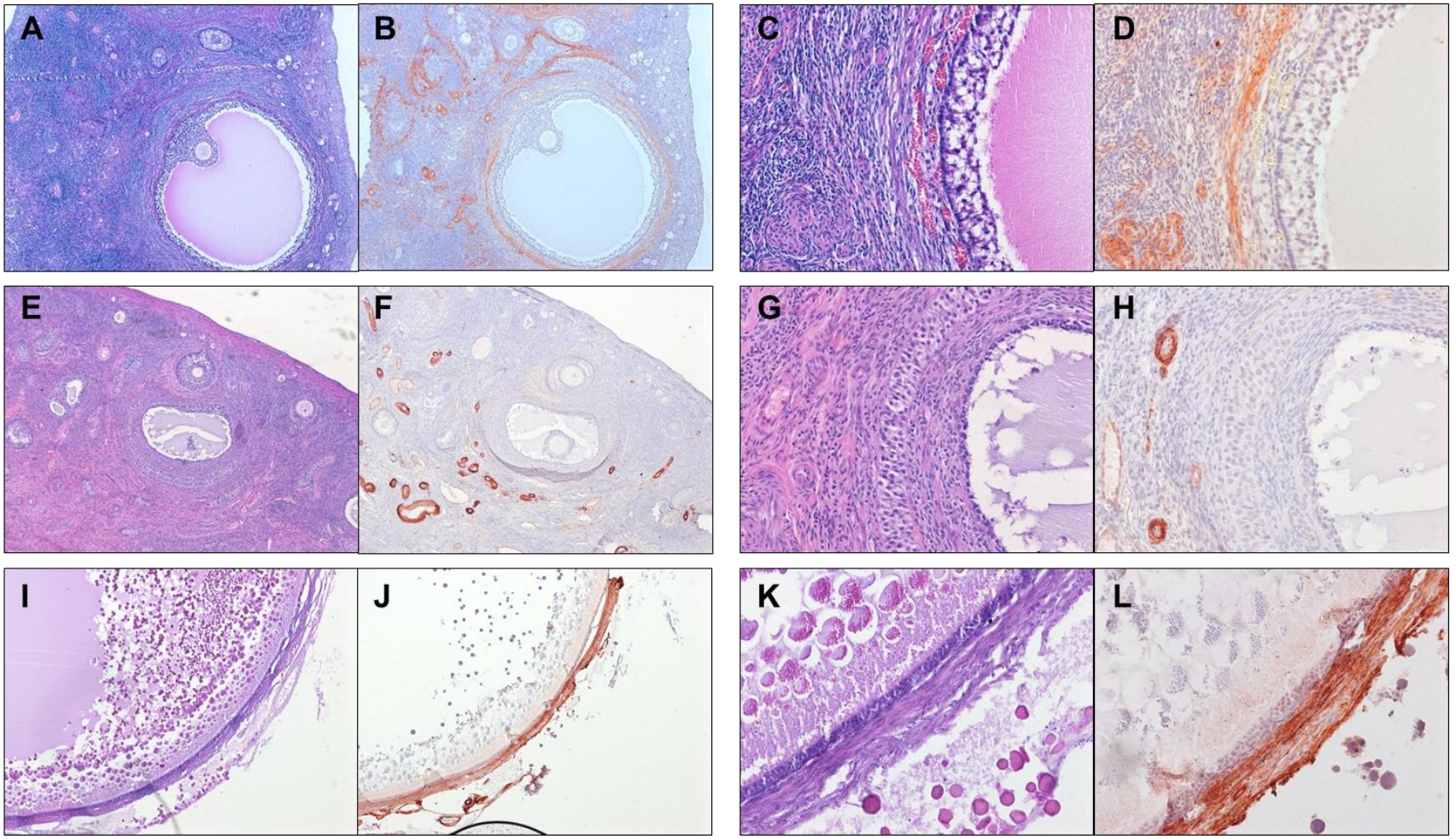

Figure 4.3. Alpha-smooth muscle actin is present around the feline and chicken follicle. Images are shown at 4X (left) and 20X magnification (right). **A-D** feline tissue; **E-H** canine tissue; **I-L** chicken tissue. There is staining of myoid cells of the theca externa layer around large follicles in the feline and chicken ovary, and consistent intense staining of the large vessels throughout all ovaries. Contractile theca externa cells are not present around immature follicles. The theca externa is approximately 3-5 cells thick in mature follicles in all three species. No anti-SMA staining is seen in the granulosa cells of follicles. Positive staining is also seen in the vessels within corpora lutea in felines and canines (not pictured). Tissues are sectioned at 5uM.

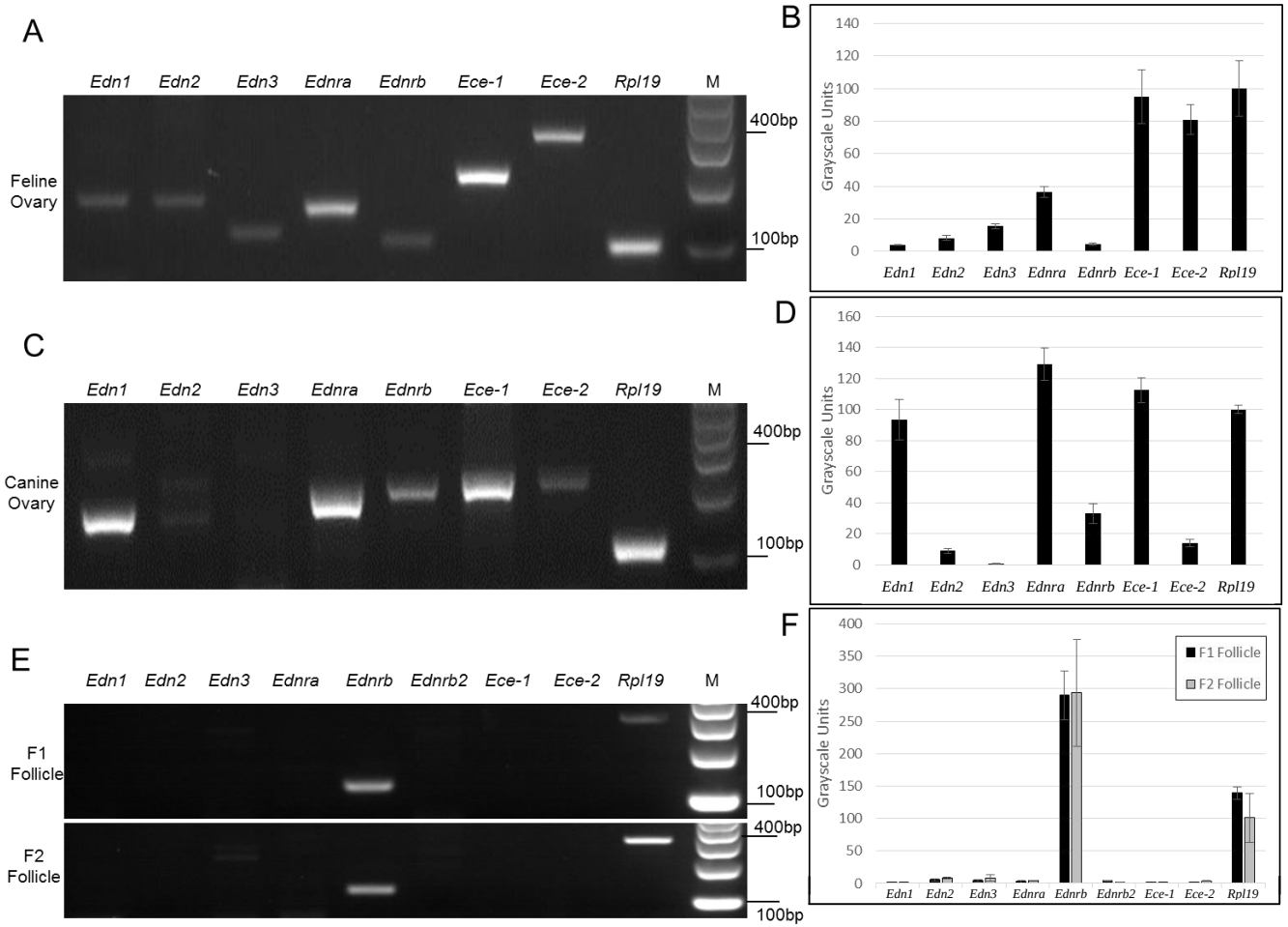

Figure 4.4. Ovaries express ligands, receptors, and enzymes of the endothelin system. **A,B.** Semiquantitative PCR of cDNA generated from RNA extracted from whole feline ovaries (grayscale units, n=5). PCR gel images were analyzed by ImageJ software for relative intensity; all amplicons for a single gene were run and imaged at the same time to reduce variation. **C,D.** Semiquantitative PCR using RNA from whole canine ovaries (n=7). **E,F.** Semiquantitative PCR comparing RNA from chicken F1 and F2 follicular cells (n=6). Expression of *Edn2* is absent in both F1 and F2 follicles.

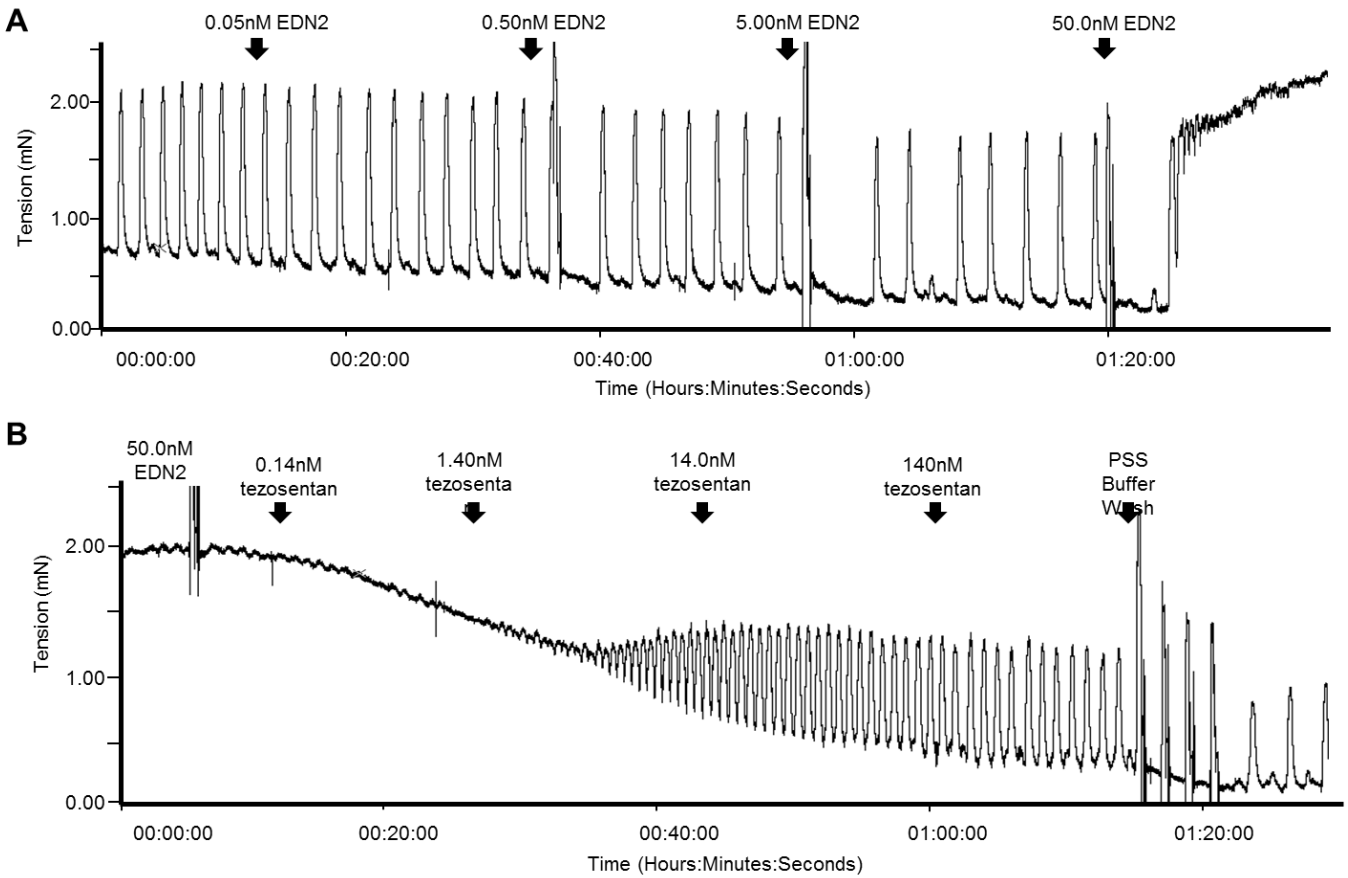

Figure 4.5. Ovaries respond to various doses of EDN2 and endothelin antagonists. A. A representative feline ovary demonstrates continuous peaks for rhythmic spontaneous contraction as increasing doses of EDN2 peptide are applied at 20 minute intervals. Contraction frequency decreases after reaching a solution concentration of 5.00 nM EDN2. A sustained contraction is present after achieving 50nM EDN2. A 5-10 minute time lapse occurs between dosing with 50nM EDN2 and ovarian contraction in response. **B.** A representative feline ovary, after stimulation with 50nM EDN2, decreases in contractile tension in response to increasing doses of an endothelin receptor antagonist drug, tezosentan. After reaching 1.40nM tezosentan, spontaneous contractions of low amplitude and high frequency return to the ovary, and increase in amplitude as the dose of the competitive antagonist drug increase. Following washing away of all ligand and antagonist (4 washes), spontaneous contractions return to normal frequency. Vertical axis: tension in millinewtons where 9.81mN = 1.00gram-force. Horizontal axis: Time (Hours:Minutes:Seconds).

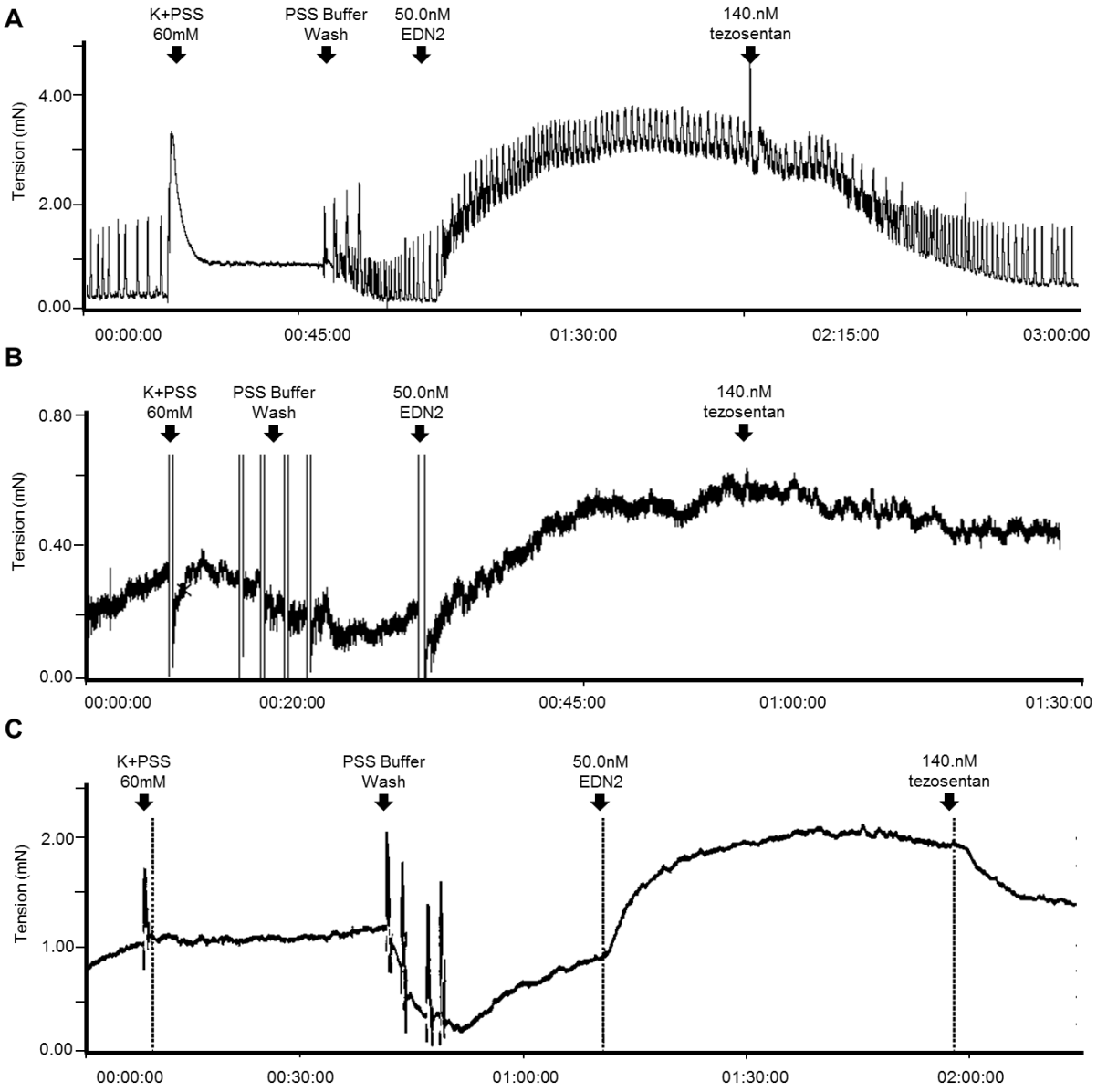

Figure 4.6. Ovaries contract in response to EDN2 peptide and relax during receptor antagonization. **A.** a representative feline ovary response to a 60mM K+PSS solution (for normalization), a 50nM EDN2 solution, and a 140nM tezosentan solution. This ovary demonstrates spontaneous contractions, which are not present during K+PSS exposure. This treatment schema was similarly used to measure responses in **B.** canine and **C.** chicken ovaries. Vertical axis: tension in millinewtons where 9.81mN = 1.00gram-force. Horizontal axis: Time (Hours:Minutes:Seconds).

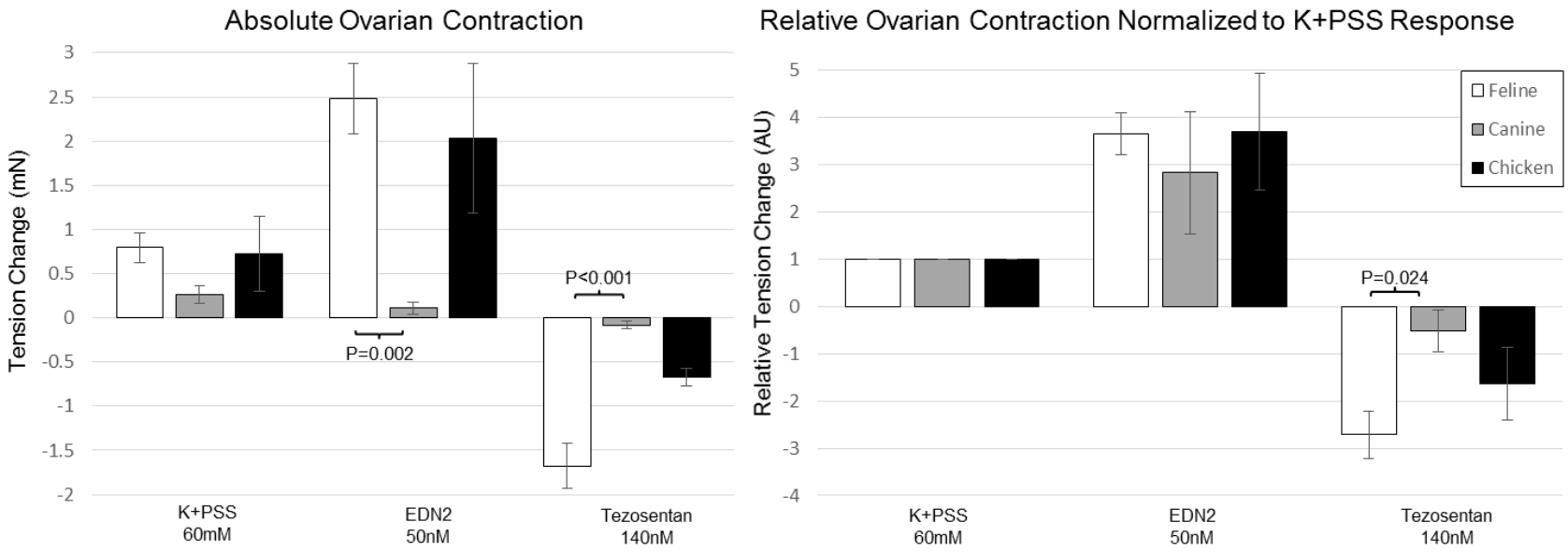

Figure 4.7. Feline, canine, and chicken ovaries respond similarly to EDN2 and tezosentan. Comparison between species of absolute (left) and relative (right) responses to endothelin receptor agonization and subsequent antagonization. Ovarian contraction was normalized to the response to K+PSS to compare relative contractile responses. Significant differences ($p<0.05$) are noted.

CHAPTER 5: GENERATION OF AN ESTROGEN RECEPTOR BETA-ICRE KNOCK-IN MOUSE

Joseph A Cacioppo[1], Yongbum Koo[1,2], Po-Ching Patrick Lin[1], Sarah A Osmulski[1], Kee Jun Kim[1], Arnon Gal[1], and CheMyong Ko[1]*

[1]Comparative Biosciences, College of Veterinary Medicine, University of Illinois, Urbana-Campaign, IL 61802, USA
[2]School of Biological Sciences, Inje University, Gimhae, South Korea.

*Corresponding author
CheMyong Ko, Ph.D.
Department of Comparative Biosciences
College of Veterinary Medicine
University of Illinois at Urbana-Champaign
3806 VMBSB, MC-002
2001 South Lincoln Avenue
Urbana, IL 61802, USA
217-333-9362 (office), 217-244-1652 (fax)
jayko@illinois.edu

This work was supported by NIH (HD071875 to CK).

Running Title: Esr2-iCre knock in mouse

Key Words: Estrogen receptor beta, Esr2-iCre, Cre recombinase, Knock-in, Granulosa cells

ABSTRACT

A novel knock-in mouse that expresses codon-improved Cre recombinase (iCre) under regulation of the estrogen receptor beta (*Esr2*) promoter was developed for conditional deletion of genes in estrogen receptor beta (ESR2, also ER[b], ERbeta, Estrb, ERβ, NR3A2) expressing cells and for the spatial and/or temporal localization of *Esr2* expression. ESR2 is one of two main estrogen nuclear receptors that alters a wide variety of gene signaling pathways, and is important for maintaining normal fertility in females. It is also implicated in a variety pathologies affecting ranging from immunologic function to memory to cardiovascular health. A cassette was constructed that contained iCre, a polyadenylation sequence, and a neomycin selection marker. It was inserted in front of the endogenous start codon of the *Esr2* gene in a mouse genome BAC clone and then transferred by homologous recombination to a C57BL/6J embryonic stem (ES) cell line. ES cells were verified and then used to generate females by blastocyst injection. Resulting Esr2-iCre mice were bred with ROSA26-lacZ and Ai9 reporter mice to visualize areas of functional iCre expression. Strong expression, observed as color/fluorescence after reporter crossing, was seen throughout the ovary, the posterior pituitary, the interstitium of the testes, the head and tail but not body of the epididymis, skeletal muscle, the coagulation gland (anterior prostate), acini of the salivary gland, acini of the pancreas, the lung, and the prepucial gland. Additional diffuse or patchy expression was observed in the cerebrum, the hypothalamus, the heart, the adrenal gland, the colon, the bladder, and the pads of the paws. To confirm effect of ovarian gene ablation, Esr2-iCre mice were crossed with progesterone receptor floxed (Pgr-flox) mice. These mice demonstrated significant loss of *Pgr* expression in the ovary, loss of PGR protein staining in the granulosa cells, anovulation, complete loss of fertility, and continued normal estrous cycling. Therefore, Esr2-iCre mice will serve as a novel line for conditional gene deletion in *Esr2*-expressing tissues, for generating homozygous *Esr2*-knock out mice, and for differentiating the downstream functions of ESR2 and ESR1. Specifically, Esr2-iCre mice may be used to remove *Edn2* in ovary and determine the effect on ovulation in a more efficient manner than other available granulosa cell-specific Cre mouse lines, as is further discussed in Chapter 6.

INTRODUCTION

Estrogens, and estradiol (E2) in particular, are a group of one of the most important steroid hormones in the human body with a plethora of actions and functions in nearly all organs. Estrogens act primarily through their two cognate receptors, estrogen receptors alpha and beta. Estrogen receptor beta (ESR2, also ER[b], ERbeta, Estrb, ERβ) is a classic nuclear receptor[356] with widespread expression throughout the body. It has also been demonstrated and confirmed that ESR2 can act as a membrane receptor as well[357,358]. The mRNA for *Esr2* has been found at high levels in the ovary, prostate, and hypothalamus with expression also seen in the testis, uterus, bladder, and lung[359-361]. ESR2 also plays a prominent role in many cancer sites, including the breast, bladder, and ovary[362,363]. Additionally, ESR2 has been found to play a critical role specifically within the granulosa cells of the ovary for successful ovulation[364]. Mice that lack ESR2 give birth to fewer and smaller litters[365] that are the result of aberrant expression of over 300 genes in the granulosa cells[366]. These mice also develop bladder and prostate hyperplasia in old age, though future work on the exact pathways underlying ESR2 signaling remains. Current available mouse models include one commercially available (Jackson Laboratories, Bar Harbor, ME) global *Esr2* knockout (KO) that was generated by neomycin cassette insertion[365] and one mouse line with a floxed 3rd exon of *Esr2*[366]. However, no models exist for conditional deletion of genes either downstream of ESR2 or localized to *Esr2*-expressing cells. Therefore, this study aimed to create a novel knock-in mouse that expresses codon-improved Cre recombinase (iCre) under the *Esr2* promotor for conditional gene deletion and localization of global *Esr2* expression. It was hypothesized that this mouse would serve as an excellent model for gene ablation specifically within the granulosa cells of the ovary, and that it would have increased effect relative to previous granulosa cell-specific Cre lines [188,367]. In order to visualize localization of *Esr2* expression, Esr2-iCre mice were crossed with two lines of reporter mice: ROSA26-lacZ[175] and Ai9 mice[177]. Additionally, the Esr2-iCre mice were used to generate homozygous ESR2 knockout mice. Due to the function of ESR2 within the granulosa cells of the ovary, this knock-in model can be utilized for removing genes specifically in granulosa cells and for marking sites of *Esr2* expression. It is an important and useful new tool within the field of reproductive biology.

The choice to develop this model was made following other attempts to remove *Edn2* in the granulosa cells of the ovary using Edn2-Floxed mice (described in the following the chapter). Results with Cyp19-iCre and Pgr-Cre mice did not display total loss of *Edn2* mRNA by RT-PCR.

Thus it was postulated that Esr2-iCre mice could instead be used for ablation of *Edn2* expression, which would in turn cause an impaired reproductive phenotype. The details and outcome of this specific hypothesis is discussed later, and the current chapter will instead first characterize Esr2-iCre mice and their potential ability to remove genes within the ovarian granulosa cells. An understanding of locality of Esr2-iCre recombinase activity is critical for data presented in the following chapter, particularly in comparison to *Edn2* localization as described in Chapter 3.

METHODS

Ethics Statement

This study was carried out in tight accordance with the recommendations in the Guide for the Care and Use of Laboratory Animals of the National Institutes of Health. Animal protocol was approved by the University of Illinois Animal Care and Use Committee (Protocols: 11205 and 14222), and all efforts were made to minimize animal suffering. Animal models generated in this study will be made readily available to the research community.

Targeting Vector Construction

An iCre-polyA-FRT-neo-FRT cassette (3266 bp) was generated similar to previous transgenic study from a pBluescript KS(+)-iCre plasmid[368] and was modified for insertion into the mouse *Esr2* gene. The cassette was inserted before the translational initiation codon of the *Esr2* gene of a BAC clone (ID RP23-342B14) that was purchased from Invitrogen (Carlsbad, CA) by recombineering according to protocols provided by Frederick National Laboratory for Cancer Research[274-276]. Briefly, a homology arm (upstream from ATG at exon 2) was amplified using primer pairs (5'-CGTCGACAAGGCCTCTCGAGCCTC-3', 5'-CGAATTCGAATTAAAAAACCTCCCACACCTC-3') and cloned between the *Eco*R1 site and the *Sal*1 site upstream of the cassette. Another homology arm downstream from ATG was amplified using primer pairs (5'-AGGATCCGGAATAGTAACTTCTCCATGGTAG-3', 5'-CGCGGCCGCGATGTGCTGCAAGGCGATTAAG-3') and cloned the between *Bam*H1 site and the *Not*1 site after the cassette. The cassette with the two homologies was cut with *Eco*R1 and *Not*1, gel purified, introduced into *E. coli* SW106 (heat-induced) carrying the BAC for insertion. Engineered BAC clones were selected on LB plate supplemented with kanamycin (25 mg/liter). The engineered *Esr2* gene was retrieved in a pL253 targeting vector. Briefly, an upstream homology arm (*Not*1/*Hin*dIII fragment) which was amplified with primer pairs (5'-GACGCGTAGACTGCATCTCTGTAGTCCAA-3' and 5'-GAAGCTTGATGCTCTCAGAGACTCACG-3') and a downstream homology arm (*Hin*dIII/*Spe*1 fragment) which was amplified with the primer pairs (5'-AGGCCGAGGCGGCCATGTCCATCTGTGCCTCCTCT-3' and 5'-AGACGTCAACACTGTAGTTCATCACAGCAG-3') were cloned between *Not*1 site and *Spe*1

site of pL253. The resulting plasmid was linearized by *Hin*dIII digestion and introduced into *E. coli* SW106 (heat-induced) carrying the engineered BAC. Retrieved clones were selected on LB medium supplemented with ampicillin (50 mg/liter). The targeting vector was linearized by *Cla*1 digestion and used for ES cell targeting.

Gene Targeting

The cassette was then inserted into the genome of embryonic stem cells (ES cells) at the University of Illinois at Urbana-Champaign Biotechnology Center. C57BL/6N-PRX-B6N #1 mouse black ES cells were purchased from Jackson Laboratory (Bar Harbor, Maine) and maintained in media according to the suppliers instructions. ES cells received cassette DNA through electroporation and homologous recombination at 75% confluence, and were then grown in selection media with G418 (200ug/ml). ES cell DNA was extracted and sent to the Murine Genetic Analysis Laboratory at the University of California Davis. Quantitative PCR, long range PCR, karyotyping, and viral screening were performed on 96 cell lines to ensure insertion of a single copy in the correct orientation without defect. Long range PCR was performed on the 5' end with primers (5'-TGAGATCTAGGTTCAGAAGGAGAAGG-3' and 5'-GGTGCACAGTCAGCAGGTTGGAG-3') to produce a 3352bp band, and on the 3' end with primers (5'-CTGTCCTTGATCCCTTCTCTGTGC-3' and 5'-CGCATCGCCTTCTATCGCCTTC-3') to produce a 3506 bp band. Six ES cell clones were identified as successful for insertion. Cells of one of these lines (#030) were expanded and used for blastocyst injection at the University of Illinois to generate black and white chimeric mice.

Animals Used

Eight chimeric mice containing the Esr2-iCre construct that were at least 50% black in color were produced from surrogate mothers. Five female chimeras were bred with albino WT C57B/6J male mice. The genotype of their offspring was determined by PCR of ear tissue using primers iCre-F (5′-TCTGATGAAGTCAGGAAGAACC-3′) and iCre-R (5′-GAGATGTCCTTCACTCTGAATC-3′)[278] to detect iCre presence. The three-primer set 5'-CAGGTGCTGTTGGATGGTCTTC-3', 5'-CTTAGTTACTCCGGCAGCTTGAAC-3', and 5'AGGGGAAGTAAGGCTTGATGGTGA-3' was later used to determine if mice were hetero- or homozygous for Esr2-iCre. The 3rd female chimera gave birth to a litter of normal size with eight

pups, of which four pups were black in color and all four were positive for the iCre gene. Given its normal fecundity and successful gene transmission, this mouse line was chosen for removal of the neomycin targeting cassette and subsequent breeding with reporter lines. These mice were first bred with B6N.Cg-Tg(ACTFLPe)9205Dym/CjDswJ (FLP) mice (Jackson Laboratory) to remove neomycin, and then backcrossed with WT mice to remove the FLP gene[369]. FLP presence was determined with the primers 5'-AACGGAACAGCAATCAAGAGAGCC-3' and 5'-TGCTTCTTCCGATGATTCGAACTG-3'. For characterization of expression, Esr2-iCre mice were bred with two homozygous reporter lines: B6;129S4-*Gt26Sor*^{tm1Sor}/J (ROSA26) reporter mice were used to visualize expression by X-gal staining[175], and B6;129S6-*Gt26Sor*$^{tm9(CAG-tdTomato)Hze}$/J (Ai9) reporter mice[177] were used to visualize expression by presence of red fluorescent protein (RFP). Of note, cells that are positive by x-gal staining or RFP presence may be either cells that positively express iCre or cells that are progeny of those that have previously expressed iCre. Lastly, Estrogen receptor beta knockout mice (Esr2KO) were used for phenotypic comparison to homozygous Esr2-iCre mice. Esr2KO mice were generated by crossing Esr2-Floxed mice[370,371] with Zp3Cre mice[173] to globally remove exon 3 of *Esr2*. Esr2KO mouse genotypes were confirmed with primers 5'-CTTCTTAGAGGTACGGATCCCAGCCCA-3', 5'-AATCTCTTTGCCTTCCAGAGCTA-3', and 5'-GCATAGCGCAGTTGGTAGAG-3'.

Characterizing Esr2-iCre Expression

Tissues were collected from sacrificed mice and washed two times in cold phosphate buffered saline (PBS). For x-gal staining, tissues were incubated in 4% paraformaldehyde (PFA) on ice for one hour. After again washing twice with PBS, the tissues were placed in individual vials of X-gal staining solution. Tissues were then placed on a shaker to be incubated for 24-48 hours in the dark at 4ºC. Following incubation, tissues were washed three times with PBS, and then incubated in the dark for one hour at room temperature in X-gal holding solution before being re-fixed overnight in 4% PFA at 4ºC. After fixation, gross images were taken of the tissues before tissues were dehydrated and embedded in paraffin blocks. Blocks were sectioned at 5um thickness using the microtome. Slides were then stained with nuclear fast red (Fisher Scientific, Pittsburg, PA) and imaged with an Olympus BX51 microscope. For RFP signal visualization, gross images were taken using a Zeiss SV11 fluorescent microscope immediately after sacrifice. Tissues were then fixed overnight in 4% PFA, embedded in paraffin, and serially sectioned at 5um. Using an

Olympus BX51 microscope, raw sections were used for fluorescence visualization; adjacent slides were stained with hematoxylin and eosin (Thermo Scientific, Kalamazoo, MI) to histologically confirm structures. Embryos were collected from pregnant females and fixed similar to whole organs prior to x-gal staining. Estrus cyclicity was determined by vaginal smears according to published guidelines for mice [116]. Vaginas were flushed with PBS and cell size, morphology, and nucleus presence were determined by bright-field microscopy.

Quantifying Esr2-iCre gene ablation: progesterone receptor

To quantify efficiency of Esr2-iCre gene ablation within the female reproductive tract and phenotypically demonstrate proof of concept, Esr2-iCre mice were crossed with progesterone receptor-floxed (Pgr-Flox, PgrF/F) mice[243]. These mice have a floxed second exon. After breeding, mice were superovulated as above and ovary, oviduct, and uterine tissues were collected 6 hours after hCG was administered. Semi-quantitative RT-PCR was performed to quantify *Pgr* expression in the reproductive tissues using the primers Pgr_RT_F 5'-GTGCTTACCTGTGGGAGCTGC-3' and Pgr_RT_R 5'-TCCGGAAACCTGGCAGAGAT-3' at 28 cycles with an annealing temperature of 58°C to produce a 481 basepair band, where the forward primer binds in the second exon and the reverse primer binds to exons four and five. RNA was extracted using Trizol® solution (Ambion, Carlsbad, CA), and then purified with a Qiagen RNEasy Kit (Valencia, CA). RNA was analyzed by a Nanodrop machine for quantity and quality. Complementary DNA was then generated by M-MLV Reverse Transcriptase using random primers. Template RNA quantities were normalized prior to reverse transcription. Amplified DNA (4.0 μL) was visualized on a 2.0% agarose gel and was quantified using ImageJ freeware (NIH, Bethesda, MD) to measure peak pixel grayscale levels within the defined areas of the bands. The ribosomal 60S subunit L19 (*Rpl19* gene; L19) was used as an internal control with (5'-CCTGAAGGTCAAAGGGAATGTG-3' and 5'-GTCTGCCTTCAGCTTGTGGAT-3') to produce a 79 basepair band.

Immunohistochemistry

To compare with other granulosa-cell specific knockout animals, Pgr-Flox mice were bred with both Esr2-iCre mice and Cyp19-iCre mice, the latter of which express Cre under the aromatase promoter which is expressed in granulosa cells during the secondary follicle stage[372]. Mice of each genotype as well as controls were superovulated and tissues collected from hCG6

hours were fixed in 4% PFA, dehydrated, embedded in paraffin wax, sectioned at 5um, and used for immunohistochemical (IHC). IHC was performed by P.L and A.G. Slide deparaffinization was achieved by drying the slides in an oven at 60˚C for 20 min followed by incubation for 5 min 3 times in xylene, and for 2 min twice in 100% alcohol, once each in 90% and 70% alcohol, and once in running tap water. Heat-induced antigen retrieval was achieved by incubating the slides for 1 hour in 10 mM sodium citrate buffer pH 6.0, 0.05% Tween-20 solution in a vegetable steamer. Slides were then cooled to room temperature, rinsed under tap water, and incubated for 20 min in 3% H_2O_2 diluted in water. Following termination of quenching of endogenous peroxides, slides were briefly rinsed under tap water and incubated twice for 5 min in Tris-buffered saline pH-7.6 with 0.1% Tween-20 (TBST; 20 mM Tris, 150 mM NaCl) and blocked for 20 min at room temperature in 5% goat serum (S-1000, vector labs, Burlingame, CA, USA) in Tris-buffered saline pH-7.6 (TBS; 20 mM Tris, 150 mM NaCl) with 1% serum bovine albumin (BSA) and avidin (SP-2001, vector labs, Burlingame, CA, USA) (200 µl/1ml). Following the serum block, a rabbit anti-mouse PGR antibody (A0098, Dako, Carpinteria, CA, USA) in 5% goat serum, TBS (pH 7.6), 1% BSA, and biotin (SP-2001, vector labs, Burlingame, CA, USA)(200 µl/1 ml) solution was applied for 60 min at room temperature in a 1:200 dilution. Slides were then incubated twice for 3 min in TBST, and a secondary biotinylated goat anti-rabbit antibody (Vectastain ABC kit, Vector labs, Burlingame, CA, USA) in 1% BSA was applied for 20 min at room temperature. Slides were then incubated twice for 3 min in TBST and incubated with avidin biotin complex solution (Vectastain Elite ABC kit, Vector labs, Burlingame, CA, USA) for 20 min at room temperature. For chromogen development, 3,3'-diaminobenzidine Nickel (DABN; SK-4100, Vector labs, Burlingame, CA, USA) was applied until color optimally developed.

Fertility Assay

For the fertility assay, control (Pgr-Flox/Flox), Esr2-iCre Pgr-Floxed, and Cyp19-iCre Pgr-Floxed mice were bred for a period of 10 days with proven male breeders. Mice were then separated from males and allowed to give birth. The percentage of females that gave birth from each treatment group, the average number of pups per litter, and the gender distribution of the pups was recorded. Litter sizes describe the number of pups present at birth. Females repeated the breeding assay two to three times. Average age describes the age at the start of mating period. Vaginal cytology was also performed in immature mice (35-60 days of age) prior to fertility assay.

Vaginal smears were assessed according to established methods[116]. A repeated 4-5 day estrous cycle was considered normal; estrous cycles were considered abnormal if estrus was not achieved or if diestrus lasted longer than three days. Additionally, some mice were euthanized at hCG20 hours and reproductive tissues were removed. Oocytes were counted after ampullary dissection of the oviduct and quantified to determine ovulatory ability prior to fertilization and implantation.

Statistical Analysis

Data analyses were performed using statistical software (SPSS, Inc., released 2013, PASW Statistics for Windows, Version 22.0, Chicago, IL). Continuous data were tested for normal distribution by a Shapiro-Wilk test. All normally distributed continuous data were analyzed with parametric tests (student's t-test, ANOVA) and a Bonferroni *post hoc* test. All non-normally distributed continuous data were analyzed by non-parametric tests (Mann Whitney U, Kruskal Wallis ANOVA). Ordinal data were similarly analyzed. Data are graphically presented as the mean and standard error of the mean unless otherwise indicated. For all analyses the alpha value was set to 0.05.

RESULTS AND DISCUSSION

The goal of this work was to generate a novel mouse line that faithfully expresses codon-improved Cre recombinase in place of endogenous estrogen receptor beta (*Esr2*) expression for future use in removing genes within the granulosa cells of the ovary. Generation of a knock-in mouse was chosen ensure that there was as little disruption of the normal *Esr2* promoter as possible, which may DNA sequences upstream, downstream, or within the *Esr2* gene itself. Additionally, though heterozygous mice have a normal phenotype, homozygous knock-in mice may be used as global knockout for the modified *Esr2* gene while retaining the ability to remove Floxed genes through Cre activity in cells that would normally express *Esr2*. Expression of Cre in place of *Esr2* is useful for both removing genes in *Esr2*-expressing cells as well as visually characterizing novel areas of *Esr2* expression.

To generate this model, a bacterial artificial chromosome containing a portion of the *Esr2* gene sequence was purchased as a vector for modification. A cassette containing iCre, a polyadenylation sequence, and an FRT-neomycin-FRT selection marker was inserted into exon 2 of the *Esr2* gene (Figure 5.1A). The second exon contains the functional region of the ESR2 protein. Homologous recombination was used to insert the iCre cassette into exon 2 of the *Esr2* gene within the BAC clone. Two homology arms were amplified from the endogenous *Esr2* gene by PCR and inserted on either side of the cassette, resulting in a total cassette length of 16193 base pairs (Figure 5.1B). The cassette was linearized by *Cla1* digestion, inserted into C57BL/6J black embryonic stem (ES) cells at the University of Illinois, and selected for with neomycin. To confirm single copy number, correct direction, and completeness, ES cell DNA was sent to the Murine Genetic Analysis Laboratory at the University of California Davis (Figure 5.1C). One ES cell colony (#30) was selected for blastocyst injection and chimera generation. One chimera gave birth to a normal number of black pups that were positive for the iCre gene. These offspring were then bred with an FLP mouse to remove the neomycin targeting vector; their pups were crossed to generate a final knock-in Esr2-iCre mouse line that expressed neither FLP nor had the neomycin portion of the cassette (Figure 5.1A).

All following mouse breeding was performed using mice heterozygous for Esr2-iCre to avoid homozygote, and Esr2-knockout mouse, generation. Mice that are heterozygous for Esr2-iCre have lost one functional *Esr2* allele, however this is expected to have little or no impact on reproductive parameters as global Esr2-KO mice are fertile[373]. Loss of both alleles results in fewer

litters and fewer pups per litter, with fewer antral follicles and fewer corpora lutea in the ovaries[373], but possessing a single functional allele is expected to be sufficient to restore function.

The Esr2-iCre mice were crossed with homozygous ROSA26 and Ai9 reporter mice, which produce beta-galactosidase and red fluorescent protein (RFP), respectively, in cells or cell lineages of Cre expression. Esr2-iCre ROSA26 mice and Esr2-iCre Ai9 showed identical reporter expression in tissues examined and otherwise maintained normal phenotypes and fertility; ROSA26 staining data are omitted here as ROSA26 reporter lines have increased background in control tissues relative to Ai9 reporter mice[176,291].

To characterize expression, adult Esr2-iCre Ai9 mice were collected at 2-4 months of age and examined for RFP. Mice were first examined as a whole during dissection, then on the individual organ level, and lastly histologically. Wild-type (WT) mice were sacrificed and imaged as negative controls: no fluorescence was observed grossly in WT mice and little background was observed histologically in unstained sections. However, it was observed that WT tissues that were fixed for more than 24 hours in PFA were subject to increased auto-fluorescence grossly and histologically. Similar increased auto-fluorescence was observed in tissues that were in 70% ethanol for extended periods of time (>2 months). Histological auto-fluorescence could be quenched by quickly staining with Sudan Black B solution (CAS 4197-25-5, Santa Cruz; data not shown), though this also diminishes any normal RFP signal.

The primary interest in generating Esr2-iCre mice was as a tool for the removal of ovarian genes, specifically within the granulosa cells. Expression of *Esr2* has been well characterized in granulosa cells of growing follicles beginning in the primary follicle stage[374-377]. Expression of *Esr2* has been controversial in the oviduct, with rodent and sheep models reporting little to no expression in the adult female reproductive tract outside of the oviduct[377,378], while hormone-dependent expression has been reported in the bovine oviduct[379]. In the immature uterus, expression of *Esr2* has been reported in both the epithelium and the stroma of the mouse[380], while in adults expression is localized in the glandular epithelial cells[381] where it is believed to play a role in modulation of ESR1 activity[380] and also likely to the stroma during days 7-15 of pregnancy[382]. In Esr2-iCre Ai9 mice, RFP was noted grossly in the ovary, oviduct, and uterus (Figure 5.2). Fluorescence was most notable from the ovary, where it was present throughout the granulosa cells as described, as well as the theca cells and stroma cells. This suggests that ovarian *Esr2* expression may be active during development in ovarian precursor cells, or during low levels

in the adult ovary. It must be noted that Ai9 reporter mice will express RFP in any cell that is or has previously expressed, or is descended from a cell that previous expressed, Cre recombinase. The oviduct demonstrated punctate expression in some of the epithelial cells, particularly concentrated towards the ampulla and away from the isthmus. Spotted expression was also observed in a few cells of the muscularis layer about the oviduct. In the uterus, few cells demonstrated RFP expression. These cells were present throughout the epithelium and stroma of the endometrium, and also present in a few myofibrils of the myometrium (Figure 5.2). These data are consistent with previous findings, and indicate that estrogen receptor beta likely does not play a major role in the oviduct or uterus.

In the male reproductive tract, multiple tissues demonstrated red fluorescence, including the testes, epididymis, ductus deferens, coagulation gland (anterior prostate), and prepucial glands (Figure 5.3). In the testes, RFP was present in the interstitium between the seminiferous tubules. This pattern has been previously reported[383], though expression has also been reported in the sertoli cells and germ cells. However, sertoli expression was not observed. Further, germ cell expression was not observed, either in the spermatogonia or spermatids of the testes, or in the sperm themselves visible throughout the epididymis; no pups were born with global RFP expression. This is similar to more recent reports of human *Esr2* expression[384]. Punctate staining was present throughout the epithelium of the rete testes, the head of the epididymis, and the tail of the epididymis, but not the body of the epididymis (Figure 5.3). Similarly, expression was seen in the epithelium of the vas deferens as well. These data are similar to previous reports using immunohistochemical localization[384-386].

In addition to a plethora of other functions, the pituitary and brain (specifically the hypothalamus) are important in reproductive regulation and hormonal feedback loops in both genders. Not surprisingly, both organs had presence of red fluorescence in each gender (Figure 5.4). Expression in the brain and pituitary was similar between genders in adult mice. In the brain, diffuse fluorescence was grossly present throughout the cerebrum, though it was absent in the hindbrain, the cerebellum, and the optical tracts. More marked fluorescence was grossly visible in the hypothalamus, through histologically expression was not observed in the arcuate nucleus. Points of increased fluorescence were also present on the ventral cerebrum, which may represent the Islands of Calleja, a portion of the limbic system[387], though this requires future analyses to confirm. Previous reports on *Esr2* expression in the brain have demonstrated expression in the

olfactory bulb, the amygdaloid nucleus, the medial geniculate nucleus, the posterior hypothalamic nucleus, and the suprachiasmatic nucleus, which are estrogen-dependent[388]. The data presented confirm previous findings, and also implicate additional *Esr2* expression throughout neurons of the cerebrum. Previous studies have also reported pituitary expression of *Esr2*: in fetal rats, ESR2 is present within the developing pituitary from post-natal day 12 (PND12) onward, though expression decreases in the adult and is then limited to the periphery and area adjacent to the intermediary lobe, with no differences between genders[389]. The data confirm previous findings regarding limited expression in the anterior pituitary near the intermediary lobe (Figure 5.4). However, strong fluorescence within the posterior pituitary was also observed in contrast to previous IHC data[389]. This may be reflective developmental expression in the posterior pituitary, especially as these cells are descended from the developing hypothalamus where *Esr2* expression has been previously observed.

Beyond the reproductive organs, *Esr2* has a widespread distribution throughout the body and has also been implicated in multiple types of cancer as well[390-397]. Global survey of Esr2-iCre mice identified RFP in multiple organs (Figure 5.5). In particular, RFP was present in a wavy or patch pattern throughout parts of the adrenal cortex, diffusely present in the detrusor muscle of the bladder, in several cells in a spotted pattern in the mucosa of the colon (but very limited in the gut-associated lymphatic tissues therein), in the most interior layer of the cornea of the eye, in the epicardium and atrial myocardium, throughout the entirety of the lung, in some acini of the pancreas, in the some serous cells of the acini of the salivary glands, and throughout the skeletal muscle fibers (Figure 5.5). A detailed list of all organs examined, as well as previous related literature, are presented in Table 5.1. Future work may specifically identify the cell types or timing of expression within these non-reproductive tissues. The expression of Esr2-iCre within the pancreatic islets is particularly interesting.

Lastly, as proof of concept and to quantify Esr2-iCre gene ablation within the ovary, Esr2-iCre mice were bred with progesterone receptor-floxed mice (*Pgr*-flox/flox, Pgr-F/F)[243]. It has previously been demonstrated that mice globally lacking progesterone receptor fail to ovulate owing to a lack of follicle rupture[70,201,244]. It was hypothesized that mice that were lacking *Pgr* expression in the ovary as a result of Esr2-iCre action would fail to ovulate similar to global progesterone receptor knockout (Pgr-KO) mice after stimulation with exogenous gonadotropins by superovulation. Loss of *Pgr* was tested in the female reproductive tract by RT-PCR. Results

demonstrated that *Pgr* expression, which peaks at hCG6 hours after gonadotropin injection in the ovaries but remains relatively constant in the oviduct and uterus throughout ovulation, was sharply reduced in Esr2-iCre PgrF/F ovaries as expected when examined at hCG6 hours (Figure 5.6A). However, there was no difference in *Pgr* expression in the oviducts or uteri of Esr2-iCre PgrF/F mice at hCG6 hours. These data indicate that Esr2-iCre is capable of gene ablation in the ovary, specifically in the granulosa cells, but not within the oviductal or uterine epithelium or stroma.

In addition to control mice and Esr2-iCre Pgr-Flox/Flox mice, a third genotype of mice were generated by crossing Pgr-Flox mice with Cyp19-iCre mice. Cyp19-iCre mice are established as having granulosa-cell specific expression of Cre recombinase[372], as Cre activity is under the aromatase enzyme promoter which becomes active in granulosa cells during estrogen production in the secondary follicular stage. However, there are also reports that Cyp19-iCre does not completely ablate gene expression within granulosa cells[188]. Immunohistochemistry for PGR in ovaries collected at hCG6 hours from control mice (Figure 5.6B) indicates that PGR is present throughout the granulosa cells of mature / antral follicles. In Cyp19-iCre Pgr-F/F mice, there is decreased staining within granulosa cells of antral follicles of the ovary at this time point, however there are some mural and cumulus granulosa cells that still stain positively (Figure 5.6B). By comparison, Esr2-iCre Pgr-F/F demonstrate no positive staining for PGR within the ovary at hCG6 hours. These data indicate that at the protein level, Esr2-iCre Pgr-F/F mice lack PGR. To test the functional significance of this, a fertility assay was performed with mice of either Cyp19-iCre or Esr2-iCre Pgr-F/F vs control animals (Figure 5.6C). Though there was no difference in fertility or fecundity between control and Cyp19-iCre Pgr-F/F mice, Esr2-iCre Pgr-F/F mice instead gave birth to 0 litters after breeding with 9 different mice ($p<0.001$ relative to control and Cyp19-iCre mice). However, vaginal cytology in all three genotypes of mice indicated normal estrous cycles (data not shown), indicating that Esr2-iCre Pgr-F/F maintain normal hormonal signaling and hypothalamic/pituitary feedback to influence vaginal keratinization. As a final test, to bypass hypothalamic pituitary feedback necessary for the luteinizing hormone surge, immature mice of all three genotypes received superovulation stimulation. Oocytes were collected from the ampulla of the oviduct at hCG20 hours and counted. Control mice ovulated an average of 24.8 oocytes/ovary, while Cyp19-iCre Pgr-F/F mice ovulated only 13.6 oocytes/ovary ($p=0.005$). However, Esr2-iCre Pgr-F/F mice did not ovulate any oocytes from any ovary ($n=10$, $p<0.001$, Figure 5.6D), a phenotype that matches global PR-KO mice.

Overall, these data demonstrate that ovarian PGR activity is likely critical for follicle rupture to proceed during ovulation; future studies may focus on differences in *Pgr* expression and protein in the brain and pituitary as well between Esr2-iCre Pgr-F/F and control mice during ovulation to confirm there were no major differences in PGR action outside of the ovary in this model. In conclusion, novel knock-in Esr2-iCre mice express Cre recombinase in cells and cell lineages that mimic endogenous *Esr2* expression. Cre activity, examined by RFP through Ai9 reporter mice, is present throughout the ovary and functionally ablates gene expression there in a manner superior to Cyp19-iCre mice. Additional high activity is observed throughout the testicular interstitium, the head and tail of the epididymis, in the hypothalamus and generally throughout the cerebrum, in the posterior pituitary, in the lungs, and in the coagulation gland. Homozygous Esr2-iCre mice are also useful as global *Esr2* knockout models. This new animal model will be useful across multiple fields for better understanding the tissue locations and the specific pathways utilized by estrogen receptor beta signaling or by other genes within *Esr2*-expressing cells.

ACKNOWLEDGEMENTS

The authors thank Dr. Lori Raetzman for ROSA26 reporter mice, Dr. Pierre Chambon for Esr2-Flox mice, Dr. Jing Yang for FLP mice and support in cassette generation, Dr. John Lydon for Pgr-Flox mice, Dr. Fuming Pan for embryonic stem cell DNA insertion and generation of chimeric mice, Stephanie Martynenko for vaginal cytology, and Karen Doty for histological assistance.

TABLES

Table 5.1. **Summary of Esr2-iCre expression**. Expression was visualized in multiple tissues in adult intact mice (60+ days of age) through RFP signal after crossing with an Ai9 reporter line. Fluorescence marks cells that may be expressing Cre recombinase or cells that previously have, or have emerged from a cell lineage with a progenitor cell that had, expressed Cre. Continued on multiple pages.

Tissue	Relative Fluorescence	Notes	Select Relevant Literature
Adipose Tissue	-	No fluorescence visualized.	398-400
Adrenal	++	Punctate or streaked fluorescence throughout the three layers of the adrenal cortex; little to none in medulla.	401,402
Aorta	-	Limited fluorescence to skeletal muscle near aorta.	403,404
Bladder	+	Diffuse, weak fluorescence throughout the detrusor muscle.	359,365,393,405
Blood (circulating)	-	No fluorescence seen (in all RBC and WBCs observed).	391,406
Bone (femur)	-	No fluorescence seen in osteocytes, bone marrow.	407,408
Brain	+	Diffuse fluorescence throughout cerebrum and hypothalamus; none in optic chiasm, cerebellum, or hind brain. Marked increased fluorescence at several small points on the ventral surface.	409-413
Coagulation gland (anterior prostate)	+++	Strong fluorescence seen in secretory cells.	407
Colon	++	Diffuse to patchy fluorescence throughout mucosa, stronger and more widespread than in proximal GI tract.	357,414
Ductus (vas) deferens	+	Limited, punctate fluorescence in some luminal epithelial cells; weaker than head and tail of epididymis.	415
Duodenum	+	Limited punctate fluorescence in mucosa and stroma of the submucosa. More points of expression are visible at the more distal portion.	416
Epididymis	++	Strong fluorescence seen in the epithelium of the tubules connecting to the rete and in the head of the epididymis. No fluorescence in the body of the epididymis. Fluorescence again present in the epithelium of the tail of the epididymis.	384,385,417
Esophagus	-	No fluorescence visualized.	418
Eye	+	Fluorescence visible in the most interior cellular layer of the cornea, not present in the lens or retina.	419,420

Table 5.1. Continued from previous page.

Heart	++	Patchy fluorescence in some of the epicardial cells, particularly those near the coronary arteries or surface adipose deposits. Fluorescence also present throughout majority of the myocardial cells of each atrium.	394,421,422
Ileum	+	Limited punctate fluorescence in mucosa and submucosa similar to the duodenum, stronger distally.	416
Jejunum	+	Limited punctate fluorescence in mucosa and submucosa similar to duodenum and ileum.	416
Kidney	+	Little fluorescence visualized, limited to cortex and particularly in some glomeruli when present.	423,424
Liver	-	No fluorescence visualized.	425-427
Lung	+++	Strong fluorescence throughout entirety of lungs and respiratory epithelium.	428-430
Nerve (thoracic vagus)	-	No fluorescence visualized.	396
Ovary	+++	Fluorescence seen throughout ovary, including granulosa cells, theca cells, stromal cells, and epithelial cells. Not seen in oocytes.	362,365,386,431,432
Oviduct	+	Punctate fluorescence in epithelial folds of the proximal oviduct (ampulla). Fluorescence diminished or not present in distal oviduct (isthmus).	379
Pancreas	++	Fluorescence present in endocrine pancreas only within some of the pancreatic acini, approximately 5%.	433
Penis	-	No fluorescence visualized externally.	434
Peyers Patch (Gut-associated lymphatic tissue)	+	Very limited punctate expression visualized within follicles, 0-2 cells/100.	
Pituitary	++	Fluorescence visible throughout cells of the posterior pituitary, none visible in intermediary pituitary, punctate or diffuse expression in medial anterior pituitary with decreased prevalence near lateral edges.	375,435,436
Preputial gland	+++	Fluorescence seen in the majority of acini in both basal and secretory cells.	
Salivary gland	++	Fluorescence present throughout the serous cells of acini, overall spotted pattern histologically.	397,437

Table 5.1. Continued from previous page.

Seminal vesicle	-	No fluorescence visualized	
Skeletal muscle	+++	Obvious, strong fluorescence throughout skeletal muscle throughout the body.	[438-440]
Skin	±	Fluorescence limited to 1-2 cells/hair follicle, otherwise not seen histologically in skin; fluorescence also present on pads of feet.	[441-443]
Spleen	-	No fluorescence visualized.	[444]
Stomach	-	No fluorescence visualized.	[445,446]
Testes	+++	Strong fluorescence in interstitial cells, potentially including Leydig cells; not present in sertoli cells of seminiferous tubules; punctate expression in epithelium lining the rete.	[383,385,386,447]
Uterus	+	Seen in some smooth muscle cells of the myometrium and some epithelial and stromal cells of the endometrium throughout the uterus.	[364,382,448,449]
Vagina	+	Expression seen in the stratified mucosa of vagina in cycling adult mice.	[449]

FIGURES

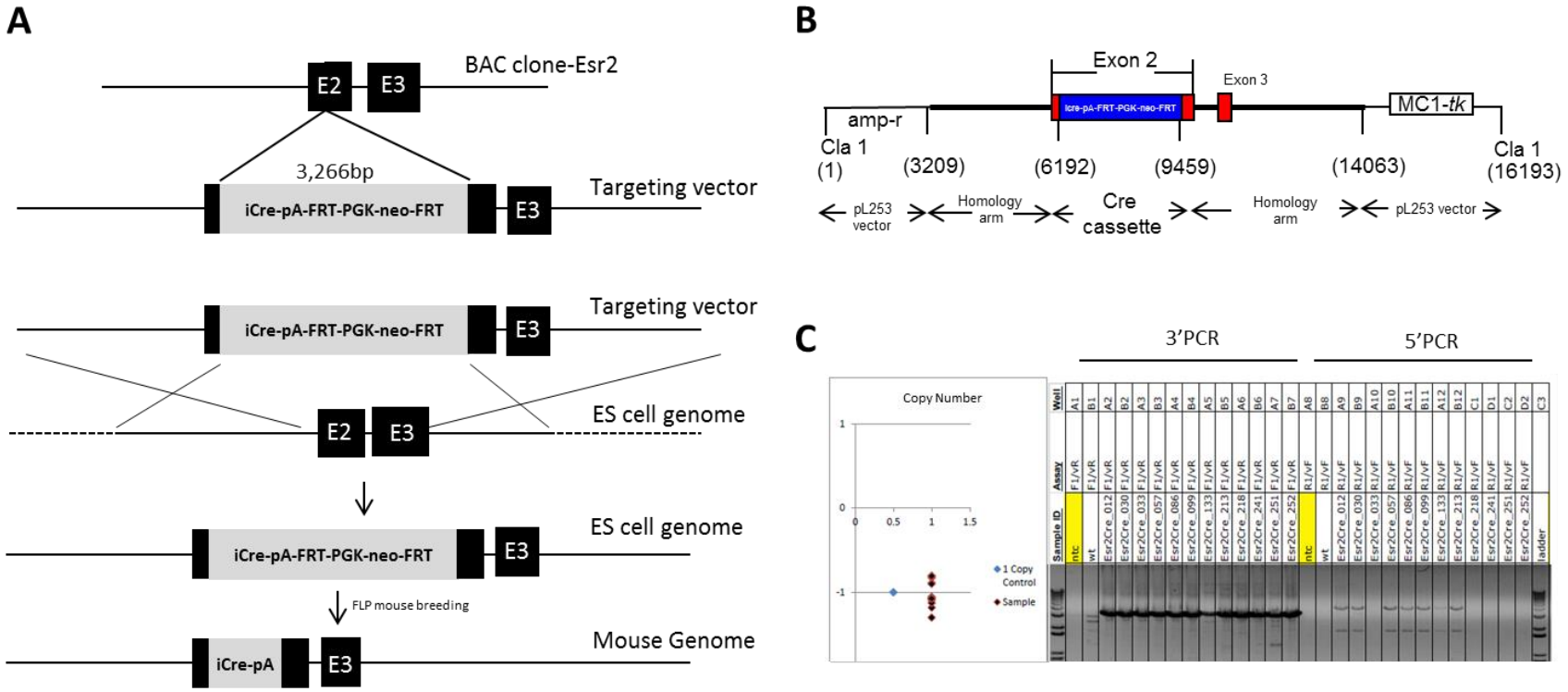

Figure 5.1. Generation of Esr2-iCre mice. To generate mice that faithfully express codon-improved Cre recombinase under regulation of estrogen receptor beta, **A.** an iCre-polyA-FRT-PGK-neomycin-FRT cassette was inserted into exon 2 of the *Esr2* gene in a BAC clone. The targeting vector **B.** was inserted into the genome of C57BL/6J embryonic stem cells using homologous recombination, thus creating a knock-in mouse line. Stem cells were screened for **C.** single copy insertion in the correct orientation using long range PCR. One chimeric mouse that gave birth to multiple black offspring was chosen as a founder and was crossed with FLP recombinase-expressing mice to remove the FRT-PGK-neo-FRT targeting vector.

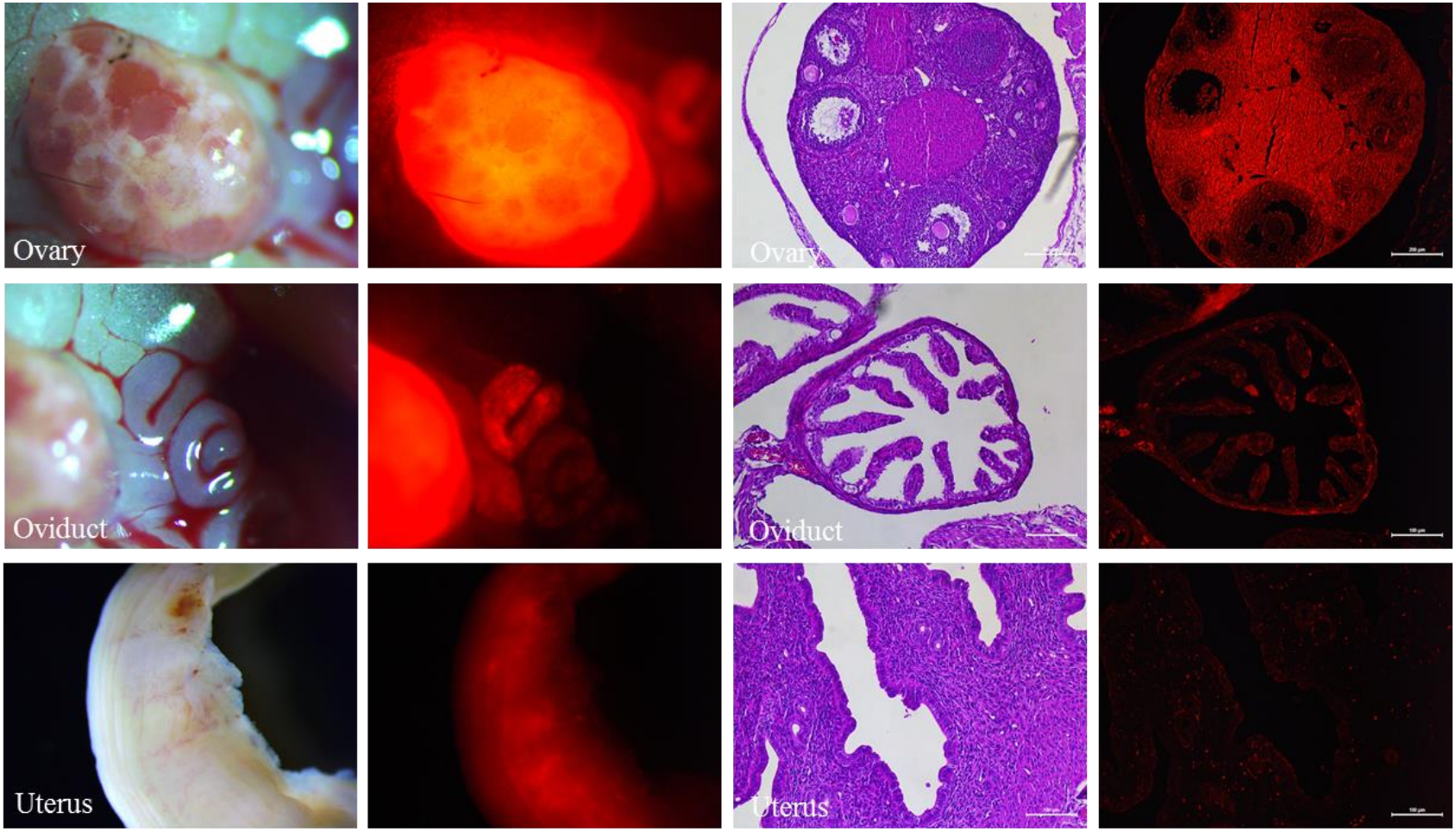

Figure 5.2. Functional expression of Esr2-iCre in the ovary, oviduct, and uterus. Female reproductive organs from post-natal day 120 females were collected; mice were unstimulated and had previously been pregnant. **Top**: Strong fluorescence was seen throughout the ovary, in the granulosa cells as well as the lutein cells of the corpora lutea and the stroma. **Middle**: Punctate fluorescence was seen in the oviduct, particularly in the proximal oviduct (ampulla). Fluorescence was limited to few individual epithelial cells. **Bottom**: In the uterus, diffuse fluorescence was observed throughout. Punctate expression was observed in few cells of both the endometrium (epithelial cells) and myometrium (smooth muscle cells).

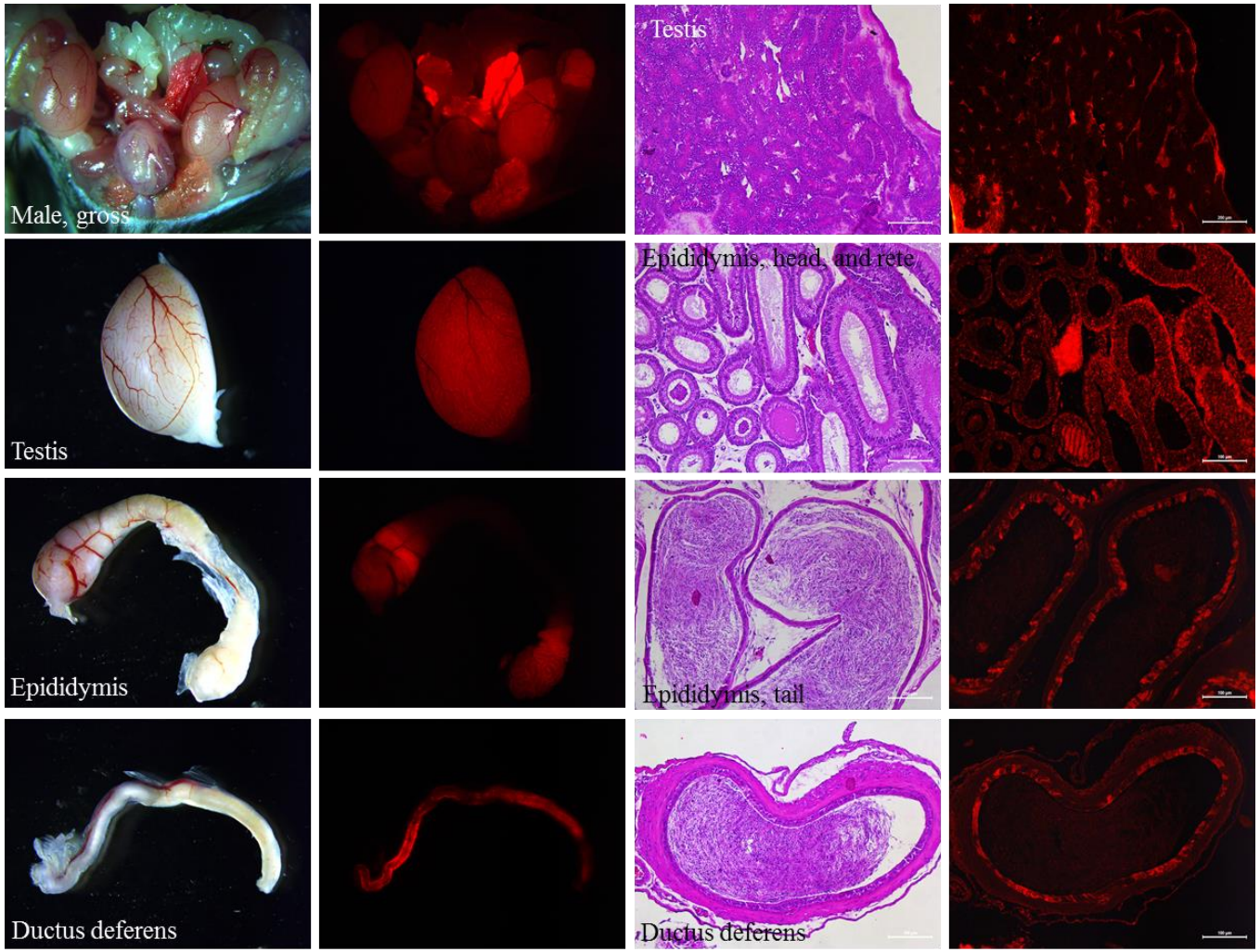

Figure 5.3. Functional expression of Esr2-iCre in the male gonad and accessory organs. Mature post-natal day 60 male mice were sacrificed and organs were fixed for histology. Grossly, fluorescence was observed in the testes, epididymis, vas (ductus deferens), the prepucial glands, and strongly in the coagulation glands (anterior prostate, top left corner). Histological analyses revealed expression in the interstitium of the testes (top right), punctate expression throughout the epithelium of the rete testis, head of the epididymis, and tail of the epididymis (mid-right), and the mucosa of the ductus deferens (bottom right).

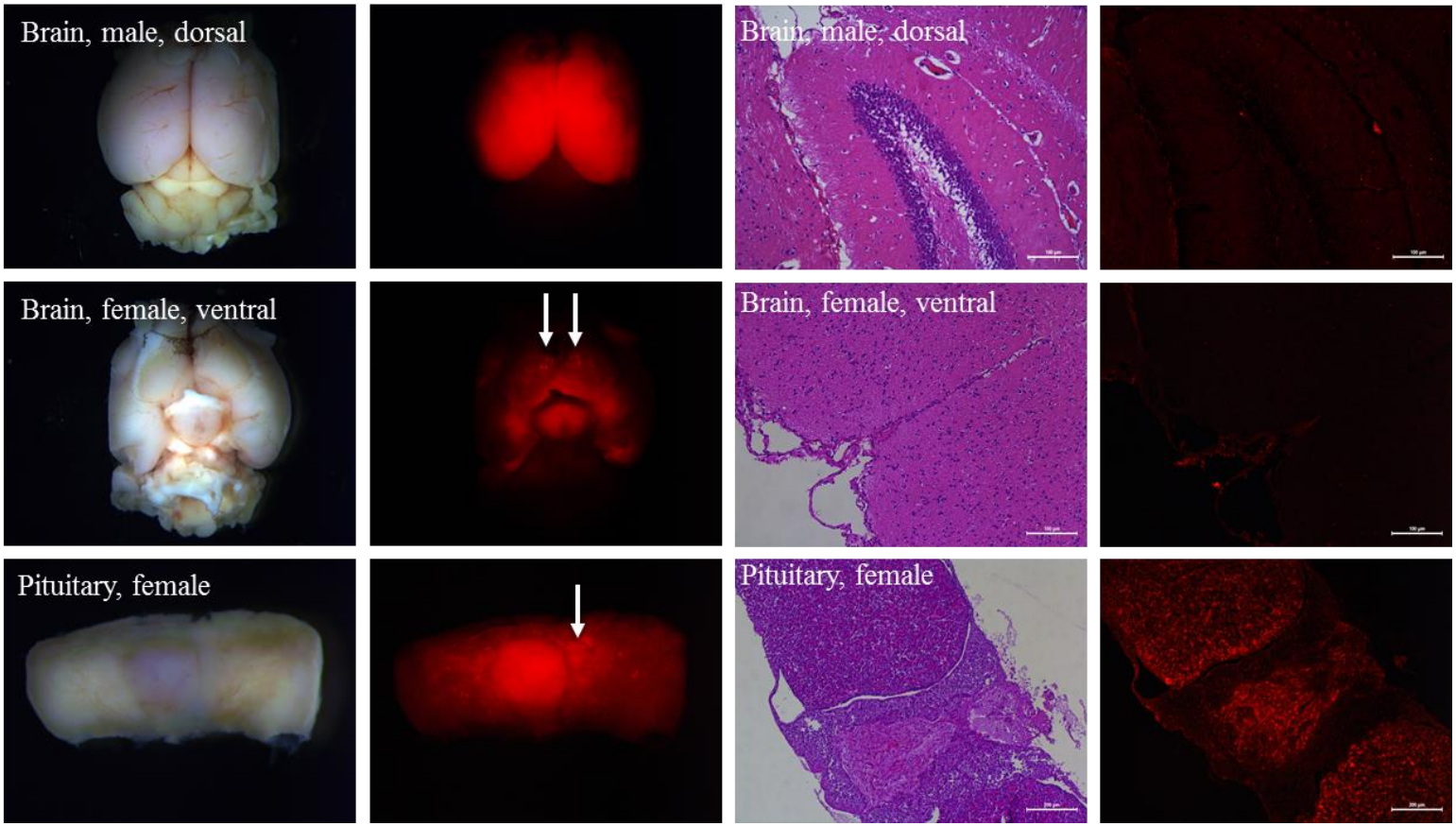

Figure 5.4. Functional expression of Esr2-iCre in the brain and pituitary. Esr2-iCre mice were crossed with Ai9 reporter mice. Adult mice were sacrificed at 2-4 months of age. Expression was similar in both the brain and pituitary of adult mice of each gender. Diffuse expression was observed throughout neurons of the cerebrum, though this was sharply limited to the forebrain. Few neurons in the cerebrum demonstrated RFP. Ventrally, expression was present throughout the hypothalamus and the ventral portion of the cerebrum; expression was absent from the optic nerve chiasm and from the arcuate nucleus (histology images at right, low power above and high power below). Uniquely, expression was observed in bilaterally symmetrical ventral point structures about the olfactory tubercle, which may represent the Islands of Calleja of the limbic system (arrows, ventral brain view). In the pituitary of each gender, expression was prominent throughout the posterior pituitary lobe. Expression was punctate throughout the medial anterior pituitary (arrow), with limited lateral expression. No expression was observed in the intermediary pituitary (histology at right).

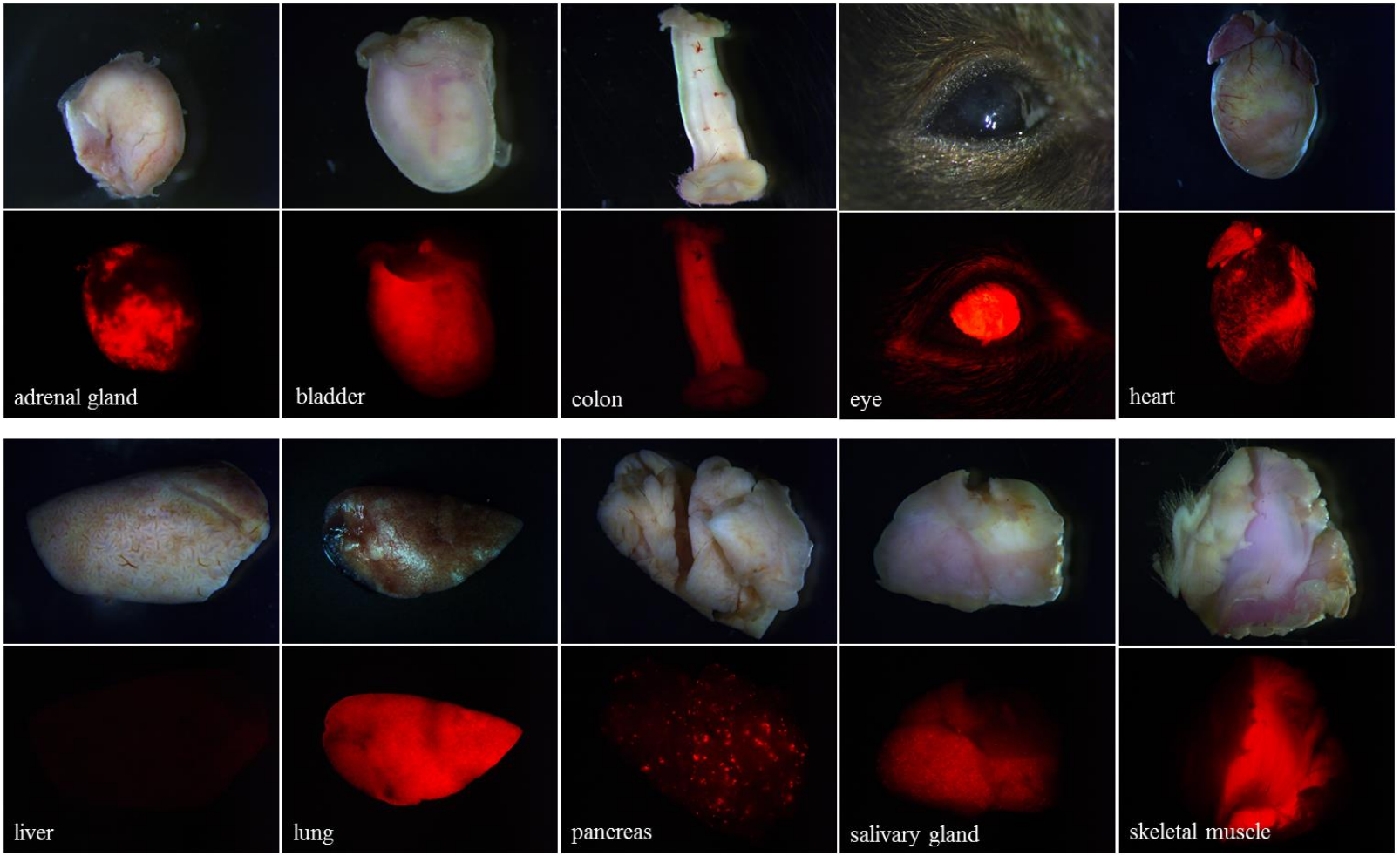

Figure 5.5. Expression of Esr2-iCre throughout the body. Esr2-iCre mice were crossed with Ai9 reporter mice and adult mice were sacrificed at 2-4 months of age. Outside the reproductive organs, multiple other areas of expression were grossly visible. Expression was observed in a wavy and fragmented pattern throughout the adrenal gland which does not correspond to underlying cell layers, consistently throughout the detrusor muscle of the bladder, the mucosa of the distal GI tract (colon, cecum), the interior cornea of the eyes, the epicardium surrounding the coronary arteries, the entirety of the lungs, select acini of the pancreas, the serous-associated acini of the salivary glands, and throughout the skeletal muscle of the body.

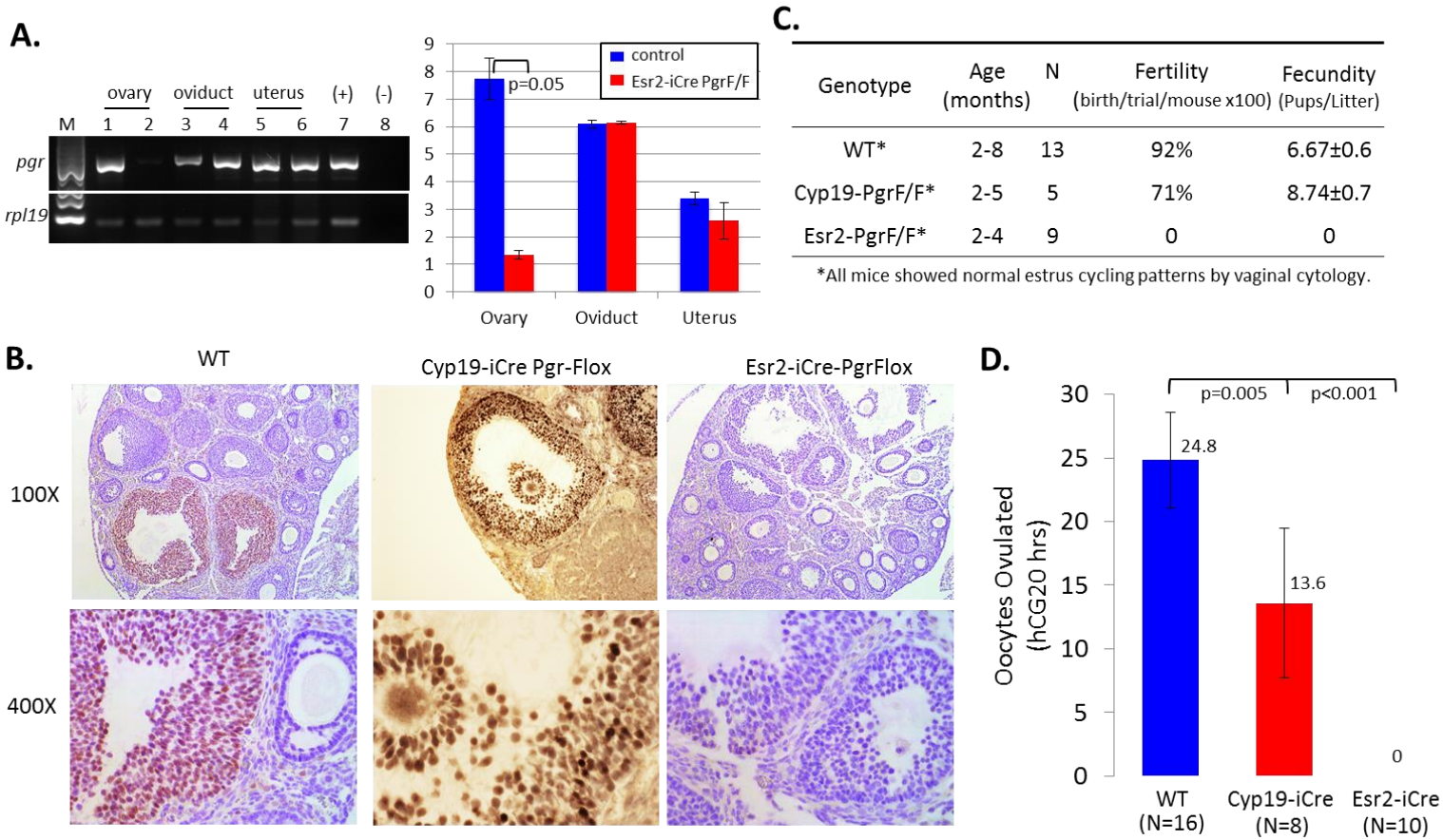

Figure 5.6. Esr2-iCre conditional Pgr-knockout mice are infertile. Esr2-iCre mice were crossed with progesterone receptor floxed (Pgr-floxed) mice. **A.** Semi-quantitative RT-PCR revealed a marked decrease in expression in the ovary, but not in the ovary or uterus. Lanes 1,3,5 are control cDNA and lanes 2,4,6 are Esr2-iCre Pgr-Floxed cDNA; lane 7 is a positive control of cDNA from a WT hCG6 hour ovary and lane 8 is a negative control from PCR mastermix without template. **B.** When checked by IHC for PGR, no positive staining was observed in Esr2-iCre Pgr-Floxed mice, though staining was still present in some granulosa cells of Cyp19-iCre Pgr-Floxed mice. Unlike both control and Cyp19-iCre Pgr-Floxed mice, Esr2-iCre Pgr-Floxed mice, **C.**, were completely infertile and did not give birth to any litters. However, cyclicity by vaginal smear was normal in all mice with 4-5 day estrus cycles. **D.** Lastly, Esr2-iCre mice did not ovulate when stimulated by exogenous gonadotropins to bypass pituitary signaling, confirming that there is efficient ablation of *Pgr* within the ovary, that this ablation is superior to that of Cyp19-iCre mice, and also that ovarian *Pgr* is necessary for ovulation.

CHAPTER 6: INTRAOVARIAN ENDOTHELIN-2 EXPRESSION IS FUNDAMENTAL FOR NORMAL OVULATION AND SUBSEQUENT FECUNDITY

Joseph A Cacioppo[1], Po-Ching Patrick Lin[1], Patrick R Hannon[1], Daniel R McDougle[1], Arnon Gal[1], and CheMyong Ko[1]

[1]Comparative Biosciences, College of Veterinary Medicine, University of Illinois, Urbana-Campaign, IL 61802, USA

*Corresponding author
CheMyong Ko, Ph.D.
Department of Comparative Biosciences
College of Veterinary Medicine
University of Illinois at Urbana-Champaign
3806 VMBSB, MC-002
2001 South Lincoln Avenue
Urbana, IL 61802, USA
217-333-9362 (office), 217-244-1652 (fax)
jayko@illinois.edu

This work was supported by NIH (HD052694 and HD071875 to CK).

Running Title: EDN2 is major player in follicle rupture in ovulation

Key Words: Endothelin-2, Ovulation, Esr2-iCre, Ovary, Edn2KO, Edn2Flox

ABSTRACT

Successful ovulation is inherently dependent upon a myriad of intrinsic ovarian and extrinsic factors that signal for follicular growth, vascularization, leukocyte invasion, and ultimately oocyte release prior to fertilization. Prior to ovulation, granulosa cells of periovulatory follicles transiently produce the potent vasoconstrictor EDN2, a gene product of endothelin-2 (*Edn2*). It was previously shown that antagonization of the endothelin receptor pathway significantly reduces ovulation, indicating a potential role of contraction in ovulation. To determine the significance of EDN2 production in the granulosa cells, the *Edn2* gene was selectively ablated by crossbreeding a floxed *Edn2* (Edn2Flox) mouse with an Esr2-iCre mouse that express codon improved Cre recombinase under the promoter of estrogen receptor beta (*Esr2*). In the ovary, *Esr2* expression begins during follicular recruitment in the primary follicle stage and is spatially limited to the granulosa cells. It was hypothesized that the loss of *Edn2* in granulosa cell results in reduced ovulation and therefore smaller litter size. The ablation of *Edn2* by Esr2-iCre significantly reduced the numbers of ovulated oocytes compared to wild type littermates when treated with gonadotropins for ovulation induction (3.75±0.88 vs 16.36±1.85 oocytes/ovary, p=0.001, respectively). Furthermore, *Edn2* ablation resulted in smaller litters than controls (4.29±1.02 vs 8.50±0.60, p=0.008, respectively). Though fecundity was decreased, the number of pregnancies to term per pairing was not different between groups (p=1.000), implying that some follicles ovulated successfully in the absence of *Edn2* expression. Histological examination showed that the ovaries of the conditional *Edn2* knockout mice had a significantly higher percentage of antral follicles and fewer corpora lutea than controls (p=0.019 and p=0.013, respectively), suggesting that follicles progress to the antral stage but some are unable to rupture at the time of ovulation. RT-PCR profiler array data suggest that EDN2 does not cause transcriptional modification to induce oocyte rupture, but instead acts through its cognate receptors to induce follicular contraction and oocyte expulsion. These data strengthen the hypothesis that the local EDN2 signaling cascade is a key player in driving smooth muscle contraction during ovulation.

INTRODUCTION

Endothelin-2 (*Edn2*) encodes the peptide EDN2 that is expressed in the ovary during ovulation and early luteinization / corpus luteum (CL) formation. *Edn2* mRNA is expressed only in the granulosa cells of mature follicles immediately prior to ovulation, and the entire duration of *Edn2* mRNA expression is about 2 hours[6,7,14,200]. One of three similar endothelin isoforms, EDN2 alone is known to be transiently expressed in the stimulated rodent and human ovary. It has been shown to be necessary for both ovulation and CL formation through pharmacological and knockout mouse approaches[6,7,171]. Recent evidence shows that mice expire from starvation, hypothermia, and/or emphysema when EDN2 is lost globally[223], and that these mice have impaired ovulatory abilities[171]. Thus, EDN2 is an important molecule to study for a variety of roles within human health, and reproduction in particular.

EDN2 has similar receptor affinity to EDN1, and has nearly the same biochemical structure. Each is a 21-residue peptide mediates its action by binding to one of two receptors, EDNRA or EDNRB[208]. However, the physiological and molecular triggers for induction of *Edn2* remain to be further elucidated; to date only hypoxia has been demonstrated to have a significant effect on *Edn2* expression in culture[246,250,252,450], while the effect of progesterone receptor (PGR) on *Edn2* expression has been controversial[7,247]. Regardless of the cause of induction, it is agreed that EDN2 has a profound effect on ovulation by influencing follicle rupture. However, the mechanisms underlying EDN2-modulated follicle rupture have not been directly proven. EDN2 is thought to act through EDNRA[170] receptors on the smooth muscle about the follicle in the theca externa layer and in the associated blood vessels. The gene *Ednra* is highly expressed in vascular smooth muscle cells but is not believed to be expressed in endothelial cells themselves[451]. It also known to be expressed in the theca externa layer around human follicles[14]. Alternatively, EDNRB is expressed largely in endothelial cells[452] where it acts to clear endothelins from circulation[453-456] and induce vasodilator production[457]. EDNRB may be expressed in smooth muscle cells too[458].

The time of *Edn2* expression coincides with ovulation of mature follicles and the initial transformation process to form CL, which are necessary for pregnancy maintenance and progesterone synthesis[241,242]. Given its timing of expression, EDN2 may influence contraction as well as angiogenesis, especially as global EDN2-knockout mice fail to form CL[171]. VEGF plays a central role in ovarian angiogenesis by activating endothelial cells and inducing hypertrophy[88,89]. Luteinizing granulosa cells secrete VEGF, activating VEGF receptors (VEGFR-1 and -2) that are

localized to both endothelial cells and steroidogenic cells[85,86]. Klipper *et al*. (2010) showed that EDN2 directly induces VEGF expression in granulosa cells of the bovine ovary[246]. Angiogenesis continues after VEGF induction with MMP-mediated dissolution of the basement membrane, sprouting of new vessels with proliferating endothelial cells, and eventual vessel anastomosis that is mediated by macrophages[91]. MMP-2 and MMP-9 are known to be significantly elevated in ovarian tumors[255], and at the time of ovulation and luteal formation MMP-2 is elevated in the rat[256-259], while MMP-9 is elevated during ovulation in the mouse[97,244]. MMP activity is critical to allow follicle rupture by weakening the ovarian walls as well as angiogenesis. Tissue inhibitors of metalloproteinases (TIMPs) are highly expressed in the ovary after the LH surge[92-96]. In particular, TIMP-1 mRNA is upregulated 10-fold after the LH surge[260], is released in large quantities during ovulation from the granulosa cells and subsequent lutein cells [97-99], and is highly produced in forming CL[97]. EDN2 may antagonize TIMP-1 action as well, as excessive TIMP-1 is associated with fewer CL, zygotes, and follicles[261,262]. EDN2 has been shown to activate macrophages[270], which secrete and mediate MMP activity; macrophages are trafficked to the ovary during ovulation, are required for ovulation[459-461], and may be critically influenced by EDN2. Together, these data suggest a role for EDN2 in regulating angiogenic, collagenase and proteinase, leukocytic, or proliferative/apoptotic pathways during ovulation and CL formation that should be explored in an *in vivo* functional setting given the involvement of multiple organ systems.

The Cre/LoxP system has been widely used to remove tissue-specific genetic expression and to evaluate resulting physiological changes[462]. To remove *Edn2* specifically in the granulosa cells of the ovary, Cre recombinase expression driven by promoters for the progesterone receptor (*Pgr*, PR-Cre)[463], cytochrome P450 family 19 A1 (aromatase, *Cyp19*; Cyp19-iCre)[367], and estrogen receptor beta (*Esr2*, Esr2-iCre) may be utilized[376,386,464,465]. Previous studies have also used Cre driven by anti-Mullerian hormone type 2 receptor (Amhr2-Cre)[466]. Though all are active within the granulosa cell, each Cre line is first expressed at a different time point in folliculogenesis, ranging from the primary follicle stage (Esr2-iCre)[376,432,435,467] to the secondary follicle stage (Cyp19-iCre)[468-470] to just 6 hours before ovulation (PR-Cre)[199,244]. This allows for removal of *Edn2* at different points during follicular development and targeting at what time point EDN2 translation is ablated, determining if EDN2 is developmentally important in the ovary and allowing for a gradient in phenotypic severity of ovulatory defects. Additionally, a mouse with Cre driven by the zona pellucida protein 3 (Zp3Cre) promoter, which is useful for removing genes only in

oocytes, was used to globally remove *Edn2* to examine its effect on ovarian development and early follicular growth[173].

The aims of this study were to generate and reproductively characterize novel mouse models where *Edn2* was lost throughout the ovary or specifically in the granulosa cells, to specifically determine the effect of *Edn2* loss on the number of oocytes ovulated and overall fertility/fecundity, and to determine if *Edn2* loss causes aberrant ovarian development, folliculogenesis, or CL formation. It was hypothesized that mice lacking *Edn2* in all or part of the ovary will have decreased oocytes ovulated and consequently smaller litter sizes and will form fewer or no corpora lutea, but will maintain normal ovarian development and folliculogenesis to the time of ovulation.

METHODS

Ethics Statement

This study was carried out in tight accordance with the recommendations in the Guide for the Care and Use of Laboratory Animals of the National Institutes of Health. Animal protocol was approved by the University of Illinois Animal Care and Use Committee (Protocols: 13032, 14222, and 14247), and all efforts were made to minimize animal suffering.

Animals Used

Mice were generated by crossing Edn2flox/flox mice purchased from Jackson Laboratory[263] with PR-Cre mice[463], Cyp19-iCre mice[367], and novel knock-in Esr2-iCre mice (Cacioppo *et al*., unpublished, previous chapter) to remove *Edn2* specifically in the granulosa cells at various time points during folliculogenesis, or with Zp3Cre mice[173] to generate global *Edn2* knockout mice (Edn2KO). Genotyping was performed on ear biopsies using the HotShot method[471]. The following five primer sets were used for genotyping:

Edn2Flox_F	CAT AGA GCG GTG AGG CCA CAG	Flox: 170bp
Edn2Flox_R	AAG TTG GCA CCC TTG GTG TTC	WT: 130bp
Edn2KO_R	CTG TTC AGC TGG CAG AGT GAA GC	KO: 400bp
PR-Cre_F1	ATG TTT AGC TGG CCC AAA TG	PR-Cre: 594bp
PR-Cre_F2	CCC AAA GAG ACA CCA GGA AG	WT: 283bp
PR-Cre_R	TAT ACC GAT CTC CCT GGA CG	
iCre_F	TCT GAT GAA GTC AGG AAG AAC C	iCre: 500bp
iCre_R	GAG ATG TCC TTC ACT CTG ATT C	WT: no band
Esr2-iCre_F	CAG GTG CTG TTG GAT GGT CTT C	Esr2-iCre: 401bp
Esr2-iCre_R1	CTT AGT TAC TCC GGC AGC TTG AAC	WT: 181bp
Esr2-iCre_R2	AGG GGA AGT AAG GCT TGA TGG TGA	
Zp3Cre_F	GGA CAT GTT CAG GGA TCG CCA GGC G	Zp3Cre: 250bp
Zp3Cre_R	GTG AAA CAG CAT TGC TGT CAC TT	WT: no band

Fertility Assay

This assay was conducted to determine if mice were capable of giving birth to a normal number of litters with a normal number of pups and gender distribution. Adult female mice, aged two months to seven months, were randomly allocated into groups of two or three females of each

treatment. Each set of females was paired for 10 days with a proven WT male breeder, aged 3 months – 7 months. Females were then removed from the male and separated into individual cages for 21 days and monitored daily. The percentage of females that gave birth from each treatment group, the average number of pups per litter, and the gender distribution of the pups was recorded. Litter sizes describe the number of pups present at birth. Females repeated the breeding assay two to four times. Average age describes the age at the start of mating period.

Superovulation, RT-PCR, and Histology

Superovulation was performed by single intraperitoneal (i.p.) injection of gonadotropins (5IU pregnant mare serum gonadotropin, PMSG, and 5IU human chorionic gonadotropin, hCG) at 48 hour intervals to 25 day old mice. Mice were sacrificed 12 or 24 hours after hCG injection. At 12 hours after, ovaries were frozen, RNA was extracted using Trizol® solution (Ambion, Carlsbad, CA), and then purified with a Qiagen RNEasy Kit (Valencia, CA). RNA was analyzed by a Nanodrop machine for quantity and quality. Complementary DNA was then generated by M-MLV Reverse Transcriptase using random primers. Template RNA quantities were normalized to 1.0μg/μL prior to reverse transcription. 1.0μL of resulting cDNA from each ovary was used as template for semi-quantitative RT-PCR with 15μL Taq Platinum (Invitrogen) and 0.3μL of each primer per PCR reaction; reactions were cycled 30x for 94°C for 1:00 min, 53°C for 1:00, and 72°C for 1:30. Amplified DNA (3.0 μL) was visualized on a 2.0% agarose gel and was quantified using ImageJ freeware (NIH, Bethesda, MD) to measure peak pixel grayscale levels within the defined areas of the bands. The ribosomal 60S subunit L19 (*Rpl19* gene; L19) was used as an internal control with (5'-CCTGAAGGTCAAAGGGAATGTG-3' and 5'-GTCTGCCTTCAGCTTGTGGAT-3'). Expression of *Edn2* was analyzed with primers (5'-CTCCTGGCTTGACAAGGAATG-3' and 5'-GCTGTCTGTCCCGCAGTGTT-3'). Expression of *Edn1* was analyzed with primers (5'-AGCCGAACTCAGCACCGGAGCT-3' and 5'-ATGATGTCCAGGTGGCAGAAGTAGAC-3'). For quantitative RT-PCR using the Taqman system (Life Technologies), primers Mm0432983_m1 were purchased for *Edn2*, primers Mm02601633_g1 for *Rpl19*, and primers Mm00435628_m1 for *Pgr* (Life Technologies). Taqman reactions were run on an ABI 7500 machine and data were analyzed using the delta delta Ct[472] method. After fixation in the 4% PFA, ovaries from hCG24 hours were embedded in paraffin and sectioned at 5 μm, mounted on charged glass slides, deparaffinized, and rehydrated. Tissues were

then stained with hematoxylin (Harris) and eosin (Surgipath) for cellular visualization for use in follicle counting.

Endothelin Protein Quantification

Soluble endothelins were extracted following protocol of Chakravarthy *et al*. (1994)[473] and measured following protocol by Choi *et al*. (2011)[14]. Briefly, individual whole ovaries from hCG12 hours were placed in individual 1.5mL tubes with 500uL 1M HCl in 100% ethanol, homogenized with a mortar and pestle, and incubated at 4°C for 48 hours on an orbital shaker. Tubes were centrifuged at 2000xg for 30 minutes liquid was transferred to a clean tube. Ethanol was then removed by 1 hour incubation in an unheated vacuum centrifuge to dry protein. To measure endothelin quantity, a commercial ELISA kit (583151) was purchased from Cayman Chemical Company (Ann Arbor, Michigan). Individual ovarian endothelins were constituted with 500uL of EIA buffer and loaded onto the plate, and plates were run according to the manufacturer's instructions. Plates were read at 405nm and analyzed with a quadratic standard curve.

Kidney-Ovarian Transplantation (KOT)

Ovaries from post-natal day six (PND6) mice were removed following CO_2 euthanasia. The PND30-32 recipient female mice were anesthetized by continuous nasal inhalation of isoflurane (2-2.5%) with 1 liter per minute (LPM) of oxygen flow. After appropriate depth of anesthesia is reached, fur was removed from an area centered over the proposed incision sites, 15 mm wide by 30 mm long. The size of the area clipped was proportional to the size of the mouse. Skin was disinfected with surgical iodine and 70% ethanol using sterile applicators. Eye gel/ointment was applied to both eyes to prevent dehydration. The mouse was placed on a heat pad (37°C) to prevent hypothermia during surgery. The donor mouse was placed in ventral-lateral recumbency. A 4-7mm skin incision was made parallel and ventral to the spine midway between the last rib and the iliac crest. An incision was made in the underlying abdominal wall. Forceps were used to spread open the incision to look inside the abdominal cavity and locate the ovary. Forceps were used to grasp and exteriorize the ovarian fat pad. The fat pad was positioned on a 2x2 Versalon sterile sponge so that the ovary was facing the surgeon and the oviduct was ventral. A Moria forceps was placed under the ovary (medial aspect) to clamp the ovarian blood vessels. A second pair of Moria forceps was placed immediately proximal to the first pair and used to shear

the ovary off of the ovarian blood vessels. Before releasing the first forceps, one drop of epinephrine was added to the vascular stump for one minute. The collected ovary was discarded and the fat pad was returned to the body. Next the kidney was exposed through the same incision site and a 2mm incision was made through the kidney capsule on one pole of the kidney. The donor ovary was pushed through the incision and pushed to the opposite pole of the kidney. The kidney was returned to the abdominal cavity. The incision in the abdominal wall was closed with 5-0 or 6-0 absorbable suture with a swaged on needle. The skin incision was closed with the same suture in a simple interrupted pattern or with wound clips. The same procedure was repeated on the opposite side of the mouse to produce a WT ovariectomized mouse (OVX) with one Edn2KO ovary under each kidney capsule. Control mice were also produced with WT ovaries inserted under the kidney capsule. Mice were allowed to recover and skin suture or wound clips were removed 7 days later. Post-surgical mice were transferred to a clean, warm cage. Mice were placed on a paper towel in ventral or lateral recumbency with head slightly extended. A paper towel was placed under the rodent to minimize bedding adhering to the incision site. Each mouse was given a subcutaneous injection of warm sterile saline (1-2 cc/25g body weight) to avoid dehydration. For pain control, carprofen 5mg/kg was be injected subcutaneously. Temperature in the recovery area was controlled to prevent hypothermia during recovery. Supplemental heat was provided by placing the recovery cage on a slide warmer. The cage was warmed to 80-86°F (26.7-30°C) and the animal was provided a means to move away from the heat source once awake. The anesthetized mouse should was observed at least every 10 minutes until it was able to move about the cage on its own to ensure that it did not crawl into a corner and obstruct its nose. Frequent stimulation such as touching and moving the mouse was performed. The followings were interpreted as signs of pain or distress: constant facial expression of discomfort (orbital tightening, nose bulge, cheek bulge, and "pulled back" ear position), facial wiping with the forelimb, licking, biting, and scratching the surgical wound, and additional carprofen was administered every 12 hours.

Serum Steroid Measurement

Progesterone was considered the principle hormone measured and all others were secondary. Samples were prepared by spinning down whole blood after clotting and removing the serum supernatant. 10 μL of mouse serum was mixed with 50 μL methanol and 1 μL of 2 μg/mL D9-progesterone, followed by the rigorous centrifugation. The supernatant was subjected to

LC/MS/MS injection at the Metabolomics Center at the University of Illinois at Urbana-Champaign by Dr. Lucas Li. The standard solutions for the calibration curve used double charcoal-stripped steroid free mouse serum provided by Dr. Kee Jun Kim and followed the same extraction protocol as the serum samples. For detection, samples were analyzed with the 5500 QTRAP LC/MS/MS system (AB Sciex, Foster City, CA) in Metabolomics Lab of Roy J. Carver Biotechnology Center, University of Illinois at Urbana-Champaign. The 1200 series HPLC system (Agilent Technologies, Santa Clara, CA) includes a degasser, an autosampler, and a binary pump. The LC separation was performed on an Agilent Zorbax SB-Aq column (4.6 x 50mm, 3.5μm.) with mobile phase A (0.1% formic acid in water) and mobile phase B (0.1% formic acid in acetonitrile). The flow rate was 0.3 mL/min. The linear gradient was: 0-2 min, 60%A; 6-12 min, 0%A; 12.5-17 min, 60%A. The autosampler was set at 5°C. The injection volume was 5 μL. Mass spectra were acquired under positive electrospray ionization (ESI) with the ion spray voltage of 5500 V. The source temperature was 550°C. The curtain gas, ion source gas 1, and ion source gas 2 were 38, 50, and 65, respectively. Multiple reaction monitoring (MRM) was used to measure progesterone (m/z 315.1-->m/z 97.1) with D9-progesterone used as internal standard (m/z 324.1 --> m/z 100.1).

For additional steroid profiling, samples were prepared by using 20 μL mouse serum sample mixed with 40 μL methanol and 1 μL 2 μg/mL D9-progesterone, followed by the rigorous centrifugation. The supernatant was subject to LC/MS/MS injection. The standards solutions for the calibration curve again used double charcoal-stripped steroid free mouse serum, and followed the same extraction protocol as the serum samples. Samples were again analyzed with the 5500 QTRAP LC/MS/MS system (AB Sciex, Foster City, CA) in Metabolomics Lab of Roy J. Carver Biotechnology Center, University of Illinois at Urbana-Champaign. The LC separation was performed on a Phenomenex C6 Phenyl column (2.0 x 100mm, 3μm.) with mobile phase A (0.1% formic acid in water) and mobile phase B (0.1% formic acid in acetonitrile). The flow rate was 0.25 mL/min. The linear gradient was as follows: 0-1 min, 80%A; 10 min, 65%A; 15 min, 50%A; 20 min, 40%A; 25 min, 30%A; 30 min, 20%A; 30.5-38 min, 80%A. The autosampler was set at 5°C. The injection volume was 5 μL. Mass spectra were acquired under positive electrospray ionization (ESI) with the ion spray voltage of 5500 V. The source temperature was 500 °C. The curtain gas, ion source gas 1, and ion source gas 2 were 36 psi, 50 psi, and 65 psi, respectively. Multiple reaction monitoring (MRM) was used to measure steroids with the following transitions

(Q1-->Q3) with D9-progesterone as internal standard (m/z 324.1 --> m/z 100.1). Progesterone Q1 (m/z): 315.1, Q3 (m/z): 97.0; 5β-corticosterone Q1 (m/z): 349.2, Q3 (m/z): 313.2; deoxycorticosterone/11β-hydroxyprogesterone Q1 (m/z): 331.2, Q3 (m/z): 97.1; pregnenolone Q1 (m/z): 317.1, Q3 (m/z): 299.0.

RT^2 Profiler PCR Array

To conduct a rapid and pathway-focused expression analysis of multiple genes, the female infertility RT^2 Profiler PCR Array (PAMM-164Z, Qiagen) was purchased. Whole ovarian RNA from hCG12 hours was compared between control mice and Edn2Flox/Flox Esr2-iCre mice. Total RNA from ovaries from five to eight mice was pooled for analysis. Six genes were used for normalization. Genes examined and their associated pathways are listed in Tables 6.1 and 6.2. Pathway analysis was conducted by averaging the fold change expression from each gene within a pathway; pathways were grouped by the manufacturing company and were not modified in name or group; data analyses were conducted according to the manufacturer's instructions.

Phenylephrine Treatment

Mice, either WT or Edn2Flox/Flox Esr2-iCre, at 25 days of age underwent superovulation treatment with PMSG and hCG as above. At 11 hours after hCG injection, the treatment group of mice also received injection with 1.0ug phenylephrine HCl dissolved in 100uL of sterile saline. Phenylephrine is a specific alpha-1 adrenergic receptor agonist; binding induces GPCR-mediated vasoconstriction. Oocytes were collected at hCG24 hours from oviducts of treated mice and quantified. As Edn2Flox/Flox Esr2-iCre mice

Statistical Analysis

Data analyses were performed using statistical software (SPSS, Inc., released 2013, PASW Statistics for Windows, Version 22.0, Chicago, IL). Continuous data were tested for normal distribution by a Shapiro-Wilk test. All normally distributed continuous data were analyzed with parametric tests (student's t-test, ANOVA, or paired student's t-test) and a Bonferroni *post hoc* test. All non-normally distributed continuous data were transformed by log function to a normal distribution if possible or analyzed by non-parametric tests (Mann Whitney U, Kruskal Wallis

ANOVA). Ordinal data were similarly analyzed. Data are graphically presented as the mean and standard error of the mean unless otherwise indicated. For all analyses the alpha value was 0.05.

RESULTS AND DISCUSSION

The aim of this study was discover the physiological role of EDN2 during ovulation in the mouse as a translational model for human ovulation. Four new mouse models were generated in which *Edn2* was lost within the granulosa cells of the ovary during the primary follicle, secondary follicle, or preovulatory stage, or throughout the entire ovary following surgical transplantation. The data demonstrated that loss of *Edn2* caused a decrease in litter size because fewer oocytes were ovulated, although mice retained the ability to give birth to healthy pups and to form morphologically and functionally normal corpora lutea.

Generation of Edn2KO mice by Edn2 *exon2 ablation*

First, global *Edn2* knockout mice (Edn2KO) were generated by breeding Edn2Flox mice with Zp3Cre mice, and then crossing heterozygotes as breeders. The Edn2KO mice generated were comparable to previous reports on global *Edn2* loss by Chang *et al.* (2013)[223], though Edn2KO mice used in this study were generated by ablating the second exon which contains the biologically active peptide sequence as opposed to previous work where a neomycin cassette was inserted into the gene. Edn2KO mice here were unhealthy and generally expired by 8-10 days of age (range 0-18 days), despite supplemental heat and nutrition with Peptamen (Nestle). This is earlier than reported by Chang *et al*., who observed expiration at 3-4 weeks[474]. Edn2KO mice in each study were noticeably smaller by post-natal day 6 (PND6) despite heat supplementation, which suggests that observed growth retardation was due to starvation (Figure 6.1). Though not quantified, milk was present in the stomachs and intestines of sacrificed Edn2KO pups similar to control siblings, confirming findings from Chang *et al*. that internal starvation is not due to failure to nurse. Starvation has a powerful impact on reproductive ability; two days of starvation is sufficient to prevent subsequent ovulation in hamsters[475], and gonadotropin stimulation is insufficient to induce follicle development or ovulation after eight days of starvation[475,476]. This suggests that previous observations by Cacioppo *et al*. (2014)[171] in which gonadotropin-stimulated Edn2KO mice failed to ovulate and form corpora lutea (CL) may be, at least partially, due to nutritional deficiencies.

Edn2KO mice have normal follicular development to PND6

Although Edn2KO mice are nearly half the size of their siblings by mass at PND6 (Figure 6.1C), ovarian / follicular development is largely unaffected. Ovaries examined at PND6 appear histologically normal (Figure 6.1B), and demonstrate follicles of all levels of maturity, excluding the antral (tertiary) and preovulatory (Graafian) stages. When these young ovaries were serially sectioned and the numbers of follicles were counted (n=10), there was no difference between Edn2KO and WT in the absolute numbers of germ cells (1032±152 vs 1496±314, p=0.068), primordial (3870±569 vs 3497±385, p=0.520), primary (1482±150 vs 1169±127, p=0.078), or preantral follicles (112±102 vs 41±34, p=0.376) per ovary (Figure 6.2). There was also no difference in the percentage of these follicles relative to total follicle+germ cell number (Figure 6.2), excepting germ cells (16.3±0.9% vs 22.6±2.4%, p=0.007) which were slightly but significantly elevated in Edn2KO PND6 ovaries. These data, in addition to a trend towards a lower percentage of primordial follicles (59.0±1.5% vs 56.9±0.7%, p=0.057) in Edn2KO ovaries (Figure 6.2), indicate that germ cell nest breakdown and/or germ cell maturation into primordial follicles may be slighted retarded. Differences between genotypes may become statistically significant if n-values were greatly increased. However, these data indicate that follicle development and maturation is largely capable of occurring in a time span comparable to control mice, and the total number of germ cells remains intact within the ovary.

Edn2KO KOT ovaries have mature follicles and form CL

To remove confounding systemic effects and focus specifically on the ovary, Edn2KO ovaries and controls were removed at PND6 and grafted under the kidney capsule of OVX WT mice (Figure 6.3A) to generate Edn2KO KOT ovaries and WT KOT ovaries, respectively. Ovaries were allowed to mature to 24 days of age, when response to gonadotropin stimulation is observed in WT intact mice. At grafted ovarian age 24 days (PND50 for the recipient mouse), superovulation as performed and ovaries and sera were collected at hCG12 and hCG24 hours. When histologically examined at hCG24 hours, corpora lutea and antral follicles were present in Edn2KO KOT ovaries similar to WT KOT ovaries and WT intact age-matched mice (Figure 6.3A). Ovaries were misshapen owing to space restriction under the kidney capsule, but were capable of successful follicle maturation and CL formation. Quantitative RT-PCR was performed at hCG12 hours to test that *Edn2* expression remained lost in Edn2KO KOT ovaries, and ovarian cells had not been

replaced by the surgical process. Additionally, *Edn1* expression was examined as EDN1 acts through the same receptors with the same affinity as EDN2[295]. Expression of *Edn2* was effectively 0 in in Edn2KO KOT ovaries, indicating that ovarian EDN2 production did not occur after surgical graft and superovulation (Figure 6.3B). Surprisingly, expression of *Edn1* was also decreased ($p=0.006$), indicating that compensatory expression did not occur. Additionally, there was a trend for decreased *Edn2* expression in WT KOT ovaries at hCG12 hours ($p=0.086$, n=5-7), indicating that the ovarian graft process itself likely impedes the ovarian ability to produce EDN2.

Edn2KO KOT ovaries have oocytes trapped within CL and more AF

No ovulated oocytes were observed under the kidney capsule in either KOT group at hCG24 hours, likely because the collagenous kidney capsule prevented extrusion of antral fluid and the cumulus oocyte complex (COC) from the ovary. As oocytes were not present in the majority of CL from WT KOT ovaries (<20%), oocytes were likely expelled from the follicle and then failed to thrive in the environment under the kidney capsule about the ovary. The number of CL may be considered a marker for potential ovulation, though it must be noted that the recipient mice were old enough to enter a natural estrus and present CL may be resultant from ovarian cycling prior to superovulation. Mouse CL persist for multiple estrous cycles[71]. To quantitatively explore folliculogenesis in Edn2KO KOT mice, ovaries from hCG24 hours were serially sectioned. By absolute count per ovary, there were significantly more antral follicles (AF) and significantly fewer CL in Edn2KO KOT ovaries than in WT intact ovaries, though there was no significant difference with WT KOT ovaries (Figure 6.4). Similarly, there was no significant difference in the percentage of AF or CL in Edn2KO KOT ovaries compared to WT KOT (Figure 6.4, Figure 6.5). However, Edn2KO KOT ovaries had a significantly increased percentage of oocytes trapped within CL compared to both WT intact and WT KOT ovaries (82.6±7.2% vs 11.9±7.0% and 16.8±8.4%, $p=0.004$, 0.004, respectively). These data strongly suggest that oocyte release from the follicle is impaired, but not completely prevented, in Edn2KO-deficient ovaries. Additionally, as there was a greater percentage of AF (64.3±5.2% WT KOT vs 44.8±4.3% intact, $p=0.036$) and decreased percentage of CL in WT KOT ovaries (35.7±5.3%) compared to WT intact (55.2±4.4%, $p=0.036$), the kidney graft itself may partially inhibit corpora lutea formation. No differences in amounts of hemorrhagic follicles were observed (Figure 6.4). No differences in serum hormone concentrations of progesterone, 5β-corticosterone, or deoxycorticosterone (Figure

6.6) were observed at hCG12 or hCG24 hours, though there may be a trend towards decreased progesterone concentrations in Edn2KO KOT ovaries at hCG24 hours (p=0.168). This may be reflective of fewer CL were present, though there is a large degree of variability in serum hormone concentration in all groups. Taken together, these data demonstrate that ovaries may form large antral follicles and functional CL though lacking ovarian EDN2 production, though the ovulatory ability of the ovaries cannot be determined.

Generation of granulosa cell-specific Edn2KO mice

To overcome limitations of surgical tissue transplantation, conditional *Edn2* knockout mice were generated. The genes progesterone receptor (*Pgr*), aromatase (*Cyp19*), and estrogen receptor beta (*Esr2*) are all expressed within the mouse ovary within the granulosa cells. Expression of *Pgr* occurs in preovulatory follicles only six hours before ovulation in the mouse[199,477]; *Cyp19* expression begins in the secondary follicles to allow estrogen production from theca cell-provided testosterone[69,478]; and *Esr2* expression occurs within the granulosa cells of primary follicles following recruitment[432,479]. Thus each of these genes may be used to target granulosa cells with the Cre/LoxP system. Mice expressing Cre recombinase (or codon-improved Cre[172], iCre) under the promoters of each of these genes were crossed with Edn2Flox mice. Mice were superovulated at 25 days of age and tissues were collected at hCG12 and hCG24 hours (Figure 6.7A, top), or mice underwent a fertility assay with proven male breeders in sets of 10 day pairings (Figure 6.7A, bottom). When ovaries were collected at hCG24 hours and histologically sectioned, ovaries from each genotype appeared healthy with immature and antral follicles and corpora lutea present (Figure 6.7B). Many antral follicles were present in Edn2Flox/Flox Cyp19-iCre and Esr2-iCre mice.

Edn2Flox/Flox Esr2-iCre mice gave birth to smaller litters and ovulate fewer oocytes

Fertility assay revealed no significant difference in the percentage of litters born per pairing in any genotype (Figure 6.8A). Occurrence of mating behavior and presence of a vaginal plug were not different between groups. However, the average number of pups per litter was significantly reduced in Edn2Flox/Flox Cyp19-iCre and Esr2-iCre mice compared to WT mice (4.67±0.71 and 4.29±1.02 vs. 8.50±0.60, p=0.022 and 0.008, respectively). Semi-quantitative RT-PCR for *Edn2* revealed a graded decrease in expression relative to the time of Cre expression. Compared to WT

mice (100±10.7%), Cyp19-iCre (17.8±3.2%, p=0.011) and Esr2-iCre (2.4±0.6%, p<0.001) mice had significantly reduced *Edn2* expression at hCG12 hours (Figure 6.8B). No increase in *Edn1* was observed in Edn2Flox/Flox PR-Cre (70.4±9.2%, p=0.214) or Cyp19-iCre mice (67.7±11.3%, p=0.800) when compared to control mice (100%±13.1%), though *Edn1* expression was slightly yet significantly elevated in Edn2Flox/Flox Esr2-iCre mice (148.6±11.4%, p=0.047). Edn2Flox/Flox Esr2-iCre mice demonstrated the greatest reduction in Esr2-iCre expression. To confirm this, quantitative RT-PCR was performed with a Taqman system. Expression of *Edn2* was reduced by 97.6% percent in Esr2-iCre conditional knockout mice (Figure 6.8C). Additionally, endothelin protein expression was significantly reduced in whole ovaries at hCG12 hours as well (Figure 6.8D). Total proteins were measured as antibodies are unable to discriminate between EDN1, EDN2, EDN3, and their prepro-forms. As *Edn1* and *Edn3* expression do not change in WT ovaries during ovulation[199], the increase in endothelin protein from hCG0 to hCG12 is caused by an increase in *Edn2* transcription. Lack of *Edn2* upregulation thus accounts for the difference in endothelin protein content between WT and Edn2Flox/Flox Esr2-iCre mice at hCG12 hours.

To confirm that differences in fertility were due to an ovulatory defect caused by *Edn2* ablation, mice were superovulated and oocytes were collected and counted from the oviduct at hCG24 hours. This bypasses pituitary signaling and accounts for possible delayed ovulation by about 12 hours. Edn2Flox/Flox Esr2-iCre mice had significantly decreased oocytes ovulated (3.75±0.88 vs 16.36±1.85 oocytes per ovary, p<0.001), further suggesting a defect in oocyte expulsion. Follicle counting was performed on Edn2Flox/Flox Esr2-iCre ovaries after serial sectioning, revealing that they had significantly more AF (43.3±4.1 vs 31.3±2.7, p=0.045), a significantly greater percentage of AF (90.5±2.7% vs 77.2±3.9%, p=0.019), and a significantly lower percentage of CL (9.5±2.7% vs 22.8±3.9%, p=0.013) (Figure 6.9). There was no difference in the number of hemorrhagic follicles, and no or few oocytes trapped within CL were observed in any ovary. These data additionally indicate a partial defect in follicle rupture which prevents CL formation after loss of *Edn2*. However, mice may become pregnant to parturition with a normal (21 day) pregnancy period despite giving birth to smaller litters. Additionally, there was no significant difference in serum progesterone concentration at hCG24 hours (Figure 6.10). The ovulation of only four oocytes on average after excessive gonadotropin stimulation and the successful birth of four pups/litter on average indicates that defects are likely exclusively in the ovary though *Esr2* and *Edn2* are both expressed in the uterus[368,382,449]. Overall, the Edn2Flox/Flox

Esr2-iCre mouse demonstrates stark loss of *Edn2* expression, and consequently endothelin proteins, and has obvious defects in follicle rupture from the ovary, and is thus an ideal tool for further investigation of the mechanisms underlying EDN2 function during ovulation.

RT^2 Profiler PCR Array reveals no major changes in Edn2Flox/Flox Esr2-iCre ovaries

Next, to determine what genetic pathways may be modified during ovulation as a consequence of EDN2 loss, an RT^2 PCR Profiler Array (Qiagen) was run to specifically examine genes known to be involved in female infertility. RNA from ovaries at hCG12 hours in Edn2Flox/Flox Esr2-iCre or WT mice was pooled, reverse transcribed to cDNA, and run on the RT^2 plate. The array examines differences in expressions in 84 genes, and normalizes expression to six housekeeping genes. The genes tested and their alternative names are listed in Table 6.1. Complete results from the array are listed in Table 6.2. It was not possible to determine p-values for individual gene expression changes as each gene was only examined once per mouse genotype, but differences in fold expression were calculated and comparisons were made relative to WT ovary expression levels. Of the 84 genes examined, only 10.7% showed greater than a two-fold change in genetic expression (fold regulation) (Figure 6.11A); genes with less than a two-fold change in fold regulation were considered to not demonstrate noteworthy differences. 5.9% of genes were upregulated and 4.7% were downregulated. Progesterone receptor (*Pgr*) had the greatest change in regulation and was upregulated 13.17 fold (Figure 6.11A). Secreted phosphoprotein 1 (*Spp1*) had the greatest downregulation of any gene (-5.28 fold). Other genes modified include *Areg*, *Pgf*, *Cfd*, *Il6*, *F3*, *Hoxa10*, and *Wnt2*. The majority of genes were not much changed as observed by RT^2 array (Figure 6.12).

Gene expression changes reflect lack of ovulation, not direct EDN2 signaling

Of those genes with differing expression, each has been implicated in the ovary or ovulation to some degree. PGR is required for ovulation and knockout mice are completely infertile, and it has highest production at hCG6 hours. It is interesting that EDN2 may downregulate the gene governing its own expression, potentially in a negative feedback loop; alternatively, *Pgr* expression may rise in response to delayed follicle rupture. Interestingly, when compared to unpublished microarray data using global Edn2KO (neomycin insertion) ovaries[171], there was no difference in *Pgr* expression. Amphiregulin is known to be downstream of the *Pgr*

gene, and its upregulation at hCG12 may directly reflect *Pgr* upregulation[480-482]. Amphiregulin may also be a stimulator of RUNX1, and may be upregulated in response to lack of *Edn2* expression[483]. As *Pgr* is upregulated and Pgr-KO mice are infertile, the differences in fertility are likely not modified by *Pgr*. The decrease in *Spp1* expression (also known as osteopontin, *Opn*) may be reflective of the lack of epidermal growth factors that are highly expressed during CL formation; *Spp1* peaks in cultured granulosa cells at hCG16 hours (post-ovulation) and enhances progesterone synthesis in the early luteal phase[484]. Placental growth factor (*Pgf*) is an angiogenic factor similar to VEGF[485] which is slightly upregulated in Edn2Flox/Flox Esr2-iCre ovaries, though there has been little exploration to its role during ovulation. Expression of *Pgf* is directly related to oxygen tension[486]. Hypoxia and hypoxic factors normally increase during ovulation, but as ovulation does not occur in the knockout ovaries, hypoxia may persist and *Pgf* may be slightly upregulated. However, the RT^2 profiler array did not examine expression of hypoxia-inducible factor genes. Previous data from the global Edn2KO ovary microarray indicates that HIF factors are slightly upregulated (1.4-1.7 fold increase), which may cause this mild change in *Pgf*.

Compliment factor D (adipsin, *Cfd*) is a serine protease that is regulated by C3bB[487], which has been implicated in trout ovulation in one study[488] as a potential contractile agent, though expression is highest 12 hours after ovulation in the trout and it is thus likely not involved directly in ovulation. Downregulation of *Cfd* in the Edn2Flox/Flox Esr2-iCre ovaries may result from changes protease activity that are normally necessary for tissue organization after ovulation. Interleukin 6 (*Il6*) is a cytokine and potent mediator of immune responses. It is a known regulator of the COC expansion process[489], and is necessary for LH receptor upregulation during granulosa cell differentiation[490]. As knockout ovaries fail to form as many CL and thus fewer granulosa cells differentiate, it is logical that *Il6* might be consequently downregulated. The observed upregulation of coagulation factor 3 (thromboplastin, tissue factor, *F3*) is surprising, given that there is no difference in observed hemorrhage and that less follicular rupture occurs which would necessitate less coagulation. Coagulation factor 3 is known to be upregulated in women with polycystic ovary syndrome (PCOS), and may be reflective of the retained antral follicles of the *Edn2*-ablated group. *HoxA10* is a homeobox gene necessary for embryonic development of the body axis, but HoxA10 knockout mice survive to adulthood and ovulate normally[491]; females only show modified implantation, while males retain testes. The ninth gene upregulated more than two-fold, *Wnt2*, is a secreted glycoprotein that is expressed in the granulosa cells and works to counteract activing-

stimulated signaling[492]. It has been previously demonstrated that *Wnt2* overexpression has no resultant transcriptional activity, and though *Wnt2* may be modified in response to changed activing levels, it is also unlikely to be directly modified by loss of EDN2.

Genes postulated to be involved in EDN2-mediated changes are not differentially regulated

It has been conjectured that EDN2 modulates ovulation via alteration of angiogenic growth factors, collagenase and proteinase activity, or apoptosis. Relevant genes analyzed in the RT^2 Array are listed in Figure 6.11B, and include *Casp3*, *Esr1*, *Esr2*, *Mmp2*, *Mmp7*, *Mmp9*, *Ptgs1*, *Pgts2*, *Timp1*, *Vegfa*, and *Trp53*. None of these genes had over a two-fold difference in expression either up or down. Additionally, the pathways involved did not show a common directional change in expression, with the exception of estrogen receptors which were both decreased. For instance, *Mmp2* and *Mmp7* showed decreased expression, while *Mmp9* and *Timp1* were upregulated. Such inconsistencies and low changes in expression suggest that the genes, their effect, and their encompassing pathways are largely unchanged by absence of EDN2. To confirm this, the expression changes of all genes within a functional pathway were averaged; pathways were pre-defined by the manufacturer (Table 6.2). No pathway showed an average fold change greater than 1.50 or less than 1.50, showing that in general there was no specific pathway that was modified in response to EDN2 loss. Surprisingly, the pathway that demonstrated the greatest average fold change were the control genes (Figure 6.11); as these controlled for contamination in the sample and the majority were read at above 35 cycles, these data can be ignored. The next two pathways with the greatest change were those described as "General Infertility" and "Receptive / Oocyte Support." As the names suggest, neither pathway has a directed influence on ovulation, but are more closely related to the uterine tissue for which this array was originally designed. The high standard deviation of each suggests that the differences observed are caused by one or two genes per group, such as *Pgr*, that modify the overall average expression change. The only pathway that demonstrated a consistent shift with little variation was upregulation of genes involved in the Cell Cycle (+1.17, Stdev=0.09). This may indicate that a greater percentage of actively growing cells were present in the Edn2Flox/Flox Esr2-iCre ovaries. As fewer cumulus oocyte complexes rupture from these ovaries compared to WTs during ovulation, and the cells of the these complexes are highly active, the overall slight increase in the Cell Cycle pathway may represent an increased amount of cumulus granulosa cells and oocytes per ovary.

The majority of genes were not much changed as observed by RT^2 array (Figure 6.12), which suggests that EDN2 mediates a direct physiological effect through its receptors rather than a transcriptional cascade. EDN2 functions through its receptors to elicit smooth muscle contraction. Muscle cell depolarization is caused by Ca^{2+} influx. Endothelin receptor A stimulates this via a $G_{q/11}$-driven phospholibase C-β pathway and a $G_{12/13}$-Rho kinase pathway[208]. Lack of stimulation of this receptor pathway would fail to cause smooth muscle contraction, which may normally mediate an increase of follicular pressure to cause rupture of the follicular wall. This contraction may also promote local vasoconstriction, which would in turn increase local blood pressure, which could then prompt vessel rupture, bleeding into the periovulatory follicle, an increase in volume and consequential follicle rupture[345,493], and early formation of the corpus hemorrhagicum[494].

Pgr expression is not significantly modified in Edn2Flox/Flox Esr2-iCre mice

To confirm RT^2 Profiler Array findings regarding an elevation in *Pgr* expression, RT-PCR was performed at hCG6 and 12 hours in ovaries from Edn2Flox/Flox Esr2-iCre and control mice using Taqman probes. Results of RT-PCR analysis revealed no significant difference in *Pgr* expression at either time point (Figure 6.13). The same ovaries used in the profiler array were combined with three additional ovaries of each genotype to confirm results. There was a significant difference in *Pgr* expression between ovaries collected at each sampling day. This is attributed to slightly different collection times in individual ovaries and individual variation, where those first ovaries used for the RT^2 Profiler had already likely achieved ovulation and begun forming corpora lutea. As *Pgr* expression rises in CL to allow a feedback loop, the increase in *Pgr*, and thus amphiregulin, is likely caused by differences in timing of collection relative to ovulation and does not reflect differences in gene expression dependent upon EDN2 signaling.

Phenylephrine decreases ovulatory ability and does not restore ovulation to conditional knockout mice

To attempt to restore ovulatory ability to Edn2Flox/Flox Esr2-iCre mice and to test the hypothesis that EDN2 ligand operates through calcium channel-induced contraction, mice were treated with phenylephrine (1.0ug/100mL i.p.) at hCG11 hours. Phenylephrine is an alpha adrenergic agonist, and activates the same three voltage and ligand operated calcium channels as

are triggered by endothelin receptor A signaling[208]. It also has a similar half-life to endothelins. However, addition of phenylephrine did not restore ovulatory ability to Edn2Flox/Flox Esr2-iCre mice (Figure 6.14). In WT mice, phenylephrine treatment significantly reduced ovulatory ability. This is in contrast to previous reports by Branstrom *et al*. (2001)[493]. Phenylephrine acts as a systemic vasoconstrictor, increasing overall blood pressure. The dose used was chosen as it is 1% of the LD50 dose, and is potent without causing vascular changes that could fatally induce hypertension. However, increases in blood pressure are inversely related to changes in follicular pressure[493]. It is most likely here that phenylephrine modifies ovulatory ability in control mice by systemic changes in blood pressure, which similarly fails to restore ovulatory ability in Edn2Flox/Flox Esr2-iCre mice. Differences between these results and previous studies in ovulation may be due to differences in dose administered or strain of mice used. Future work may focus instead on methods to specifically induce calcium channel-dependent contraction within the ovary without modifying global vascular tension as a method to demonstrate ovulatory dependency upon EDN2-induced ovarian contractions.

Conclusions and future directions

In summary, systemic loss of *Edn2* causes early juvenile death, likely through starvation, though ovarian development is little affected by PND6. Whole-ovarian loss of *Edn2* does not prevent CL formation in healthy adult mice, though follicle rupture remains impaired. Granulosa cell-specific loss of *Edn2* at various times during folliculogenesis causes smaller litter size and fewer oocytes ovulated (subfertility), although all mice retain the ability to give birth to healthy pups and to form morphologically normal corpora lutea. The range of severity varies with timing of Cre expression, which is likely because of the time required for Cre recombinase to remove *Edn2*. A novel Esr2-iCre mouse successfully ablates the majority of ovarian *Edn2* expression and protein production during ovulation. These mice have few changes in gene expression at hCG12 hours, though protein is sharply reduced. Interestingly, *Pgr* is upregulated, which may otherwise be normally suppressed by EDN2. As few genes are changed, the cause of subfertility likely occurs through the normal contractile and vasoconstrictive properties of EDN2. These data support that EDN2 acts as a final trigger for ovulation. Speculatively, it may also have an effect on tension in the oviduct or uterus to increase the frequency or intensity of their continual contractions for fluid or germ cell transport. Future studies may focus on the physiological role of EDN2 through

supplementation of endothelins to conditional knockout mice during ovulation compared to other contractile agents that act through unchanged receptor pathways. Successful ovulation in Edn2Flox/Flox Esr2-iCre would be indicative for an EDN2-driven follicular contractile force during ovulation to drive oocyte expulsion and subsequent CL formation.

ACKNOWLEDGEMENTS

The authors thank Dr. Lucas Li for serum hormone measurements, Karen Doty and Dr. Juan Davila for histological assistance, and Dr. Levent Dirikolu for pharmacological advice.

TABLES

Table 6.1. Genes examined in RT^2 Female Infertility Profiler Array. Symbol correlates with NCBI gene database. Housekeeping genes used for normalization are listed last. Continued on multiple pages.

Symbol	Description	Alt. Gene Names
Akt1	Thymoma viral proto-oncogene 1	Akt/ PKB/ PKB/ Akt/ PKBalpha/ Rac
Anxa2	Annexin A2	AW215814/ Cal1h
Apod	Apolipoprotein D	-
Ar	Androgen receptor	AW320017/ Tfm
Areg	Amphiregulin	AR/ Sdgf
Bax	Bcl2-associated X protein	-
Bcl2	B-cell leukemia/lymphoma 2	AW986256/ Bcl-2/ C430015F12Rik/ D630044D05Rik/ D830018M01Rik
C2	Complement component 2 (within H-2S)	-
C3	Complement component 3	AI255234/ ASP/ HSE-MSF/ Plp
Calca	Calcitonin/calcitonin-related polypeptide, alpha	CA/ CGRP-1/ CGRP1/ Calc/ Calc1/ Cgrp/ Ct/ Ctn/ calcitonin
Casp3	Caspase 3	A830040C14Rik/ AC-3/ Apopain/ CASP-3/ CC3/ CPP-32/ CPP32/ Caspase-3/ Lice/ SCA-1/ Yama/ mldy
Ccl5	Chemokine (C-C motif) ligand 5	MuRantes/ RANTES/ SISd/ Scya5/ TCP228
Ccnb1	Cyclin B1	Ccnb1-rs1/ Ccnb1-rs13/ CycB1/ Cycb-4/ Cycb-5/ Cycb1-rs1
Cd55	CD55 antigen	Daf/ Daf-GPI/ Daf1/ GPI-DAF
Cdh1	Cadherin 1	AA960649/ E-cad/ Ecad/ L-CAM/ UVO/ Um
Cfd	Complement factor D (adipsin)	Adn/ DF
Cldn4	Claudin 4	Cep-r/ Cpetr/ Cpetr1
Comp	Cartilage oligomeric matrix protein	TSP5
Crabp2	Cellular retinoic acid binding protein II	AI893628/ Crabp-2/ CrabpII
Csf1	Colony stimulating factor 1 (macrophage)	C87615/ Csfm/ MCSF/ op
Ctnnb1	Catenin (cadherin associated protein), beta 1	Bfc/ Catnb/ Mesc
Cxcl12	Chemokine (C-X-C motif) ligand 12	Pbsf/ Scyb12/ Sdf1/ Tlsf/ Tpar1

Table 6.1. Continued from previous page.

Dkk1	Dickkopf homolog 1 (Xenopus laevis)	mdkk-1
Egf	Epidermal growth factor	AI790464
Egfr	Epidermal growth factor receptor	9030024J15Rik/ AI552599/ Erbb/ Errb1/ Errp/ Wa5/ wa-2/ wa2
Esr1	Estrogen receptor 1 (alpha)	AA420328/ AU041214/ ER-alpha/ ER[a]/ ERa/ ERalpha/ ESR/ Estr/ Estra/ Nr3a1
Esr2	Estrogen receptor 2 (beta)	ER[b]/ ERbeta/ Estrb
F3	Coagulation factor III	AA409063/ CD142/ Cf-3/ Cf3/ TF
Fbn1	Fibrillin 1	AI536462/ B430209H23/ Fib-1/ Tsk
Fn1	Fibronectin 1	E330027I09/ Fn/ Fn-1
Gadd45a	Growth arrest and DNA-damage-inducible 45 alpha	AA545191/ Ddit1/ GADD45
Gast	Gastrin	GAS
Gdf15	Growth differentiation factor 15	MIC-1/ NAG-1/ SBF
Gpx3	Glutathione peroxidase 3	AA960521/ EGPx/ GPx/ GSHPx-3/ GSHPx-P
Hbegf	Heparin-binding EGF-like growth factor	AW047313/ Dtr/ Dts/ Hegfl
Hoxa10	Homeobox A10	Hox-1.8/ Hoxa-10
Hoxa11	Homeobox A11	Hox-1.9/ Hoxa-11
Icam1	Intercellular adhesion molecule 1	CD54/ Icam-1/ Ly-47/ MALA-2
Igf1	Insulin-like growth factor 1	C730016P09Rik/ Igf-1/ Igf-I
Igfbp1	Insulin-like growth factor binding protein 1	-
Il11	Interleukin 11	IL-11
Il15	Interleukin 15	AI503618/ IL-15
Il1a	Interleukin 1 alpha	Il-1a
Il1b	Interleukin 1 beta	IL-1beta/ Il-1b
Il1r1	Interleukin 1 receptor, type I	CD121a/ CD121b/ IL-iR/ Il1r-1
Il6	Interleukin 6	Il-6
Itga4	Integrin alpha 4	CD49D/ Itga4B
Itgav	Integrin alpha V	1110004F14Rik/ 2610028E01Rik/ CD51/ D430040G12Rik
Itgb3	Integrin beta 3	CD61/ GP3A/ INGRB3

Table 6.1. Continued from previous page.

Kdr	Kinase insert domain protein receptor	6130401C07/ Flk-1/ Flk1/ Krd-1/ Ly73/ VEGFR-2/ VEGFR2/ sVEGFR-2
Lama1	Laminin, alpha 1	AA408497/ Lama
Lamc2	Laminin, gamma 2	AA589349
Lep	Leptin	ob/ obese
Lif	Leukemia inhibitory factor	-
Lifr	Leukemia inhibitory factor receptor	A230075M04Rik/ AW061234/ LIF
Maoa	Monoamine oxidase A	1110061B18Rik/ AA407771
Mid1	Midline 1	61B3-R/ DXHXS1141/ Fxy/ Trim18
Mki67	Antigen identified by monoclonal antibody Ki 67	D630048A14Rik/ Ki-67/ Ki67
Mmp2	Matrix metallopeptidase 2	Clg4a/ GelA/ MMP-2
Mmp7	Matrix metallopeptidase 7	MAT
Mmp9	Matrix metallopeptidase 9	AW743869/ B/ MMP9/ Clg4b/ MMP-9/ pro-MMP-9
Msx1	Homeobox, msh-like 1	AA675338/ AI324650/ Hox-7/ Hox7/ Hox7.1/ msh
Muc1	Mucin 1, transmembrane	CD227/ EMA/ Muc-1
Olfm1	Olfactomedin 1	AMY/ AW742568/ Noe1/ OlfA/ Pancortin/ Pancortin3
Pcna	Proliferating cell nuclear antigen	-
Pgf	Placental growth factor	AI854365/ PIGF/ Plgf
Pgr	Progesterone receptor	9930019P03Rik/ BB114106/ ENSMUSG00000074510/ NR3C3/ PR/ PR-A/ PR-B
Prl	Prolactin	AV290867/ Prl1a1
Ptgs1	Prostaglandin-endoperoxide synthase 1	COX1/ Cox-1/ Cox-3/ PGHS-1/ PHS 1/ Pghs1
Ptgs2	Prostaglandin-endoperoxide synthase 2	COX2/ Cox-2/ PGHS-2/ PHS-2/ Pghs2/ TIS10
Sell	Selectin, lymphocyte	AI528707/ CD62L/ L-selectin/ LECAM-1/ Lnhr/ Ly-22/ Ly-m22/ Lyam-1/ Lyam1
Sfrp4	Secreted frizzled-related protein 4	-
Sod1	Superoxide dismutase 1, soluble	B430204E11Rik/ Cu/ Zn-SOD/ CuZnSOD/ Ipo-1/ Ipo1/ SODC/ Sod-1
Spp1	Secreted phosphoprotein 1	2AR/ Apl-1/ BNSP/ BSPI/ Bsp/ ETA-1/ Eta/ OP/ Opn/ Opnl/ Ric/ Spp-1
Stat3	Signal transducer and activator of transcription 3	1110034C02Rik/ AW109958/ Aprf

Table 6.1. Continued from previous page.

Stmn1	Stathmin 1	19k/ Lag/ Lap18/ Op18/ P18/ P19/ Pig/ Pp17/ Pp18/ Pp19/ Pr22/ Smn
Tgfb1	Transforming growth factor, beta 1	TGF-beta1/ TGFbeta1/ Tgfb/ Tgfb-1
Timp1	Tissue inhibitor of metalloproteinase 1	Clgi/ TIMP-1/ Timp
Tnf	Tumor necrosis factor	DIF/ TNF-a/ TNF-alpha/ TNFSF2/ TNFalpha/ Tnfa/ Tnfsf1a
Tnfrsf10b	Tumor necrosis factor receptor superfamily, member 10b	DR5/ KILLER/ Ly98/ MK/ TRAILR2/ TRICK2A/ TRICK2B/ TRICKB
Trp53	Transformation related protein 53	Tp53/ bbl/ bfy/ bhy/ p44/ p53
Vcam1	Vascular cell adhesion molecule 1	CD106/ Vcam-1
Vegfa	Vascular endothelial growth factor A	Vegf/ Vpf
Wnt2	Wingless-related MMTV integration site 2	2610510E18Rik/ Int1l1/ Irp/ Mirp/ Wnt-2/ Wnt2a
Actb	Actin, beta	Actx/ E430023M04Rik/ beta-actin
B2m	Beta-2 microglobulin	Ly-m11/ beta2-m/ beta2m
Gapdh	Glyceraldehyde-3-phosphate dehydrogenase	Gapd
Gusb	Glucuronidase, beta	AI747421/ Gur/ Gus/ Gus-r/ Gus-s/ Gus-t/ Gus-u/ Gut/ asd/ g
Hsp90ab1	Heat shock protein 90 alpha (cytosolic), class B member 1	90kDa/ AL022974/ C81438/ Hsp84/ Hsp84-1/ Hsp90/ Hspcb

Table 6.2. Results from RT^2 Female Infertility Profiler Array. Symbol correlates with NCBI gene database. Housekeeping genes used for normalization are listed last. Comparison is of Edn2Flox/Flox Esr2-iCre whole ovaries relative to age-matched WT ovaries. Pathways are supplied by the RT^2 Profiler and were not modified to focus specifically on the ovary. Comments were automatically generated by the Profiler software and have not been modified. Fold change is resultant from one run using cDNA combined from 5 or 8 ovaries from 5 or 8 mice (n=1), and p-values may not be generated. The Ct threshold was set to 35 (default) and values greater than 35 are recorded as 35. "Comments: A: This gene's average threshold cycle is relatively high (> 30) in either the control or the test sample, and is reasonably low in the other sample (< 30). These data mean that the gene's expression is relatively low in one sample and reasonably detected in the other sample suggesting that the actual fold-change value is at least as large as the calculated and reported fold-change result. This fold-change result may also have greater variations if p value > 0.05; therefore, it is important to have a sufficient number of biological replicates to validate the result for this gene. B: This gene's average threshold cycle is relatively high (> 30), meaning that its relative expression level is low, in both control and test samples, and the p-value for the fold-change is either unavailable or relatively high (p > 0.05). This fold-change result may also have greater variations; therefore, it is important to have a sufficient number of biological replicates to validate the result for this gene. C: This gene's average threshold cycle is either not determined or greater than the defined cut-off value (default 35), in both samples meaning that its expression was undetected, making this fold-change result erroneous and un-interpretable. Fold-Change (2^(- Delta Delta Ct)) is the normalized gene expression (2^(- Delta Ct)) in the Test Sample divided the normalized gene expression (2^(- Delta Ct)) in the Control Sample. Fold-Regulation represents fold-change results in a biologically meaningful way. Fold-change values greater than one indicate a positive- or an up-regulation, and the fold-regulation is equal to the fold-change. Fold-change values less than one indicate a negative or down-regulation, and the fold-regulation is the negative inverse of the fold-change." Continued on multiple pages.

Table 6.2. Continued from previous page.

Position	Symbol	Control Ct	Edn2Flox/Flox Esr2-iCre Ct	Fold Regulation	Comment	Pathway	
A01	Akt1	22.71	23.28	-1.19	C	3	Signal Transduction
A02	Anxa2	21.28	22.07	-1.38		9	Other
A03	Apod	29.80	30.54	-1.34	A	9	Other
A04	Ar	23.99	24.58	-1.21		9	Other
A05	Areg	27.51	25.25	5.97		2	Receptive / Oocyte Support
A06	Bax	24.64	25.03	-1.04		7	Apoptosis
A07	Bcl2	26.49	26.96	-1.11		7	Apoptosis
A08	C2	26.26	26.22	1.29		6	Coagulation
A09	C3	22.07	22.75	-1.28		6	Coagulation
A10	Calca	29.44	29.56	1.15		4	Leukocyte Migration
A11	Casp3	26.22	26.76	-1.17		7	Apoptosis
A12	Ccl5	30.38	30.91	-1.16	B	4	Leukocyte Migration
B01	Ccnb1	24.29	24.45	1.12		5	Cell Cycle
B02	Cd55	24.01	24.35	-1.01		6	Coagulation
B03	Cdh1	25.19	25.59	-1.05		3	Signal Transduction
B04	Cfd	25.21	26.91	-2.60		1	General Infertility
B05	Cldn4	29.38	30.23	-1.44	A	1	General Infertility
B06	Comp	28.34	29.04	-1.30		1	General Infertility
B07	Crabp2	25.05	25.31	1.05		1	General Infertility
B08	Csf1	27.20	27.39	1.10		8	Cytokines
B09	Ctnnb1	21.84	22.17	-1.00		3	Signal Transduction
B10	Cxcl12	24.14	24.76	-1.23		4	Leukocyte Migration
B11	Dkk1	32.84	33.24	-1.06	B	3	Signal Transduction
B12	Egf	30.92	31.17	1.05	B	3	Signal Transduction
C01	Egfr	24.75	25.28	-1.15		3	Signal Transduction
C02	Esr1	24.29	24.81	-1.14		9	Other
C03	Esr2	24.27	24.88	-1.23		1	General Infertility

Table 6.2. Continued from previous page.

C04	F3	23.62	22.87	2.10		6	Coagulation
C05	Fbn1	24.35	24.75	-1.06		4	Leukocyte Migration
C06	Fn1	23.18	23.94	-1.35		4	Leukocyte Migration
C07	Gadd45a	24.19	24.66	-1.11		1	General Infertility
C08	Gast	33.22	33.72	-1.13	B	1	General Infertility
C09	Gdf15	31.75	31.79	1.21	B	1	General Infertility
C10	Gpx3	20.35	21.48	-1.75		1	General Infertility
C11	Hbegf	30.42	30.34	1.31	B	9	Other
C12	Hoxa10	29.18	30.54	-2.05	A	2	Receptive / Oocyte Support
D01	Hoxa11	32.38	32.82	-1.08	B	2	Receptive / Oocyte Support
D02	Icam1	26.74	26.89	1.13		4	Leukocyte Migration
D03	Igf1	22.55	22.73	1.10		9	Other
D04	Igfbp1	33.71	33.57	1.38	B	1	General Infertility
D05	Il11	28.38	28.65	1.04		8	Cytokines
D06	Il15	29.30	29.86	-1.18		8	Cytokines
D07	Il1a	31.72	31.75	1.22	B	8	Cytokines
D08	Il1b	29.96	30.10	1.14	A	8	Cytokines
D09	Il1r1	23.92	24.23	1.00		8	Cytokines
D10	Il6	26.75	28.40	-2.50		8	Cytokines
D11	Itga4	29.23	29.53	1.02		4	Leukocyte Migration
D12	Itgav	22.67	22.44	1.46		4	Leukocyte Migration
E01	Itgb3	25.10	25.81	-1.31		4	Leukocyte Migration
E02	Kdr	25.06	25.27	1.08		9	Other
E03	Lama1	25.67	25.63	1.28		4	Leukocyte Migration
E04	Lamc2	26.19	26.68	-1.13		4	Leukocyte Migration
E05	Lep	31.64	32.12	-1.11	B	2	Receptive / Oocyte Support
E06	Lif	29.00	30.19	-1.83	A	2	Receptive / Oocyte Support
E07	Lifr	24.07	24.74	-1.27		2	Receptive / Oocyte Support
E08	Maoa	27.48	27.83	-1.02		1	General Infertility

Table 6.2. Continued from previous page.

E09	Mid1	23.61	23.14	1.73		9	Other
E10	Mki67	23.91	24.00	1.18		5	Cell Cycle
E11	Mmp2	24.66	25.35	-1.29		4	Leukocyte Migration
E12	Mmp7	31.07	31.54	-1.11	B	4	Leukocyte Migration
F01	Mmp9	30.37	30.54	1.11	B	4	Leukocyte Migration
F02	Msx1	28.70	28.47	1.46		7	Apoptosis
F03	Muc1	30.16	30.32	1.12	B	2	Receptive / Oocyte Support
F04	Olfm1	26.11	26.55	-1.08		1	General Infertility
F05	Pcna	22.13	22.05	1.32		5	Cell Cycle
F06	Pgf	29.53	28.43	2.67		9	Other
F07	Pgr	27.48	24.08	13.17		2	Receptive / Oocyte Support
F08	Prl	32.65	33.26	-1.23	B	9	Other
F09	Ptgs1	27.03	28.26	-1.87		3	Signal Transduction
F10	Ptgs2	23.25	22.74	1.78		3	Signal Transduction
F11	Sell	31.45	31.91	-1.10	B	2	Receptive / Oocyte Support
F12	Sfrp4	20.93	21.78	-1.44		1	General Infertility
G01	Sod1	23.58	23.56	1.26		9	Other
G02	Spp1	24.49	27.21	-5.28		1	General Infertility
G03	Stat3	24.14	24.59	-1.09		3	Signal Transduction
G04	Stmn1	23.48	23.70	1.07		5	Cell Cycle
G05	Tgfb1	24.59	24.72	1.14		5	Cell Cycle
G06	Timp1	24.70	25.68	-1.58		9	Other
G07	Tnf	32.30	31.83	1.73	B	7	Apoptosis
G08	Tnfrsf10b	26.18	26.25	1.19		7	Apoptosis
G09	Trp53	25.53	25.57	1.22		7	Apoptosis
G10	Vcam1	28.12	27.78	1.58		4	Leukocyte Migration
G11	Vegfa	24.41	24.35	1.30		9	Other
G12	Wnt2	33.31	32.61	2.02	B	3	Signal Transduction
H01	Actb	18.70	19.19	-1.13		10	House Keeping Gene

Table 6.2. Continued from previous page.

H02	B2m	20.25	20.56	1.01		10	House Keeping Gene
H03	Gapdh	20.40	20.67	1.03		10	House Keeping Gene
H04	Gusb	26.86	27.13	1.03		10	House Keeping Gene
H05	Hsp90ab1	20.05	20.32	1.04		10	House Keeping Gene
H06	MGDC	34.66	33.78	2.30	B	11	Controls
H07	RTC	35.00	35.00	1.25	C	11	Controls
H08	RTC	35.00	35.00	1.25	C	11	Controls
H09	RTC	35.00	35.00	1.25	C	11	Controls
H10	PPC	23.48	23.47	1.25		11	Controls
H11	PPC	23.52	23.45	1.31		11	Controls
H12	PPC	24.03	23.41	1.92		11	Controls

FIGURES

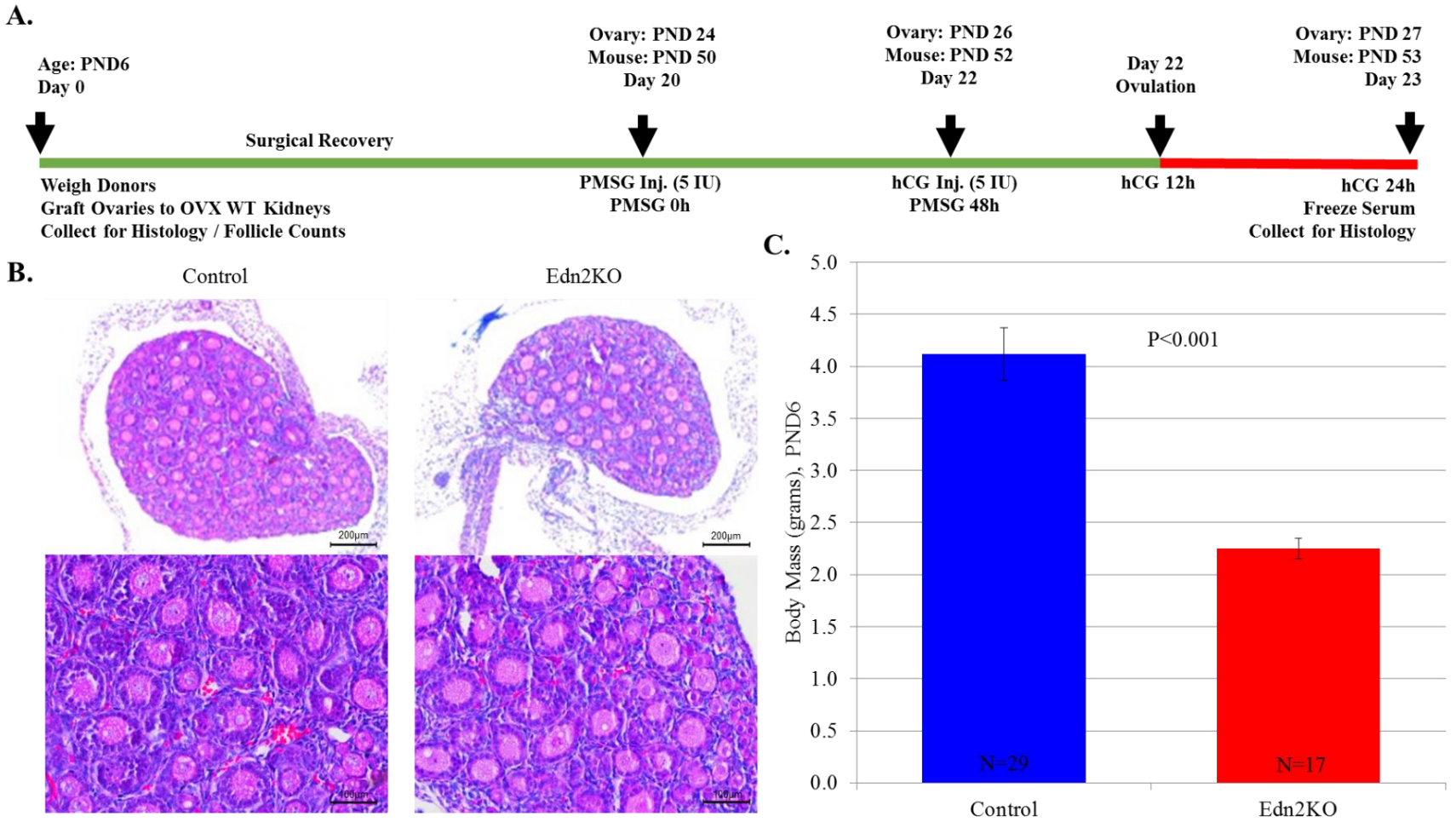

Figure 6.1. Edn2KO PND6 pups are smaller but have normal ovarian development. A. Experimental plan for Edn2KO pups and control litter mates. Pups were euthanized at post-natal day 6 (PND6) and ovaries were removed and used for histology or grafted under the kidney capsule of 28-32 day old control females. Mice were then superovulated and ovaries were collected. **B.** At PND6, collected ovaries were serially sectioned at 5uM. Histology images are shown at 10X and 20X. No histological differences are apparent; all ovaries have a mix of germ cells, primordial follicles, primary follicles, and a few preantral follicles, despite a **C.** significant difference in body weight between Edn2KO and control sibling pups. Edn2KO pups (2.25±0.10g) are nearly half the mass of control siblings (4.12±0.25g) at PND6 ($p<0.001$), and the majority expire by PND8.

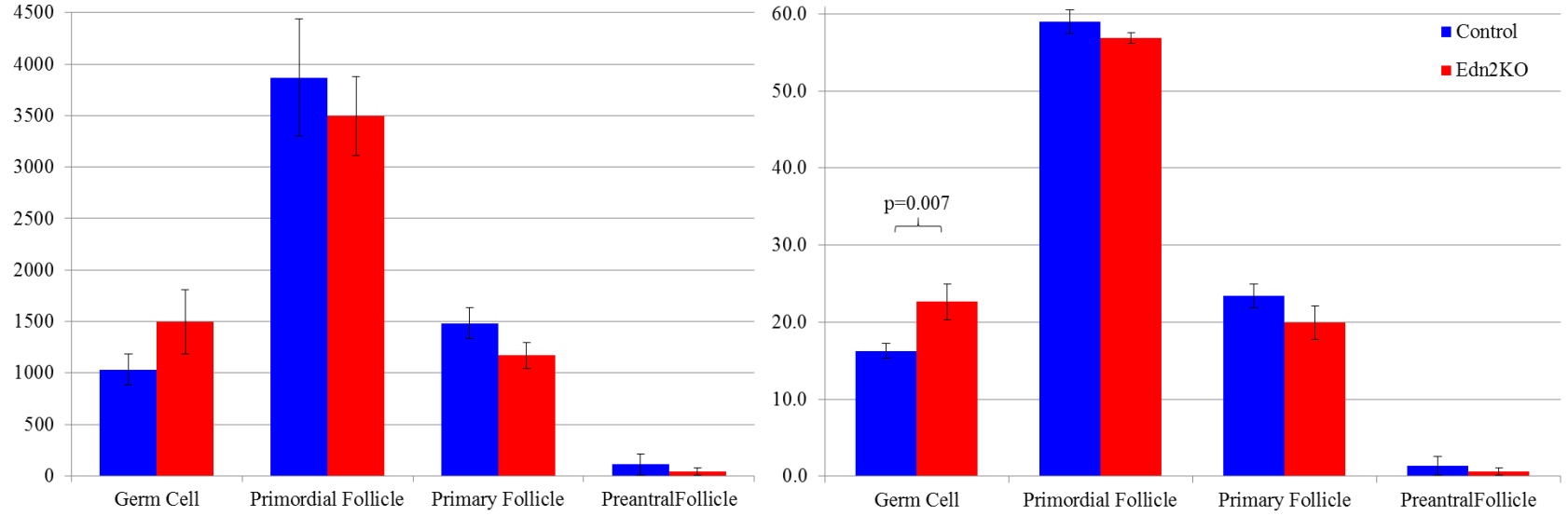

	Absolute Number / Ovary				Percent Type / Ovary			
n=10	**Germ Cell**	**Primordial Follicle**	**Primary Follicle**	**Preantral Follicle**	**Germ Cell**	**Primordial Follicle**	**Primary Follicle**	**Preantral Follicle**
Control	1032 ± 152	3870 ± 569	1482 ± 150	112 ± 102	16.3 ± 0.9	59.0 ± 1.5	23.4 ± 1.5	1.3 ± 1.2
Edn2KO	1496 ± 314	3497 ± 385	1169 ± 127	41 ± 34	22.6 ± 2.4	56.9 ± 0.7	19.9 ± 2.1	0.6 ± 0.5
p-value	0.068	0.520	0.078	0.376	0.007*	0.057	0.121	0.440

Figure 6.2. PND6 Edn2KO pups have significantly more ovarian germ cells than control mice. Follicle and germ cell counting was performed on PND6 Edn2KO and control ovaries (n=10) by PRH. Absolute cell counts are displayed at left and the percentage of total cells per ovary is displayed at right. A significant difference was seen between the percentage of germ cells present (p=0.007). No other significant differences were noted. Error bars display the S.E.M.

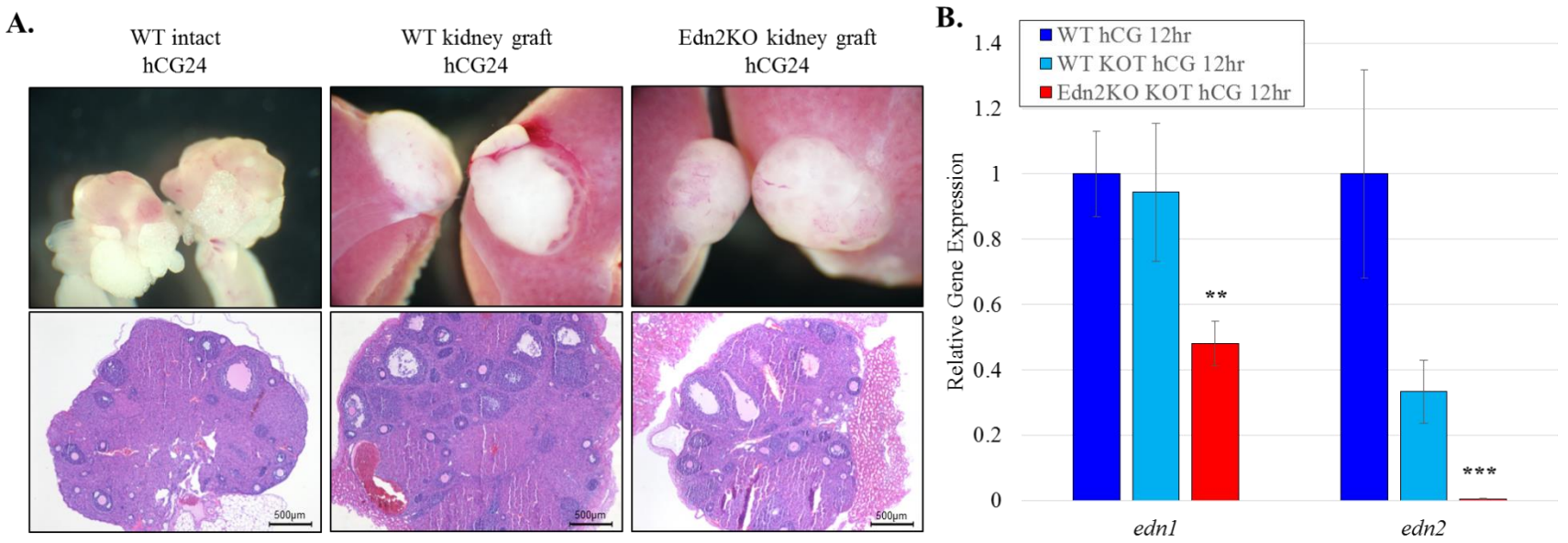

Figure 6.3. Edn2KO ovaries grafted under the kidney capsule successfully form corpora. Twenty-one days after transplanting Edn2KO PND6 ovaries into the kidneys of WT OVX mice, mice were injected with gonadotropins. **A.** At hCG 24hrs, ovaries were collected and serially sectioned. Images are shown grossly before removal from the kidney and at 4X. Grafted ovaries become flattened with a greater diameter and are less deep. Antral follicles, corpora lutea, and immature follicles were present in all groups. **B.** Ovaries were also collected at hCG12 hours; RNA was extracted and RT-PCR was performed for *Edn1* and *Edn2* expression to confirm gene loss. Grafted Edn2KO ovaries had significantly lower *Edn1* ($p=0.006$) and *Edn2* ($p<0.001$) expression, confirming CL formation in the absence of EDN2. Additionally, grafted WT ovaries trended towards decreased *Edn2* expression ($p=0.086$). KOT=kidney ovarian transplant.

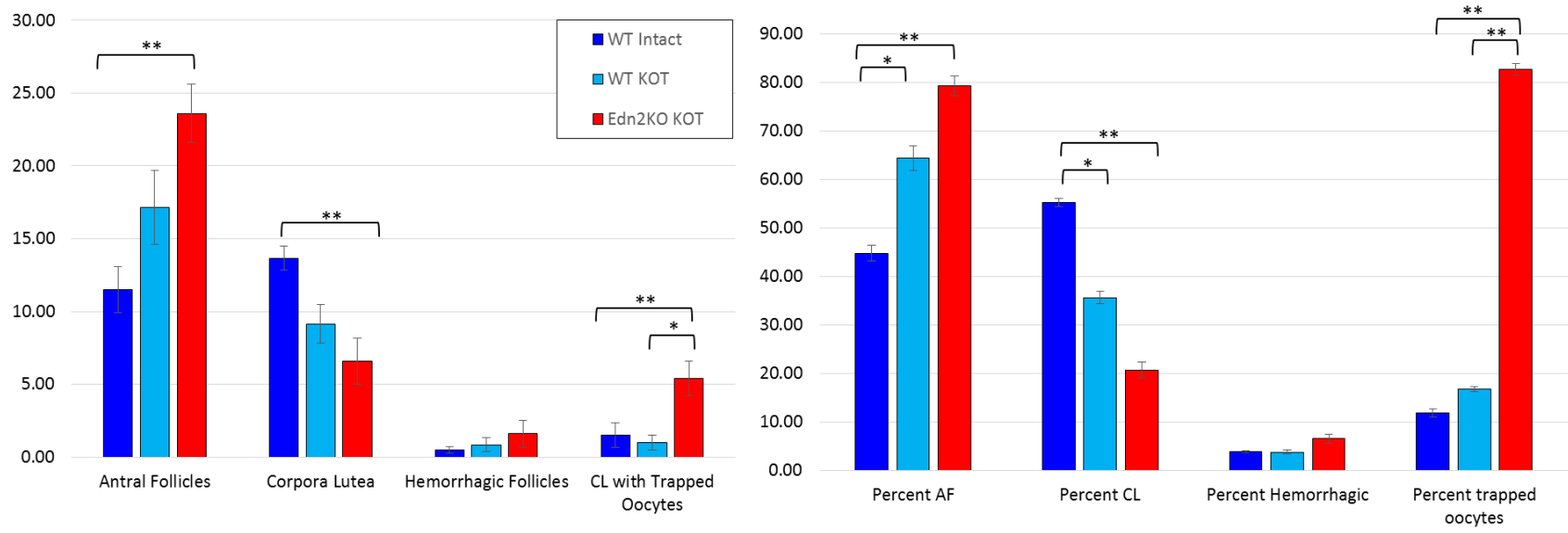

Figure 6.4. Follicle counting reveals significantly more oocytes trapped in corpora lutea in grafted Edn2KO ovaries. Twenty-one days after transplanting Edn2KO PND6 ovaries into the kidneys of WT OVX mice, ovaries were collected at hCG 24hrs and serially sectioned. The total numbers of antral follicles (AF) and corpora lutea (CL) were determined (n=5-7). Absolute counts are displayed at left and percentages are displayed at right. When compared to transplanted control ovaries, transplanted Edn2KO ovaries trended towards a higher percentage of antral follicles and fewer CL (p=0.088). Grafted Edn2KO ovaries had significantly more oocytes trapped within corpora luteal (p=0.010) and a significantly greater percentage of CL with trapped oocytes (p=0.004). Errors bars represent the SEM. KOT=kidney ovarian transplant.

Averages	Coding	Antral Follicles AF	Corpora Lutea CL	Hemorrhagic Follicles	CL with Trapped Oocytes	AF:CL Ratio	Percent AF	Percent CL	Percent Hemorrhagic	Percent trapped oocytes
WT Intact	1.00	11.50	13.67	0.50	1.50	0.86	44.76	55.24	3.95	11.90
WT KOT	2.00	17.14	9.14	0.86	1.00	2.24	64.33	35.67	3.80	16.84
Edn2KO KOT	3.00	23.60	6.60	1.60	5.40	4.15	79.24	20.76	6.58	82.62
STDEVs										
WT Intact	1.00	3.94	1.97	0.55	2.07	0.30	10.71	10.71	4.42	17.11
WT KOT	2.00	6.67	3.53	1.21	1.41	1.37	13.96	13.96	4.92	22.28
Edn2KO KOT	3.00	4.51	3.51	2.07	2.70	1.41	6.34	6.34	7.86	16.14
SEMs										
WT Intact	1.00	1.61	0.80	0.22	0.85	0.12	4.37	4.37	1.80	6.98
WT KOT	2.00	2.52	1.34	0.46	0.53	0.52	5.27	5.27	1.86	8.42
Edn2KO KOT	3.00	2.01	1.57	0.93	1.21	0.63	2.83	2.83	3.52	7.22
ANOVA:		0.007	0.006	N/A	N/A	0.001	N/A	N/A	N/A	N/A
KruskalWallis:		N/A	N/A	0.672	0.021	N/A	0.007	0.007	0.893	0.004
Post hoc values:										
WT Intact vs WT KOT		0.229	0.057		0.695	0.137	**0.036**	**0.036**		0.756
WT KOT vs Edn2KO KOT		0.168	0.542		**0.010**	**0.036**	0.088	0.088		**0.004**
WT Intact vs Edn2KO KOT		**0.006**	**0.006**		**0.030**	**0.001**	**0.004**	**0.004**		**0.004**

Figure 6.5. Follicle counting data for grafted Edn2KO ovaries vs WT intact and WT grafted ovaries at hCG24 hours. Normally distributed data were analyzed by an ANOVA and a Bonferroni *post hoc* test; non-normally distributed data could not be log transformed and were analyzed nonparametrically by a Kruskal Wallis ANOVA with follow up Mann Whitney U tests. Both the standard deviation and the standard error of the mean are provided. For WT Intact, WT grafted, and Edn2KO grafted, n values are 6,7, and 5, respectively. KOT=kidney ovarian transplant.

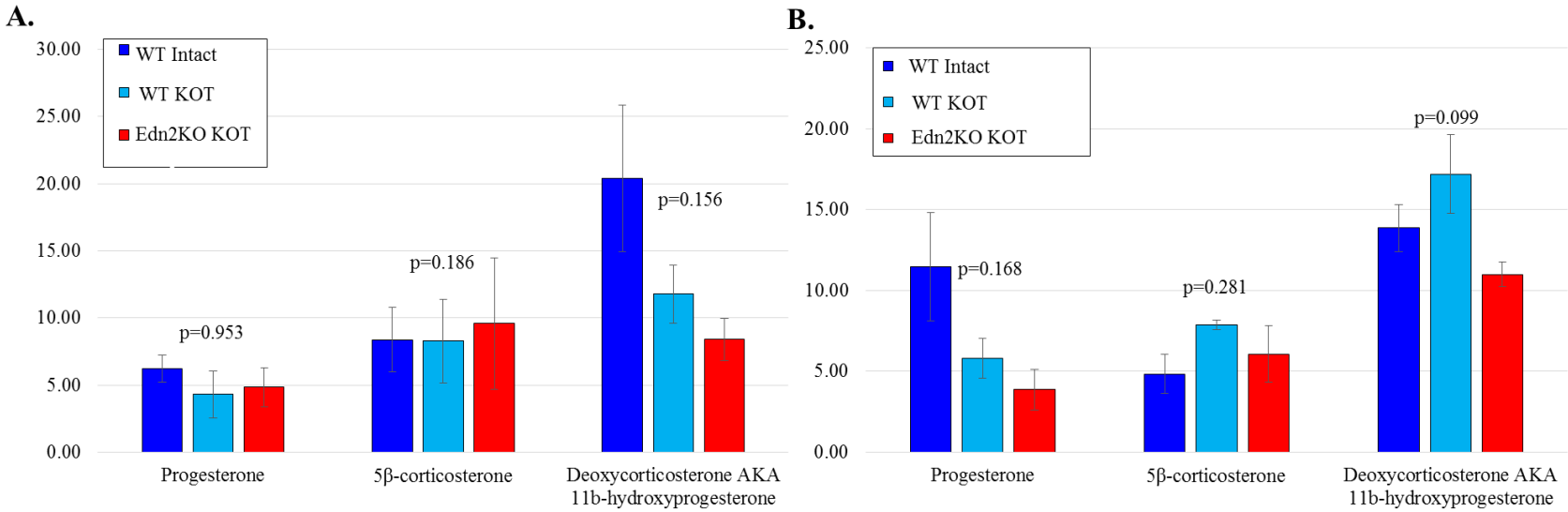

Figure 6.6. Serum hormones are not different in ovarian graft mice from intact mice. Serum was extracted from mice at hCG12 **A.** and hCG24 hours **B.** Serum hormone concentrations (in ng/mL) were not different between intact WT mice, OVX WT mice with one WT ovary grafted to each kidney, or WT mice with one Edn2KO ovary grafted to each kidney. However, a high degree of variability was present between mice within treatment groups; future results may reveal a trend towards a lower progesterone concentration at hCG24 hours in mice receiving ovaries grafted to kidneys, as a reflection of the trend towards fewer corpora lutea. P-values represent ANOVA score by hormone. Error bars represent the SEM.

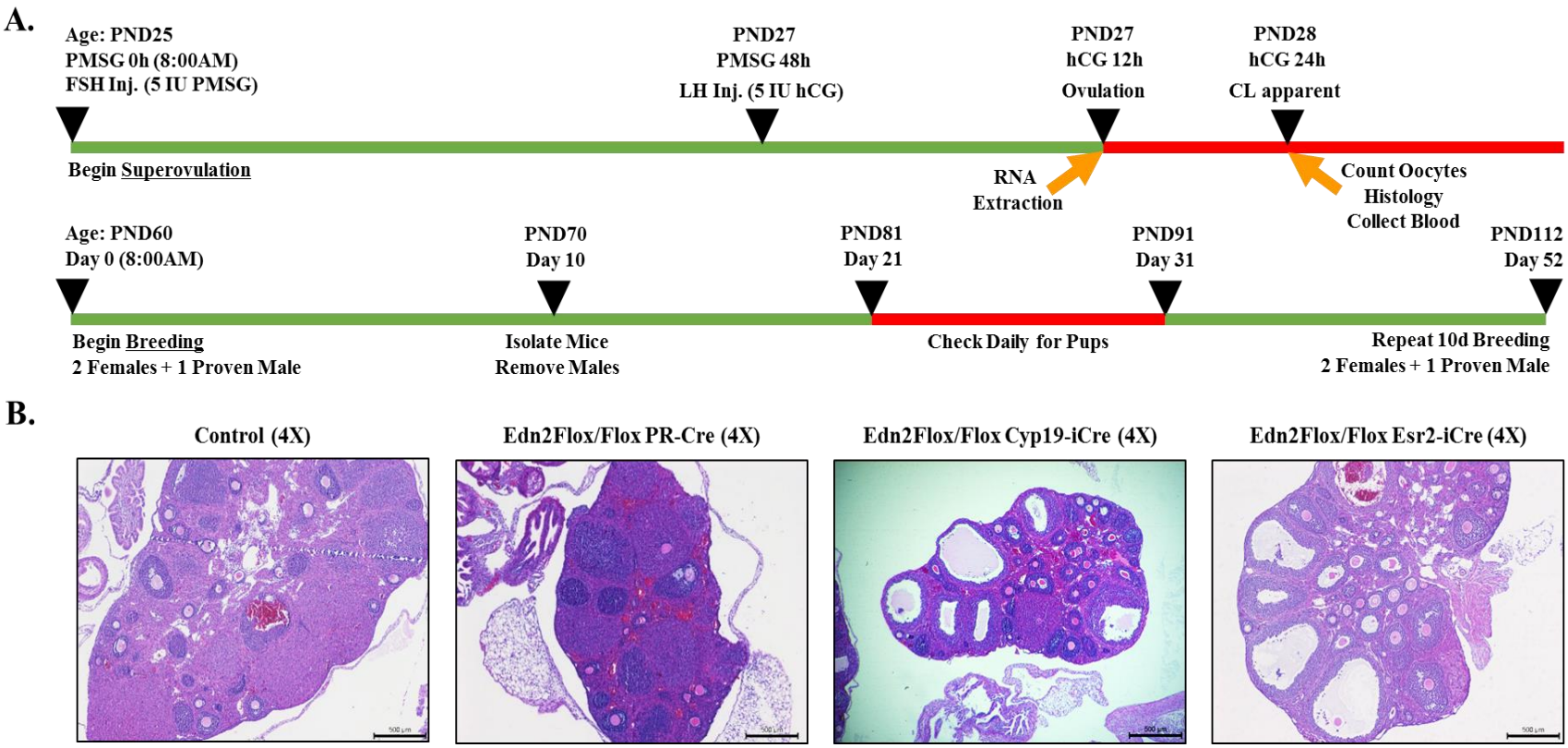

Figure 6.7. Generation of granulosa cell-specific endothelin-2 conditional knockout mice. To examine the ovarian effects of EDN2 loss without surgical transplantation, Edn2Flox mice were crossed with mice from three different Cre recombinase lines: PR-Cre, Cyp19-iCre, and novel Esr2-iCre mice. **A.** Experimental plan involving superovulation of immature mice for RNA collection at hCG12 hours, and serum hormone measurement, histology, and oocyte counting at hCG24 hours (top line). A breeding study was also performed by placing females with proven male breeders for 10 days and monitoring daily for the number of pups born (bottom line) from mice ages 2-7 months. **B.** Representative histological images from ovaries of each genotype at hCG24 hours (4X). Ovaries from each genotype appeared healthy and all had corpora lutea, antral follicles, and immature follicles with no difference in hemorrhage between groups. Note the multiple antral follicles with trapped oocytes present in Cyp19-iCre and Esr2-iCre Edn2Flox/Flox mouse lines.

A.

Genotype (average age)	N (mice)	N (pairings)	Fertility	P-value	Pups/Litter	Median	P-value	Oocytes/Ovary	Median	N (ovaries)	P-value
Control (2.6 months)	9	14	71.4%	-	8.50±0.60	8.5	-	16.36±1.85	19.0	28	-
Edn2Flox/Flox PR-Cre (2.6 months)	2	4	75.0%	1.000	6.33±1.76	7.0	0.969	15.57±2.36	16.5	14	0.779
Edn2Flox/Flox Cyp19-iCre (4.0 months)	6	8	87.5%	1.000	4.67±0.71	5.5	0.022	11.50±2.64	12.5	14	0.149
Edn2Flox/Flox Esr2-iCre (2.8 months)	5	11	63.6%	1.000	4.29±1.02	3.0	0.008	3.75±0.88	4.0	12	<0.001

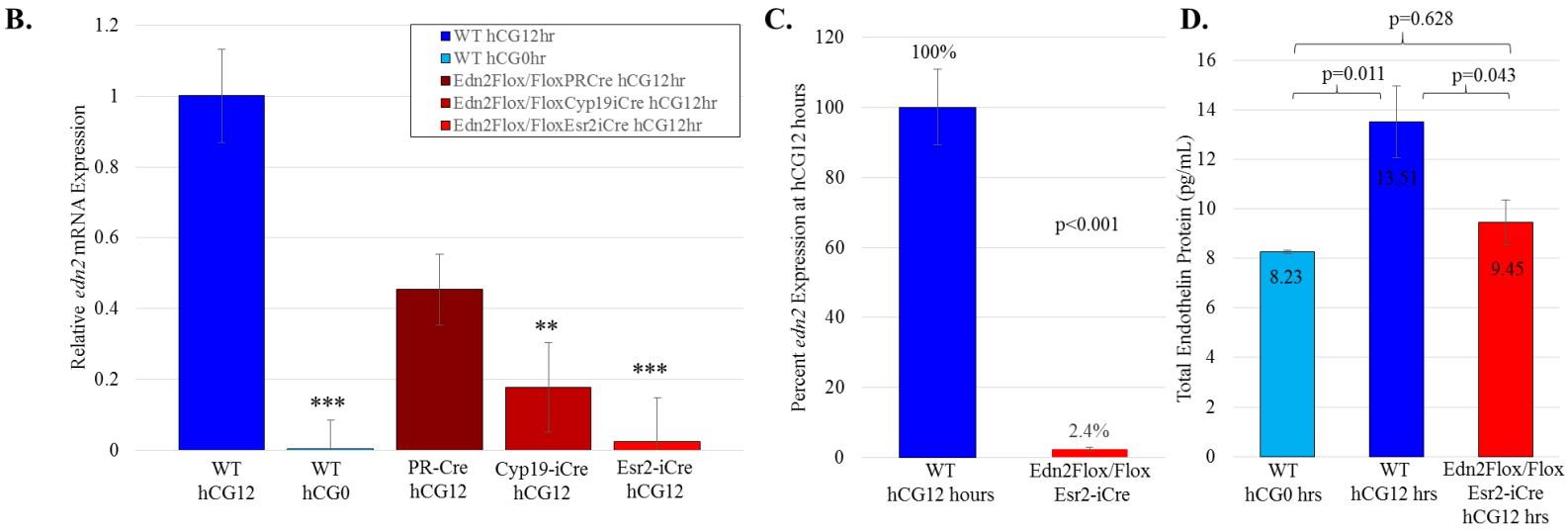

Figure 6.8. Loss of EDN2 reduces oocytes ovulated and decreases average litter size. Edn2Flox mice were crossed PR-Cre, Cyp19-iCre, and Esr2-iCre mice to remove *Edn2* expression in granulosa cells. **A.** Breeding study and superovulation oocyte collection results. Each pairing lasted 10 days; litter size represents pups born instead of weaned; oocytes were collected from the ampulla of the oviduct at hCG24 hours. P-values are from post hoc test relative to control mice. **B.** Relative *Edn2* mRNA expression in whole ovaries at hCG0 and hCG12 hours determined by semi-quantitative RT-PCR. Expression of *Edn2* is significantly lower in WT mice at hCG0 and in Edn2Flox/Flox Cyp19-iCre and Esr2-iCre mice at hCG12 hours. **C.** Taqman quantitative RT-PCR results comparing WT and Edn2Flox/Flox Esr2-iCre mice at hCG12 hours; 97.6% of *Edn2* expression is lost. **D.** ELISA quantitation of total endothelin protein per ovary. Endothelin mass is significantly reduced at hCG12 hours in Edn2Flox/Flox Esr2-iCre mice from *Edn2* loss and is not different from endothelin mass at hCG0 hours in WT mice. All error bars represent the SEM. Asterisks denote significant differences from control mice when p-values are not provided.

A.

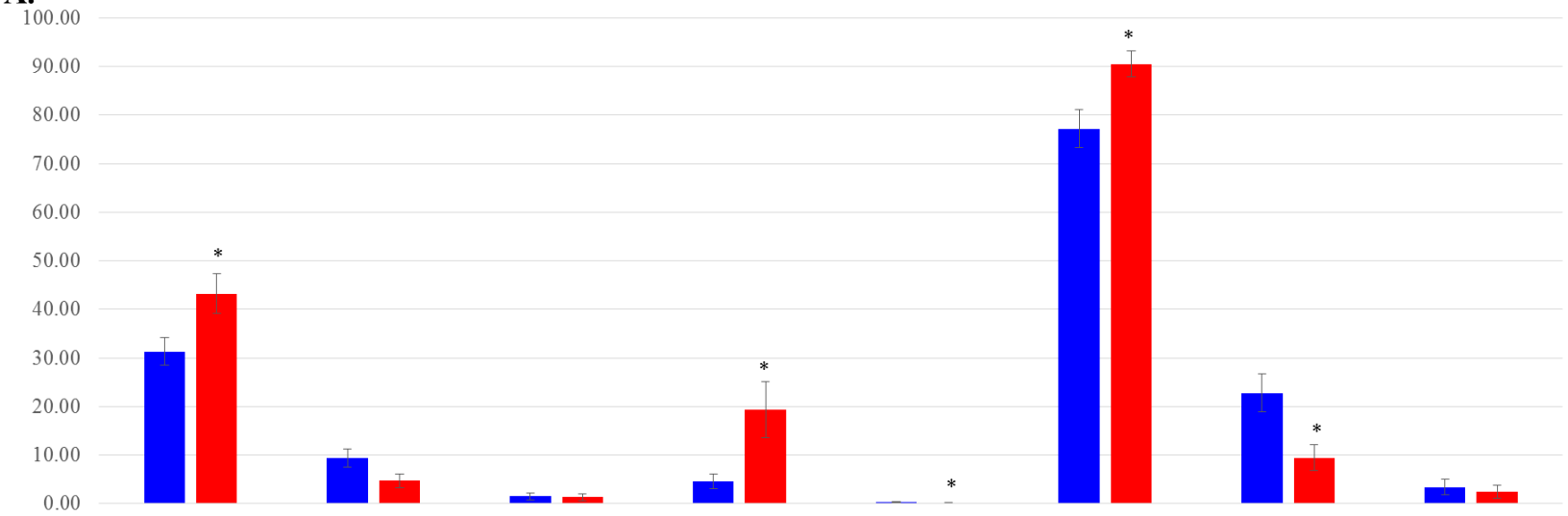

B.

Averages	Antral Follicles AF	Corpora Lutea CL	Hemorrhagic Follicles	AF/CL	CL/AF	Percent AF	Percent CL	Percent Hemorrhagic
Control (n=6)	31.33	9.33	1.50	4.58	0.31	77.19	22.81	3.42
Edn2Flox/Flox Esr2-iCre (n=8)	43.25	4.75	1.38	19.33	0.11	90.53	9.47	2.44
STDEVs								
Control	6.76	4.58	1.64	3.87	0.17	9.48	9.48	3.85
Edn2Flox/Flox Esr2-iCre	11.60	4.02	2.01	16.21	0.11	7.67	7.67	3.62
SEMs								
Control	2.76	1.87	0.67	1.58	0.07	3.87	3.87	1.57
Edn2Flox/Flox Esr2-iCre	4.10	1.42	0.71	5.73	0.04	2.71	2.71	1.28
P-value	**0.045***	0.070	0.825	**0.018***	**0.015***	**0.019***	**0.013***	0.617

Figure 6.9. Edn2Flox/Flox Esr2-iCre ovaries have more antral follicles and fewer corpora lutea after ovulation. Ovaries were collected at hCG24 hours from immature mice, fixed, and serially sectioned. The absolute number of corpora lutea (CL), antral follicles (AF), and follicles with hemorrhage present were counted. The each value is also expressed as a percentage of total ovarian structures. **A.** Graphical presentation of follicle counts. Asterisks represent significant differences ($p<0.05$). Error bars represent the SEM. **B.** Tabular presentation of data. Standard deviation (STDEV) and standard error of the mean (SEM) are provided. P-values of significantly different groups are bolded.

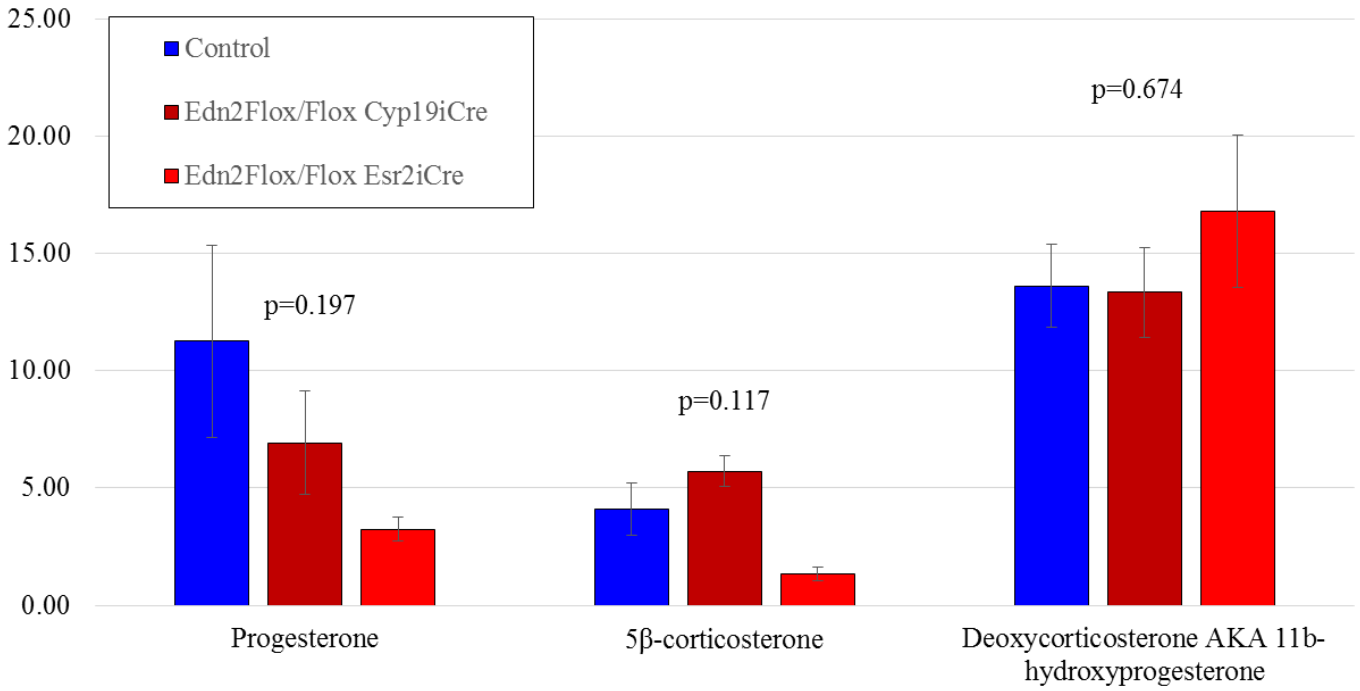

Figure 6.10. Serum hormones are not different significantly different after ovulation in Edn2Flox/Flox Esr2i-Cre mice. Serum was extracted from mice at hCG24 hours. Serum hormone concentrations (in ng/mL) were not different between intact WT mice, Edn2Flox/Flox Cyp19-iCre or Esr2-iCre mice. A high degree of variability was present between mice within treatment groups; future results may reveal a trend towards lower progesterone concentration at hCG24 hours in conditional knockout mice. P-values represent ANOVA score by hormone. Error bars represent the SEM.

A.

Position	Gene Symbol	Gene Name	Fold Regulation	Functional Gene Group
F07	Pgr	Progesterone receptor	13.17	Receptive / Oocyte Support
A05	Areg	Amphiregulin	5.97	Receptive / Oocyte Support
G02	Spp1	Secreted phosphoprotein 1	-5.28	General Infertility
F06	Pgf	Placental growth factor	2.67	Other
B04	Cfd	Complement factor D (adipsin)	-2.60	General Infertility
D10	Il6	Interleukin 6	-2.50	Cytokines
C04	F3	Coagulation factor III	2.10	Coagulation
C12	Hoxa10	Homeobox A10	-2.05	Receptive / Oocyte Support
G12	Wnt2	Wingless-related MMTV integration site 2	2.02	Signal Transduction

B.

Position	Gene Symbol	Gene Name	Fold Regulation	Functional Gene Group
A11	Casp3	Caspase 3	-1.17	Apoptosis
C02	Esr1	Estrogen receptor 1 (alpha)	-1.14	Other
C03	Esr2	Estrogen receptor 2 (beta)	-1.23	General Infertility
E11	Mmp2	Matrix metallopeptidase 2	-1.29	Leukocyte Migration
E12	Mmp7	Matrix metallopeptidase 7	-1.11	Leukocyte Migration
F01	Mmp9	Matrix metallopeptidase 9	1.11	Leukocyte Migration
F09	Ptgs1	Prostaglandin-endoperoxide synthase 1	-1.87	Signal Transduction
F10	Ptgs2	Prostaglandin-endoperoxide synthase 2	1.78	Signal Transduction
G06	Timp1	Tissue inhibitor of metalloproteinase 1	-1.58	Other
G11	Vegfa	Vascular endothelial growth factor A	1.30	Other
G09	Trp53	Transformation related protein 53	1.22	Apoptosis

C.

Functional Gene Group	Average Fold Change (no change = 0)	Standard Deviation	n	SEM
General Infertility	-1.12	1.68	14.00	0.45
Receptive / Oocyte Support	1.31	5.10	9.00	1.70
Signal Transduction	-0.36	1.40	10.00	0.44
Leukocyte Migration	-0.06	1.27	15.00	0.33
Cell Cycle	1.17	0.09	5.00	0.04
Coagulation	0.28	1.68	4.00	0.84
Apoptosis	0.33	1.35	7.00	0.51
Cytokines	0.26	1.49	6.00	0.61
Other	0.20	1.51	13.00	0.42
House Keeping Genes	0.60	0.96	5.00	0.43
Controls	1.51	0.43	7.00	0.16

Figure 6.11. Differential gene expression between control and Edn2Flox/Flox Esr2-iCre mice. Ovaries from immature mice were collected at hCG12 hours and gene expression was compared by an RT ^{2}Prolifer PCR Array kit. **A**) Genes with greater than two-fold regulation difference between ovaries where 1.00 = no change. **B**) Genes known to be influentially involved in ovulation show no major differences other than progesterone receptor, where 1.00 = no change. **C**) Overall average fold expression change by functional gene group. Functional gene groups were used based on grouping from the RT^{2} kit. Though certain groups have an average that indicates general upregulation or downregulation where no fold change = 0.00, the high standard deviations and errors of the mean do not allow conclusion that any functional gene group shows significant up or downregulation. EDN2 likely plays little role in modifying gene expression.

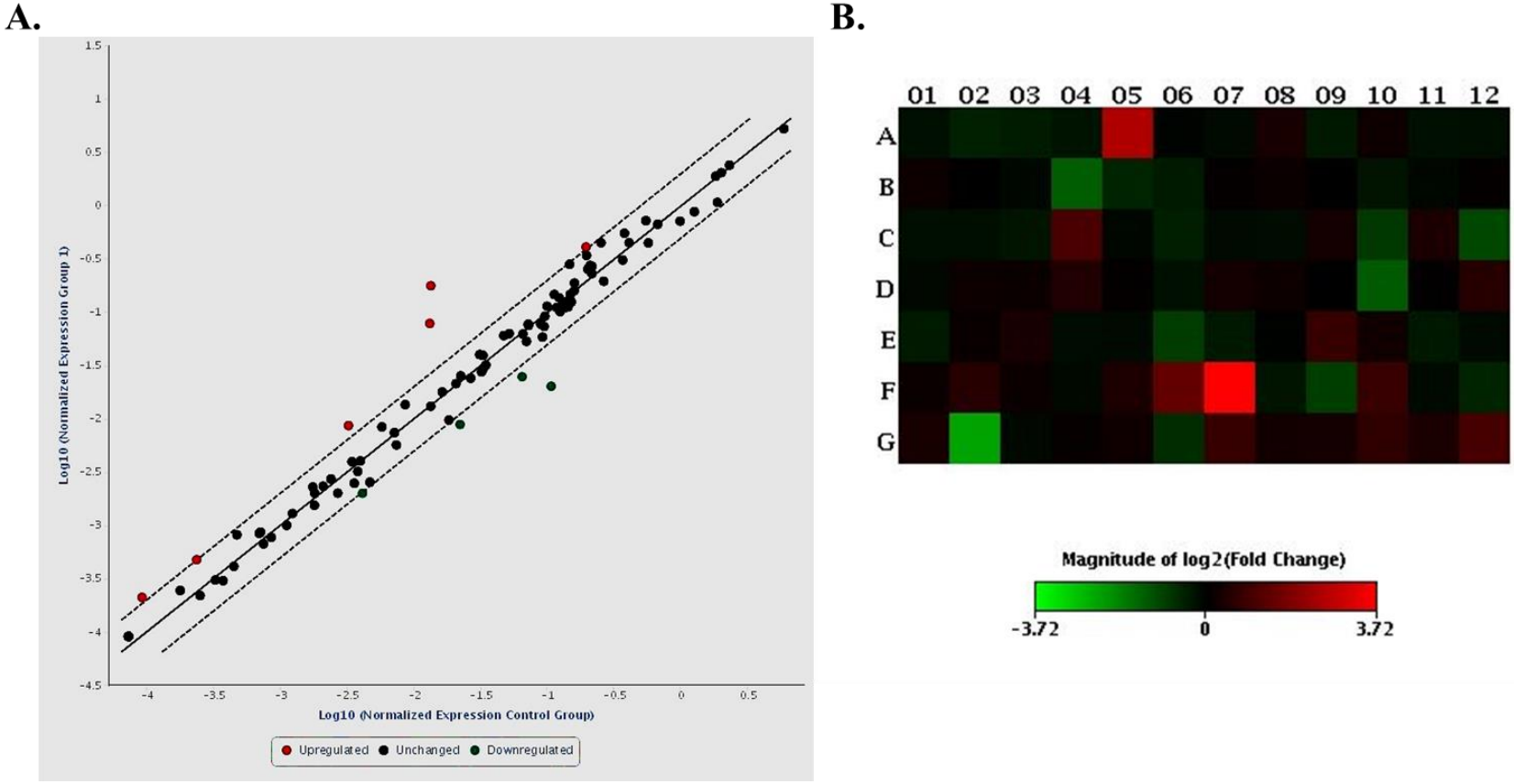

Figure 6.12. RT^2 Profiler PCR Array shows few gene expression differences between control and Edn2Flox/Flox Esr2iCre mice. A. Scatter plot of normalized gene expression between immature control ovaries (x-axis) and Edn2Flox/Flox Esr2-iCre ovaries (y-axis) at hCG12 hours. Dashed lines represent a two-fold increase or decrease from control expression levels. Genes with less than a twofold difference from controls are presented as black circles; genes with expression greater than controls are in red and genes with expression less than controls are in green. **B.** Heat map of gene expression between genotypes. Each square represent one gene (and one well on the PCR Array). Square color indicates fold change in expression; red cells are upregulated and green cells are downregulated.

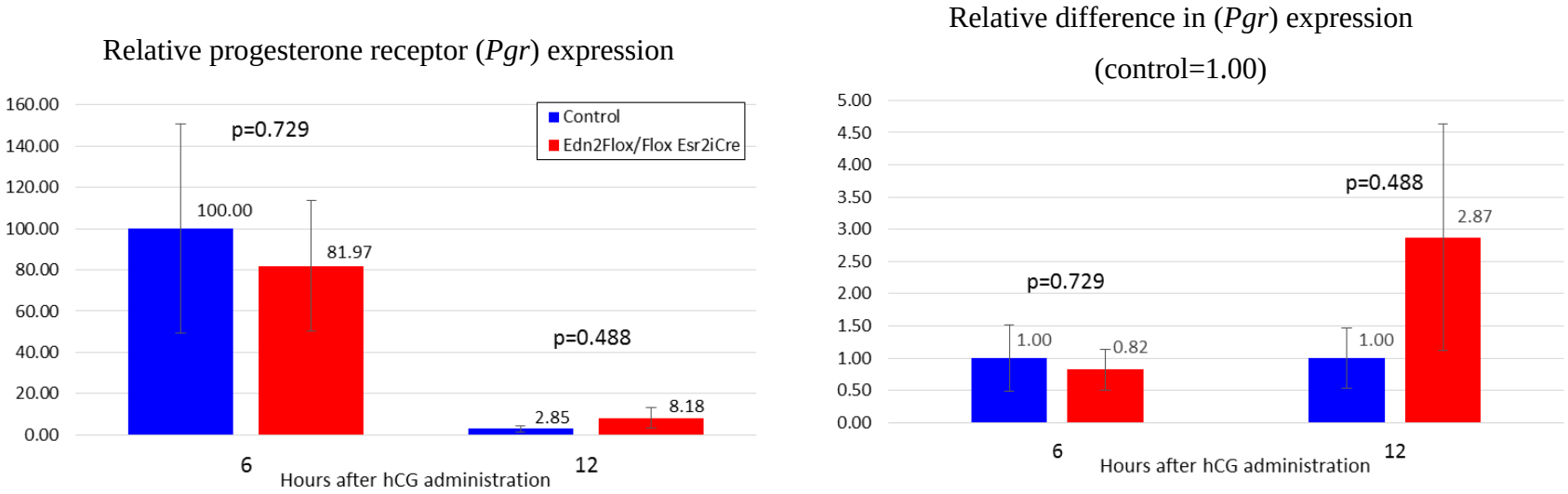

Figure 6.13. Edn2Flox/Flox Esr2iCre ovaries have no difference in *Pgr* expression. To confirm RT^2 profiler data, whole ovaries were collected at hCG6 and 12 hours from immature mice, and cDNA was generated for RT-PCR (n=6). At each time point, there was no significant difference in progesterone receptor expression. **A**. The relative progesterone receptor expression decreases from hCG6 to hCG12 in control and conditional knockout animals. **B**. When normalized to control *Pgr* expression at each time point (1.00), there is no significant difference when *Edn2* expression is lost. Large ranges and error bars in conditional knockout mice result from a few ovaries with high *Pgr* expression, likely from early times of ovulation and luteinization. Errors bars represent the standard error of the mean (SEM).

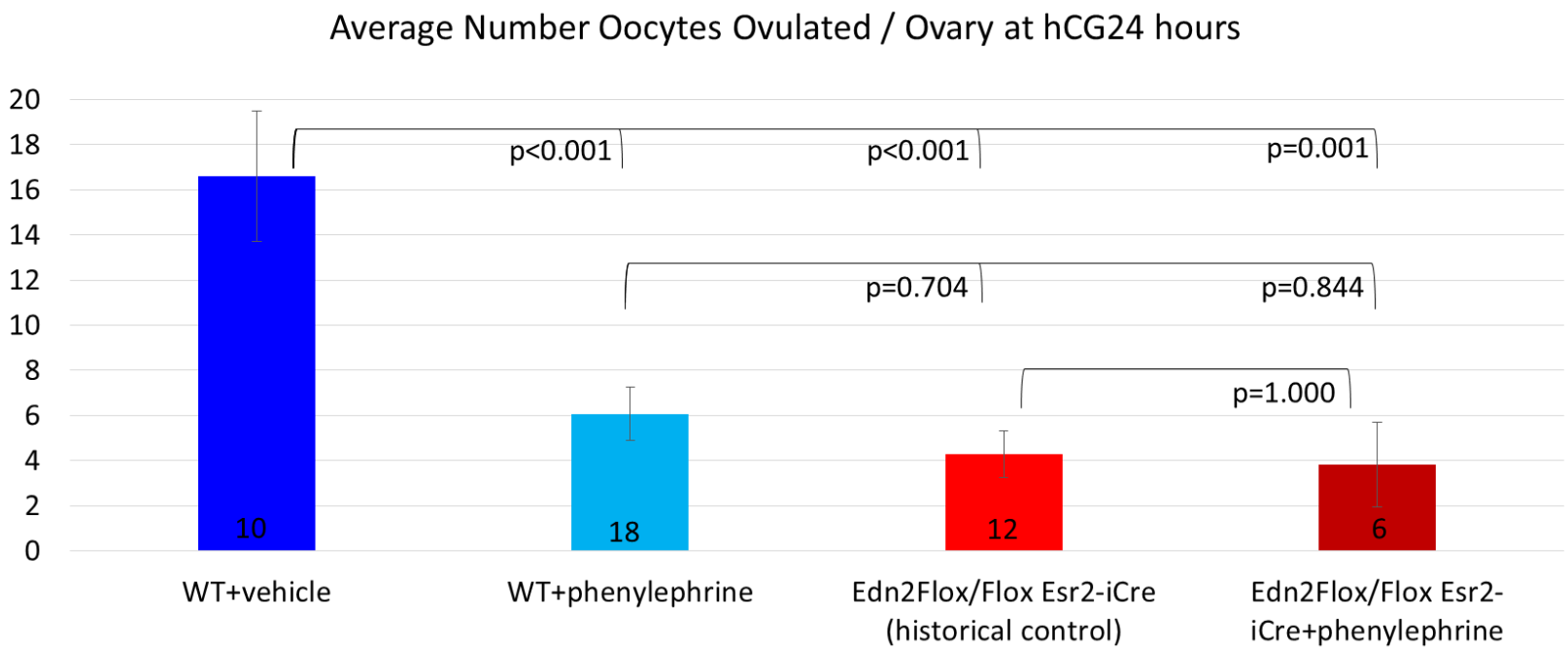

Figure 6.14. Phenylephrine treatment reduces the number of oocyte ovulated in WT mice. To determine if activation of calcium channels by alpha adrenergic receptors could restore ovulatory ability, twenty-five day old mice received superovulation treatment and also received injection of phenylephrine (1.0 µg i.p.) at hCG11 hours. Oocytes were collected from the oviduct at hCG24 hours to quantify ovulatory ability. Phenylephrine treatment significantly reduced ovulation in WT mice. In Edn2Flox/Flox Esr2-iCre mice, phenylephrine treatment did not significantly change the number of oocytes ovulated. There was no significant difference between Edn2Flox/Flox Esr2iCre mice and WT receiving phenylephrine injection. Owing to low n values, Edn2Flox/Flox Esr2-iCre mice from a previous study were used as a historical control in place of vehicle-treated mice. N-values are displayed at the base of each column and errors bars represent the standard error of the mean (SEM).

CHAPTER 7: INVESTIGATION INTO THE SIGNIFICANCE OF *EDNRA* EXPRESSION IN OVARIAN SMOOTH MUSCLE CELLS IN OVULATION

Joseph Cacioppo[1], Jongki Cho[1,2], Patrick Lin[1], Arnon Gal[1], and CheMyong Ko[1]*

[1]Comparative Biosciences, College of Veterinary Medicine, University of Illinois, Urbana-Campaign, IL 61802, USA
[2]College of Veterinary Medicine, Research Institute of Veterinary Medicine, Chungnam National University, Daejon, South Korea

* Corresponding author
CheMyong Ko, Ph.D.
Department of Comparative Biosciences
College of Veterinary Medicine
University of Illinois at Urbana-Champaign
3806 VMBSB, MC-002
2001 South Lincoln Avenue
Urbana, IL 61802, USA
217-333-9362 (office), 217-244-1652 (fax)
jayko@illinois.edu

Grant Support:
Supported by a grant for research from the National Institutes of Health (R01HD052694 to C. Ko)

Running Title: EDNRA in Ovulation

Summary Sentence: Mice with a smooth muscle-specific knockout of the endothelin-2 gene demonstrate ovulation

Keywords: endothelin-2, ovulation, EDNRA, ETa, oocytes, tamoxifen, smooth muscle actin, gonadotropins

ABSTRACT

During ovulation, the precise physiological mechanism governing follicle rupture and oocyte expulsion from the ovary remains to be revealed. Ovulation is a multifactorial process and it is known that many factors contribute including collagenase digestion of the follicular wall, leukocyte invasion of the ovary, cumulus complex expansion, and prostaglandin production. However, the exact trigger governing the time of oocyte discharge is unknown. It was previously demonstrated that endothelin-2 (EDN2) produced in granulosa cells is important for follicle rupture and corpus luteum formation, and that this is mediated by endothelin receptor A (EDNRA) through a contractile mechanism in the ovary. To determine if EDNRA on smooth muscle cells in the ovary was responsible for contraction and force generation during follicular rupture, mice that express Cre recombinase in smooth muscle cells in a tamoxifen-inducible manner were bred with EdnraFlox mice to attempt to characterize the effect of *Ednra* loss on ovulation. However, tamoxifen treatment had significant and confounding effects on ovulation. Untreated control mice ovulated 34.7±3.5 oocytes/ovary, whereas WT mice ovulated 15.6±4.4 oocytes per ovary after tamoxifen treatment and SMACre^{ERT2}EdnraFlox mice ovulated 9.2±2.0 oocytes per ovary after tamoxifen; $p<0.001$ before and after tamoxifen treatment within either genotype; $p=0.462$ between genotypes after tamoxifen treatment. In the ovary, *Ednra* expression is increased 30 days after tamoxifen injection, implying gene loss is impermanent as smooth muscle cells are replaced. Overall, it was demonstrated that ovulation may occur in tamoxifen-treated SMACre^{ERT2}EdnraFlox mice, though tamoxifen exposure inhibits the number of oocytes ovulated in both control and SMACre^{ERT2}EdnraFlox mice. It is possible that *Ednra* may play a significant role in ovulation, either in smooth muscle or other ovarian cells, but SMACre^{ERT2}EdnraFlox mice do not allow for dissection of this signaling pathway owing to the confounding role of tamoxifen.

INTRODUCTION

The study of ovulation remains an ongoing and relevant issue as new contraceptives and molecular targets are discovered to control the rising human population. It has long been debated what mechanism within the ovary specifically controls the release of the oocyte from the follicle to the oviduct prior to fertilization. The wall of the follicle is composed of the granulosa cells, the theca interna cells, and the theca externa cells[65]. The granulosa cells function for both protein synthesis and steroidogenic synthesis during follicular maturation; these cells are responsible for estrogen production from a testosterone precursor via the aromatase enzyme[495,496]. The theca interna cells appear fibrotic and steroidogenic, while the theca externa cells are myeloid and fibrotic[497] and may generate contractile forces. Theca interna cells are responsible for testosterone synthesis from cholesterol[498]. A basement membrane exists between the granulosa and theca cells and blood and lymph vessels are confined to the theca layers. Following ovulation, theca and granulosa cells luteinize and produce progesterone rather than testosterone or estrogen; these cells reside within the corpus luteum, which becomes highly vascular following ovulation[499].

Numerous effects must come together to allow for a follicle to rupture, including growth of the follicle and hypertrophy of the granulosa and theca cell layers[500], weakening of the basement membrane and surrounding collagenous tissue through metalloproteinase action, invasion of leukocytes and cytokine release, and expansion of the cumulus cells surrounding the oocyte. It has also been debated if there exists a change in pressure or a contractile force that expels the oocyte from the ovary at the time of ovulation, though there exists little definite and conclusive evidence in this area. It is well agreed that contractile cells containing bundles of thin filaments parallel to the long axis of the cytoplasm exist in many mammalian species[501-507], thus providing potential for a contractile force. Some authors claim that fewer contractile cells are present at the apical region of the protruding follicle[508,509], while others dispute this[510-515]. It is likely that species variation exists within mammalian ovaries. Other authors have also argued that contractile filaments in cells surrounding the follicle function for cellular locomotion rather than a unison contractile effect[516], especially as fibroblasts are mobile cells[517-519] and a large amount of collagen is needed to be rapidly deposited within the corpora lutea just after ovulation to maintain internal cellular and vascular support[66]. An excellent review on early literature on ovarian contraction is provided by Espey, 1978[66].

Contraction of the ovary as a whole rather than the follicles has been previously well documented in the human[163,520,521] as well as cats[343], rabbits[164,165,167], and several other mammalian species[345,522]. Spontaneous ovarian contraction has also been observed, though often *ex vivo*[167]; however, it has been proposed that such contractions may originate in the vascular hilus of the ovary rather than the follicular cortex[158-160,162,506,507,523]. It has also been debated if there is a difference in strength of ovarian contraction during ovulation or not[524-526] and particularly if there is an increase in intrafollicular pressure just prior to ovulation[527,528]. This argument has largely gone unanswered, and with the advent of new molecular technologies and gene identification, new avenues in molecular reproduction have been largely focused on over large-scale contractile physiology. However, it has been reported recently that intrafollicular pressure and the follicular wall tension index increase in rat ovarian follicles after gonadotropin stimulation[100], though the necessary role of collagenases during ovulation is noted. Measured changes in individual follicular pressure were less than two-fold increases[100,493], though a second similar study concluded that NO was likely a local mediator of pressure changes as well as systemic blood pressure[493]. It has also been postulated that smooth muscle cells near periovulatory follicles can undergo stress relaxation[166] to selectively prevent ovulation of certain follicles. Summarily, changes in tension occur within the ovary as a whole during ovulation as follicle walls weaken, intrafollicular pressure increases during ovulation but not severely, and changes in tension may be mediated by vascular tension about the follicles themselves or throughout the body; the necessity of such pressure changes *in vivo* remains debatable.

Within the last decade, it was reported that the protein endothelin-2 (EDN2, also ET-2) is essential for contraction of the follicle and release of the oocyte through the follicular wall[6]. EDN2 has been well characterized as a potent vasoconstricting agent[212,529]. It is a short peptide composed of 21 amino acids that acts through binding to one of its two G protein-coupled receptors (GPCRs): endothelin receptor A (EDNRA, also ETa, *Ednra* gene) and endothelin receptor B (EDNRB, also ETb, *Ednrb* gene)[217]. EDN2 is part of the endothelin system, which is composed of two other isomers, EDN1 and EDN3, the two receptors, and at least two endothelin converting enzymes (ECEs). EDN1 and EDN2 differ by only two amino acids and have equivalent affinity for each receptor[213,295,530]. Within the ovary, EDN1 is constitutively produced in the endothelial cells[12,531,532] while EDN2 is produced in the granulosa cells at the time of ovulation[6,7]. EDN1 is involved in follicular development as an inhibitor of premature luteinization of granulosa cells[533],

an inhibitor of premature luteolysis[534-536] and an inhibitor of oocyte meiosis[537]. The time and location specific production of EDN2 at very high concentrations, relative to constitutively low EDN1, indicates direct involvement with the ovulatory process. The endothelin-2 gene, *Edn2*, is regulated largely at the transcriptional level[287,318,450], and is known to be under regulation by both hypoxia inducible factor 1 alpha (HIF1α)[245-247,450,538] and progesterone receptor (PGR, PR)[7].

In general, EDNRA is thought to have the opposite effect of EDNRB, which also may act to clear the ligand during receptor recycling[539]. EDNRA acts through the Gs or Gq pathway, whereas EDNRB acts through the Gi or Gq pathway[218,540]. Smooth muscle contraction is initiated by an influx of intracellular calcium to cause depolarization. Intracellular calcium is released from the endoplasmic reticulum to cause a transient increase in polarity, while the main action of endothelin receptors occurs through an influx of extracellular calcium through the opening of receptor-operated calcium channels (ROCCs). Additionally, extracellular calcium increases through store-operated and voltage-operated calcium channels (SOCCs and VOCCs), though these play a minor role relative to ROCCs[208,278,541-546]. Calcium influx can be modulated by either EDN1 or EDN2[6] via EDNRA, though only *Edn2* expression increases during ovulation[6,170]. There is evidence that in humans, luteinized granulosa cells have EDNRA, but not EDNRB,[547] which may act as secondary EDN2 targets.

Previous work by Bridges *et al*., (2010)[170,200] using specific endothelin receptor antagonists suggest that EDNRA is the critical receptor involved in ovulation: EDN2-mediated contraction was reduced by a specific EDNRA antagonist but not by a specific EDNRB antagonist. However, no effect was observed *in vivo* on ovulation rate owing to the rapid degradation of these inhibitors by proteolytic enzymes. These results are supported by a large body of evidence that EDNRA induces prolonged vasoconstriction[529,548-550] whereas EDNRB acts in the opposite fashion for NO_2-dependent vasodilation[551-553]. Additionally, and most convincingly, mice that selectively lack EDNRB demonstrate no reproductive deficits; instead, mice with *Ednrb* ablation throughout the ovary give birth to more pups per litter and produce more corpora lutea[233].

The precise physiological responses governed by EDN2 and its receptor-mediated action in the ovary remain to be further investigated. Given the limitations in previous studies using pharmacological approaches, a transgenic animal model approach was chosen to dissect the receptor-mediated action of EDN2 during ovulation. EDN2 is a known potent vasoconstrictor that is produced in the granulosa cells specifically during ovulation, *Ednra* is expressed in the smooth

muscle cells that are present around mature follicles and responds to drive cellular contraction in response to EDN2, and EDNRA can be pharmaceutically inhibited to prevent ovulation. It was postulated that EDNRA, which is expressed by smooth muscle cells, causes contraction of mature follicles at the time of ovulation which acts as a final trigger for oocyte release and expulsion from the ovary. The LoxP-Cre recombinase system was used to generation a conditional knockout of EDNRA specifically in the smooth muscle cells following Cre activation by exogenous tamoxifen administration; thus a model that has temporally-controlled removal of *Ednra* from only smooth muscle cells was created. This approach was chosen because global EDNRA knockout is embryonically fatal, resulting in facial, cranial, and cardiac defects; additionally, smooth muscle-specific *Ednra* knockout mice often fail to survive to reproductive age and exhibit systemic defects which may cause developmental abnormalities that may influence reproduction. It was hypothesized that, in SMACre^{ERT2}EdnraFlox mice, smooth muscle-specific ablation of EDNRA within would ovary inhibit ovulation and consequently prevent corpus luteum formation and progesterone production.

MATERIALS AND METHODS

Ethics Statement

This study was carried out in tight accordance with the recommendations in the Guide for the Care and Use of Laboratory Animals of the National Institutes of Health. Animal protocol was approved by the University of Kentucky Animal Care and Use Committee (Protocol 1111M2006) and the University of Illinois Animal Care and Use Committee (Protocols: 11184, 12090, 14222), and all efforts were made to minimize animal suffering.

Animal models and genotyping

Animals were maintained under a 12 hour light-dark cycle and given a continuous supply of Harlan (Indianapolis, IN) rodent chow and water. A tamoxifen inducible smooth muscle–specific Cre recombinase transgenic mouse line (SMACre^{ERT2}) was provided by Dr. Pierre Chambon[193,554]. To characterize Cre recombinase expression, B6;129S6-Gt^{279}26Sortm9(CAG-tdTomato)Hze/J reporter mice[177] (Ai9 mice) were purchased from Jackson Laboratories (Bar Harbor, Maine). These animals have a floxed stop codon in front of a constitutively active red fluorescent protein (RFP) gene; thus RFP is produced in cells that have been exposed to active Cre recombinase. To generate specific loss of the endothelin receptor A gene (*Ednra*), a floxed *Ednra* (EdnraFlox) mouse line, which carries two LoxP sites in the introns flanking exon 6, 7, and 8 of the *Ednra* gene (Figure 7.5), was used as a target for *Ednra* gene excision[555]. EdnraFlox mice were provided by Dr. Masashi Yanagisawa.

To generate reporter mice for SMACre^{ERT2} expression, heterozygous male SMACre^{ERT2} mice were crossed with homozygous Ai9 female mice. Offspring were examined for presence of the SMACre^{ERT2} gene by PCR using primers TK139 (5’-ATTTGCCTGCATTACCGGTC-3’) and TK141 (5’- ATCAACGTT TTGTTTTCGGA-3’)[193] with an amplicon size of 349 base pairs. Mice lacking the inducible Cre gene were used as controls. To generate smooth muscle-specific loss of *Ednra*, female EdnraFlox/Flox mice were first bred with male SMACre^{ERT2} mice, which resulted in the production of F1 heterozygotes, SMACre^{ERT2}EdnraFlox/+. Then SMACre^{ERT2}EdnraFlox/Flox female mice were generated by breeding male F1 SMACre^{ERT2}EdnraFlox mice and female EdnraFlox mice[177]. To confirm the EdnraFlox gene in the pups by PCR genotyping the primers EtaF (5'-CCTCAGGAAGGAAGTAGCAAGATTA-3')

and EtaR (5'-ACACAACCATGGTGTCGA-3') were used[555] with an amplicon size of 650 basepairs (floxed) or 610 base pairs (WT allele).

Tamoxifen-induced Cre recombinase activation and superovulation

To induce Cre recombinase in smooth muscle cells, post-natal day 28 (PND28) mice were exposed to tamoxifen (TAM) following Jackson Laboratories protocol by dissolving tamoxifen in corn oil at a concentration of 20mg/ml at 37°C in the dark and storing at 4°C and then injecting mice with 100uL solution intraperitoneally (i.p.) once every 24 hours for a total of 5 days (approximately 75mg TAM / kg body weight)[177,556]. Mice were monitored for adverse reaction to injection and were removed from experiment in that instance.

To induce ovulation and synchronize follicular development, mice were stimulated with gonadotropins following superovulation protocol. Mice were given a single i.p. injection of 5 IU pregnant mare serum gonadotropin (PMSG) in 100uL phosphate buffered saline (PBS) followed 48 hours later by a single i.p. injection of 5 IU human chorionic gonadotropin (hCG) in 100uL PBS. PMSG and hCG were purchased from Sigma (St. Louis, MO). Mice normally ovulate 12-14 hours after hCG injection.

Visualization of Cre recombinase activity

Twenty-eight day old SMACre^{ERT2} Ai9/+ mice received TAM treatment for 5 days, were allowed to recover for two days or 30 days, and were then superovulated (Figure 7.1A). Mice were euthanized by CO_2 asphyxiation and perfused intracardially with cold PBS solution and then a 4% paraformaldehyde (PFA) solution to assist in fixation. Tissues were fixed in 4% PFA overnight, then dehydrated in an ethanol series, embedded in paraffin blocks, and sectioned by microtome at 5um thickness. One section was used for fluorescence visualization and an adjacent slide was stained with hematoxylin and eosin staining for cellular visualization (Thermo Scientific, Kalamazoo, MI). Images were taken with a Zeiss SV11 fluorescent microscope, or an Olympus BX51 microscope for brightfield images and gross tissue images throughout all experiments.

Vaginal Cytology

Vaginal cytology was performed according to previously established guidelines for rats and mice[116]. Briefly, mice were smeared daily at approximately 1100 hours by application of

100uL of PBS into the distal aspect of the vagina followed by aspiration of fluids. Samples were placed into a clear 96-well plate and read using an inverted microscope (Olympus CKX41, Center Valley, PA). Proestrus (P) was characterized by predominantly round to polygonal cells that occasionally have a discernable nucleus with several leukocytes; Estrus (E) was characterized by many anucleate polygonal cells and a lack of leukocytes; Metestrus (M) was characterized by a combination of an equivalent number of leukocytes and anucleate polygonal cells; and Diestrus (D) was characterized by a marked dominance of small, round leukocytes. All smears were performed by one individual (JC).

Ednra *deletion after tamoxifen injection by RT-PCR*

Total RNA was extracted from ovaries 24 hours after TAM treatment and hCG injection (hCG 24hrs). Animals were euthanized by CO_2 asphyxiation and cervical luxation, ovaries were removed, and homogenized. RNA was extracted by Trizol® solution (Ambion, Carlsbad, CA), washed twice with ethanol, and then purified with a Qiagen RNEasy Kit (Valencia, CA). RNA was analyzed by a Nanodrop machine for quantity and quality. Complementary DNA was then generated by M-MLV Reverse Transcriptase using random primers. Template RNA quantities were normalized to 1.0μg/μL prior to reverse transcription. 1.0μL of resulting cDNA from each ovary was used as template with 15μL Taq Platinum (Invitrogen) and 0.3μL of each primer per PCR reaction; reactions were cycled 30x for 94°C for 1:00 min, 59°C for 1:00, and 72°C for 1:30. Amplified DNA (3.0 μL) was visualized on a 2.0% agarose gel and was quantified using ImageJ freeware (NIH, Bethesda, MD) to measure peak pixel grayscale levels within the defined areas of the bands. To confirm the deletion of *Ednra* in smooth muscle cells, the primer set EDNRAKO_F (5'-GAGAACCTACAACTGGGGACACAAACAC-3') and EDNRAR (5'-ACACAACCATGGTGTCGA-3') was used to produce a 1200bp amplicon (Figure 7.5). PCR products were visualized on an agarose gel; band intensity was analyzed using ImageJ software (NIH, Bethesda, MD) for relative intensity. The ribosomal 60S subunit L19 (*Rpl19* gene; L19) was used as an internal control with (5'-CCTGAAGGTCAAAGGGAATGTG-3') and (5'-GTCTGCCTTCAGCTTGTGGAT-3'). Five animals were used for each treatment and cDNA was used from each for each gene.

Histology and immunohistochemistry (IHC)

After fixation in the 4% PFA, tissues were then embedded in paraffin and sectioned at 5 μm, mounted on charged glass slides, deparaffinized, and rehydrated. Tissues were then either stained with hematoxylin (Harris) and eosin (Surgipath) for cellular visualization, or were processed for immunohistochemistry to localize contractile cells or those actively involved in steroidogenesis. For IHC, smooth muscle actin was chosen as a target to identify smooth muscle cells; P450scc, which converts cholesterol to pregnenolone, was chosen as a steroidogenic enzyme target. Antigen retrieval was done with Tris EDTA buffer pH 9.2 for 60 minutes in an Oster 5711 Food Steamer, rinsed under deionized water for 5 minutes, loaded in a humidifying chamber, and washed with PBS + 0.2% tween20 to remove bubbles. Tissues were then blocked with 5% rabbit serum for 30 minutes, treated with the primary polyclonal antibody rabbit anti-mouse alpha Smooth Muscle Actin (αSMA) Abcam ab5694 at a 1:200 dilution, goat anti-mouse Cyp11a1 (P450scc, also cytochrome P450 XIA) Santa Cruz sc-18043 at a 1:200 dilution, or Dako negative control rabbit immunoglobulin fraction (8.7μL in 700 μL of PBST normalized to the SMA concentrate), washed twice with PBST, treated with fresh Avidin Biotin complex solution for 20 minutes at room temperature, washed twice with PBS, and incubated with Nova Red for 2 min at room temperature, prior to 10% hematoxylin counterstaining. Molecular reagents were purchased from Invitrogen (Invitrogen, Carlsbad, CA).

Ovary mounting and isometric tension measurement

Ovaries used for tension analysis were placed into a 4°C physiological saline solution (PSS) at 37°C, where a wire myograph system (Tissue Bath System 620M, Danish Myo Technology, DMT-USA Inc., Ann Arbor, MI) was located. Whole ovaries were used after the removal of ovarian vessels, and pin mounting was chosen to minimize tissue damage and increase mounting speed. Each ovary was punctured on each end by one of the 4mm mounting pins on each arm of the myograph. The myograph was then turned on, to gradually heat the PSS back to 37°C (minor cooling during mounting) while also slowly bubbling a mixture of 50% oxygen, 45% nitrogen, and 5% carbon dioxide through the chamber. Meanwhile, fresh PSS and a 60mM K+ in PSS (K+PSS) were placed into a water bath to also reach a physiological temperature. Two ovaries were processed at the same time for each set of experiments. Ovarian tensile measurements were recorded via LabChart software (ADInstruments, Colorado Springs, CO). After about 20 min when

the test chamber containing the ovary had reached the appropriate temperature, the PSS solution was removed and fresh, warm PSS buffer was added. The system was then zeroed. Tension was next repeatedly applied to the half ovary over the following 20 min to maintain a constant tension of 3mN. Optimal tension-contraction response in ovaries occurred with ~1mN of passive tension applied per whole ovary. Lastly, a 'wake-up' protocol was used to finish the equilibration: K+PSS was applied to the stretched ovary, and was removed 3 min later. The ovary was then washed 4 times over 5 min with PSS, and allowed to sit for 5 more min. This procedure was repeated twice. The PSS was then replaced a final time and the contractile experiment began, time zero.

To determine strength of ovaries contraction in response to endothelin-2 agonization, ovaries were first allowed to sit in fresh PSS at a physiological temperature and pH with supplied oxygen and CO_2 for five minutes to generate a baseline tensile measurement, the average tension in mN during this treatment. For ovaries that demonstrated cyclical contractions during this period, baseline measurements were averages of the trough tension for five troughs between peaks. Next, K+PSS solution was applied a third time for a duration of 5 minutes. This served as a reference point for the relative contractility of that ovary to account for variation in mounting, ovary size, and ovary health. Any ovary that failed to demonstrate contraction in response to K+PSS was discarded. K+PSS was then removed with four PSS washes at 1 minute intervals, and the ovary was allowed to equilibrate for 5 additional minutes. Next, human endothelin-2 purified peptide (American Peptide Co, Sunnyvale, CA) was added to the PSS solution of the chamber to generate a 50nM solution. After 20 minutes, without changing the buffer solution or removing the ligand, the dual-endothelin receptor antagonist drug tezosentan was added to a concentration of 140nM and left for 20 minutes. These concentrations were calculated from titration experiments in which increasing amounts of EDN2 peptide were added to ovaries and the relative change in tension was recorded. 50nM of EDN2 was the lowest dose that consistently produced the strongest contraction (Figure 7.8). Tensile measurements represent the difference from resting measurement (the average of 5 minutes prior to the final K+PSS addition) to either average K+ contraction (the average of minutes 2:00-5:00 after the K+PSS addition at 0:00) or average EDN2 contraction (the average of the 5 minutes prior to tezosentan administration for EDN2-induced contraction). The average of the final 5 minutes of the experiment was subtracted from peak EDN2-induced tension to calculate the change after tezosentan addition. All measurements were made in mN, and were later converted to arbitrary units (AU) for relative comparison by dividing each by the contractile

response to K+PSS for that ovary. Titrations of EDN2 or tezosentan to determine minimum concentrations for optimum effect were made as above, except varying doses of each were added in 20 minute intervals without washing away previous buffer solution to those ovaries; aortic and uterine tissues were used as smooth muscle controls (data not shown).

Ovarian transplantation

The mice were anesthetized by continuous nasal inhalation of isoflurane (2-2.5%) with 1 liter per minute (LPM) of oxygen flow. After appropriate depth of anesthesia was reached, fur was removed from an area centered over the proposed incision sites, 15 mm wide by 30 mm long. The size of the area clipped was proportional to the size of the mouse. Skin was disinfected with surgical iodine and 70% ethanol using sterile applicators. Eye gel/ointment was applied to both eyes to prevent dehydration. The mouse was placed on a heat pad (37°C) to prevent hypothermia during surgery. The donor mouse was placed in ventral-lateral recumbency. A 4-7mm skin incision was made parallel and ventral to the spine midway between the last rib and the iliac crest. An incision was made in the underlying abdominal wall. Forceps were used to spread open the incision to look inside the abdominal cavity and locate the ovary. Forceps were used to grasp and exteriorize the ovarian fat pad. The fat pad was positioned on a 2x2 Versalon sterile sponge so that the ovary was facing the surgeon and the oviduct was ventral. A Moria forceps was placed under the ovary (medial aspect) to clamp the ovarian blood vessels. A second pair of Moria forceps was placed immediately proximal to the first pair and used to shear the ovary off of the ovarian blood vessels. Before releasing the first forceps, one drop of epinephrine was added to the vascular stump for one minute. The collected ovary and fat pad were placed in a petri dish of sterile PBS. Each ovary was dissected free of the ovarian bursa and fat pad using Dumont forceps and fine scissors. The donor ovary may also have been bisected at this point.

The same procedures were performed to the recipient mouse until exteriorization of the ovarian fat pad, and the fat pad was positioned the same way as the donor mouse. The ovarian bursa was incised cranially at the junction of bursa and fat pad using Vannas micro-scissors. Dumont forceps were used to slide the bursa ventrally off the ovary and place it proximal to the oviduct. A Dumont forceps was placed under the ovary (medial aspect) to clamp the ovarian blood vessels. A second pair of Dumont forceps was placed immediately proximal to the first pair and used to shear the ovary off of the ovarian blood vessels. Before releasing the first forceps,

epinephrine was again added. The excised recipient ovary was discarded. If bleeding was observed from the ovarian vessels, hemorrhage was controlled using direct pressure with a sterile cotton tipped applicator. The donor ovary or half ovary was placed on top of the ovarian blood vessels. The ovarian bursa located near the oviduct was retracted over the donor ovary and tucked back into its original position using one or both pairs of Dumont forceps. The fat pad and ovary were returned to the abdominal cavity. The incision in the abdominal wall was closed with 5-0 or 6-0 absorbable suture with a swaged on needle. The skin incision was closed with the same suture in a simple interrupted pattern or with wound clips. Skin suture or wound clips were removed 7 days later.

The post-surgical mice were transferred to a clean, warm cage. Mice were placed on a paper towel in ventral or lateral recumbency with head slightly extended. A paper towel was placed under the rodent to minimize bedding adhering to the incision site. Each mouse was given a subcutaneous injection of warm sterile saline (1-2 cc/25g body weight) and carprofen 5mg/kg was injected subcutaneously. Supplemental heat was provided by placing the recovery cage on a slide warmer. The cage was warmed to 80-86°F (26.7-30°C) and the animal was provided a means to move away from the heat source once awake. The anesthetized mouse was observed every 10 minutes until it was able to move about the cage on its own to ensure that it did not obstruct its nose. Frequent stimulation such as touching and moving the mouse was performed. The following were interpreted as signs of pain or distress: constant facial expression of discomfort (orbital tightening, nose bulge, cheek bulge, and "pulled back" ear position), facial wiping with the forelimb, licking, biting, and scratching the surgical wound, and additional carprofen was administered every 12 hours.

Serum Steroid Measurement

Progesterone was considered the principle hormone measured and all others were secondary. Samples were prepared by spinning down whole blood after clotting and removing the serum supernatant. 10 μL of mouse serum was mixed with 50 μL methanol and 1 μL of 2 μg/mL D9-progesterone, followed by centrifugation. The supernatant was subjected to LC/MS/MS injection at the Metabolomics Center at the University of Illinois at Urbana-Champaign by Dr. Lucas Li. The standard solutions for the calibration curve used double charcoal-stripped steroid free mouse serum provided by Dr. Kee Jun Kim and followed the same extraction protocol as the

serum samples. For detection, samples were analyzed with the 5500 QTRAP LC/MS/MS system (AB Sciex, Foster City, CA) in Metabolomics Lab of Roy J. Carver Biotechnology Center, University of Illinois at Urbana-Champaign. The 1200 series HPLC system (Agilent Technologies, Santa Clara, CA) includes a degasser, an autosampler, and a binary pump. The LC separation was performed on an Agilent Zorbax SB-Aq column (4.6 x 50mm, 3.5μm.) with mobile phase A (0.1% formic acid in water) and mobile phase B (0.1% formic acid in acetonitrile). The flow rate was 0.3 mL/min. The linear gradient was: 0-2 minutes, 60%A; 6-12 minutes, 0%A; 12.5-17 minutes, 60%A. The autosampler was set at 5°C. The injection volume was 5 μL. Mass spectra were acquired under positive electrospray ionization (ESI) with the ion spray voltage of 5500 V. The source temperature was 550°C. The curtain gas, ion source gas 1, and ion source gas 2 were 38, 50, and 65, respectively. Multiple reaction monitoring (MRM) was used to measure progesterone (m/z 315.1-->m/z 97.1) with D9-progesterone used as internal standard (m/z 324.1 --> m/z 100.1).

For additional steroid profiling, samples were prepared by using 20 μL mouse serum sample mixed with 40 μL methanol and 1 μL 2 μg/mL D9-progesterone, followed by the rigorous centrifugation. The supernatant was subject to LC/MS/MS injection. The standards solutions for the calibration curve again used double charcoal-stripped steroid free mouse serum, and followed the same extraction protocol as the serum samples. Samples were again analyzed with the 5500 QTRAP LC/MS/MS system (AB Sciex, Foster City, CA) in Metabolomics Lab of Roy J. Carver Biotechnology Center, University of Illinois at Urbana-Champaign. The LC separation was performed on a Phenomenex C6 Phenyl column (2.0 x 100mm, 3μm.) with mobile phase A (0.1% formic acid in water) and mobile phase B (0.1% formic acid in acetonitrile). The flow rate was 0.25 mL/min. The linear gradient was as follows: 0-1 minutes, 80%A; 10 minutes, 65%A; 15 minutes, 50%A; 20 minutes, 40%A; 25 minutes, 30%A; 30 minutes, 20%A; 30.5-38 minutes, 80%A. The autosampler was set at 5°C. The injection volume was 5 μL. Mass spectra were acquired under positive electrospray ionization (ESI) with the ion spray voltage of 5500 V. The source temperature was 500 °C. The curtain gas, ion source gas 1, and ion source gas 2 were 36 psi, 50 psi, and 65 psi, respectively. Multiple reaction monitoring (MRM) was used to measure steroids with the following transitions (Q1-->Q3) with D9-progesterone as internal standard (m/z 324.1 --> m/z 100.1). Progesterone Q1 (m/z): 315.1, Q3 (m/z): 97.0; 5β-

corticosterone Q1 (m/z): 349.2, Q3 (m/z): 313.2; deoxycorticosterone/11β-hydroxyprogesterone Q1 (m/z): 331.2, Q3 (m/z): 97.1; pregnenolone Q1 (m/z): 317.1, Q3 (m/z): 299.0.

Fertility assay

This assay was conducted to determine if mice were capable of giving birth to a normal number of litters with a normal number of pups (approximately 8/litter) and gender distribution (50% male). Adult female mice being tested, age two months to six months, were randomly allocated into groups of two or three females of each treatment. Each set of females was paired for 10 days with a proven WT male breeder, age 3 months – 7 months. Females were then removed from the male and separated into individual cages for 21 days and monitored daily. The percentage of females that gave birth from each treatment group, the average number of pups per litter, and the gender distribution of the pups was recorded. Females then continued with the experiment (Figure 7.15) or repeated the breeding assay (Figure 7.16) two to four more times.

Experiments

Three sets of experiments and one pilot study were conducted to determine what effect loss of *Ednra* in smooth muscle cells in the ovary has on ovulation and the ability of the ovary to contract, following confirmation of *Ednra* loss and model validation. 1) Twenty-eight day old SMACre^{ERT2}EdnraFlox and sibling EdnraFlox (control) female mice were treated with tamoxifen and given either two or 30 days to recover (Figure 7.1A). Mice were then superovulated. Young mice were chosen to prevent confounding estrous cycling from having already occurred. To allow for any potential delay in ovulation, ovaries were collected at hCG24 hours and histology was performed; concurrently, oocytes were collected from the oviduct and the number of oocytes were counted. Serum hormones were measured at hCG24 hours. Isometric tension analyses were performed with whole ovaries at hCG12-16 hours, approximately the time of ovulation, to measure the contractile effects of a physiological concentration of EDN2 peptide.

2) Global loss of *Ednra* in smooth muscle cells occurs in SMACre^{ERT2}EdnraFlox mice after TAM as a confounding factor. In the second experiment, this effect was minimized by first exposing the mice to tamoxifen, then surgically transplanting half of an exposed ovary to a WT ovariectomized (OVX) recipient female mouse (Figure 7.13B). Recipients received one half ovary of each genotype (n=16). Vaginal smears were conducted to confirm return to estrous stage and

successful ovarian function. Mice were then superovulated and tissue was collected. Histology was performed on ovaries at hCG 24 hours; oocytes were collected at hCG24 hours, counted, and their ability to expand the cumulus oocyte complex was examined by treatment of hyaluronidase (80 IU/ml). Immunohistochemistry for P450scc was performed on ovaries, and progesterone was measured and compared to WT mice that had not received surgery to monitor if progesterone production remained normal.

3) A third experiment was performed to examine the effect of *Ednra* loss after TAM treatment on fertility (Figure 7.15). Sixty day old OVX females received whole ovaries from untreated 28 day old donors, either SMACre^{ERT2}EdnraFlox or control mice. Recipients received two whole of the same genotype (n=4 of each). Vaginal smears were conducted to ensure normal ovarian function. Mice were then superovulated and a baseline blood sample was collected at hCG24 hours. Next, mice received TAM and then underwent a fertility study. Vaginal smears were again recorded after the fertility study to ensure normal cyclicity as a proxy for function. Mice then received TAM again for 5 days, were superovulated, and sacrificed. Tissues were collected and oocytes were counted at hCG24 hours. Blood was also collected, and histology was also performed on uterine tissues.

4) In a fourth pilot experiment to examine the alternative hypothesis that loss of *Ednra* specifically in granulosa cells inhibits ovulation, Cyp19-iCre[372] mice and Amhr2-Cre[557-560] mice were crossed with EdnraFlox mice and underwent a fertility assay as described previously. Some mice were sacrificed, and ovarian histology was performed in naturally cycling adult female mice (age 3-7 months). Cyp19-iCre mice[372] were obtained from Dr. Joanne Richards and Amrh2-Cre mice[561] were purchased from Jackson Laboratories.

Statistical Analysis

Data analyses were performed using statistical software (SPSS, Inc., released 2013, PASW Statistics for Windows, Version 22.0, Chicago, IL). Continuous data were tested for normal distribution by a Shapiro-Wilk test. All normally distributed continuous data were analyzed with parametric tests (student's t-test, ANOVA, or paired student's t-test) and a Bonferroni *post hoc* test. All non-normally distributed continuous data were analyzed by non-parametric tests (Mann Whitney U, Kruskal Wallis ANOVA). Ordinal data were similarly analyzed. Data are graphically

presented as the mean and standard error of the mean unless otherwise indicated. For all analyses the alpha value was set to 0.05.

RESULTS

Recombination occurs in ovarian smooth muscle after tamoxifen (TAM) treatment

This study sought to determine the role of endothelin receptor A (*Ednra*) in ovulation in the ovary, specifically in smooth muscle cells. To accomplish this, transgenic mouse models were utilized. A mouse that expresses Cre recombinase under the smooth muscle actin promoter with a tamoxifen-inducible mutation in the promoter was selected and validated to prevent developmental defects that otherwise occur[555,562]. These SMACre^{ERT2} mice were crossed with Ai9 tomato reporter mice in order to demonstrate areas of Cre activity by red fluorescence. Mice were exposed to tamoxifen (TAM) and tissues were collected (Figure 7.1A). In control ovaries that did received vehicle (corn oil) injection without TAM, no fluorescence was observed grossly or histologically (Figure 7.1B, left). No fluorescence was observed in ovaries of mice that were superovulated immediately after vehicle treatment or that were allowed to recover for 30 days before superovulation (Figure 7.2, top right). With only vehicle treatment, mild fluorescence was observed in the bladder and several cells per section of the heart. When observed grossly, visible fluorescence was only present in the bladder but no other organs (data not shown). In general, Cre activity without TAM is punctate or scattered in the bladder, and severely limited in other organs including the heart, GI tract, ovary, aorta, and skeletal muscle; such limited recombination is unlikely to contribute to a phenotype when coupled with a floxed gene of interest.

In mice that received TAM and were then superovulated (Figure 7.1B, center), marked fluorescence was observed in ovary, oviduct, and uterus grossly, indicating successful recombination. Fluorescence was observed in the smooth muscle cells surrounding the follicles, in the large and medium vessels, and in the newly forming corpora lutea of the ovaries as expected. Similarly, fluorescence was noted in the smooth muscle cells of the oviduct, the aorta, the GI tract (specifically in the longitudinal and circular muscle about the tubular organs as well as in the center of individually villi), in the myometrium of the uterus, in all three layers of the detrusor muscle of the bladder as well as on the luminal edge of the transitional epithelium therein, and in arteries and arterioles throughout the body (Figure 7.2). Consistent fluorescence was not observed after TAM treatment in cardiac or skeletal muscle, except for the vessels within (Figure 7.2, bottom right). In SMACre^{ERT2}Ai9 mice that received TAM treatment and then had a 30 day delay before superovulation, fluorescence was again grossly observed in the ovary, oviduct, and uterus (Figure 7.1B, bottom right). However, gross intensity was decreased. Thirty days was chosen based on the

half-life of tamoxifen, which is approximately 7 days *in vivo*[563,564]; a time greater than four half-lives was chosen as the potential effect of tamoxifen is reduced. When observed histologically 30 days after TAM, ovaries had fewer red fluorescent cells. Cell number was reduced by approximately 75%. Those cells retaining fluorescence were present around follicles and vessels, and some were also present within corpora lutea. This indicates a relatively rapid turnover of smooth muscle cells within active mouse ovaries, and that this Cre recombinase is not active in parent stem cells giving rise to new smooth muscle cells. When SMACre^{ERT2}Ai9 mice that did not receive TAM were examined for expression (Figure 7.3), mild exogenous Cre activity was detected in the bladder and several cells of the heart, but not in the GI tract, the female reproductive tissues, aorta, or skeletal muscle.

Additionally, it was observed that TAM treatment alone modified vaginal cytology when smears were performed. Beginning approximately 1-2 days after the first TAM injection, normal cyclicity (4-6 day cycle) ceased. On vaginal smears, cells were predominantly leukocytes, though many rounded anucleate epithelial cells lacking the more sharply defined edges commonly seen during estrus or diestrus were also present (Figure 7.4). This cytology remained consistent throughout TAM treatment and for several days following. Given the high prevalence of leukocytes, it is most similar to diestrus and was marked as such for later graphs of vaginal smears. These data indicate tamoxifen at the given dose causes significant changes in the vaginal epithelium that may affect function and receptivity.

Ablation of Ednra *in ovarian smooth muscle cells*

To determine the effect of loss of *Ednra* during ovulation, SMACre^{ERT2} mice were crossed with EdnraFlox mice. Tamoxifen treatment and subsequent recombination resulted in the loss of three critical exons within the *Ednra* gene, exons 6, 7, and 8 (Figure 7.5). A 1200 base pair band was detected following successful recombination through PCR of genomic DNA extracted from whole ovaries. Amplification of this sequence occurred in SMACre^{ERT2}EdnraFlox following TAM treatment, but not with vehicle treatment (Figure 7.5A) or in any control ovaries with TAM or vehicle treatment. To roughly quantify the amount of recombination occurring in SMACre^{ERT2}EdnraFlox ovaries at hCG24 hours, total RNA was extracted from ovaries and subjected to semi-quantitative RT-PCR (Figure 7.5B). Ovaries were from control mice with vehicle treatment (lanes 1-2), control mice with TAM treatment (lanes 3-4),

SMACre^{ERT2}EdnraFlox mice with TAM treatment and a 30 day delay before superovulation (lanes 5-6), or SMACre^{ERT2}EdnraFlox mice with TAM treatment and no delay (lanes 7-8). The gene *Rpl19* was used as an internal control for each sample (n=5/group). Band intensity was quantified as a relative marker of the amount of RNA present (Figure 7.5C). No differences in the amount of *Ednra* RNA were observed, likely because of the many ovarian cells present in which recombination did not occur in each treatment group and the wide-spread expression of *Ednra*. As expected, only SMACre^{ERT2}EdnraFlox ovaries that had been exposed to TAM had a knockout band present. Amplification was significantly greater in ovaries that had recently been exposed to TAM rather than a 30 day delay before superovulation, likely indicating renewal of *Ednra* expression to some smooth muscle cells during the delay, though partial gene deletion remains present.

Tamoxifen treatment does not prevent ovulation or corpus luteum formation

To determine if TAM treatment modifies ovarian function, ovaries were collected from superovulated control adult mice 2 months of age at hCG18 hours immediately after TAM or vehicle treatment (Figure 7.6). Ovarian histology was performed and compared by hematoxylin and eosin staining. To examine the localization and effect of TAM on the smooth muscle network of the ovary, immunohistochemistry (IHC) was performed with anti-alpha smooth muscle actin (αSMA). Additionally, to examine one aspect of steroidogenic function necessary for progesterone production, IHC was performed with anti-P450scc. No significant qualitative differences were observed between treatments. Ovaries appear normal with follicles of all stages present as well as corpora lutea. No difference was observed in the smooth muscle network present; anti-αSMA staining is present around follicles and corpora lutea, around vessels, and within corpora lutea of each group. Staining is also visible within the oviduct on some slides. This pattern matches the red fluorescence pattern seen in SMACre^{ERT2} Ai9 mice (Figure 7.1). Anti-P450scc staining was observed in the stroma of each ovary and also within the corpora lutea of each. Follicular development, the smooth muscle network, and P450scc expression were not modified during superovulation following TAM treatment.

Tamoxifen treatment reduces the number of oocytes ovulated

To examine the effect of *Ednra* loss in the smooth muscle on ovulation, 28 day old mice were superovulated after TAM or vehicle treatment. Oocytes were collected from the oviduct 18 hours after hCG was administered. Histology was performed on collected ovaries. No differences were noted between ovaries of any treatment group (Figure 7.7). There were no differences in follicle count by stage, number of corpora lutea, or ovarian size; mild hemorrhage was present within some ovaries of each treatment group. Oocyte quantification (Figure 7.7B) revealed a significant difference between WT ovaries with vehicle treatment and WT ovaries with TAM treatment ($p=0.003$). There was also a significant difference between WT ovaries with vehicle treatment and SMACre^{ERT2}EdnraFlox ovaries with TAM treatment ($p<0.001$), and between SMACre^{ERT2}EdnraFlox ovaries with vehicle treatment and either WT or SMACre^{ERT2}EdnraFlox ovaries with TAM treatment. There was no significant difference between WT and SMACre^{ERT2}EdnraFlox ovaries with vehicle treatment ($p=1.000$). However, there was no significant difference between WT and SMACre^{ERT2}EdnraFlox ovaries with TAM treatment ($p=0.462$). These data indicate that vehicle treatment alone has no difference in impact on ovulation. TAM treatment has a significant impact on ovulation in each group, likely because of its role as an estrogen receptor antagonist throughout the body. This is a confounding issue with this model system; TAM alone causes more than a 50% reduction in ovulation. Furthermore, as there is no difference between genotypes with TAM treatment, it is not possible to discern if a difference in ovulatory ability with loss of *Ednra* exists or not, as the changes caused by TAM may be masking any differences in ovulation. There is a slight decrease in the average number of oocytes ovulated in SMACre^{ERT2}EdnraFlox mice with TAM treatment, from 15.6±4.4 in the WT to 9.2±2.0 in conditional knockout animals, but this difference is not significant. The large variation may be accounted for by multiple ovaries failing to ovulate in each group (5 and 10, respectively) and the normal large variation seen even in WT ovaries with vehicle treatment (34.7±3.5, range 19-57). However, the percentage of ovaries that failed to ovulate in each group (0% in WT+vehicle, 4.5% in SMACre^{ERT2}EdnraFlox +vehicle, 35.7% in WT+TAM, and 43.5% in SMACre^{ERT2}EdnraFlox +TAM) indicate that TAM alone prevents nearly half of the exposed ovaries from ovulating regardless of genotype. Also of note, the majority of the time it was only one ovary in each mouse that failed to ovulate. These data support that TAM treatment alone

inhibits ovulation regardless of gene loss, preventing conclusion on the effect of *Ednra* loss on ovulation alone.

No difference in contraction immediately after TAM treatment

To determine if smooth muscle loss of *Ednra* influences ovarian contraction in response to EDN2 peptide, isometric contraction was performed on ovaries at hCG12-16 hours. First, the response of WT ovaries to EDN2 was compared without TAM treatment (Figure 7.8). Following mounting, ovaries were normalized to K+PSS and then exposed to increasing concentration of EDN2 in PSS, from 50pM to 50nM (n=4). Contraction increased linearly in response to increasing doses of EDN2. At 50nM, contraction response reached a near maximum with little increase in tension from previous concentration (Figure 7.8, bottom graphs). The average increase in tension from baseline in response to 50nM EDN2 for an ovary without TAM treatment was approximately 0.3 mN, or about 2.5 times the average response to K+PSS. This concentration was also used previously by Ko *et al*. 2006[6], and allows for simple comparison. Thus 50nM was used as an EDN2 concentration for future study on EDN2-induced contraction in conditional *Ednra* knockout ovaries.

Ovaries at hCG 12-16 hours from SMACre^{ERT2}EdnraFlox and control mice (n=8) that had previously received TAM were mounted and the response to compared EDN2 was compared (Figure 7.9). Representative responses are shown. The average response to EDN2 at 50nM in control ovaries was 0.4 mN and 2.2 times the average response to K+PSS. Similarly, the average response to SMACre^{ERT2}EdnraFlox ovaries to EDN2 was 0.3 mN and 2.0 times the average response to K+PSS. To confirm that this was specific to endothelin receptors, the dual endothelin receptor antagonist tezosentan was added at a concentration of 140nM after EDN2 and without washing away the solution. This concentration of tezosentan was previously shown to prevent EDN2-induced contraction when administered first (data not shown). The average reduction in tension after tezosentan in control tissues was 0.2 mN and 0.9 times the response to K+PSS; similarly, the response to tezosentan in SMACre^{ERT2}EdnraFlox ovaries was 0.1 mN and 0.9 times the response to K+PSS. There were no significant differences in tensile response to K+PSS, EDN2 at 50nM, or tezosentan at 140nM in ovaries of either genotype ($p>0.05$ for all comparisons). It is also interesting that the response to K+PSS occurs immediately after the solution is changed. However, there is a delay of between 5 and 10 minutes from when EDN2 50nM solution is added

and ovarian contraction occurs, demonstrating that smooth muscle depolarization is not immediate. This may occur simply because of the signaling response time required for the GPCR endothelin receptors to act through downstream mediators, or because signaling may be occurring between cell types in an autocrine or paracrine fashion.

No difference in oocytes ovulated 30 days after TAM treatment

Ovaries were collected at hCG24 hours from superovulated PND 65 mice, 30 days after receiving TAM treatment (Figure 7.10). Oocytes were collected from the oviduct and counted after hyaluronidase treatment. There was no significant difference (p=0.389) in the number of oocytes ovulated between control mice (n=4) and SMACre^{ERT2}EdnraFlox mice (n=6); all ovaries ovulated. The amount of oocytes ovulated per ovary (12.8±1.2 vs 10.1±2.5, respectively) was more similar to that ovulated by younger mice with TAM and no delay than to vehicle treated mice with no delay before superovulation. Histologically (Figure 7.10), there were no differences in ovarian morphology between groups. Follicles of various stages and corpora lutea were present in ovaries of each group. There was no significant difference between control and conditional knockout mice in the number of corpora lutea per ovary (19.8±2.1 vs 18.0±1.4, p=0.494), the number of antral follicles per ovary (6.8±1.3 vs 8.8±2.5, p=0.550), or the ratio between them (3.7±1.3 vs 4.9±2.8, p=0.522). Serum sex hormones were also compared at hCG24 hours (Figure 7.11). There were no significant differences between progesterone (6.4±2.2 vs 5.7±0.6 ng/mL, p=0.779), 5β-corticosterone (1.9±0.5 vs 3.6±1.2 ng/mL, p=0.331), deoxycorticosterone (9.1±0.9 vs 14.7±4.6 ng/mL, p=0.354), or pregnenolone (0.8±0.2 vs 2.3±1.1 ng/mL, p=0.295). Though the n-value is relatively low, the high variation in this sample size and the similar means indicate that a very large number of animals would be needed to determine if slight differences between groups exist. As there are no significant differences between groups, it is possible that either *Ednra* loss has little effect on ovulation and related parameters, that *Ednra* loss was only partial given 75% reduction in red fluorescence in ovaries in earlier experiments after 30 days and this loss did not have a significant phenotype, or that TAM treatment permanently alters ovulatory ability given relatedness of the number of oocytes ovulated compared to superovulated mice with and without TAM treatment.

No difference in contraction 30 days after TAM treatment

Isometric contraction was performed on ovaries at hCG12-16 hours 30 days after TAM treatment from SMACre^{ERT2}EdnraFlox (n=6) and control mice (n=4). The response to K+PSS, 50nM EDN2, and 140nM tezosentan was quantified (Figure 7.12). Representative responses from each genotype are shown. The average response to EDN2 at 50nM in control ovaries was 0.4 mN and 2.7 times the average response to K+PSS. Similarly, the average response to SMACre^{ERT2}EdnraFlox ovaries to EDN2 was 0.4 mN and 3.1 times the average response to K+PSS. To confirm that this was specific to endothelin receptors, the dual endothelin receptor antagonist tezosentan was added at a concentration of 140nM after EDN2 and without washing away the solution. The average reduction in tension after tezosentan in control tissues was 0.3 mN and 1.7 times the response to K+PSS; similarly, the response to tezosentan in SMACre^{ERT2}EdnraFlox ovaries was 0.3 mN and 2.8 times the response to K+PSS. There were no significant differences in tensile response to K+PSS, EDN2 at 50nM, or tezosentan at 140nM in ovaries of either genotype ($p>0.05$ for all comparisons). These contractile responses were also similar to younger ovaries that did not have 30 day delay before collection. All ovaries demonstrate approximately a 0.4mN response to EDN2. Ovaries after the 30 day delay have a slightly stronger contraction in response to EDN2 relative to K+PSS than younger ovaries. Similarly, ovaries after the 30 day delay have a similar absolute change in tension in response to tezosentan, but this response is again elevated relative to the K+PSS response compared to younger ovaries. These slight differences in contraction response between age groups, but not genotypes, suggest that 50nM EDN2 is a consistently potent contractile agent, but that the response to K+PSS is slightly decreased in older mice.

Half ovary transplantation decreases oocytes ovulated

In a second set of experiments, half of an ovary from a control mouse and half of an ovary from a SMACre^{ERT2}EdnraFlox mouse were transplanted into the bursas of ovariectomized WT recipient mice. Half ovaries were used for their small size, which decreases the chances of leaving the bursa after surgery (Figure 7.13); additionally, the cut side of the ovary may expose the vasculature allowing for improved angiogenesis. The goal of this method was to decrease potentially confounding effects of TAM on the hypothalamus and pituitary within the reproductive axis, while allowing one ovary of each genotype to be under the same influence from a mature WT

reproductive axis. Previous data (Lin *et al.*, submitted for review) indicates that half ovaries are integrated normally after vascular reestablishment and can successfully respond to gonadotropins and ovulate within one week of surgery. Ovaries were exposed to TAM prior to transplantation and were superovulated after a recovery period. Though shorter than 30 days, this recovery period may have modified gene ablation; it was chosen as being necessary to allow vascular reformation and being one half-life of tamoxifen. However, tamoxifen concentrations inside the transplanted ovary likely decreased after the vascular supply was reestablished.

To confirm ovarian function and return of blood supply after surgery, vaginal smears were performed on the day of surgery before transplantation and for 8 days afterwards. All but one mouse was able to reach estrus (Figure 7.14A). Mice were superovulated and euthanized at hCG 24 hours. Ovaries were collected (n=16) and fixed for histology and oocytes within the oviduct were counted. Few oocytes were ovulated by ovaries of either genotype (Figure 7.14B) and though there was no significant difference between control and SMACre^{ERT2}EdnraFlox ovaries (1.4±0.7 vs 0.3±0.1 oocytes/ovary, p=0.093), there was a trend for more oocytes to be ovulated by control ovaries than SMACre^{ERT2}EdnraFlox ovaries (range 0-13 vs 0-2). The majority of the ovaries (9 and 11 per group, respectively) from either genotype failed to ovulate. Histologically (Figure 7.14E), ovaries exhibited infiltration of many leukocytes in each genotype. This may represent vascular remodeling continuing to occur after surgery; it may also represent graft rejection, though previous pilot studies demonstrated successful graft survival for up to 60 days and successful ovulation. Leukocyte invasion may also be occurring in response to previous TAM exposure. Ovaries of each genotype also had multiple corpora lutea and antral follicles. There were significantly more corpora lutea in control ovaries (8.8±1.3 vs 5.1±0.6, p=0.012), though there was no difference between control mice and SMACre^{ERT2}EdnraFlox in the number of antral follicles (4.7±1.0 vs 6.3±1.0, p=0.258). If corpora lutea are used as a proxy for ovulation, this suggests that move ovulations occur in SMACre^{ERT2}EdnraFlox ovaries in this treatment. However, as so few oocytes are recovered from any ovary, the oocytes themselves may be atretic prior to ovulation, or luteinization may occur without ovulation, though oocytes trapped within corpora lutea were not observed in either group of ovaries.

Transplanted half ovaries have normal CL formation and progesterone production

The functionality of the corpora lutea in each ovary was additionally examined. Ovarian sections were stained with anti-P450scc as a steroidogenic marker. Positive staining was seen in the new or forming corpora lutea in ovaries of each genotype (Figure 7.15A), confirming CL presence and presence of steroidogenic enzymes. Additionally, progesterone was measured from blood collected at hCG24 hours (Figure 7.15B). It was not possible to collect blood that had received steroids from only one ovarian genotype. However, if one or both ovaries were deficient in progesterone production, serum progesterone levels may have been lower overall, either from surgical treatment, TAM treatment, bisection, and/or gene loss. However, when serum progesterone from WT intact mice without TAM at hCG24 hours was compared to serum progesterone from mice receiving transplanted TAM treated half ovaries of each genotype, there was no significant difference (2.2±0.3 vs 1.9±0.1 ng/mL, p=0.320) (Figure 7.15B). Thus, even ovaries that have been exposed to tamoxifen, bisected, and surgically transplanted can still successfully ovulate within one week of surgery and exposure, albeit to a lower number of oocytes than non-surgical ovaries; these ovaries can also produce progesterone at concentrations similar to control mice, implying that they are likely able to maintain uterine function for implantation and pregnancy. Oocytes collected from these ovaries (Figure 7.15C) appear histologically normal and may be dissociated from the cumulus oocyte complex with hyaluronidase treatment as well.

Tamoxifen exposure prevents pregnancy

As mice given half ovary transplants after ovarian TAM exposure demonstrated severe ovulatory defects in each genotype whereas previous work demonstrates that half ovary transplant alone does not prevent ovulation, the TAM exposure might prevent transplant integration and function. To circumvent this issue, mice were generated with ovary-specific genotypes (n=4) and then provided TAM treatment for gene removal (Figure 7.16). Whole ovaries were transplanted to WT recipients; mice received two ovaries of the same genotype, either WT ovaries or SMACre^{ERT2}EdnraFlox ovaries. After recovering from surgery, mice were superovulated for baseline blood hormones, then exposed to TAM before immediately undergoing a breeding assay. Considering the loss of fluorescence previously observed 30 days after TAM in SMACre^{ERT2}Ai9 mice, these double ovarian transplant females received a second dose of TAM for five days before being superovulated and sacrificed at hCG24 hours (see Figure 7.16 for timeline).

After surgery, vaginal smears were used to confirm return of ovarian function (Figure 7.17). Each mouse experienced estrus at least once after surgery, confirming functionality of at least one ovary for sufficient hormone production to induce cycling. Blood was then collected at hCG24 hours, and mice were next dosed with TAM. Immediately after, mice underwent a breeding assay. Interestingly, no mouse became pregnant after being placed with a male for 10 days; thus TAM exposure inhibits reproductive receptivity up to 10 days after exposure. Though mice were not checked during fertility assay, vaginal smears after the last day of potential births indicated that mice were still cycling normally and were able to enter estrus (Figure 7.17); a fertility assay occurring with an intermittent period after TAM exposure may have yielded different results, though this may also have decreased the percentage of smooth muscle cells with *Ednra* ablation. Mice were again exposed to TAM and tissues were collected at hCG24 hours. No oocytes were obtained from any ovary of either genotype, further demonstrating that chronic TAM exposure alone prevents ovulation despite gonadotropin stimulation. Histologically (Figure 7.17C), some ovaries of each genotype appeared healthy with obvious follicles in multiple stages and visible corpora lutea, likely from previous ovulations. Alternatively, multiple ovaries of each genotype were shrunken, fibrotic, and lacked discernable follicles or even oocytes with no corpora lutea. Additionally, a high degree of inflammation was observed; these are likely from transplanted ovaries that did not establish a healthy vascular supply or/and were rejected. No remarkable changes were histologically observed in the oviducts of the mice. The uteri from the double TAM treated mice all had obvious and severe cystic endometrial hyperplasia at the end of the study (Figure 7.17C). The many large uterine cysts may likely have prevented pregnancy from occurring during the breeding study, even though mice may have been cycling. It is possible that an effect of TAM in the oviduct may also prevent oocytes from reaching the uterus, and would account for their absence during tissue collection.

TAM exposure after surgery decreases 5β-corticosterone and deoxycorticosterone production

At hCG24 hours at the time of euthanasia, mice with double whole ovarian transplants were weighed; ovaries were removed and weighed as well, and serum was collected for hormone analysis and comparison to serum hormones prior to TAM exposure at hCG24 but after surgery (Figure 7.18). There were no significant differences in body weight between mice with different ovarian genotype transplants. Additionally, there was no significant difference in ovarian weight

or the ovarian weight to body weight ratio between control and SMACre^{ERT2}EdnraFlox ovaries. When serum hormones were measured, there was no significant difference in serum progesterone between mice with differing ovarian genotypes either before TAM treatment or after TAM treatment, nor from before TAM to after TAM within a group. Similarly, there was no difference in 5β-corticosterone and deoxycorticosterone between mice of different ovarian genotypes at either time point. However, there was a significant decrease in 5β-corticosterone in mice from before TAM to after TAM treatment, though this was present in mice with ovaries of each genotype. The same is true for deoxycorticosterone, which sharply decreased from before to after TAM treatment (Figure 7.18). These decreases in steroid production outside what are normally considered reproductive hormones likely indicate a decrease throughout the body of all steroid production, as corticosterone is produced from cholesterol at an upstream junction in the steroid synthesis pathway from estrogen or testosterone. Parsimoniously, this is most likely occurring through the rejection of transplanted ovaries and their chronic inflammation throughout the duration of the experiment; similar changes in progesterone are likely not observed because it is lower in serum concentration and more highly variable within groups, though progesterone in all groups is lower than in WT intact control mice at hCG24 hours (Figure 7.18). Overall, it appears that two treatments with TAM decrease steroid production in general and inhibit pregnancy, ovulation, transplanted organ uptake, and cyclicity during the time of TAM exposure. Tamoxifen-dependent gene ablation in cells with a rapid turnover such as smooth muscle is considered a poor tool for reproductive studies in vivo where multiple systems are at the regulation of numerous steroids. Tamoxifen itself demonstrates a systemic confounding effect, and its modifications of steroid production similarly create a lasting systemic confounding effect as well.

Granulosa-cell specific loss of Ednra *causes decreased fertility and litter size*

Given challenges using tamoxifen dependent models, a new pilot study was conducted to examine the role of *Ednra* in the ovary in granulosa cells as an alternative hypothesis. It was postulated that *Ednra* expression in the granulosa cells may instead mediate endothelin action during ovulation. It was hypothesized that loss of *Ednra* in the granulosa cells would cause fewer or smaller litters during normal mating as a consequence of decreased oocyte release. Mice that produce Cre recombinase under the Cyp19 (aromatase) promoter or the Amhr2 promoter were crossed with EdnraFlox/Flox mice. These mice express Cre recombinase in the granulosa cells,

specifically during and after the primary follicle stage, thus preventing most developmental confounding influences. Two Cre lines were used because of their different Cre recombinase DNA sequences: Cyp19-iCre mice use codon improved Cre recombinase, which is reported to have better recombination efficacy than traditional Cre lines like the Amhr2-Cre mouse, the latter of which has been widely used and well characterized. Both of these granulosa cell-specific *Ednra* knockout mice underwent a fertility assay in comparison to WT mice. Mice were sacrificed without gonadotropin stimulation after several rounds of breeding and histology was performed (Figure 7.19). Reproductive function of the resulting mice was measured by fertility and litter size (number of pups per mouse and pups per litter, respectively) after breeding with proven males. Amhr2CreEdnraFlox mice demonstrated a slight trend towards reduced fertility while Cyp19iCreEdnraFlox mice had significantly reduced fertility (57.9% in Amhr2Cre mice and 42.3% in Cyp19iCre mice compared to 76.5% in WT mice, $p=0.22$ and $p=0.02$, respectively). In addition, Amhr2Cre and Cyp19iCre mice had significantly smaller litter sizes (3.55 +/-0.45 and 4.56+/- 0.53 vs 7.08 +/- 0.48 in WT, $p<0.01$ for each). Interestingly, these data are similar to fertility data observed in female mice that have lost endothelin-2 production specifically in the granulosa cells (data not published, previous chapter). Each group demonstrates approximately a 50% reduction in litter size, though only mice with loss of *Ednra* and not *Edn2* demonstrated decreased litters / pairing. These early data suggest that EDN2 plays a role in reproduction in the granulosa cells from which it is produced via an autocrine/paracrine pathway through *Ednra* signaling, as opposed to direct receptor stimulation of smooth muscle cells, and this pilot study conclusively demonstrates that *Ednra* in granulosa cells plays an important role for female fertility in mice and should be further explored.

DISCUSSION

A smooth muscle-specific tamoxifen-inducible Cre mouse (SMACre^{ERT2}) was crossed with an endothelin receptor A floxed (EdnraFlox) mouse to create a conditional loss of *Ednra* after tamoxifen (TAM) treatment in smooth muscle cells. It was hypothesized that loss of *Ednra* in ovarian smooth muscle cells would prevent ovulation by inhibiting the physiological contractile mechanism during ovulation. The data presented here established that tamoxifen successfully induced Cre recombinase throughout the smooth muscle system of the ovary as well as the rest of body when provided in the once per day for five day injection scheme developed by Jackson Laboratories for that purpose. Additionally, mild Cre recombinase activity occurred without TAM, particularly in the bladder in a punctate manner, though also in other organs in a highly dispersed and likely non-influential manner. At 30 days after TAM treatment, some smooth muscle cells within the ovary were no longer fluorescent in an Ai9 reporter line, indicative of cellular turnover and replacement by a precursor cell that lacks Cre activity. Use of this mouse model established that impaired ovulation occurs in mice after loss of *Ednra* in ovarian smooth muscle. However, TAM treatment alone significantly impacts ovulation, preventing further conclusions from being drawn. Loss of *Ednra* in granulosa cells also impaired ovulation in a pilot study, suggesting that EDNRA may influence ovulation through other pathways beyond smooth muscle contraction.

Tamoxifen is a known endocrine disrupting chemical (EDC) and acts as a competitive estrogen receptor antagonist throughout the body. It is now widely used for the treatment of human breast cancer. Estrogen receptors normally form a complex with the natural steroid hormones in the cellular cytosol and are then translocated to the nucleus[565] to influence RNA and DNA polymerase, estrogen response elements within the DNA, and RNA synthesis[566], which in turn modify protein production, metabolism, and cell cycling and proliferation[567]. Thus, estrogen exerts a profound and widespread influence throughout the body in both males and females. Chronic and acute TAM treatment inhibit estradiol uptake *in vivo*[568]. A single dose will produce an antiestrogenic effect in rats for up to three weeks after treatment[569,570]. Similarly, mice exhibit long term vaginal refractoriness[570], and both the uterus and vagina have inhibited estrogen binding for up to 6 weeks *in vivo* with a 1.5mg dose on two consecutive days[571]. The influence of tamoxifen is related both to the concentration of the drug given and to the relative estrogen concentration in the animal, the latter of which influences bioavailability through receptor presence[572]. TAM has a dissociation almost 100 times faster than estradiol[573]; it was generally considered to have

estrogenic effects in mice and will cause vaginal cornification at 1.5mg/kg doses[574] and increases in uterine weight. However, prolonged administration can cause antiestrogenic and antifertility responses[570,571,575-577]. TAM also inhibits estrogen-induced pituitary sensitization[578], terminates pregnancy[579-581], and induces cystic endometrial hyperplasia of the uterus[582,583]. At the given dose of 2mg/mouse/5 days or 75mg/kg/5 days used for successful Cre recombinase induction, TAM assuredly has an effect lasting multiple weeks with a systemic antiestrogenic influence. This is the major weakness of the approach presented in this study, and of using tamoxifen-inducible Cre mice in general. It is important to consider the systemic impact of both tamoxifen and estrogen for future use of tamoxifen-inducible Cre model organisms. It is unsurprising that roughly 50% of adult mice without any surgery or delay after TAM of either genotype tested failed to ovulate in response to gonadotropins after TAM treatment, and those that did ovulate had a marked reduction from vehicle treated mice (Figure 7.7). Additionally, as TAM has a lasting effect for up to 6 weeks at a lower dose, it is not unexpected that treated mice ovulated relatively few oocytes even 30 days after TAM (Figure 7.10) and did not become pregnant during a fertility test. TAM treatment may also account for the decreased steroidogenesis in the whole ovary transplant mice as well (Figure 7.18), which showed low progesterone levels at all points relative to the expected concentration, and a decrease in both corticosterone pathway products after TAM. The presented results are similar to those from early studies that focused on TAM alone without genetic modification.

This study presents novel data on ovarian contraction relative to endothelin-2 (EDN2) treatment. Previous work by Ko *et al*. (2006)[6] demonstrated that rat ovaries contract in response to EDN2 at a 50nM dose and that this tension could be modified by treatment with tezosentan at 605nM (10mg/mL) as well, when compared to a K+ control (concentration not reported). The presented data show that EDN2 at 50nM produces a similar relative response in mouse ovaries (2.5x K+ solution) and that tezosentan reduces this contraction (1x-1.5x), albeit at approximately 15% the dose of tezosentan previously reported. This is also the first reported use of a commercially available digital system to measure mouse ovarian contraction, whereas previous experiments have used custom analog systems. The dose of EDN2 used for contraction in these experiments was chosen based on the concentration needed for maximal contractile response (Figure 7.8). This is approximately 500 times the calculated amount of EDN2 present in a human ovarian follicle when collected for IVF (100pg/mL[14] and 3.7mL volume[584], about 0.1nM). However, 100pg/mL was determined in follicular fluid that was collected prior to ovulation[14], and

rat ovaries have many more follicles and a larger change in ovarian volume than humans near ovulation[585,586]. As IVF collection occurs prior to ovulation when EDN2 mRNA dramatically increases in rodents, it is possible that much higher EDN2 concentrations are present in antral fluid during ovulation, which may be similar to 50nM used in this study. An additional finding in mouse ovarian contraction was a linear response to EDN2 concentrations between 50pM and 1nM, showing that EDN2 may exerts a contractile effect on smooth muscle cells after ovulation when antral fluid has become diluted. Considering the expulsion of antral fluid into the peri-ovarian space and the oviduct during ovulation, EDN2 may act to cause rupture of multiple follicles at the same time as a coordinator of ovulation or may modify oviductal motion for oocyte conduction. Indeed, ovarian contraction was present even with EDN2 concentrations as low as 0.05nM; lower concentrations were not tested. Also, EDN-induced oviductal contraction has been previously reported[314,315,587,588], which may facilitate sperm, oocyte, or zygote transfer.

Despite consistent contraction in response to EDN2 in all treated ovaries, no difference was observed in contraction between genotypes in response to EDN2 after TAM treatment (Figure 7.9, Figure 7.12). This is in contrast to expected results. Previous recent work with EdnraFlox mice by Donato *et al*. (2014)[562] using a smooth muscle Cre recombinase (that is not inducible) demonstrated a decreased vasoconstrictive response to EDN1 peptide from 10pM to 100nM compared to control mice. However, the sensitivity to EDN1 did not differ in that study; additionally, there was no difference in maximal diameter of isolated femoral arteries in response to EDN1 when an EDNRB antagonist was present. Key differences between studies are that application of a passive tension was not reported by Donato *et al*., and EDNRB antagonists were not employed in the presented data. Furthermore, smooth muscle in vessels is arranged in a uniform circular pattern within the tunica media whereas ovarian smooth muscle is haphazardly arranged relative to the follicles, meaning strong and directional contractions are not possible on the whole ovarian level and are not directly comparable to that of vessels. The lack of difference in contraction between genotypes in the present study may be a result of incomplete loss of EDNRA via TAM or return of EDNRA after TAM and prior to tension analysis, signaling through EDNRB, or signaling through other cell types. Future work using a high dose of EDNRB antagonist drugs or *Ednrb*-knock out mice may determine if EDN2 can induce contraction through EDNRB alone, though this seems unlikely given the higher fertility of *Ednrb*-knock out mice. If EDN2 signals through EDNRA in only a few cells to induce contraction, this may be sufficient for

ovarian contraction; it remains unknown how long *Ednra* ablation lasts after TAM treatment but if TAM effects are present six weeks after treatment but fluorescence as a marker of gene ablation is mostly lost by 30 days then *Ednra* may return quickly after TAM treatment ceases. As *Ednra* was not lost throughout the ovary, it is possible that other cells may signal for contraction through a secondary method; the 5-10 minute delay between EDN2 addition and observed contraction (Figures 7.9) as well as the phenotype of Cyp19-iCre EdnraFlox mice (Figure 7.19) lends credence to this idea.

Furthermore, it was reported by Donato *et al*. that mice with constitutively active smooth muscle Cre recombinase and EdnraFlox were growth retarded with vascular deformations, thymic insufficiencies, and decreased viability (85% fatality rate before weaning). However, fertility was not notably affected (personal communication, Tokyo 2013) in breeding mothers that carried both transgenes, though fertility defects may have been overshadowed by other more obvious phenotypic differences and the few pups that survived to weaning. A strength of the Donato *et al*. study in this aspect is the lack of TAM needed, thus preventing systemic interference with the estrogen receptor system; however, as global changes to vascular development, vascular reactivity, and blood pressure were present which are all potentially influential in follicular rupture, it also fails to prevent a conclusive result on the role of EDNRA during ovulation in smooth muscle cells. It may be possible to transplant ovaries from the mice used in the Donato study to control mice prior to superovulation; if smooth muscles about follicles develop from local stem cells and not from the recipients' population, this mouse would conclusively demonstrate the role of EDNRA in ovulation without the confounding influence of TAM, though the effect of surgery must still be considered.

Ovarian transplantation or ovarian grafting has been previously used to transfer live ovarian tissues between animals, and is a procedure that is now being undertaken in humans as well, particularly in cancer survivors[589,590]. Lack of blood flow to the ovary (ischemia) is the main complication following surgery that prevents ovarian survival[591-594]. Reformation of vessels takes more than 48 hours after ovarian grafting[595,596], but corpora lutea are present within 7 days in non-stimulated ovaries[597]. In this study, ovarian transplantation was used to create ovary-specific transgenic models; in the second set of experiments, TAM was provided before surgery, and in the third set, TAM was provided after surgery; half ovaries were used in the second set and whole ovaries were used in the third. Marked leukocyte infiltration in a large number of ovaries of each

group was observed; this is likely not due to transplant rejection in a conventional sense. Mice are inbred and have the same genotypes excepting the presence of the Cre, and previous work by Lin and Ko (2013, unpublished) in an aging study demonstrates that bisected ovarian grafts transferred into the bursa of WT C57B/6 mice from GFP mice remain viable for up to 45 days and can successfully ovulate. It is more likely that the observed leukocyte infiltration follows an ischemic event that causes widespread apoptosis, necessitating collagen deposition and scar tissue formation as some of the tissue is also resorbed. This is a result of a surgical complication, and not of genetic incompatibility. Future surgeries may consider the use of gonadotropins following surgery to induce vascular reformation via VEGF signaling as well[597]. Also, as the kidneys are more highly vascular, studies looking at ovarian expression or corpus luteum formation, and not directly requiring oocytes passage through the reproductive tract, should consider kidney grafting to increase the likelihood of vascular reformation[598-600]. Additionally, the use of histology and/or RT-PCR to check ovaries for leukocyte invasion in the future and screen out unsuccessful transplants may improve accuracy of results by removing unhealthy ovary bias.

Vascular formation in a graft begins from the recipient's tissue and grows into the donor ovary[601]. The larger incoming vessels are surrounded by smooth muscle at the completion of the revascularization process. In our study where TAM was applied before transplantation, it is possible that the change in estrogen signaling modified graft uptake and increased ischemia as estrogen is known to be involved in cellular growth and angiogenesis[602-605]. Additionally, TAM has been shown to directly decrease angiogenesis in mice after experimental pulmonic ligation[606]. In our third study using whole ovary transplantation, even though TAM was given about two weeks after surgery, it is still possible that it prevented further angiogenesis prior to the breeding study as well as having effects on ovulation itself. As some of the grafts from this experiment appeared healthy (Figure 7.17, top row) and gonadotropins were supplied before TAM, it is more likely that TAM had an effect on ovulation than graft survival. A second point to consider is the effect of *Ednra* loss on angiogenesis in the second experimental set where TAM was supplied before the transplantation. Endothelin receptors have been shown to modify angiogenesis. Recently, Rattner *et al*. (2013) showed that EDNRA signaling in the retina prevents angiogenesis by maintaining tip cell endothelial state in growing vessels[263]. In support of this, Zhang *et al*. (2014) also showed that EDNRB mediates EDN1-induced pulmonary angiogenesis in mice with hepatopulmonary syndrome[607], and Leonard and Gulati (2013) reported that the EDNRB agonist IRL-1620 enhances

angiogenesis in rat brains after ischemia[608,609], though there is some conflict from past pharmacological approaches[610,611]. Therefore it is likely that loss of EDNRA before transplantation does not prevent angiogenesis, and may in fact enhance it. This may also help explain the increased fertility in EDNRB-knock out mice[233], as increased vascularity via VEGF has been shown to increase fertility by promoting follicle growth[612,613]. EDNRA-selective inhibition may enhance surgical recovery in ovarian transplantation, as well as a multitude of other surgeries. However, the potential for EDNRA-loss to influence ischemia and reperfusion remains an important consideration and limitation of the present study.

Though TAM treatment presents obvious complications, this study did consistently demonstrate a slight difference in ovulation and ovarian histology throughout. In young SMACre^{ERT2}EdnraFlox mice, there was no significant difference in the number of oocytes ovulated, but there was a 40% difference in the average number of oocytes obtained from control mice also treated with TAM. Similarly, after a 30 day delay, intact mice also had a slightly lower average number of oocytes ovulated. This was seen in mice that had received a half ovary from transplantation surgery as well. The range in this half ovary transplantation group, from the second experiment, was quite different between genotypes as well (0-13 vs 0-2, n=16). In support, mice in the 30 day delay experiment and the half ovary transplant experiment had ovaries with more antral follicles and fewer CL on average when *Ednra* was lost than in controls, although differences were only significant for CL count in the half ovary transplant group. As CL form after successful ovulation, these data taken together suggest that there is a slight difference in ovulation resulting from loss of *Ednra*, but that it is masked in the present model by TAM.

A strength of this study is that a second and alternative hypothesis was tested in a pilot study with a relatively large number of mice, and it yielded significant and interesting results. A fertility assay was used to test if the loss of *Ednra* in granulosa cells in the ovaries of naturally cycling mice influences fertility. Mice lacking *Ednra* via a codon-improved Cre recombinase driven by the aromatase promoter had a lower percentage of litters per pairing and a decreased number of pups per litter (Figure 7.19), with no difference in the expected 50/50 ratio of females to males. Pups born to these mothers appeared healthy and matured into healthy breeders. As Cyp19-iCre is specific to the ovary, this implies that the signaling defect may lie in the ovary itself but that it is not a major change preventing all functionality. Ovarian histology revealed multiple CL and antral follicles in each group with no obvious differences, though mice were sacrificed

after reaching maturity and going through multiple cycles, and no gonadotropin stimulation was performed. It is interesting to note that the reduction in litter size, from about 8 pups to about 4 pups per litter, was similar to that observed in mice that lack *Edn2* in the granulosa cells by the same or a related Cre recombinase system (Cacioppo *et al*. 2015, unpublished). As significance was observed in both granulosa cell-specific gene knockout studies and the same fertility phenotype was observed, a different fertility effect from whole-ovarian loss of *EDNRB* by Cho *et al*. (2012), it may be that EDN2 acts through EDNRA in the granulosa cells rather than the smooth muscle cells of the ovary in a manner that facilitates up to 50% of oocyte expulsion. This may be occurring through an autocrine or paracrine method to facilitate contraction as a physiological mechanism, or EDNRA may induce further downstream genetic changes to weaken follicle walls or promote vascular invasion which then aid in rupture. It must also be cautiously considered that EDN2 may act through EDNRA in granulosa cells in a positive feedback loop, and that effects seen in Cyp19-iCreEdnraFlox mice simply result from lack of EDN2 ligand production which would otherwise stimulate receptors on smooth muscle cells. These new and significant data do not rule out that *Ednra* may also play a role through the muscle cells of the ovary. The results of this entire study as a whole suggest that the granulosa cells of the ovary may be significant contributors to ovulation via the endothelin system, particularly EDN2 and EDNRA.

Future work in the ovarian endothelin system may take several routes to determine which endothelin receptor mediates ovulation. At present, the use of a granulosa-cell specific *Ednra* knock out mouse appears promising given fertility differences, and further downstream genetic and physiological implications can be explored in the immediate future, as well as confirming normal endothelin protein production. To better examine the role of *Ednra* in smooth muscle cells, and rule out its direct effect on contractility or not, a new mouse line may be generated in which smooth muscle actin-drive Cre is induced under a tetracycline system, which would remove the confounding effects of TAM or surgery. As a mouse of this type is not currently available, such questions may be examined at a future date. A third approach is to modify the ligand rather than the receptor, such as with a granulosa cell-specific loss of *Edn2*. The phenotype of this model may then be matched to receptor-specific deletions. Recovery experiments that induce ovarian contraction via non-endothelin candidates can then be tested. As two of these three proposed models are already available, the role of endothelin receptors in the ovary during ovulation may soon be elucidated; this may in turn offer recommendations for improvement of infertility

treatment or contraceptive development, and will help explain what changes occur in the ovary during treatment with endothelin antagonists such as macitentan for nonreproductive issues, including pulmonary arterial hypertension, systemic sclerosis, and renovascular disease.

ACKNOWLEDGEMENTS

The authors thank Dr. Pierre Chambon for use of SMACre^{ERT2} mice, Dr. Masashi Yanigasawa for EdnraFlox mice, Dr. Joanne Richards for the Cyp19-iCre mice, Dr. James Park for instruction with the myograph tensile analyses, and Karen Doty for histological advice and assistance.

FIGURES

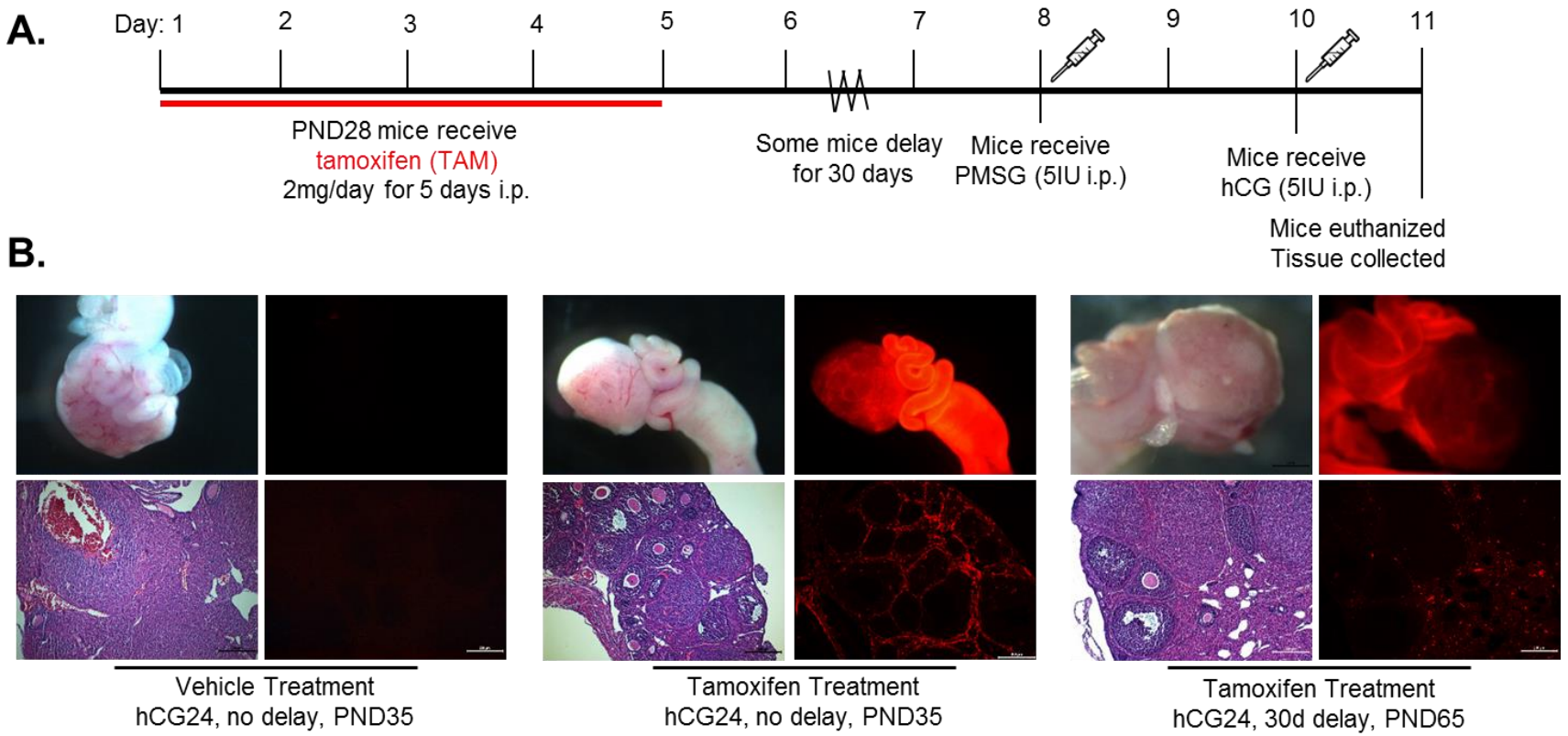

Figure 7.1. Tamoxifen treatment induces Cre recombinase activity in smooth muscle cells of the ovary in SMACre^{ERT2} Ai9 mice. A. Schema used for tamoxifen (TAM) treatment to induce Cre recombinase activity in smooth muscle cells. Tamoxifen was given once daily for five days by i.p. injection to 28 day old mice. Mice were then allowed to recover for two or 32 days. Mice then received superovulation treatment to induce ovulation with injections of PMSG and hCG 48 hours apart. Tissues were collected 24 hours after hCG injection. **B.** SMACre^{ERT2} mice were bred with Ai9 reporter mice. Red fluorescence indicates areas of successful recombination. No recombination is visualized in the vehicle treated ovary. When ovaries are superovulated and collected immediately after TAM treatment, red fluorescence is visible in the smooth muscle cells of the ovary which surround follicles and vessels. Recombination is also present in the smooth muscle cells of the oviduct and uterus. When there is a 30 day delay between TAM treatment and superovulation and tissue collection, smooth muscle cells of the ovary, oviduct, and uterus continue to demonstrate fluorescence. However, gross intensity is decreased from tissues with no delay. Histology reveals that fewer smooth muscle cells of the ovary maintain red fluorescence after 30 days, though some fluorescence around follicles is visible. Fluorescence is reduced by approximately 75%.

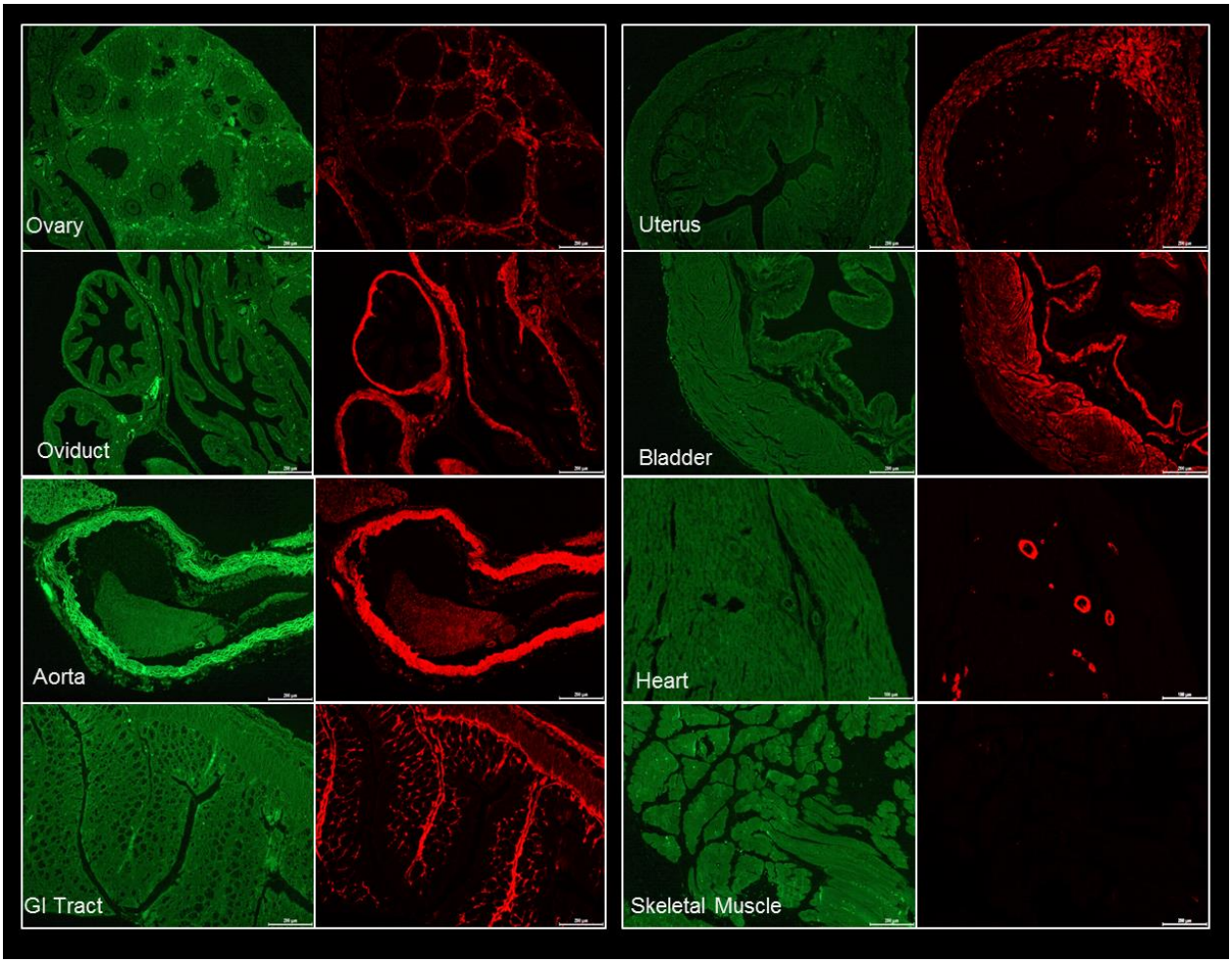

Figure 7.2. Tamoxifen treatment induces Cre recombinase activity in smooth muscle cells throughout the body. SMACre^{ERT2} Ai9 mice at 28 days old received TAM treatment for 5 days and were then superovulated after a two day recovery period. In addition to the ovary, smooth muscle cells of the oviduct, uterus, GI tract, aorta, and bladder demonstrate red fluorescence and successful recombination. There is limited to no Cre recombinase activity in skeletal and cardiac muscle, except for in the smooth muscle cells in the walls of the arteries and arterioles.

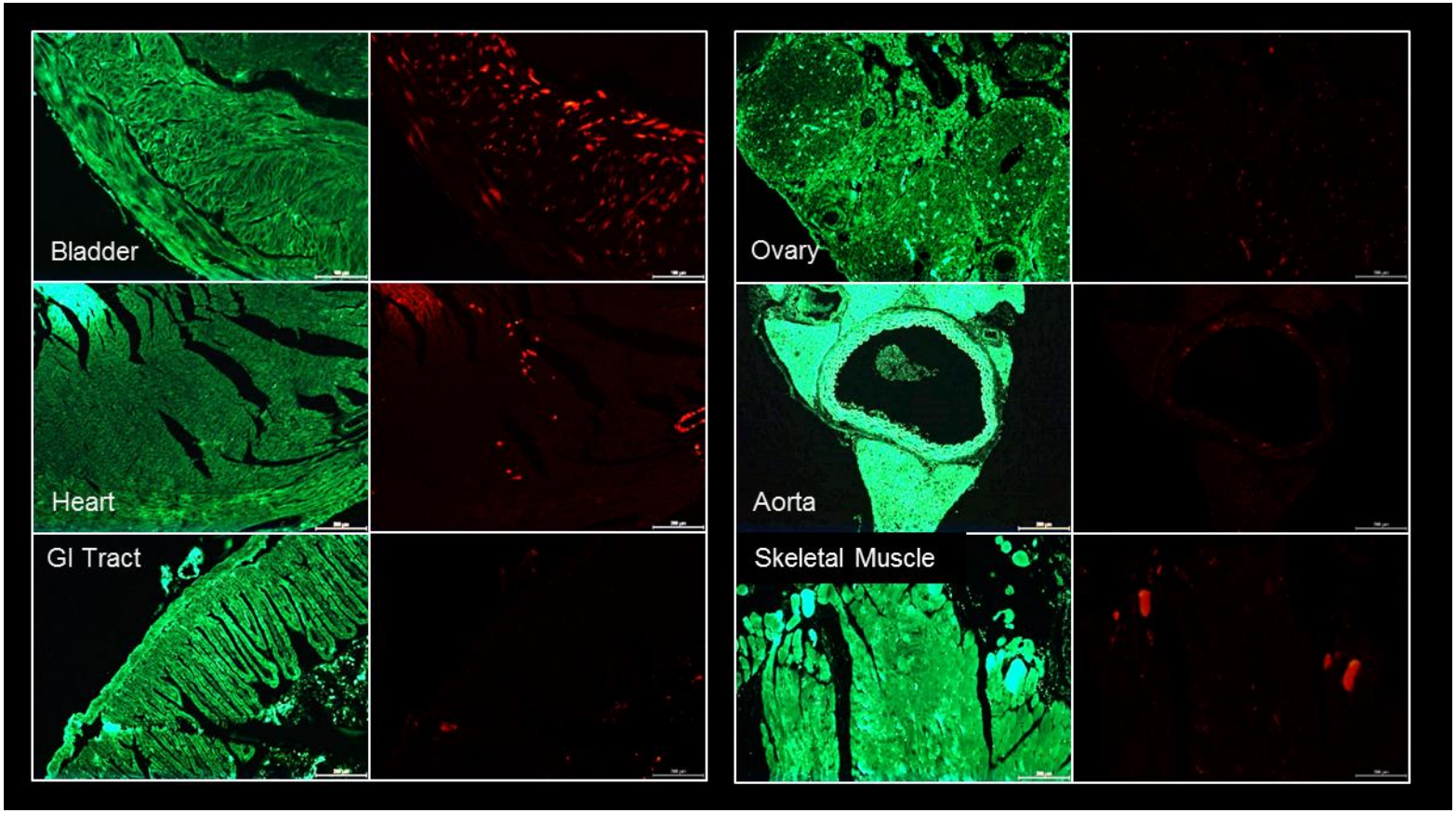

Figure 7.3. Exogenous SMACre^{ERT2} expression occurs without tamoxifen treatment. Twenty-eight day old SMACre^{ERT2} Ai9 mice received vehicle injection for five days and were then superovulated and sacrificed without delay as in Figure 7.1A. Red fluorescence indicates areas of exogenous Cre recombination in the bladder and several cells of the heart, but not in the GI tract, ovary, aorta, skeletal muscle, or uterus.

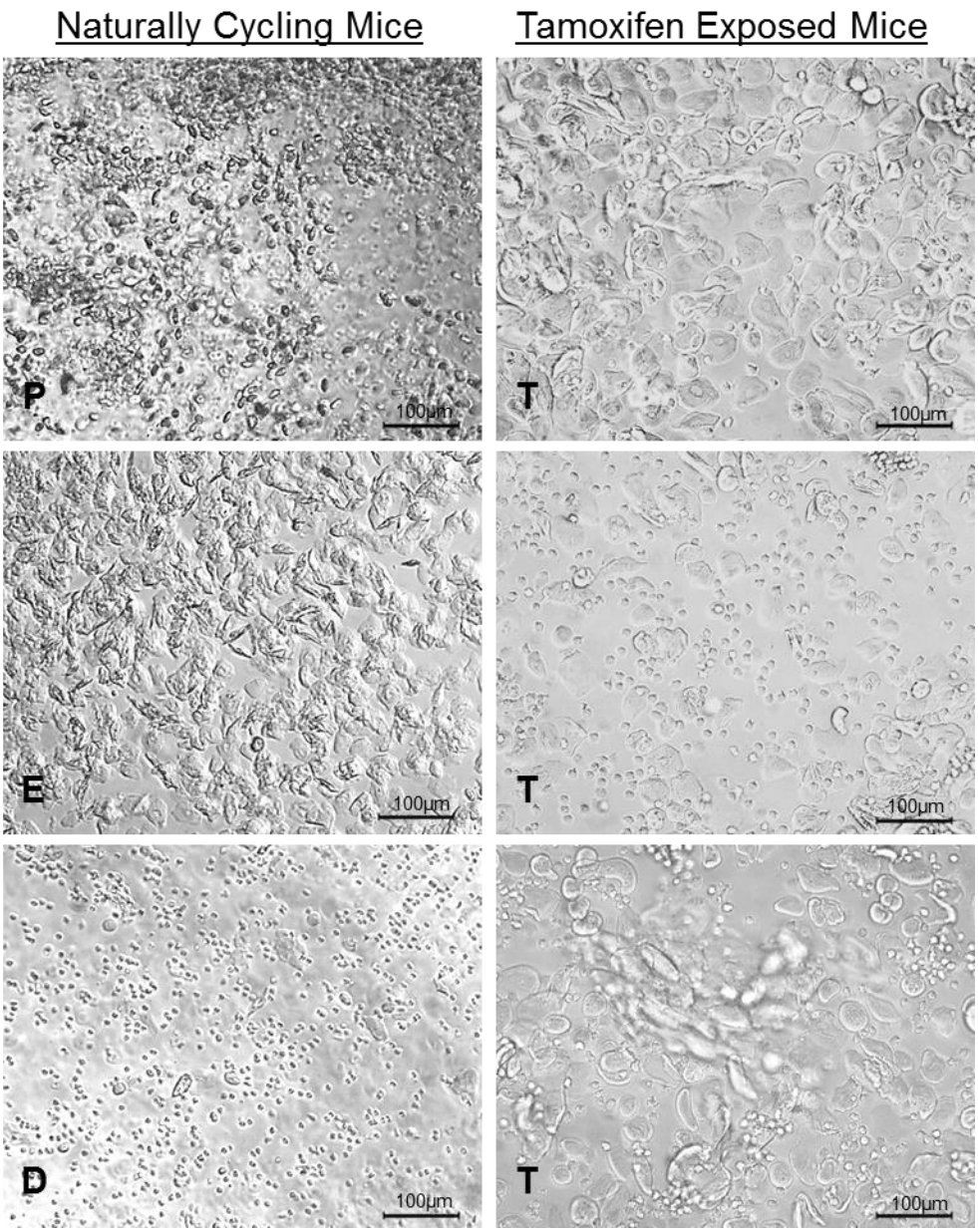

Figure 7.4. Tamoxifen causes prolonged acyclicity in exposed mice. Vaginal cytology from three naturally cycling (left) and three tamoxifen-treated (right) shows abnormal cell patterning seen in tamoxifen-treated mice. Cytology matches none of the four major stages seen in mice (proestrus(P), estrus(E), and diestrus(D) pictured for reference from mice prior to tamoxifen treatment). Cytology is consistent with multiple leukocytes present as well as many rounded anuclear epithelial cells that lack the sharp polyhedral edges normally seen on estrus swabs. No change in this cytology result is seen throughout the duration of tamoxifen treatment; this result is most consistent with diestrus owing to the high number of leukocytes present.

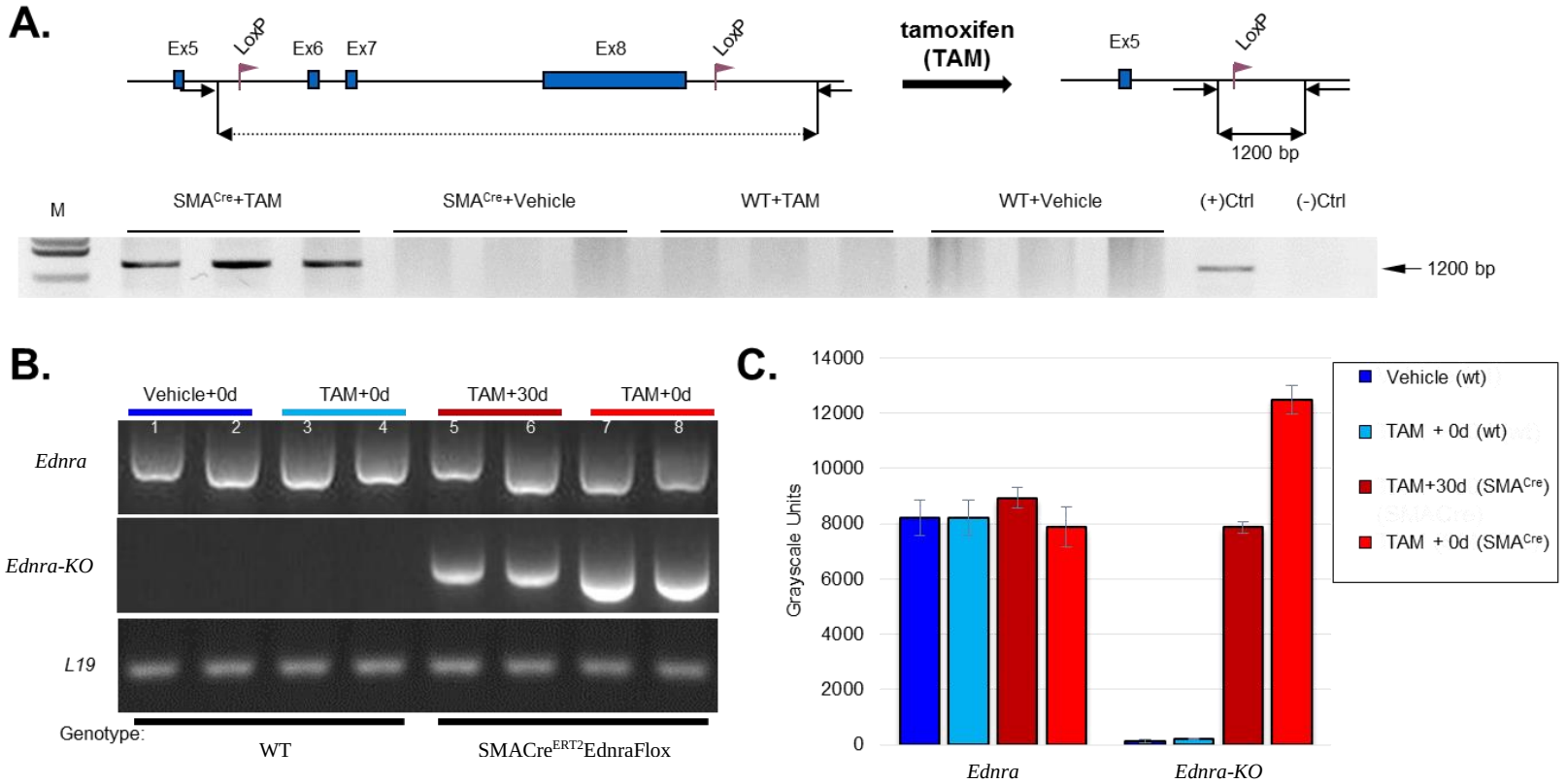

Figure 7.5. Tamoxifen treatment induces loss of endothelin receptor A (*Ednra*) in smooth muscle cells. A. Schematic of Cre recombinase-mediated deletion of Exons 6, 7, and 8 of the *Ednra* gene following five days of TAM treatment. Horizontal arrows indicate primer binding sites for the Ednra-KO band. The Ednra-KO amplicon is 1200 bp following successful deletion of *Ednra* exons; areas of primer binding are indicated by horizontal arrows. Recombination was confirmed by PCR from genomic DNA extracted from whole ovaries following TAM treatment as in Figure 7.1A. Both vehicle treatment of SMACre^{ERT2} EdnraFlox mice and TAM treatment of control mice fail to induce recombination. M: 1000bp ladder (New England Biolabs). "SMA^{Cre}" indicates SMACre^{ERT2}EdnraFlox ovarian gDNA; n=3. **B.** TAM treatment induces loss of *Ednra* in the ovary of SMACre^{ERT2}EdnraFlox mice when superovulation immediately follows TAM (lanes 7-8, red) or when there is a 30 day delay prior to superovulation (lanes 5-6, maroon). Semi-quantitative RT-PCR was performed on RNA extracts from whole ovaries. No recombination is observed in control mice (lanes 1-4) with vehicle or TAM treatment. **C.** Quantification of semi-quantitative RT-PCR of whole ovary RNA after TAM or vehicle treatment reveals no difference in *Ednra* expression between groups (blue, teal). There is a significant decrease in Ednra-KO transcript in SMACre^{ERT2} EdnraFlox mice when there is a 30 day delay between TAM treatment and superovulation (maroon) compared to two days (red), though the gene deletion remains present. Error bars represent the SEM; n=5.

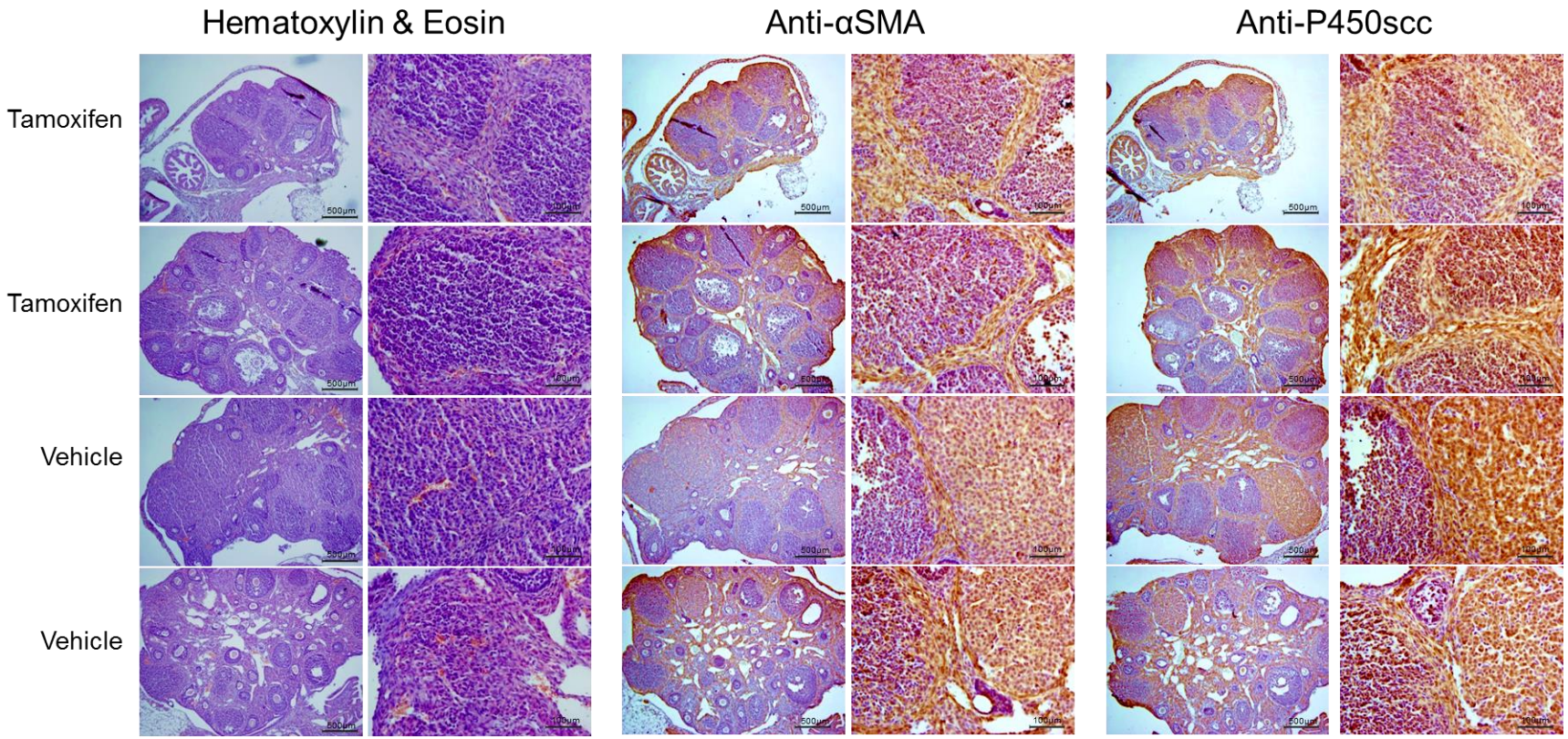

Figure 7.6. Ovarian immunohistochemistry demonstrates smooth muscle in the stroma and functional corpora lutea. Ovaries were collected from adult female (2 months of age) WT mice 18 hours after hCG injection, and were frozen, serially sectioned, and stained with hematoxylin and eosin, anti-SMA, and anti-P450scc. Note the presence of the smooth muscle network throughout the ovarian stroma around follicles and within corpora lutea (CL), and the positive staining of corpora lutea by P450scc. No differences were noted between ovaries of any treatment group in staining. Tamoxifen treatment does not prevent CL formation following gonadotropin induced ovulation nor does it modify the intraovarian smooth muscle scaffolding of either the stroma or forming CL. Magnification is shown at 4X and 20X.

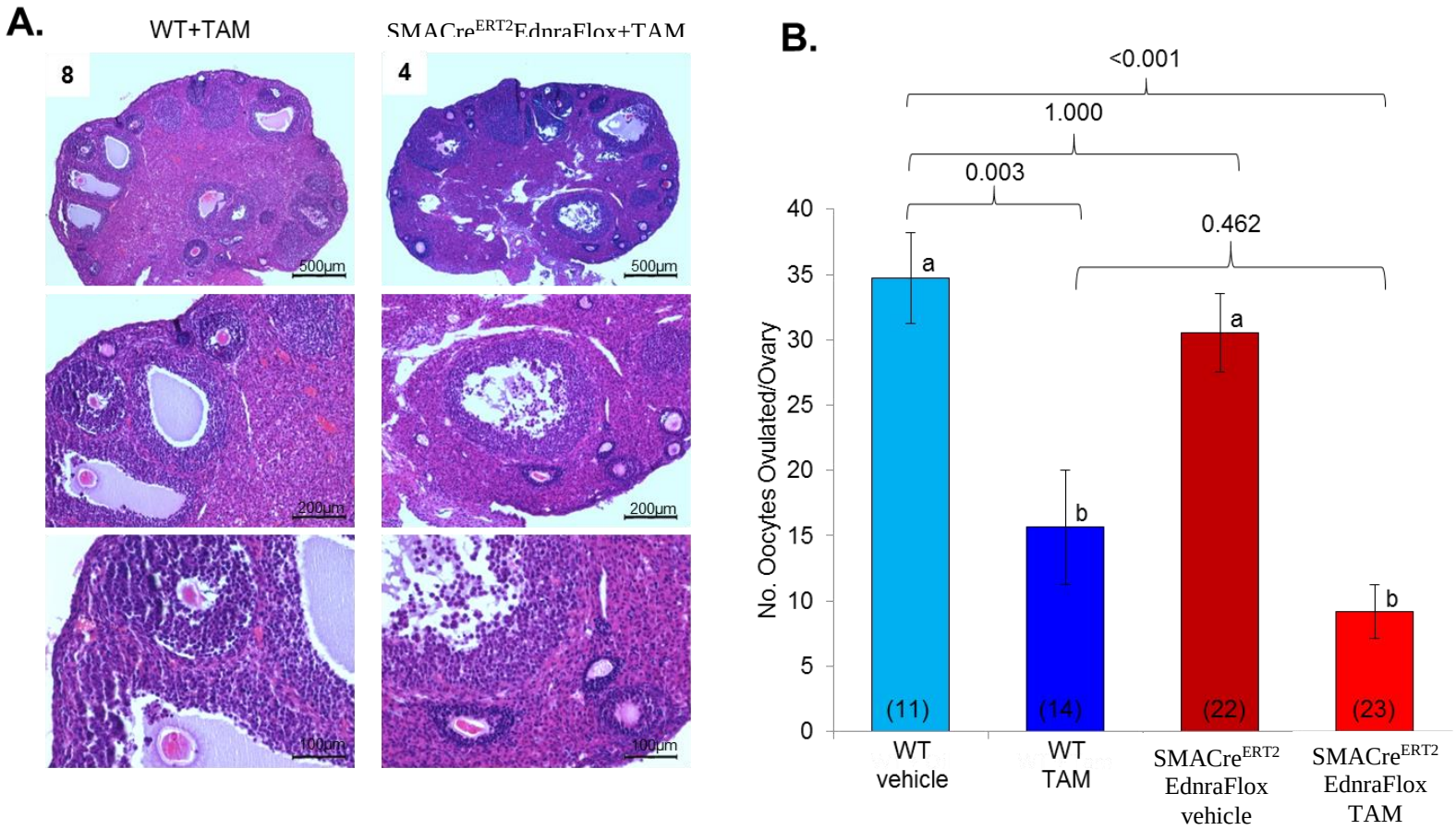

Figure 7.7. Tamoxifen treatment reduces the number of oocytes ovulated. Twenty eight day old adult mice received intraperitoneal injections of 0.5mg tamoxifen in oil 1/day for 5 days and were then given gonadotropins to induce ovulation. Oocytes were collected 18 hours after hCG injection and were quantified to determine the effect of tamoxifen and *Ednra* loss on ovulation. **A.** Histology of ovaries at hCG 18hrs following TAM treatment and superovulation. No differences were noted between ovaries of any treatment group in staining, follicle count by stage, CL count, or size. Mild hemorrhage was present within some ovaries of each group. Note the presence of antral follicles in each group. Images are shown at 4X, 10X, and 20X. Numbers in upper-left corner indicate oocytes ovulated by each ovary. **B.** Tamoxifen treatment significantly reduces the number of oocytes ovulated in both SMACre^{ERT2}EdnraFlox and control mice. P-values are displayed above the brackets between the two groups being compared. There is no significant difference in oocytes ovulated between SMACre^{ERT2}EdnraFlox mice and control mice of the same treatment. Numbers in parenthesis indicate the n-value for each group (ovaries). Error bars represent the SEM.

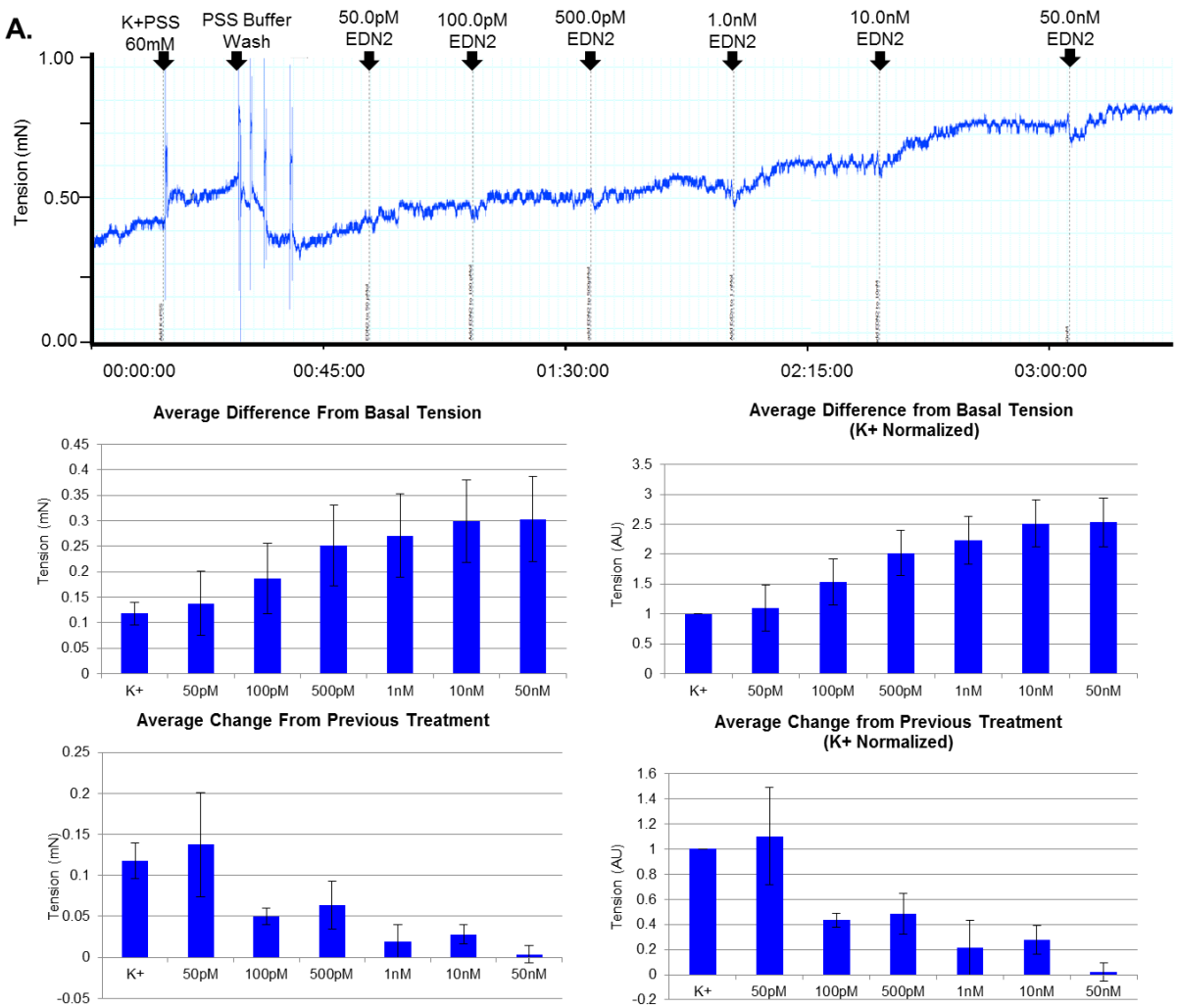

Figure 7.8. WT ovaries contract in response to EDN2 administration. Control mice (n=4) were superovulated at 28 days old and ovaries were collected at hCG12-16 hours. Ovaries were placed in a myograph machine for tension analysis. **A.** A representative control ovary (blue) response to a 60mM K+PSS solution (for normalization) and increasing concentrations of EDN2 solution. This ovary demonstrates a contraction in response to EDN2 that linearly increases with concentration. Vertical axis: tension in millinewtons where 9.81mN = 1.00gram-force. Horizontal axis: Time (Hours:Minutes:Seconds). **B.** Comparison of tension between concentrations with absolute (left) and relative (right) responses to endothelin receptor agonization by EDN2. Ovarian contraction was normalized to the response to K+PSS to compare relative contractile responses. The lowest increase in tension occurs at 50.0nM EDN2, indicating near saturation of receptors. Error bars represent the SEM. This treatment schema was similarly used to measure responses from treated ovaries, where EDN2 at 50.0 induces a strong contraction near the receptor saturation point, approximately 3.0 times as strong as the contraction from a 60mM K+ solution.

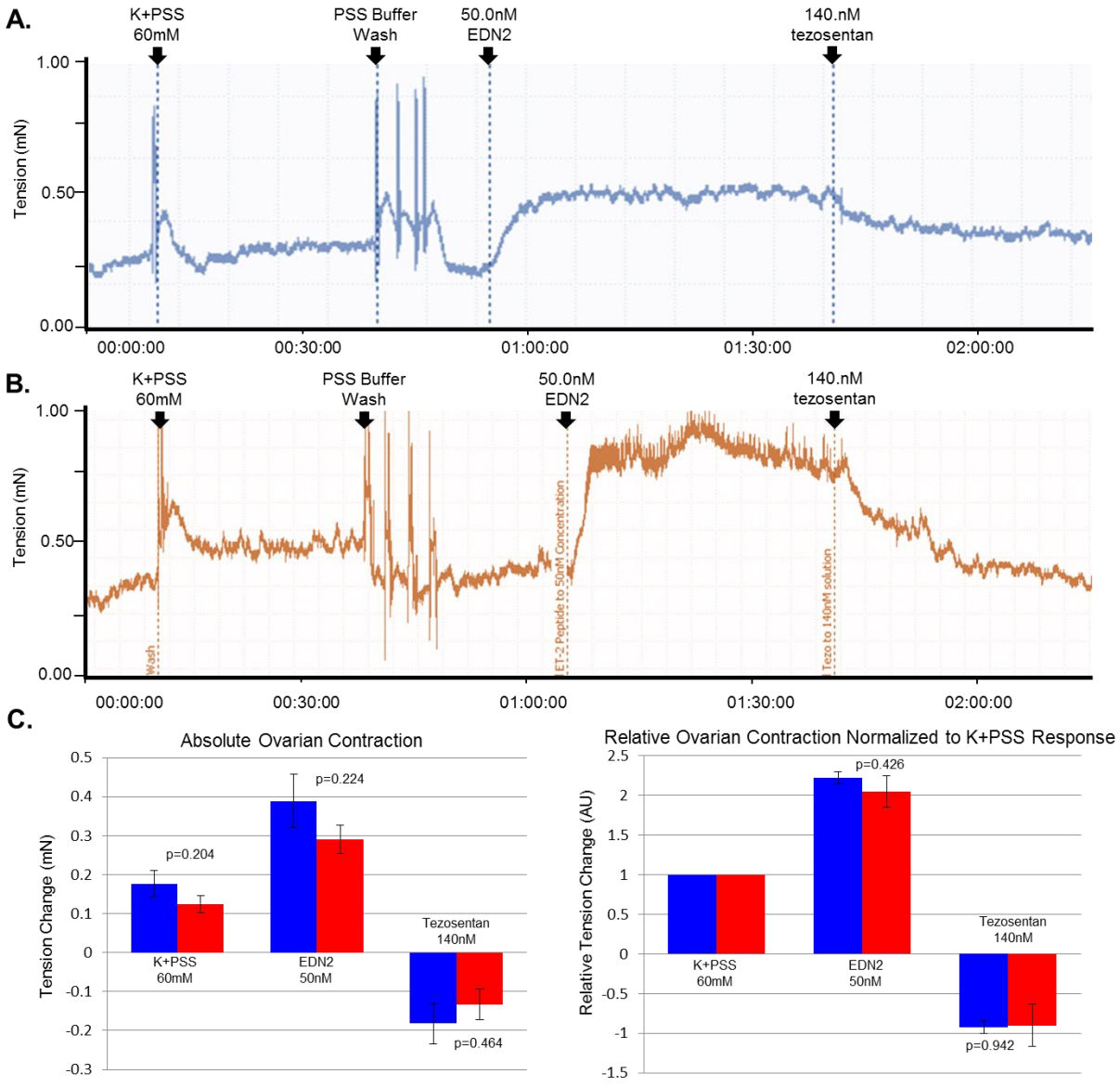

Figure 7.9. No difference in EDN2-induced ovarian contraction after TAM treatment. SMACre^{ERT2}EdnraFlox mice (n=8) and control mice (n=8) were exposed to tamoxifen for 5 days at 28 days old and were then given superovulation protocol to induce ovulation without delay. Ovaries were collected at hCG12-16 hours and were placed in a myograph machine for tension analysis. **A.** A representative control ovary (blue) response to a 60mM K+PSS solution (for normalization), a 50nM EDN2 solution, and a 140nM tezosentan solution. This ovary demonstrated contraction in response to the K+PSS and the EDN2 solution. This treatment schema was similarly used to measure responses in **B.** SMACre^{ERT2}EdnraFlox ovaries, orange. Vertical axis: tension in millinewtons where 9.81mN = 1.00gram-force. Horizontal axis: Time (Hours:Minutes:Seconds). **C.** Comparison of tension between treatment groups of absolute (left) and relative (right) responses to endothelin receptor agonization and subsequent antagonization. Ovarian contraction was normalized to the response to K+PSS to compare relative contractile responses. No significant differences were present. Blue bars (left) indicate WT tissues and red bars (right) indicate SMACre^{ERT2}EdnraFlox tissues. P-values are provided with each graph. Error bars represent the SEM.

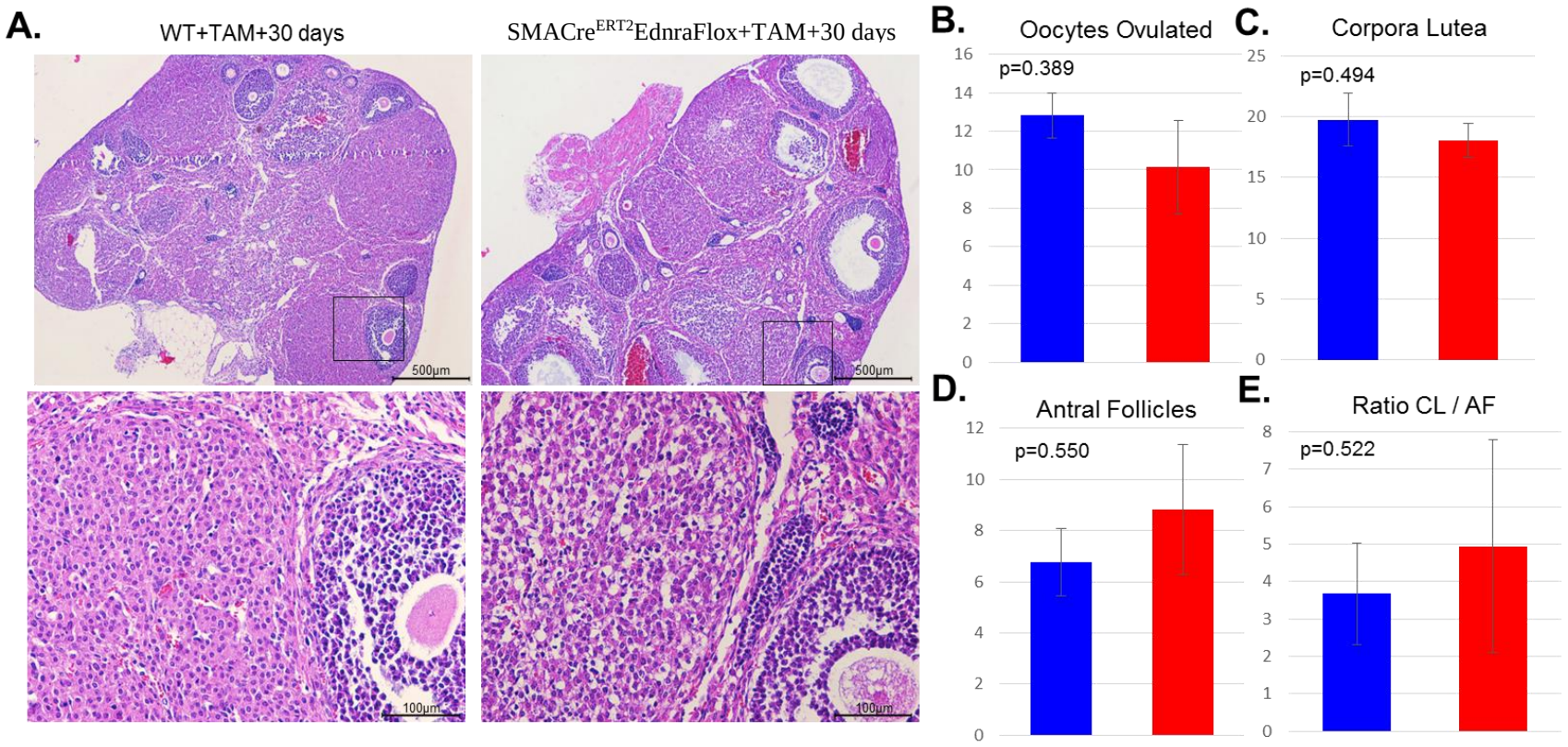

Figure 7.10. Superovulation 30 days after TAM treatment shows no difference in oocytes ovulated or ovarian histology. SMACre^{ERT2}EdnraFlox mice (n=6) and control mice (n=4) were exposed to tamoxifen for 5 days at 28 days old, allowed to recover for 30 days, and were then given superovulation protocol to induce ovulation. **A.** Ovaries were collected at hCG24 hours and were fixed and serially sectioned; **B.** oocytes were also collected from the oviduct at this time and counted. There was no significant difference in the average number of oocytes ovulated per ovary (n=8-12). No obvious histological differences were present between ovaries in each group. All ovaries appeared healthy and contained both corpora lutea and antral follicles. There was no significant difference in the number of **C.** corpora lutea or **D.** antral follicles per ovary between treatment groups. Additionally, there was no significant difference in **E.** the ratio of corpora lutea to antral follicles per ovary. Images are shown at 4X and 20X magnification. Blue bars (left) indicate WT tissues and red bars (right) indicate SMACre^{ERT2}EdnraFlox tissues. P-values are provided with each graph. Error bars represent the SEM.

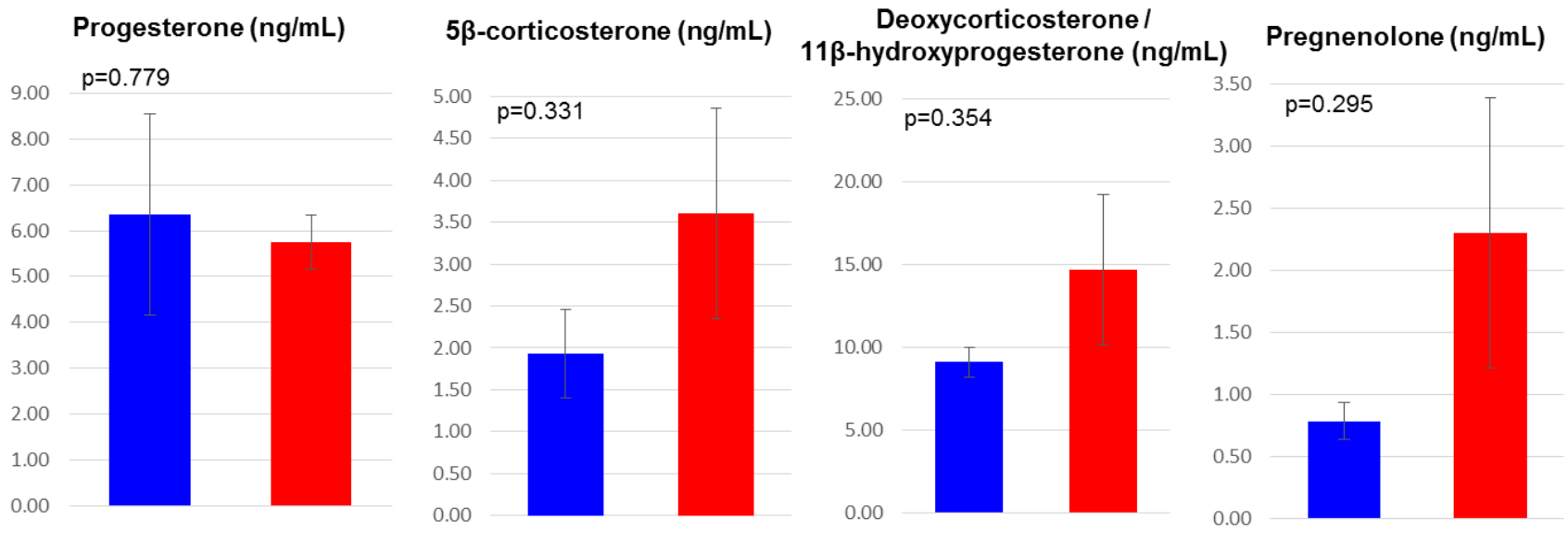

Figure 7.11. No difference in serum sex hormone concentrations 30 days after tamoxifen treatment. SMACre^{ERT2}EdnraFlox mice (n=6) and control mice (n=4) were exposed to tamoxifen for 5 days at 28 days old, allowed to recover for 30 days, and were then given superovulation protocol to induce ovulation. Serum was collected 24 hours after hCG was administered and serum sex hormones were quantified by LC/MS. No significant differences were present in serum hormones of progesterone, 5β-corticosterone, deoxycorticosterone/11β-hydroxyprogesterone, or pregnenolone. Blue bars (left) indicate WT tissues and red bars (right) indicate SMACre^{ERT2}EdnraFlox tissues. P-values are provided with each graph. Error bars represent the SEM.

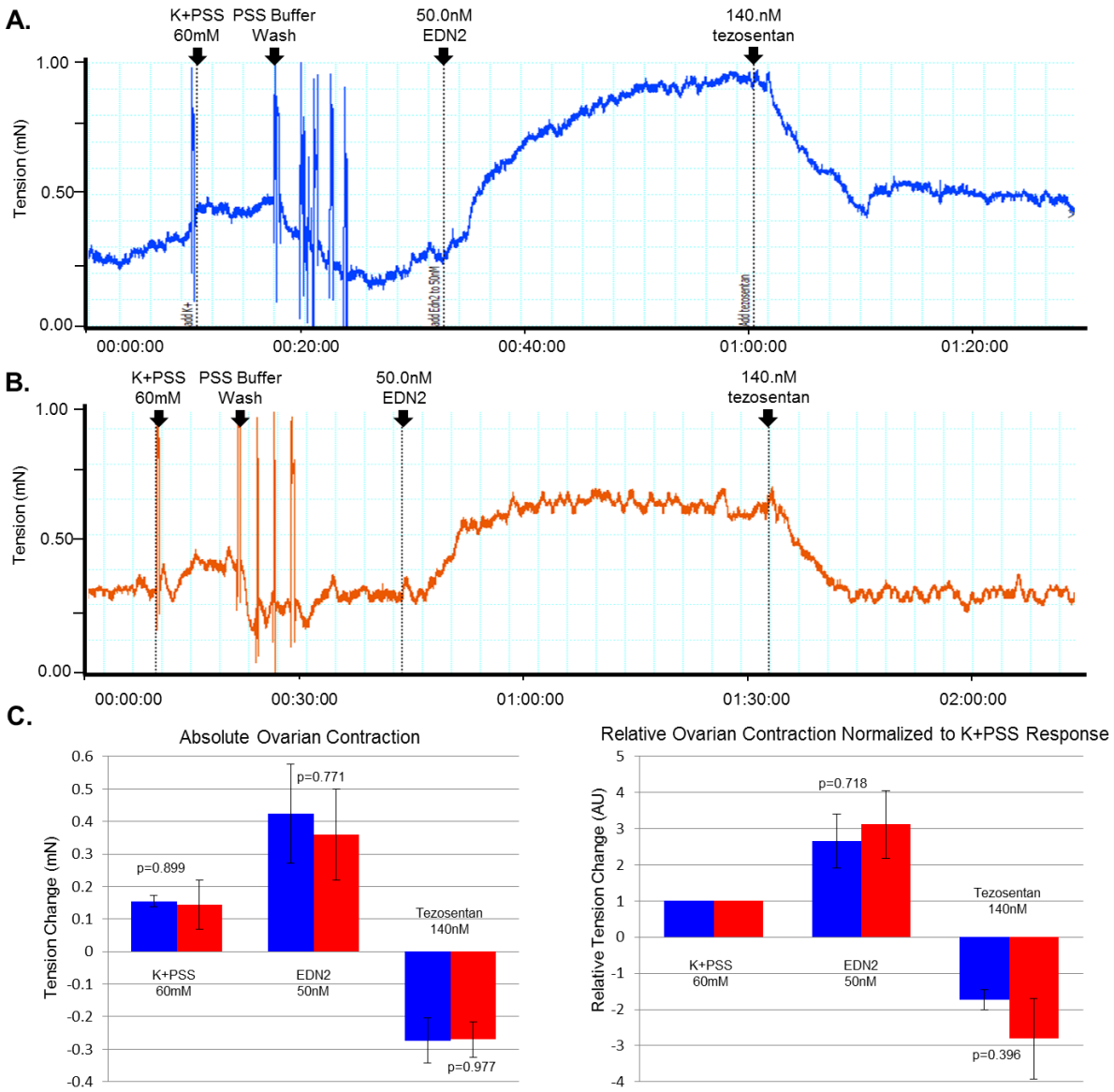

Figure 7.12. No difference in EDN2-induced ovarian contraction 30 days after TAM treatment. SMACre^{ERT2}EdnraFlox mice (n=6) and control mice (n=4) were exposed to tamoxifen for 5 days at 28 days old, allowed to recover for 30 days, and were then given superovulation protocol to induce ovulation. Ovaries were collected at hCG12-16 hours and were placed in a myograph machine for tension analysis. **A.** A representative control ovary (blue) response to a 60mM K+PSS solution (for normalization), a 50nM EDN2 solution, and a 140nM tezosentan solution. This ovary demonstrates a contraction in response to the K+PSS and the EDN2 solution. This treatment schema was similarly used to measure responses in **B.** SMACre^{ERT2}EdnraFlox ovaries, orange. Vertical axis: tension in millinewtons where 9.81mN = 1.00gram-force. Horizontal axis: Time (Hours:Minutes:Seconds). **C.** Comparison of tension between treatment groups of absolute (left) and relative (right) responses to endothelin receptor agonization and subsequent antagonization. Ovarian contraction was normalized to the response to K+PSS to compare relative contractile responses. No significant differences were present. Blue bars (left) indicate WT tissues and red bars (right) indicate SMACre^{ERT2}EdnraFlox tissues. P-values are provided with each graph. Error bars represent the SEM.

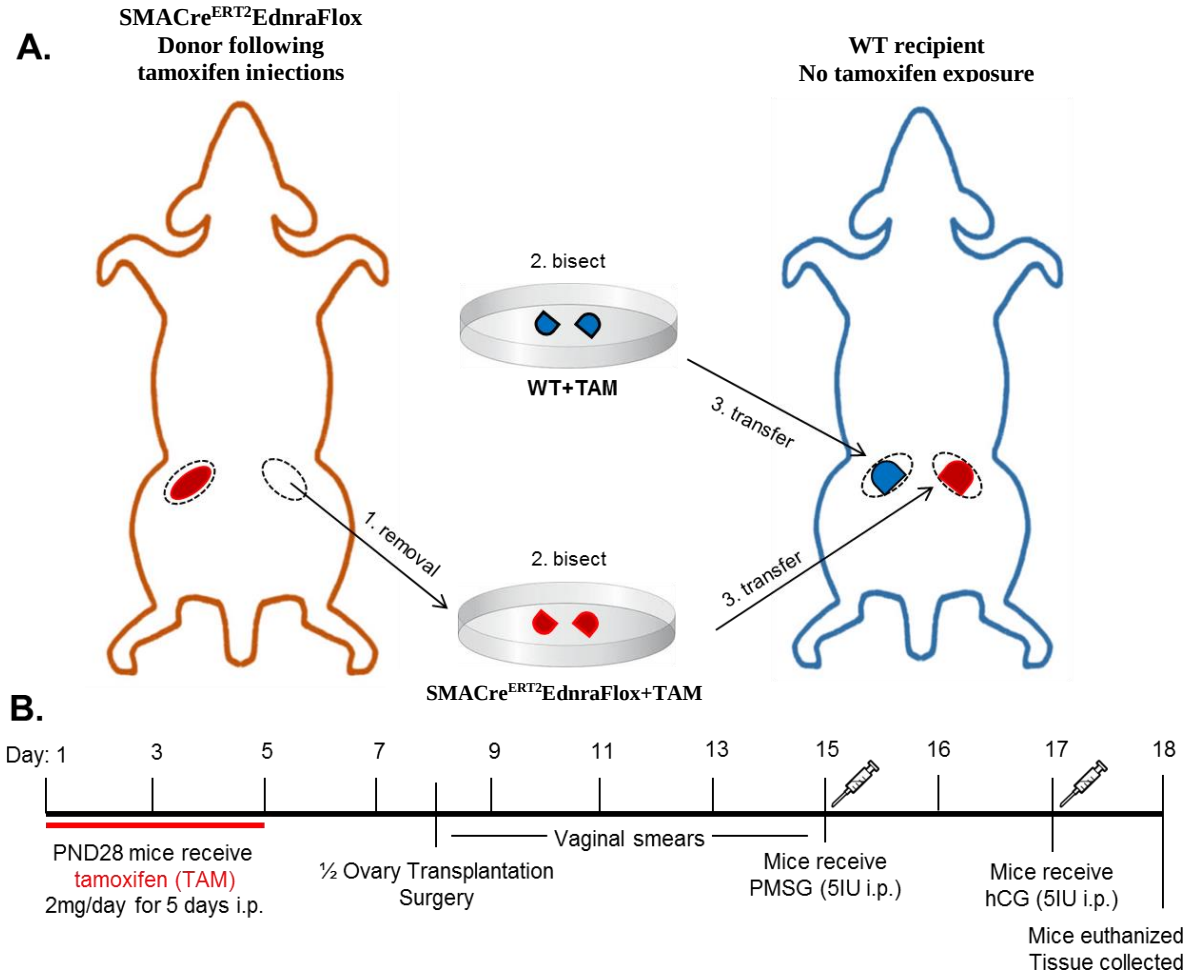

Figure 7.13. Transplantation of half ovary after TAM treatment creates ovary-specific smooth muscle cell *Ednra* loss. A. Visualization of transplantation procedure. Twenty-eight day old SMACre^{ERT2}EdnraFlox and control mice received tamoxifen (TAM) treatment for 5 days to activate Cre recombinase and remove the *Ednra* gene in smooth muscle cells. Ovaries were then removed and bisected to limit graft size. Ovaries were transplanted into the ovarian bursa of 60 day old WT ovariectomized recipients. Each recipient received one half knockout ovary and one half control ovary that had each been treated with tamoxifen. Following surgery, mice were checked by vaginal smear for ovarian cyclicity as a marker of return to ovarian functionality. After one week recovery from surgery, mice were superovulated and tissues were collected 24 hours after hCG stimulation as previously. **B.** Timeline of TAM treatment, surgery, recovery, superovulation, and collection. Note that days elapsed are not to scale.

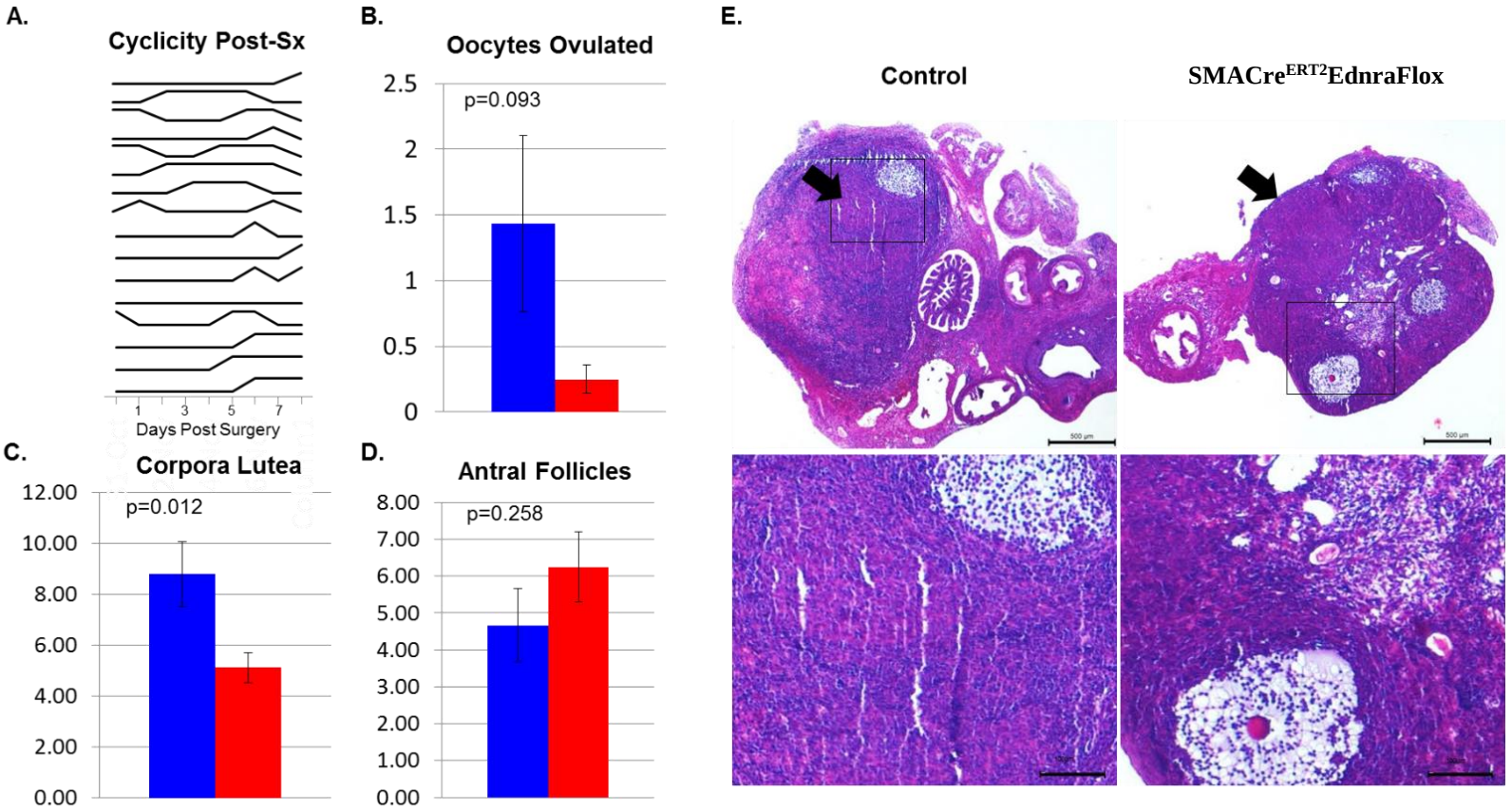

Figure 7.14. Ovary-specific *Ednra* loss decreases oocytes ovulated. Tamoxifen treatment followed by half-ovary transplantation was performed prior to superovulation**. A.** Vaginal cytology was performed once per day following surgery to monitor estrous cyclicity. Mice were able to enter estrus following ovary transplantation, usually after 5-7 days. Each line in graph represents one mouse; peaks represent estrus and base represents diestrus, proestrus, or metestrus. **B.** At hCG24 hours, mice were euthanized, ovaries were removed and fixed, and oocytes were collected from the oviduct of each mouse. Left bar (blue) is control ovaries and right bar (red) is SMACre^{ERT2}EdnraFlox ovaries. There was a trend towards **B.** fewer oocytes ovulated and **D.** more antral follicles present in the SMACre^{ERT2}EdnraFlox ovaries, and there were **C.** significantly fewer corpora lutea present when ovaries were histologically examined. There was a high degree of variation in the number of antral follicles in each group, while many ovaries from each group failed to ovulate. **E.** Representative histological comparison of superovulated ovaries at hCG24hrs. Left: Control ½ mouse ovaries with TAM treatment and surgical transplant to WT recipient. Right: SMACre^{ERT2}EdnraFlox mouse ½ ovary with TAM treatment and surgical transplant to WT recipient. Marked leukocyte infiltration was present in the majority of ovaries of each group. Images at 4X and 20X. N=16 animals and 16 ovaries of each genotype. Error bars represent the SEM.

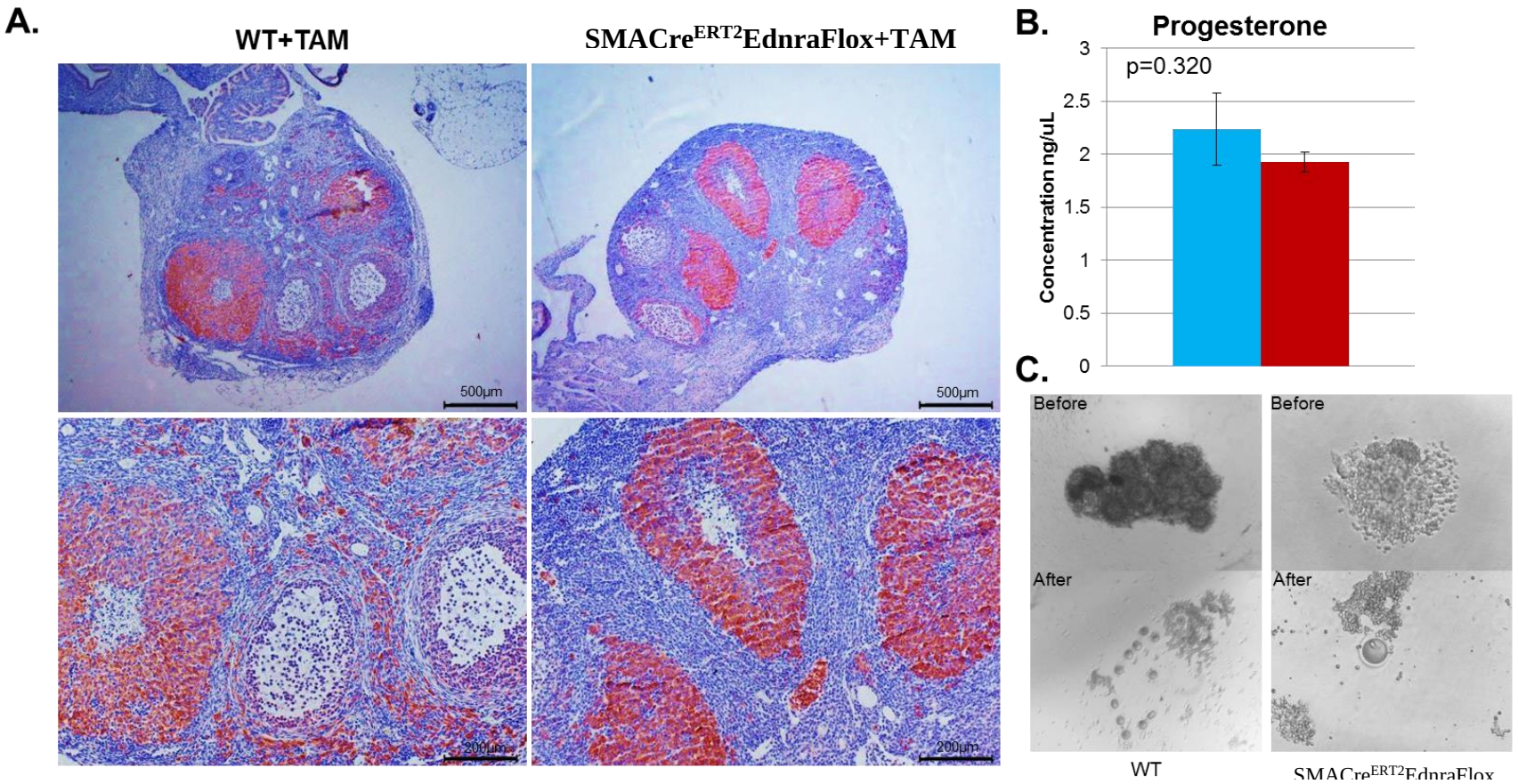

Figure 7.15. SMACre^{ERT2}EdnraFlox half ovaries have normal cytochrome P450scc expression, progesterone secretion, and oocyte expansion. To determine if mice could produce corpora lutea after half ovary transplantation, histology was performed on ovaries at hCG24. **A.** Ovaries were stained with anti-P450scc, a steroidogenic enzyme and CL marker. Newly forming corpora lutea are present in both the SMACre^{ERT2}EdnraFlox and control ovaries. Images are shown at 4X and 10X magnification. To determine if these corpora lutea were functionally capable of steroidogenesis necessary for pregnancy maintenance, **B.** serum progesterone was measured in mice that had received ovarian transplantation, one half ovary of each treatment, and compared to intact control mice at hCG24. Error bars represent the SEM. There was no significant difference in serum progesterone concentration between groups. Teal bar: control; maroon bar: SMACre^{ERT2}EdnraFlox. **C.** To determine if oocytes ovulated form SMACre^{ERT2}EdnraFlox ovaries were healthy, oocytes were collected from the oviduct at hCG24. Cumulus complexes were successfully dissociated with hyaluronidase treatment in each group and no differences were observed in oocyte gross morphology.

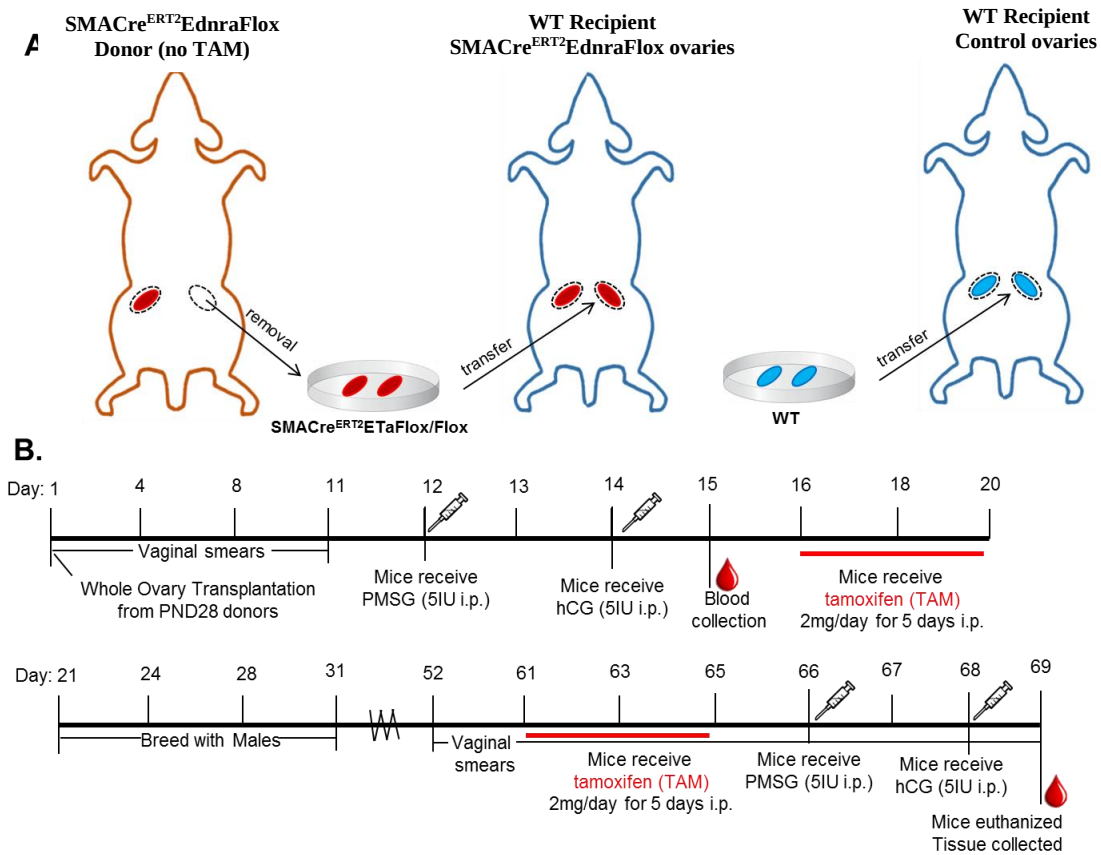

Figure 7.16. Transplantation of whole ovary before TAM treatment creates ovary-specific smooth muscle cell *Ednra* loss. A. Visualization of transplantation procedure for model generation. Twenty-eight day old SMACre^{ERT2}EdnraFlox and control mice were sacrificed with no prior treatment and whole ovaries were removed and transplanted into the ovarian bursa of 60 day old WT female recipient mice. Each recipient received two whole ovaries of the same genotype. **B.** Timeline of treatment procedure which was the same for each genotype group. Following surgery, mice were checked by vaginal smear for ovarian cyclicity as a marker of return to ovarian functionality. After one week recovery from surgery, mice were superovulated and serum samples were collected 24 hours after hCG stimulation from the mandibular vein. Mice then received tamoxifen treatment for five days to induce Cre recombinase and *Ednra* loss. Following this, mice were bred proven breeder males for 10 days. Females were then isolated for 21 days during pregnancy period. After the fertility assay, mice again received tamoxifen for five days to induce Cre recombinase. Mice were then again superovulated and serum and tissue samples were collected at 24 hours after hCG stimulation for serum hormone assays and histological examination.

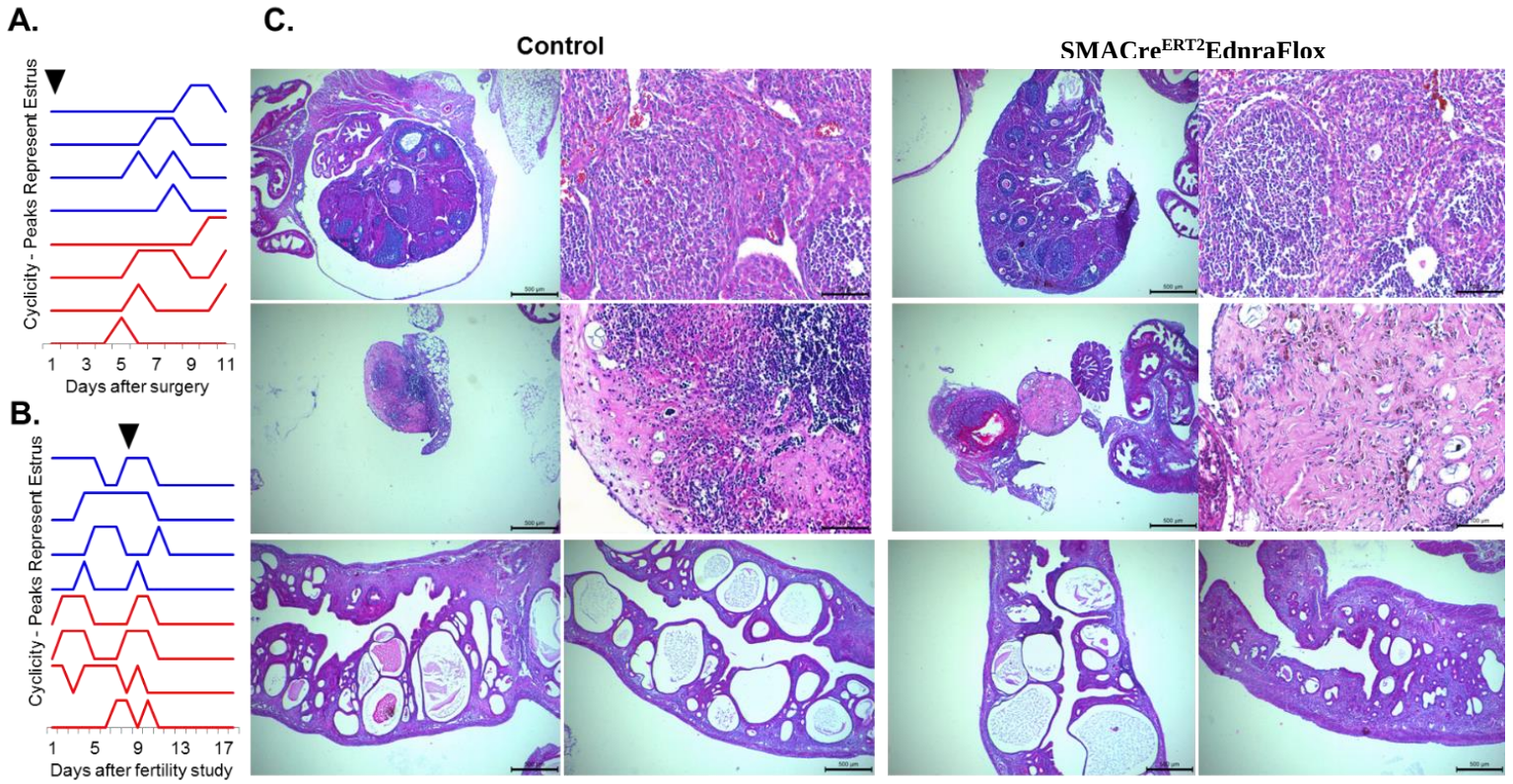

Figure 7.17. Tamoxifen-treated mice with ovarian transplantation do not ovulate normally or become pregnant. A. Vaginal smears of mice were taken daily following double ovarian transplantation procedure and prior to tamoxifen treatment. All mice were able to return to normal cyclicity within one week of surgery. Peaks represent estrus. Top four blue lines represent mice with two control ovaries. Bottom four red lines represent mice with two SMACre^{ERT2}EdnraFlox ovaries. Arrow represents time of surgical transplant. No pups were born to any mother of either group during the breeding study. **B.** Vaginal smears of mice were taken daily following the breeding study. Peaks represent estrus. Top four blue lines represent mice with two control ovaries. Bottom four red lines represent mice with two SMACre^{ERT2}EdnraFlox ovaries. Arrow represents start day of second tamoxifen treatment. Mice displayed normally cyclicity prior to second tamoxifen treatment, and no mouse entered estrus following tamoxifen treatment until the end of the study. **C.** Histology of mouse ovaries and uteri at the completion of the experiment, hCG 24 hours, hematoxylin and eosin staining. Representative ovaries of each group are shown that appear generally healthy with multiple follicles (top row) and unhealthy ovaries with a high degree of fibrosis and inflammation (middle row). Images are shown at 4X and 20X. No oocytes were obtained from any oviduct of either group at hCG 24 hours. All uteri from mice consistently demonstrate severe cystic endometrial hyperplasia (bottom row); all uteri are WT. Images are shown at 4X.

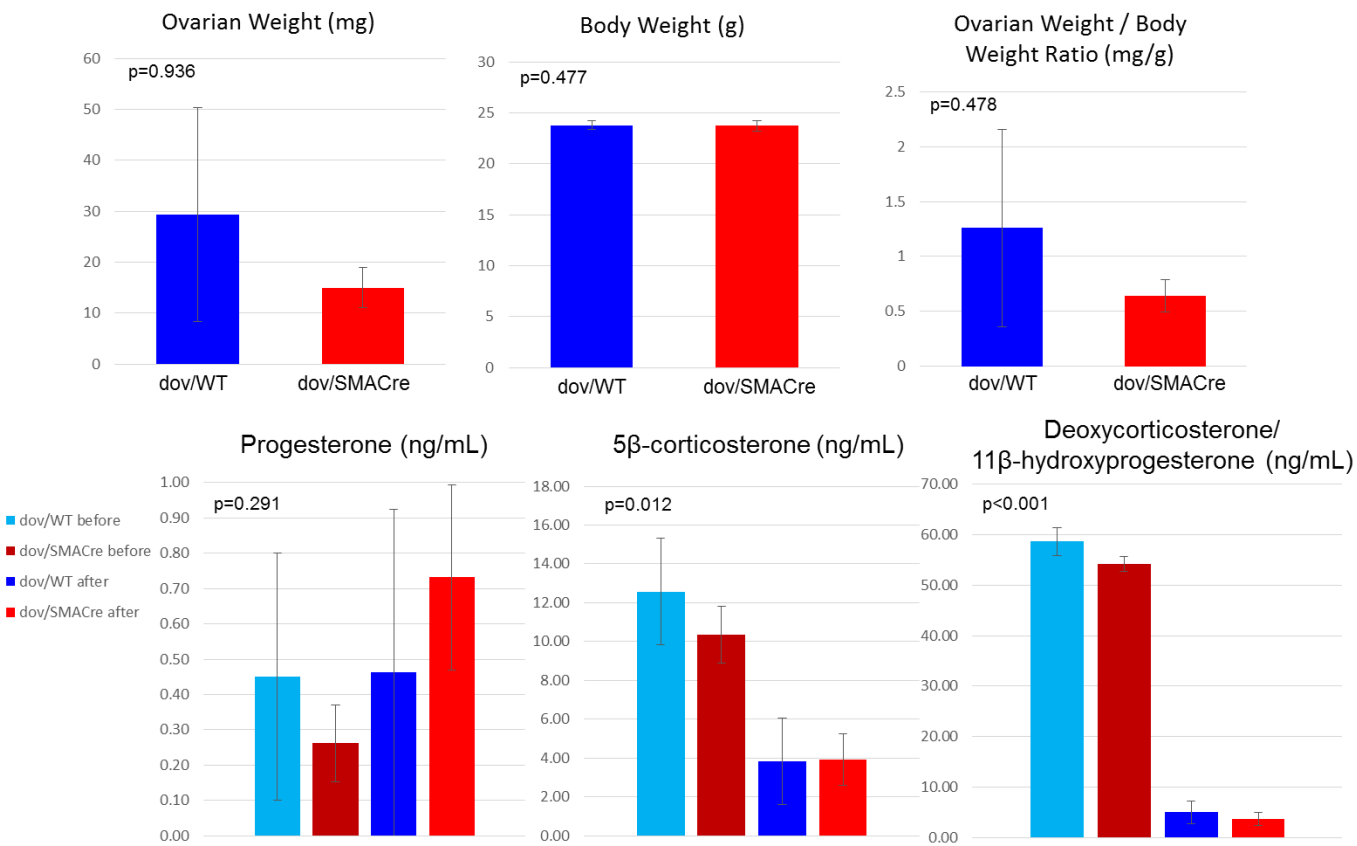

Figure 7.18. Tamoxifen-treated mice with ovarian transplantation do not differ in body weight, ovarian weight, or serum progesterone concentration. Mice with double whole ovary transplantation were superovulated and had serum collected at hCG24, then received tamoxifen treatment twice and were superovulated again and euthanized at hCG24 as in Figure 7.16. Mice were weighed, and then ovaries were removed and gross wet weight was recorded. Serum was separated from whole blood and analyzed for concentrations of progesterone, 5β-corticosterone, and deoxycorticosterone/11β-hydroxyprogesterone. Mice with double ovarian transplantation of WT ovaries (dov/WT) are displayed at left in blue and mice with double ovarian transplantation of SMACre^{ERT2}EdnraFlox ovaries (dov/SMACre) are displayed at right in red. No significant differences were present between body weight (n=4), ovarian weight (n=8), or the ratio of ovarian to body weight (n=8). No significant differences were present in progesterone concentration at any time (n=4). Both 5β-corticosterone , and deoxycorticosterone/11β-hydroxyprogesterone were significantly decreased from before tamoxifen treatment (teal and maroon) to after tamoxifen treatment (blue and red) at euthanasia in each group, but no difference existed between ovarian transplant genotype at either serum sampling point (n=4). Error bars represent the SEM.

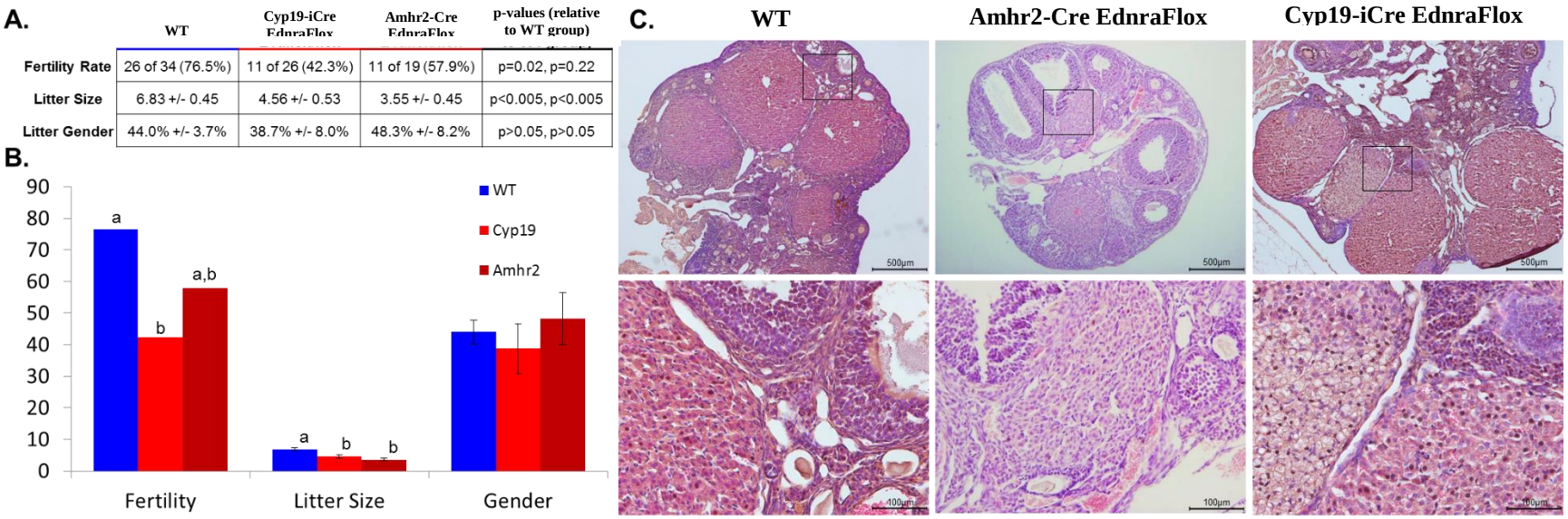

Figure 7.19. Granulosa-cell specific loss of EDNRA causes decreased fertility and litter size. Two granulosa cell-specific *Ednra*-knockout transgenic mouse lines were generated and compared by fertility assay. Females were bred with control fertile males for 10 days and then isolated. **A,B.** Mice containing Cre recombinase under the aromatase promoter (Cyp19, red) had significantly fewer litters per total mating cycles and also significantly fewer pups per litter. Mice with Cre recombinase under the anti-Mullerian hormone receptor type II (Amhr2, maroon) trended towards decreased fertility and also had a significant reduction in the average number of pups per litter. There was no difference between groups in the gender ratio of females to males. Error bars represent the SEM. Mice were sacrificed without stimulation after breeding and ovaries were collected and fixed. **C.** Histological comparison of WT and Cyp19iCreEdnraFlox ovaries. Each genotype is capable of producing normal corpora lutea and antral follicles; no obvious morphological differences are present between treatments. Representative images are shown at 4X and 20X.

CHAPTER 8: PROMOTER ANALYSIS OF ENDOTHELIN-2: REGULATION BY PROGESTERONE RECEPTOR DURING OVULATION AND POTENTIAL ROLE OF RUNT-RELATED TRANSCRIPTION FACTOR 1

Joseph Cacioppo[1], Yongbum Koo[1,2], Po-Ching Patrick Lin[1], Saurabh Sinha[3], and CheMyong Ko[1]*

[1]Comparative Biosciences, College of Veterinary Medicine, University of Illinois, Urbana-Campaign, IL 61802, USA
[2]School of Biological Sciences, Inje University, Gimhae, South Korea.
[3]Department of Computer Science, College of Engineering, University of Illinois, Urbana-Campaign, IL 61802, USA

*Corresponding author
CheMyong Ko, Ph.D.
Department of Comparative Biosciences
College of Veterinary Medicine
University of Illinois at Urbana-Champaign
3806 VMBSB, MC-002
2001 South Lincoln Avenue
Urbana, IL 61802, USA
217-333-9362 (office), 217-244-1652 (fax)
jayko@illinois.edu

This work was supported by NIH (HD052694 to CK).

Running Title: *Edn2* is regulated by PGR, potentially via RUNX1

Key Words: endothelin-2, progesterone receptor, hypoxia, ovary, Runx1

ABSTRACT

Endothelin-2 (EDN2, ET-2) is a short 21 amino acid peptide that is produced in a variety of tissues. It plays a role in the cardiovascular system, in the ovary during ovulation, in the immune system as a chemoattractant or for chemotactic response induction, and likely in a variety of cancers. EDN2 is produced from prepro-form, which must be cleaved to become active. However, the regulation of expression of the *Edn2* gene has yet to be determined. First, two pilot studies were performed: the role of progesterone receptor in *Edn2* regulation within the ovary by using progesterone receptor knockout (PRKO) mice was confirmed, and then it was determined whether acute hypoxia could induce expression throughout the body. Expression of *Edn2* was downregulated approximately 90 fold in PRKO mice; there was no difference in *Edn2* expression in mouse ovaries, kidneys, or lungs immediately after 2 hours of hypoxia in an 8% O_2 chamber, or 6 hours after normoxia recovery. Second, a promoter analysis was performed that examined 3000 base pairs upstream and downstream of the *Edn2* gene as well as the internal intron sequences. The analysis identified 88 transcription factors that may directly regulate *Edn2* expression. When coupled with ovarian microarray data, the hypothesis that *Edn2* is regulated by *Runx1* within the ovary during ovulation was developed, and a possible mechanism for this regulation through repression by BCL6 has been generated for future experimental testing.

INTRODUCTION

Endothelin-2 (EDN2, also ET-2) is a short 21 amino acid peptide[212] that plays an important role throughout the body during development[223], and it also regulates vessel growth and formation[263,614], tissue fibrosis[615,616], and leukocyte migration[270]. Mice that lack the gene *Edn2* do not survive long after birth from starvation, hypothermia, and emphysema[223]; mice that lack endothelin receptor A (*Ednra*, EDNRA) do not survive in utero to birth[617]. Though important, the mechanisms that control *Edn2* expression have not been fully explored, in the ovary or in other tissues throughout the body. Similar to the nearly identical EDN1 protein from *Edn1*, EDN2 is first translated as a prepro form and then cleaved twice into an active form[618]. The *Edn2* gene is believed to be under transcriptional regulation[619,620]. Control by transcription factors may involve binding to promoters, enhancers, and locus-control regions of DNA to help recruit the DNA polymerase complex and/or co-activators. Transcription factors may also act as repressors to prevent transcription; transcription factors exhibit sequence-specific binding and form bonds of varying strength to specific DNA sequences[621]. Transcription factors that bind weakly to one sequence but strongly to another may yet influence the transcription of each. Identification of a binding site that a transcription factor has a high affinity for in the promoter region of a gene suggests that that transcription factor plays a role in regulating that gene's expression. But the sequences transcription factors recognize are often only several base pairs long and allow for partial mismatch. Thus specific binding sites for any one factor can be found at random every few hundred to a thousand base pairs, making the search for transcriptional regulators difficult while adding complexity to a whole organism. This overall mechanism allows for different cells to express the same gene at different times or at different levels. As *Edn2* expression is widespread throughout the body but in a punctate manner[368], *Edn2* expression is likely regulated by different mechanisms in different tissues.

EDN2 has been shown to be expressed in the ovary at the time of ovulation after gonadotropin stimulation in rodents, where it is necessary for normal oocyte release and corpus luteum formation for pregnancy maintenance[6,171]. It is thought to induce contraction of the outer theca cells as a final trigger for follicle rupture[200]. Endothelin-2 is specifically expressed in the granulosa cells in a two hour window, from 11 to 12 hours after stimulation by a luteinizing hormone (LH) mimetic gonadotropin[7], while ovulation occurs from 12 – 14 hours in mice after this gonadotropin stimulation[622-624]. It has been previously shown that ovarian *Edn2* expression is

sharply decreased when the progesterone receptor gene (*Pgr*) is removed[7]. However, the peak timing of *Pgr* expression is nearly six hours before *Edn2* expression in mice (six hours after stimulation)[70,244,625], implying an indirect mechanism for regulation which is supported by the many downstream signaling cascades triggered by *Pgr*. Additionally, a study where mice were treated with RU-486 (progesterone receptor antagonist) or indomethacin (cyclooxygenase inhibitor, PTGS2 inhibitor) did not change *Edn2* expression[247], indicating further exploration is needed into the direct regulation of *Edn2*.

Hypoxia has also been shown to induce *Edn2* expression, specifically through hypoxia-inducible factors (HIFs) that couple to enhance expression[246,247,250,626]. However, luciferase assays have revealed that hypoxia inducible factors are not solely responsible for *Edn2* transcriptional regulation in mice[247]. The *Edn2* gene has multiple binding sequences for HIF upstream of exon 1, and HIF action is increased in the ovary during ovulation, but removal of HIF binding sites shows only a partial reduction in *Edn2* expression by luciferase assay[247], indicating that HIF factors may play a role in *Edn2* induction in the ovary, but may not be solely responsible for expression. Other work using granulosa cell cultures also indicates that HIF may play a role in the timing of *Edn2* expression[245,246,626]. A challenge in studying hypoxia and ovulation is examining the event at a whole tissue level, as multiple organs participate in ovulation from hormonal signaling from the pituitary to leukocyte invasion from the spleen[58]. Whole-animal hypoxic exposure also effects the other systems of the body as well. Specifically, the kidneys suffer necrosis that becomes obvious within 12 hours of acute hypoxia (ischemic injury)[627,628] via downregulation of vascular endothelial growth factor (VEGF) and hypoxia inducible factor 1 alpha (HIF1α)[629]. However, endothelin receptor antagonization may prevent hypoxia-induced damage[630]; additionally, osteopontin (secreted phosophoprotein 1, *Spp1*) knockout mice have reduced macrophage invasion and reduced fibrosis[628], and osteopontin expression itself is decreased in *Edn2*-knockout ovaries during ovulation while *Pgr* is increased (Cacioppo *et al*., unpublished). Generally, these organs have not been well evaluated for *Edn2* expression after acute hypoxia in the mouse, but acute hypoxia may directly or indirectly regulate *Edn2* expression.

To examine potential transcription factors that regulate a new gene of interest, recent large collaborative efforts have produced databases relating the genomic sequences of many species to sequenced RNA and protein sources. Regulatory elements have been investigated through DNA hypersensitivity assays, methylation assays, and now through chromatin immunoprecipitation

(ChIP) assays of proteins themselves[631]. Sequencing of ChIP results relative to DNA regions (ChIP-Seq) allows construction of a library of the proteins that interact with specific DNA regions and also allows for quantification of the strength of these interactions. Other scientists have recorded the specific DNA sequences that known transcription factors interact with and compiled these into a library from previous work using consensus sequence binding[621]. The collaborative ENCODE Consortium effort aims to build a list of regulatory elements that interact with the human genome and utilizes many search options, including ChIP-Seq data, to display possible transcription factors[631]. Alternatively, the program TESS allows for transcription factor identification through string and positional weight matrices that identify DNA sequences related to known consensus sequences[621]. Furthermore, the new MET tool from the University of Illinois statistically examines DNA for over-represented DNA sequences in a promoter region and then incorporates ChIP-Seq and DNA-Seq data from ENCODE or modENCODE to more accurately identify likely transcription factors for a particular gene[632]. One or each of these tools may be used to identify transcription factors responsible for *Edn2* regulation. To then expand upon results from TESS, ENCODE, or MET, species-specific tissue-specific time-specific RNA or protein microarray data may be used to eliminate transcription factors that are not present or not transcribed, or show no change. Transcription search tools and gene expression or protein microarray results are now available publicly online and may be coupled for a powerful new search method. In the interest of *Edn2* in the ovary during ovulation, related microarrays are present through the University of Kentucky examining rats[199] and Stanford University examining humans[198,268,633,634], and may also now be relatively cheaply privately generated for a specific species, tissues, or situations[635-638]. Given the wide utilization of knockout mouse models and the necessity of examining ovulation *in vivo*, transcription factor expression observed through a mouse RNA microarray during ovulation would provide a tool to generate hypotheses on *Edn2* regulation.

The goals of this study were to confirm previous findings regarding *Pgr* regulation of *Edn2*, to test the effect of acute hypoxia *in vivo* on *Edn2* expression in the mouse, to examine potential direct regulators of *Edn2* expression in the body through computational analysis of the gene and known transcription factors, and to generate a model method and testable hypothesis for a possible molecular mechanism underlying ovarian *Edn2* expression based on known expression in that tissue specifically during ovulation. It was hypothesized that genetic loss of *Pgr* would significantly impair expression of *Edn2*, but exposure to a low oxygen environment would not be

sufficient to increase *Edn2* expression. It was further postulated that combined analyses of microarray and ChIP-Seq data would reveal a single transcription factor that binds to the *Edn2* gene that is increased in expression during ovulation just prior to *Edn2* induction.

MATERIALS AND METHODS

Ethics Statement

This study was carried out in tight accordance with the recommendations in the Guide for the Care and Use of Laboratory Animals of the National Institutes of Health. Animal protocol was approved by the University of Illinois Animal Care and Use Committee (Protocols: 11184, 13336, and 14222) and the University of Kentucky Animal Care and Use Committee (Protocol: 1111M2006), and all efforts were made to minimize unnecessary animal suffering.

Animals

Progesterone knockout mice (PRKO) were generated by crossing mice with a floxed progesterone receptor[243] (PgrFlox/Flox) gene with mice that express Cre recombinase under the zone pellucida 3 protein promoter[173] (ZP3-Cre) to cause the deletion of exon 2 in both alleles. Genotyping for progesterone receptor was performed with the primers FPRf 5'-GTA TGT TTA TGG TCC TAG GAG CTG GG-3', fPR-R 5'-TGC TAA AGG TCT CCT CAT GTA ATT GGG-3', and fPR-DR 5'-ATA TTT ATG ACT TTG AGA CTT G-3'. Amplicons of 226, 276, and 481 base pairs indicate WT, floxed, and knockout alleles, respectively; PCR annealing temperature was 58°C with 30 cycles. These mice were on an inbred C57B/6 background. Thirteen global PRKO and 13 control immature (PND25-28) female mice received superovulation. Superovulation consists of intraperitoneal (i.p.) injections of 5IU of pregnant mare serum gonadotropin (PMSG, Sigma-Aldrich, St. Louis, MO) in 100uL saline followed 48 hours later by i.p. injection of 5IU of human chorionic gonadotropin (hCG, Sigma-Aldrich, St. Louis, MO). Mice ovulate 12-14 hours after hCG injection. Mice were euthanized by CO_2 asphyxiation and cervical luxation at hCG0 (PMSG48), hCG6, hCG9, and hCG12 hours and ovaries and uteri were collected (n=4) and flash frozen before RNA extraction. WT mice for hypoxia examination were produced from pairings from the authors' breeding colony on an inbred C57B/6 background. Mice used for ovarian database production were purchased from Jackson Laboratories (Bar Harbor, Maine). These mice were superovulated at 25 days of age and were sacrificed for RNA extraction at PMSG0, PMSG12, PMSG48/hCG0, hCG6, hCG12, and hCG24 hours, and were on a CD31/J background.

RT-qPCR and semi-quantitative PCR

Following euthanasia, ovaries, lungs, or kidneys were removed, and homogenized in Trizol solution (Life Technologies, Grand Island, NY) for RNA extraction. RNA was purified with an RNeasy kit (Qiagen, Germantown, MD), and cDNA was generated using a reverse transcription superscript VILO synthesis kit (Invitrogen). Real time-qPCR was performed to assess *Edn2* and *Rpl19* expression in PRKO and control mice. *Rpl19*, encoding murine ribosomal 60S protein L19, was chosen as an internal control based on previous publications[280,281]. RT-qPCR was run with primers purchased from Life Technologies (Carlsbad, CA): *Edn2* was quantified with primers catalog number Mm00432983_m1 (74bp) and *Rpl19* was quantified with primers catalog number Mm02601633_g1 (69bp) on an ABI 7500 machine. Results were quantified by the delta delta Ct method[472]. Semi-quantitative PCR was similarly used to quantify *Edn2* and *Rpl19* expression after hypoxia exposure in mice. The *Edn2* gene was amplified with (5'-CTCCTGGCTTGACAAGGAATG-3') and (5'-GCTGTCTGTCCCGCAGTGTT-3'), and *Rpl19* was amplified with (5'-CCTGAAGGTCAAAGGGAATGTG-3') and (5'-GTCTGCCTTCAGCTTGTGGAT-3'). PCR products were visualized on an agarose gel; band intensity was analyzed using ImageJ software (NIH, Bethesda, MD) for relative intensity.

Hypoxia Induction

To determine the effect of acute moderate hypoxia on *Edn2* expression in the ovary, lungs, and kidney, mice were exposed to a reduced oxygen atmosphere for two hours. Adult female mice (n=3/group) in diestrus, approximately 125 days of age (125±15.4 days), were placed into a hypoxia chamber (normal ventilation initially) and allowed to acclimate for two days. The chamber is a Plexiglas box with dimensions 12 x 6 x 4 in. At time=0 hours during diestrus, hypoxia was induced for the experimental group of mice by connecting the chamber to a S. J. Smith & Co. (Davenport, IA)-certified gas cylinder containing 8% O_2 and excess nitrogen. Control mice were exposed to normal room air (20.9% O_2) from a similar cylinder at matching times and rates. The hypoxia chamber was flushed for 5 minutes by using a high rate of gas flow (8L/min) to achieve the desired FiO_2. The flow was then maintained for 2 hours at 1L/minutes to induce moderate hypoxia in the experimental group. The O_2 concentration was continually monitored using a gas analyzer (OxyStar-100; CWE, Inc., Ardmore, PA). Following hypoxia exposure, gas flow was shut off and mice were returned to normal room atmospheric conditions. Mouse tissues were

collected at times t=0 (after hypoxia) and t=6 hour (6 hour recovery after hypoxia). The animals were sacrificed using CO_2 inhalation and cervical luxation, and tissues were collected, snap frozen, and stored at -80°C until RNA extraction.

Histology

Tissues were fixed in the 4% paraformaldehyde overnight and were then embedded in paraffin and sectioned at 5 μm, mounted on charged glass slides. Tissues were then stained with hematoxylin (Harris) and eosin (Surgipath) for cellular visualization. Molecular reagents were purchased from Invitrogen (Invitrogen, Carlsbad, CA).

Transcription factor search with TESS, ENCODE, and MET and binding site consensus alignment

To determine potential transcription factors that may regulate expression of *Edn2* during ovulation, multiple searches were conducted using the Transcriptional Element Search System (TESS)[621] and the motif cluster search through ENCODE[631] and the Motif Enrichment Tool (MET)[632]. TESS predicts transcription factor binding sites based on DNA sequences provided by the user using information pulled from TRANSFAC[639,640], JASPAR[641,642], IMD[643], and CBIL-GibbsMat[644]. TESS was publicly available through the University of Pennsylvania (http://www.cbil.upenn.edu/tess). MET predicts transcription factors through enrichment tests on user-defined genes by first determining a set of genes that are targets of a transcription factor and then quantifying the significance of their overlap with the gene in question. Data used for mouse and human genomes were extracted from chromatin immunoprecipitation (ChIP) data representing known binding sites and used to generate probability scores integrating strength of transcription factor binding. MET is publicly available through the University of Illinois at Urbana-Champaign (http://veda.cs.uiuc.edu/cgi-bin/MET/interface.pl). The ENCODE (Encyclopedia of DNA Elements Consortium) human genome database was examined for possible binding sites through the in a similar manner using ChIP data. The ENCODE data set is publicly available through the University of California, Santa Cruz (http://genome.ucsc.edu/ENCODE/). The TESS computation search examined 2000 base pairs upstream of the *Edn2* ATG start codon for DNA sequences in the mouse genome that match known sequences for transcription factor binding. The ENCODE and MET cluster searches examined 3000 base pairs upstream and downstream, as well as introns

of the *Edn2* gene in the human and mouse genomes. Potential transcription factors identified by TESS were scored as 1 per site. ENCODE and MET motif cluster searches were scored as 1.0 for sites above two standard deviations above the binding threshold and 1.5 for sites above four standard deviations above the binding threshold. The total score from all search methods was summed as 'Total Hits' in column 2. All genes identified by any of the three search tools are provided. Binding consensus alignment of RUNX1 was done by first identifying binding sites in the mouse *Edn2* gene. The mouse *Edn2* gene was then aligned using VISTA[645] (Visual Tools for Alignments) to rat, human, and multiple mammal genomes that are annotated and available through the National Center for Biotechnology Information (http://www.ncbi.nlm.nih.gov/). VISTA is publicly available through the University of California, the DOE Joint Genome Institute, and US Department of Energy (http://genome.lbl.gov/vista/index.shtml).

Mouse Ovarian Gene Database (mOGED) generation and use for change in gene expression searches

The mOGED was constructed in 2005 following the same principles as the publicly available rOGED freeware hosted by the University of Kentucky[199]. Briefly, RNA was extracted from four whole ovaries per time point from CD31/J mice and run in duplicate. Five micrograms of RNA were used as template for cDNA synthesis, and biotinylated antisense cRNA probe was prepared by the SuperScript System kit (Invitrogen) and the ENZO BioArray HighYield RNA labeling kit (Enzo Diagnostics, Farmingdale, NY) according to the manufacturer's instructions. Unincorporated nucleotides were removed by using the RNeasy Mini kit (Qiagen). The Affymetrix Mouse oligonucleotide array sets were hybridized, washed, and scanned using Affymetrix equipment and protocols (Affymetrix; DNA Microarray Core Facility, University of Kentucky, Lexington, KY). The total data were compiled as an Access Database file in Excel (Microsoft, Redmond, WA) and run with the GEDT software previously developed for use with rOGED. This allows interface users to search for mapped gene expression at various time points during ovulation. Gene expression at PMSG0 hours was considered baseline expression. P=Present, A=Absent, M=Marginal. Genes with a call of "absent" were considered too low to be detected at that time point and were not considered. Data from mOGED were compared to potential transcription factors identified by TESS and MET to identify genes that had both increased expression and possible binding sites about the *Edn2* gene. Data from mOGED were scored based

on the standard deviation from hCG0, hCG6, and hCG12 hours divided by the mean of those time points, times 100%, to generate a percentage describing relative change in expression just prior to ovulation. Values of less than 50% were not considered significant.

Statistical Analyses

Data analyses were performed using statistical software (SPSS, Inc., released 2013, PASW Statistics for Windows, Version 22.0, Chicago, IL). Continuous data were tested for normal distribution by a Shapiro-Wilk test. All data were normally distributed and were analyzed with parametric tests (student's t-test, ANOVA) and a Bonferroni *post hoc* test. Data are graphically presented as the mean and standard error of the mean. For all analyses the alpha value was set to 0.05.

RESULTS AND DISCUSSION

The endothelin-2 gene (*Edn2*) is implicated in several diseases and is proven important for development and ovulation in mouse models. However, the mechanistic regulation of *Edn2* expression is largely unexplored. The ovary was focused on owing to the predictable and high expression pattern of *Edn2* there during stimulated ovulation. The data demonstrated below confirm that *Edn2* is under regulation by PGR in the ovary, that acute exposure to low oxygen content is insufficient to induce expression, and RUNX1 is a likely regulator of ovarian *Edn2* expression through an epigenetic mechanism.

There are currently two conflicting studies that claim or refute that *Edn2* is under regulation by the progesterone receptor gene (*Pgr*); one utilizes a knockout animal approach[7] while the other uses a pharmacological approach[247]. To first determine if *Edn2* is under regulation of *Pgr*, a novel *Pgr*-deficient mouse (PRKO) was generated by globally deleting the second exon of the gene. These mice were superovulated and compared to control age-matched (25 days) mice. Mice were sacrificed at hCG0 and hCG12 hours, and relative expression of *Edn2* was quantified by RT-PCR and normalized to *Rpl19*. In control mice, *Edn2* expression rose from 1.0±0.1 at hCG0 hours to 926.7±177.5 units at hCG12 hours. (Figure 8.1A). However, in PRKO mice *Edn2* expression increased only from 0.48±0.1 to 10.3±1.2 units. There was no significant difference at hCG0 hours ($p=0.845$), but *Edn2* expression was greatly decreased at hCG12 hours ($p=0.019$, Figure 8.1B). Thus global loss of functional progesterone receptor decreases *Edn2* expression during ovulation approximately 90 fold. This initial study confirms that PGR directly or indirectly regulates *Edn2* expression as described originally by Palanisamy *et al*. 2006. Further study may definitively determine if lack of follicle rupture from PGR loss is responsible for loss of *Edn2* induction, or vice-versa. Conflicting results from Na *et al.* 2008 may have resulted from insufficient RU-486 dosing, a short-acting halflife, late administration of RU-486 relative to PGR action prior to ovulation, or incomplete blockage of PGR. It has been shown by Lin *et al*. (2015, unpublished) that genetic knockout of *Pgr* by a lower efficiency Cyp19-iCre transgene is insufficient to prevent ovulation and it may be that only a small amount of granulosa cells need to express progesterone receptor to mediate its effects. Future work may examine the signaling that occurs between PGR activation and *Edn2* expression, as *Edn2* does not seem to contain a PGR-response element (below).

The aforementioned conflicting authors do both agree that *Edn2* expression is regulated through hypoxic factors. Na *et al.* 2008 state that *Edn2* is under hypoxia inducible factor 1 (HIF1) regulation through ACGTG sequence sites in the promoter. Kim *et al*. 2009 similarly state that HIF1-alpha, HIF2-alpha, and HIF1-beta are transcription factors that form heterodimers during ovulation in PGR-dependent manner[251]. Na *et al*. 2008 utilized a dual luciferase assay to demonstrate loss of certain promoter regions decreased *Edn2* expression; however, *Edn2* expression was never fully lost to the extent seen in PRKO mice and was at most reduced by 2-fold. Kim *et al*. 2009 showed a 90% reduction in *Edn2* expression in the ovary at hCG11 hours when mice were treated with 5mg/kg echinomycin which inhibits HIF heterodimer binding, which is more similar to the changes in expression observed through PRKO mice. As a brief and non-exhaustive pilot study into physiological hypoxia as a trigger for *Edn2* expression, hypoxemia and consequently hypoxia were induced by exposing adult mice to 8% O_2 for two hours. Mice were then sacrificed immediately after hypoxia, or at 6 hours after hypoxia to mimic the time seen between the rise in HIF factors at hCG6 (Figure 8.3B) and expression of *Edn2* at hCG11-12. It is interesting to note here that in the rOGED, HIF1-alpha expression throughout the whole ovary increases from hCG0 hours to hCG6 hours, but that this occurs within the theca cells; there is no change observed within the granulosa cells during this time where *Edn2* expression occurs[199].

Although mice underwent obvious hypoxic stress and remained in sternal recumbency with labored rapid breathing for the duration of low oxygen exposure, no increase in *Edn2* expression was observed in the ovary, kidney, or lungs at either time point (Figure 8.2A, $p>0.05$). Kidney histology was performed as noticeable histologic changes occur there after ischemia-reperfusion injury. However, no major changes could be observed (Figure 8.2B), though this is attributed to the early time of kidney collection at hCG6 hours. At 12-24 hours after hypoxia, tubular lumen dilation of the kidney, flattened epithelial cells, nuclear loss, and apoptosis would be histologically visible[646]. Together, these data suggest that physiological hypoxia and consequential damage is not sufficient to induce *Edn2* expression, at least at the two examined time points. However, one weakness of this study is the lack of confirmation of increases in HIF1-alpha subunit expression; the alpha subunit is oxygen-labile and is rapidly degraded under normoxia while the beta subunit is constantly present[647], and increased presence of HIF1-alpha would be a positive confirmation of hypoxia and presence of one factor that may influence *Edn2* expression. Similarly, qPCR would also be useful for examining the HIF2-alpha subunit as described by Kim *et al.* 2009 to further

confirm or deny that hypoxic factors regulate *Edn2* expression in the ovary. Additionally, as the body has many ways of coping with low atmospheric oxygen to keep tissues viable, it may be more beneficial to study the effect of ovarian artery clamping on *Edn2* expression to ensure tissue hypoxia occurs and is not managed through low activity and high respiration rate.

Though they are the most closely explored, it is possible that other transcription factors beyond HIF1 and downstream of PGR may directly regulate *Edn2* expression; these factors may also vary between tissue types and may not all be present in the granulosa cells of the ovary. To identify potential transcription factors that directly regulate *Edn2* expression in any tissue, four computational searches were used based on the *Edn2* gene sequence in humans and mice and available ChIP-Seq data or a transcription factor consensus binding sequence library. Searches were conducted through TESS, ENCODE, and MET, and the methods are described above. A summary of results are listed in Table 8.1 (continued on multiple pages in two sections). Transcription factor scores ranged from 1-6, with the average being 1.90. Agreement between searches was surprisingly low and few genes were identified in multiple search methods or in the same position across searches. The highest scoring transcription factors were Sp1 (6), CTCF (5), EBF1 (5), NFKB1 (5), Zfp423 (5), Tcfcp2l1 (4), TFAP2A (4), and TLX1_NFIC (4); the full name of these factors are Sp1 transcription factor, CCCTC-binding factor (zinc finger protein), early b-cell factor 1, nuclear factor of kappa light polypeptide gene enhancer in B-cells 1, zinc finger protein 423, transcription factor CP2-like 1, transcription factor AP-2 alpha, and t-cell leukemia homeobox 1 - nuclear factor 1/c(CCAAT-binding transcription factor) complex. These transcription factors are of the greatest interest, though presence of any single binding site for any of the transcription factors listed in Table 8.1 may be sufficient for increasing expression. Of these eight transcription factors, none were similarly identified through all searches. NFKB1 scored 2 for binding within the mouse and human *Edn2* genes within both MET searches, and was the most similar between searches. No papers exist at present in NCBI's PubMed linking any of these eight transcription factors with *Edn2*. Also of interest, HIF1 scored 1.5 and HIF1A-ARNT (HIF1 is synonymous with alpha-aryl hydrocarbon nuclear translocator, ARNT) scored 2.0 (Table 8.1); these hits occurred in TESS and both MET searches and indicate that HIF1 has DNA binding about the *Edn2* gene, specifically within the 3kbp downstream of the gene as confirmed by ChIP-Seq, though this did not matched published TESS search data[247]. Lastly, though both ESR1 and ESR2 (estrogen receptor alpha and beta) had possible sites for *Edn2* regulation, no search identified PGR

as a possible transcriptional regulator of *Edn2*. This implicates that *Edn2* is indirectly downstream of PGR during ovulation in the ovary, given both binding sequence data and ChIP-Seq data in the human and mouse genome.

Transcription factor search data identify what factors associate with DNA at particular regions; however, they do not identify if those factors are present in the tissue of interest at the time of interest. Transcription factor searches require a second negative filter of what transcription factors are truly present. In examination of *Edn2* expression in the ovary, it is necessary that such a transcription factor is present during ovulation, but is absent prior to and after ovulation. To generate a negative filter for a transcription factor regulating *Edn2* expression during ovulation, it was postulated that such a factor would have a large change, either increase or decrease, in expression and protein presence just prior to ovulation when *Edn2* expression spikes. A mouse ovarian gene expression database was created using CD31 mice by extracting RNA from various time points during ovulation and comparing expression through Affymetrix microarrays, similar to the construction of the rOGED database[199]. The change in transcription factor expression during ovulation was calculated as the percent standard deviation divided by the mean expression of the transcription factor. Gene expression and expression changes during ovulation were compared to transcription factors previously identified (Table 8.2). Transcription factors that scored 50% or lower were discarded. Not all genes were present as transcript in the ovary during ovulation according to microarray data (A=absent, P=present, M=marginal). Sixteen genes scored greater than 50% deviation/mean change; the average number of transcription factor binding site hits among these was 1.72. Of those eight factors that scored 4 or higher, only EBF1 had a major change in transcript level during ovulation. However, of those 16 genes with a large transcript change, 13 were called as Absent for all or part of the critical time periods leading up to ovulation and *Edn2* expression. These 13 included EBF1. Those three transcription factors that had >50% change and were called as present and were identified by transcription factor search included JUNB (Jun B proto oncogene), RUNX1 (runt related transcription factor 1), and EGR1 (early growth response 1, also Krox24, NGFIA, zif268, Zenk, and TZs8,) (Table 8.2, bold). Each of these demonstrates significant increase in transcript just prior to ovulation, similar to *Edn2* which spikes at hCG12 hours (Figure 8.3A). JUNB increases from 127 transcriptional units (AU) at hCG0 to 629 at hCG6 to 1633 at hCG12 hours. RUNX1 increases from 106 at hCG0 to 2029 at hCG6 to 1537 at hCG12 hours. EGR1 increases from 1103 at hCG0 to 4620 at hCG6 to 7443 at hCG 12

hours (Figure 8.3). Of these three transcription factors, RUNX1 has peak expression at about hCG6 hours while JUNB and EGR1 peak at hCG12 hours near ovulation. In the first transcription factor search, JUNB scored 1 with one site identified by ENCODE upstream of human *Edn2*; RUNX1 scored 2 with one site upstream and one site within introns of *Edn2* with each site identified by MET in the human genome; EGR1 scored 2 with one site upstream and one stream downstream of mouse *Edn2* with each identified by MET (Table 8.1).

Each of these transcription factors is quite different, and it is unlikely that they simultaneously regulated *Edn2*. JUNB is a member of the activator protein-1 (AP-1) transcription factor family, similar to FOS and other JUN proteins, and is best known for its ability to modulate cellular proliferation[648,649]. JUNB inhibits cell growth through antagonization of c-Jun and suppresses proliferation by inhibiting transcription of p16INK4A[650] and cyclin-D[651], but promotes transcription of cyclin A to induce proliferation[652]. JUNB responds to plasma insulin and glucose concentrations as well[653]. Importantly, JunB-KO mice were recently generated and characterized; JunB-KO mice have growth retardation, low survival rate, and reduced fat[654]. About 65% of JunB-KO mice die by age 12 weeks, and weigh less by 3 months of age even though they are born at the same weight and have nearly the same food intake[654]. This phenotype is similar to *Edn2* global knockout mice, which also die young from starvation and demonstrate reduced rate of growth[223]. As JUNB may not be the only regulator of *Edn2*, and because JunB-KO mice were generated through crossing flox mice with Cre mice rather than ablating alleles in the oocyte, it is possible that JUNB regulates *Edn2* expression and the less severe phenotype seen in JunB-KO mice results from some remaining *Edn2* function.

RUNX1 and RUNX function as transcriptional activators or repressors depending on the target gene, cell type, and available cofactors[655]. RUNX1 has been implicated in stem cell homeostasis and lineage specification in many cell types. RUNX1 binds to DNA and associates with HATs (histone acetyltransferases) or HDACs (histone deacetylases) to direct deacetylation[656]. Deacetylation modulates DNA affinity for histones by exposing positive charges of lysine residues of the histones and increasing the interaction of histone lysine N-termini with negatively charged phosphate groups of DNA, while HATs have the opposite effect. An increased histone-DNA interaction generally promotes a heterochromatic structure and prevents gene transcription[657]. RUNX1 interacts with a DNA sequence known as MTG8 (myeloid translocation gene on chromosome 8, also ETO) or similar sequences; this sequence specifically recruits NCOR

(nuclear receptor corepressor), SMRT (silencing mediator of retinoid and thyroid hormone receptors, also NCoR2), and several HDACs[658]. To mediate these actions, RUNX1 interacts with CBFβ (core binding factor-beta) to form a heterodimer[659] that then binds the DNA. Global loss of RUNX1 is embryonically lethal[660]. In the ovary, RUNX1 has been shown to modulate expression of many genes following the LH surge[483]. Expression of *Runx1* is controlled by PGR[483]. Specifically, RUNX1 knockdown in cultured granulosa cells showed downregulation of *Mt1a*, *Hapln1*, *Rgc32*, and *Ptgs2*[483,661], while changes in *Edn2* expression were not then reported. RUNX1 has been knocked out in the intestines using a Villin-Cre system, though no phenotypes were observed in development though the incidence of tumor growth was higher[655]. Similarly, loss of *Edn2* using Villin-Cre showed no early phenotype that might lead to starvation, as seen in global *Edn2*-KO mice[223].

EGR1 is a transcription factor with three zinc finger structures that was originally identified for its expression by nerve growth factor in rat cell lines[662]. EGR1 has consequently been largely studied for its role in the brain, particularly on neuron growth and memory. It has also been shown that EGR1 is necessary for macrophage differentiation and T lymphocyte proliferation[663,664]. A global EGR1 knockout mouse line was generated in 2005 by Lee *et al*.[662]. The mice exhibit normal growth and lack defects in cellular differentiation, though reproductive characteristics were not explored[662]. However, given their normal growth and survival, it is unlikely that EGR1 influences *Edn2* expression unless it is specific to the ovary.

To specifically influence the effect of *Edn2* during ovulation for only a brief time period, it is necessary that the promoting transcription factor also be active for a brief period of time, and that it is expressed and translated prior to EDN2 peptide. Of the three likely factors examined, only RUNX1 is higher at hCG6 hours than hCG12 hours in the ovary. Given its role as a transcriptional activator and the lethal phenotype resulting from *Runx1* ablation, RUNX1 is a likely transcription factor to influence *Edn2* expression. To further examine its potential, consensus binding sites for RUNX1 were examined (Figure 8.4A). In the mouse *Edn2* gene, four binding sites were observed based on the consensus sequences TGTGGTT, TGTGGTC, TGCGGTT, and TGCGGTC or their reverse complements. Of these, one site that is present between the second and third exon of *Edn2* is conserved across mammals, excepting the rabbit and panda. This high level of conservation within an intron suggests the binding RUNX1 is important within *Edn2*.

RUNX1 is associated indirectly with BCL6 (B cell lymphoma 6 protein), which may be responsible in turn for regulation of *Edn2* in the ovarian granulosa cells. BCL6 is a sequence-specific repressor that binds to DNA that interacts with NCOR and SMRT[656], and also binds to MTG8/ETO[665]. Thus BCL6 and RUNX1 compete for the same or similar sites. During ovulation, *Bcl6* is constitutively expressed except for the time points hCG6 and hCG12 hours, where it is absent (Figure 8.3F), which is inverse to *Runx1* and is prior to and during *Edn2* expression. BCL6 consensus sequences were also examined; as in RUNX1, four sites were observed in the mouse and one of these, upstream of the first exon, is conserved across all mammals' sequences examined (Figure 8.4B); this region is within 70 basepairs of a conserved binding RUNX1 region in rats and mice. Also, as both RUNX1 and BCL6 are known to associate with MTG8-similar regions, a directly matching consensus sequence may not be required between them for DNA binding competition.

As BCL6 interacts with NCOR and SMRT, and RUNX1 with CBFβ, their expression levels were examined in the mOGED. NCOR decreases slightly from baseline at hCG6 and hCG12 hours and is present throughout ovulation; SMRT is present throughout ovulation and decreases markedly during hCG6 and hCG12 hours; and CBFβ is relative constant and present throughout ovulation with slight increase of about 10% expressing at hCG6 hours. Lastly, the protein CRLZ1 (charged amino acid rich leucine zipper 1, *Utp3*) was also examined. CRLZ1 was recently discovered as a CBFβ binding factor, which mobilizes CBFβ from the cytoplasm to the nucleus[666] where it can then associate with RUNX1. CRLZ1 also remains bound to the RUNX1-CBFβ heterodimer throughout DNA binding. CRLZ1 is present throughout ovulation in the mOGED; it remains relatively constant during ovulation except for hCG6 hours, where it increases in expression by 22%, before dropping again at hCG12 hours.

Taken together, a hypothesis for a mechanism of molecular control of *Edn2* transcription may now be constructed (Figure 8.5): Prior to ovulation and during the majority of the cycle in the mouse granulosa cells, the repressor BCL6 is bound about the *Edn2* gene with the corepressors NCOR and SMRT. These corepressors recruit HDACs which deacetylate histones to cause tight DNA binding and prevent transcription. Following the LH surge, via PGR downstream signaling, expression of BCL6, NOCR, and SMRT all decrease at hCG6 hours. Concurrently, RUNX1, CBFβ, and CRLZ1 levels increase. As BCL6 expression is absent at hCG6-hCg12 hours, this then allows the binding of RUNX1 to the *Edn2* gene; this binding is mediated by the heterodimer

formed with CBFβ and mediated through CRLZ1 translocation. RUNX1 binding recruits HATs (likely MOZ, MORF, or $p300^{656}$), which acetylate lysine residues to decrease histone-DNA affinity and allow for rapid *Edn2* transcription. This transcription is further enhanced through the presence of the HIF1 complex. After translation, EDN2 causes follicular rupture through a contractile mechanism, and mediates other downstream effects through local endothelin receptors.

Future experiments may focus on all or portions of this mechanistic hypothesis for the ovarian regulation of *Edn2* via RUNX1, and may also rule out the possible involvement of JUNB and EGR1. A solid early approach may utilize breeding studies with conditional knockout mice in which *Runx1* is lost specifically in the granulosa cells. Of note, a mouse that expresses Cre recombinase under the progesterone receptor promoter has been crossed with *Runx1*-flox mice. This mouse demonstrates normal ovulation (Kannan, 2015, unpublished data, personal communication). However, *Pgr* is expressed relatively late in ovulation at nearly the same time point as *Runx1* and Cre recombinase may not have time to sufficiently remove the *Runx1* gene before transcription begins. Furthermore, Pgr-Cre may not remove *Runx1* from all granulosa cells and incomplete ablation may result in no change. It is thus important for protein analyses to accompany transgenic mouse studies of this nature. The use of the new Esr2-iCre mouse line may be sufficient to remove *Runx1* prior to ovulation in the granulosa cells to determine if RUNX1 directly regulates *Edn2* expression; phenotypes of Runx1-FloxFlox Esr2-iCre mouse are postulated to match those of Edn2-Flox/Flox Esr2-iCre mice and exhibit significant reduction in oocytes ovulated and pups per litter. *In vitro* studies using granulosa derived from this mouse model may then allow use of pharmacological stimulation, antagonization, and knockdown technology to confirm the role of the protein intermediaries.

Overall, this study confirms the role of progesterone receptor as a regulator of *Edn2* expression within the ovary and presents a molecular hypothesis for the mechanism behind it centered about RUNX1 modulation of acetylation. The method of comparison used here between DNA sequence analyses, transcription factor binding analyses through ChIP-Seq, and tissue and time-specific microarrays may be similarly implemented to develop and test future hypothesis for genetic regulation as well, and may also combine developing protein arrays to improve accuracy and success.

ACKNOWLEDGEMENTS

The authors thank Dr. John Lydon from Baylor College of Medicine for progesterone receptor floxed mice, Dr. Stuart Clark Price for instruction and use of an oximeter to monitor oxygen content, and Dr. Matthew Wallig for his examination of kidney histology following hypoxia.

TABLES

Table 8.1. Transcription factor search using Transcriptional Element Search System (TESS) computational search and ENCODE and Motif Enrichment Tool (MET) motif cluster searches. Multiple searches were performed to identify potential transcription factors that regulate *Edn2* expression. The TESS computation search examined 2000 base pairs upstream of the *Edn2* ATG start codon for DNA sequences in the mouse genome that match known sequences for transcription factor binding. The motif cluster searches through UCSC and UIUC examined 3000 base pairs upstream and downstream, as well as introns of the *Edn2* gene in the human and mouse genomes. Potential transcription factors identified by TESS were scored as 1 per site. Motif cluster searches were scored as 1.0 for sites above two standard deviations above the binding threshold and 1.5 for sites above four standard deviations above the binding threshold. The total score from all search methods was summed as 'Total Hits' in column 2. Transcription factors with a high number of hits include CTCF, EBF1, NFKB1, Sp1, and Zfp423; however, different transcription factors are likely present in different tissues or at different times. No transcription factor examined had a score of less than 1 or greater than 6. HIF-1 and HIF1A-ARNT had a combined score of 3.5 and is the only representative score from a known inducer of *Edn2* in multiple tissues and species. Continued on multiple pages, shown as left side followed by right side:

Left side:

		TESS Upstream Computational Search	**ENCODE Human *Edn2* Search**		
Transcription Factor Name	**Total Hits**	**Upstream 2Kbp**	**Upstream 3Kbp**	**In Gene**	**Downstream 3Kbp**
AP-2alpha	1				1
AP-2gamma	3		2		1
Arnt	2				
Arnt_Ahr	2				
CEBPB	1.5				1.5

Table 8.1, left side. Continued from previous page.

c-Fos	1		1		
c-Jun	1		1		
c-Myc	2		2		
CTCF	5		1		1
CTCF_(C-20)	1		1		
CTCF_(SC-5916)	1		1		
E2F1	1				
EBF1	5				
eGFP-FOS	1.5		1.5		
eGFP-GATA2	1		1		
eGFP-JunB	1		1		
eGFP-JunD	1.5		1.5		
Egr1	2				
ELK1	1				
ELK4	2				
ERalpha-a	3		1	1	1
ESR1	2				
ESR2	1				
Esrrb	2				
FOX1	1	1			
FOXA1_(C-20)	1		1		
FOXC1	1				
FOXF2	1				
GABPA	2				
GATA-2	2.5		1.5		1
GR	3		3		
HA-E2F1	1			1	
HIF-1	1	1			
HIF1A_ARNT	2				

Table 8.1, left side. Continued from previous page.

HNF41	1				
HNF4A	1				1
HNF4A_(H-171)	1.5				1.5
HNF4G_(SC-6558)	1				1
Ini1	2		2		
INSM1	1				
JunD	1		1		
Klf4	3				
Max	1		1		
Myb	3				
Myc	2				
Myc_Max	2				
Myf	3				
MZF1_5-13	2				
NF-1	1	1			
NFIC	1				
NF-kappaB	2				
NFKB	2		1	1	
NFKB1	5				
NHLH1	1				
NR1H2_RXRA	2				
NR2F1	2				
p300	1				1
Pax5	1				
PAX5-C20	1		1		
Pax6	1				
Pit-1	1	1			
PLAG1	2				
Pol2	1.5		1.5		

Table 8.1, left side. Continued from previous page.

PPARG_RXRA	1				
PU.1	1	1			
Rad21	2		1		1
REL	1				
RELA	2				
REST	1				
RUNX1	2				
RXR_RAR_DR5	4				
RXRα	1	1			
Sp1	6	3			
Spz1	1				
STAT1	3.5		1.5		
STAT3	1				
T	1				
TBP	2	1	1		
Tcfcp2l1	4				
TEAD1	2				
TFAP2A	4				
TLX1_NFIC	4				
TP53	1				
USF1	3				
XPF-1	1	1			
Zfp423	5				
Zfx	3				
ZNF263	1		1		

Table 8.1, right side. Continued on multiple pages.

	MET Human Edn2 Search			MET Mouse Edn2 Search		
Transcription Factor Name	**Upstream 3Kbp**	**In Gene**	**Downstream 3Kbp**	**Upstream 3Kbp**	**In Gene**	**Downstream 3Kbp**
AP-2alpha						
AP-2gamma						
Arnt		1				1
Arnt_Ahr		1				1
CEBPB						
c-Fos						
c-Jun						
c-Myc						
CTCF	1	2				
CTCF_(C-20)						
CTCF_(SC-5916)						
E2F1				1		
EBF1	1	1	1		2	
eGFP-FOS						
eGFP-GATA2						
eGFP-JunB						
eGFP-JunD						
Egr1				1		1
ELK1		1				
ELK4		2				
ERalpha-a						
ESR1	1	1				
ESR2	1					
Esrrb			1	1		

Table 8.1, right side. Continued from previous page.

FOX1						
FOXA1_(C-20)						
FOXC1						1
FOXF2						1
GABPA		1	1			
GATA-2						
GR						
HA-E2F1						
HIF-1						
HIF1A_ARNT			1			1
HNF41				1		
HNF4A						
HNF4A_(H-171)						
HNF4G_(SC-6558)						
Ini1						
INSM1		1				
JunD						
Klf4		1		1	1	
Max						
Myb		1	1		1	
Myc			1			1
Myc_Max			1			1
Myf		1			1	1
MZF1_5-13		1		1		
NF-1						
NFIC		1				
NF-kappaB		1			1	
NFKB						
NFKB1		2		1	2	

Table 8.1, right side. Continued from previous page.

NHLH1					1	
NR1H2_RXRA		1		1		
NR2F1		1		1		
p300						
Pax5			1			
PAX5-C20						
Pax6			1			
Pit-1						
PLAG1	1			1		
Pol2						
PPARG_RXRA			1			
PU.1						
Rad21						
REL					1	
RELA			1		1	
REST	1					
RUNX1	1	1				
RXR_RAR_DR5			1	1	1	1
RXRα						
Sp1		1		1	1	
Spz1						1
STAT1		1		1		
STAT3			1			
T					1	
TBP						
Tcfcp2l1		1		1	1	1
TEAD1		1	1			
TFAP2A		2	1	1		
TLX1_NFIC		1		1		2

Table 8.1, right side. Continued from previous page.

TP53		1				
USF1		1	1			1
XPF-1						
Zfp423		1	1	1	2	
Zfx		1		1	1	
ZNF263						

Table 8.2. Comparison of potential regulatory transcription factors to mouse ovarian gene expression changes during ovulation. For transcription factors identified by gene search (Table 1), expression of each was examined in mouse ovaries during ovulation through microarray data downloaded from the mouse ovarian gene expression database (mOGED, unpublished). The amount of transcript at hCG0, 6, and 12 hours was recorded. To search for large changes in expression during ovulation, the standard deviation of expression from the three time points was recorded and divided by the mean of expression from those times to generate a percentage of change during ovulation. Transcription factors were ranked by decreasing percent deviation. Those with changes greater than 50% were also examined for presence or absence of transcript from the mOGED. Two transcription factors, RUNX1 and EGR1, were identified as having a large change in transcript that were also present during ovulation. No gene had a percentage greater than 100% (range 0-93%). Twenty transcription factors were not present in the mOGED and were not analyzed for expression change or presence during ovulation. Continued on multiple pages.

TF Name	Sum Score	mOGED Expression: Ovary			StDev/Mean	mOGED ID	Presence
		hCG0	hCG6	hCG12			
eGFP-JunB	1	127	629	1633	96.29%	[jun-b]	**P for all**
FOXC1	1	3	30	51	85.94%	[foxc1]	A for all
EBF1	5	6	16	3	81.68%	[irebf1]	A for all
RUNX1	2	106	2029	1537	81.62%	[runx1]	**P for all**
INSM1	1	4	36	35	72.77%	[insm1]	A for all
Egr1	2	1103	4620	7443	72.38%	[egr1]	**P for all**
HIF1A_ARNT	2	35	123	184	65.71%	[hif1a] cDNA	A hCG0 A hCG6
ELK1	1	146	42	64	65.25%	[elk1]	A hCG12
E2F1	1	224	100	72	61.28%	[e2f1]	A hCG6 A hCG12
HA-E2F1	1	224	100	72	61.28%	[e2f1]	A hCG6 A hCG12
Spz1	1	23	18	5	60.60%	[spz1]	A for all
Pax6	1	18	67	39	59.48%	[pax6]	A for all
eGFP-GATA2	1	85	117	30	56.90%	[gata2] cDNA	A hCG6

Table 8.2. Continued from previous page.

GATA-2	2.5	85	117	30	56.90%	[gata2] cDNA	A hCG6
AP-2gamma	3	37	25	10	56.37%	[tcfap2c]	A for all
ELK4	2	112	140	38	54.52%	[elk4]	A for all
T	1	6	9	3	50.00%		
Klf4	3	225	654	466	47.97%		
STAT3	1	956	2355	2790	47.12%		
Myb	3	34	27	12	46.19%		
Pax5	1	42	32	16	43.72%		
Myf	3	5	2	5	43.30%		
PPARG_RXRA	1	1462	1390	584	42.56%		
ESR2	1	1183	682	564	40.59%		
c-Fos	1	433	215	523	40.57%		
eGFP-FOS	1.5	433	215	523	40.57%		
TEAD1	2	47	113	91	40.17%		
CEBPB	1.5	2098	4968	3968	39.61%		
Esrrb	2	49	25	52	35.23%		
Myc	2	709	789	1300	34.38%		
GABPA	2	176	344	347	33.87%		
PU.1	1	47	27	55	33.54%		
NR2F1	2	84	45	55	33.03%		
Ini1	2	188	122	238	31.85%		
FOXF2	1	26	41	50	31.09%		
NFKB	2	327	439	605	30.61%		
TLX1_NFIC	4	58	37	34	30.41%		
NFIC	1	43	35	23	29.90%		
Pit-1	1	15	16	25	29.50%		
ERalpha-a	3	33	48	58	27.16%		
ESR1	2	33	48	58	27.16%		
RXRα	1	182	244	151	24.62%		
GR	3	53	86	66	24.33%		
MZF1_5-13	2	26	23	36	24.02%		

Table 8.2. Continued from previous page.

Zfx	3	93	143	103	23.41%		
RXR_RAR_DR5	4	655	453	445	22.99%		
REST	1	57	57	38	21.65%		
eGFP-JunD	1.5	1035	1555	1510	21.08%		
JunD	1	1036	1555	1510	21.03%		
USF1	3	239	366	329	20.98%		
STAT1	3.5	275	180	250	20.96%		
NF-kappaB	2	545	771	604	18.32%		
NFKB1	5	545	771	604	18.32%		
HIF-1	1.5	794	1107	921	16.74%		
NHLH1	1	74	80	59	15.23%		
Sp1	6	1748	1347	1431	14.02%		
NR1H2_RXRA	2	840	637	718	13.97%		
PLAG1	2	21	26	21	12.74%		
Zfp423	5	5	5	4	12.37%		
TBP	2	338	309	388	11.58%		
Rad21	2	1313	1047	1169	11.32%		
Arnt_Ahr	2	284	230	253	10.60%		
CTCF	5	985	1063	897	8.46%		
Arnt	2	64	57	56	7.39%		
Max	1	642	649	608	3.46%		
Tcfcp2l1	4	251	265	258	2.71%		
AP-2alpha	1	58	55	57	2.70%		
FOXA1_(C-20)	1	2	2	2	0.00%		
c-Jun	1	not in database 100807			N/A		
c-Myc	2	not in database 100807			N/A		
CTCF_(C-20)	1	not in database 100807			N/A		
CTCF_(SC-5916)	1	not in database 100807			N/A		
FOX1	1	not in database 100807			N/A		
HNF41	1	not in database 100807			N/A		
HNF4A	1	not in database 100807			N/A		

Table 8.2. Continued from previous page.

HNF4A_(H-171)	1.5	not in database 100807	N/A		
HNF4G_(SC-6558)	1	not in database 100807	N/A		
Myc_Max	2	not in database 100807	N/A		
NF-1	1	not in database 100807	N/A		
p300	1	not in database 100807	N/A		
PAX5-C20	1	not in database 100807	N/A		
Pol2	1.5	not in database 100807	N/A		
REL	1	not in database 100807	N/A		
RELA	2	not in database 100807	N/A		
TFAP2A	4	not in database 100807	N/A		
TP53	1	not in database 100807	N/A		
XPF-1	1	not in database 100807	N/A		
ZNF263	1	not in database 100807	N/A		

FIGURES

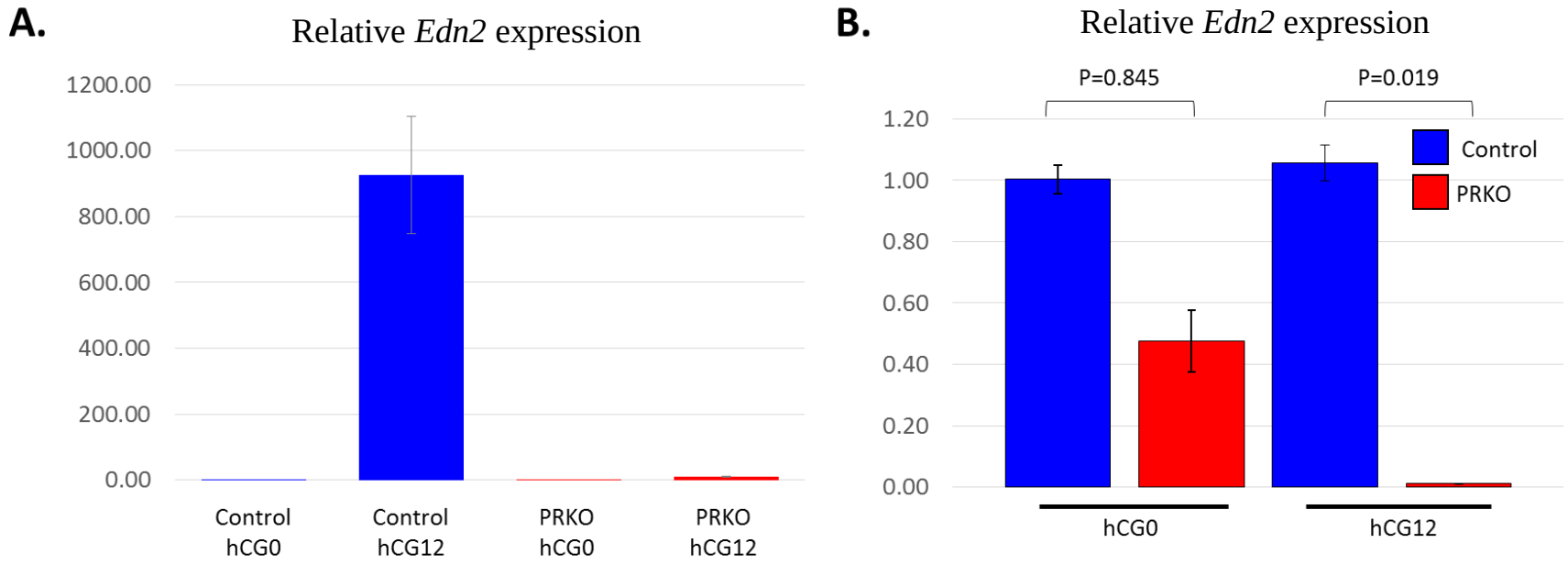

Figure 8.1. PRKO mice lack *Edn2* expression during ovulation. Female mice that globally lack the progesterone receptor gene and control siblings were superovulated at 25 days of age. Mice were sacrificed at hCG 0 hours or hCG 12 hours and ovaries were removed. Total RNA was extracted and RT-PCR was performed for *Edn2* expression (n=4 mice / group), and normalized to *Rpl19*. **A.** The change in *Edn2* expression was quantified relative to control mice at hCG 0 hours. In control mice *Edn2* expression increases 926.7±177.5 times from 1.0±0.1 from hCG0 to hCG12 hours; in PRKO mice *Edn2* expression increases from 0.48±0.1 to 10.3±1.2. **B.** Relative to control mice, PRKO mice have a significant reduction in *Edn2* expression at hCG 12 hours (p=0.019). In PRKO mice, expression of *Edn2* is decreased approximately 90 fold at hCG12 hours (1.06±0.20 to 0.01±0.00). There was no significant difference in *Edn2* expression at hCG0 hours (p=0.845). Error bars show the S.E.M.

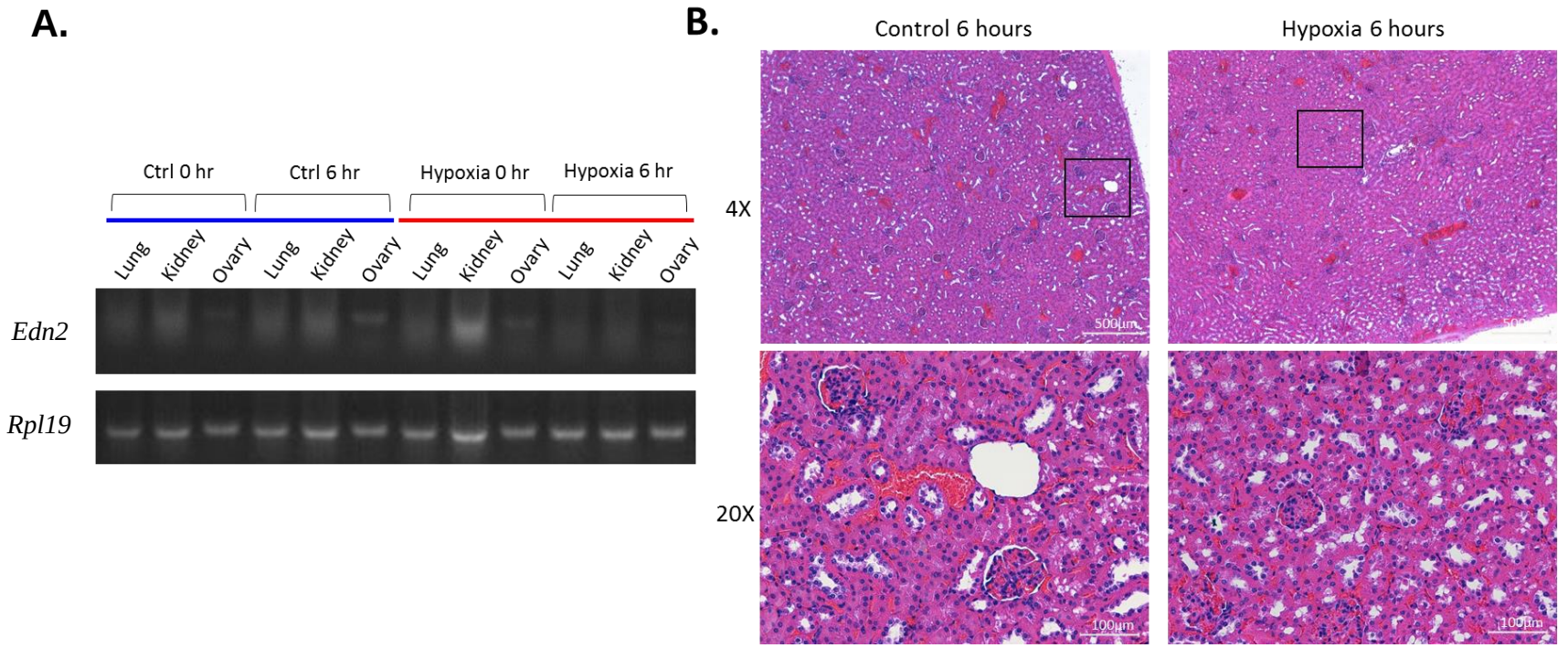

Figure 8.2. *Edn2* expression is not changed in ovaries, kidneys, or lungs following acute hypoxia. A. Adult WT mice (n=3 / group) of approximately 125 days of age (±15.4) in diestrus were exposed to 8% oxygen in a hypoxia chamber for two hours. Mice were sacrificed immediately after (0 hours), or were returned to normoxia for 6 hours and then sacrificed. Ovaries, lungs, and kidneys were collected, RNA was extracted, and mRNA expression of *Edn2* was examined by semi-quantitative RT-PCR. No significant differences were observed ($p>0.05$ for all). *Rpl19* was used as internal control. **B.** Kidney histology was examined for early signs of hypoxic damage. No qualitative differences were observed between kidneys of mice that had and had not been exposed to hypoxia. Pathological analysis at the University of Illinois suggested that microscopic changes may be apparent on a cellular level by SEM, but no histologic changes were able to be observed.

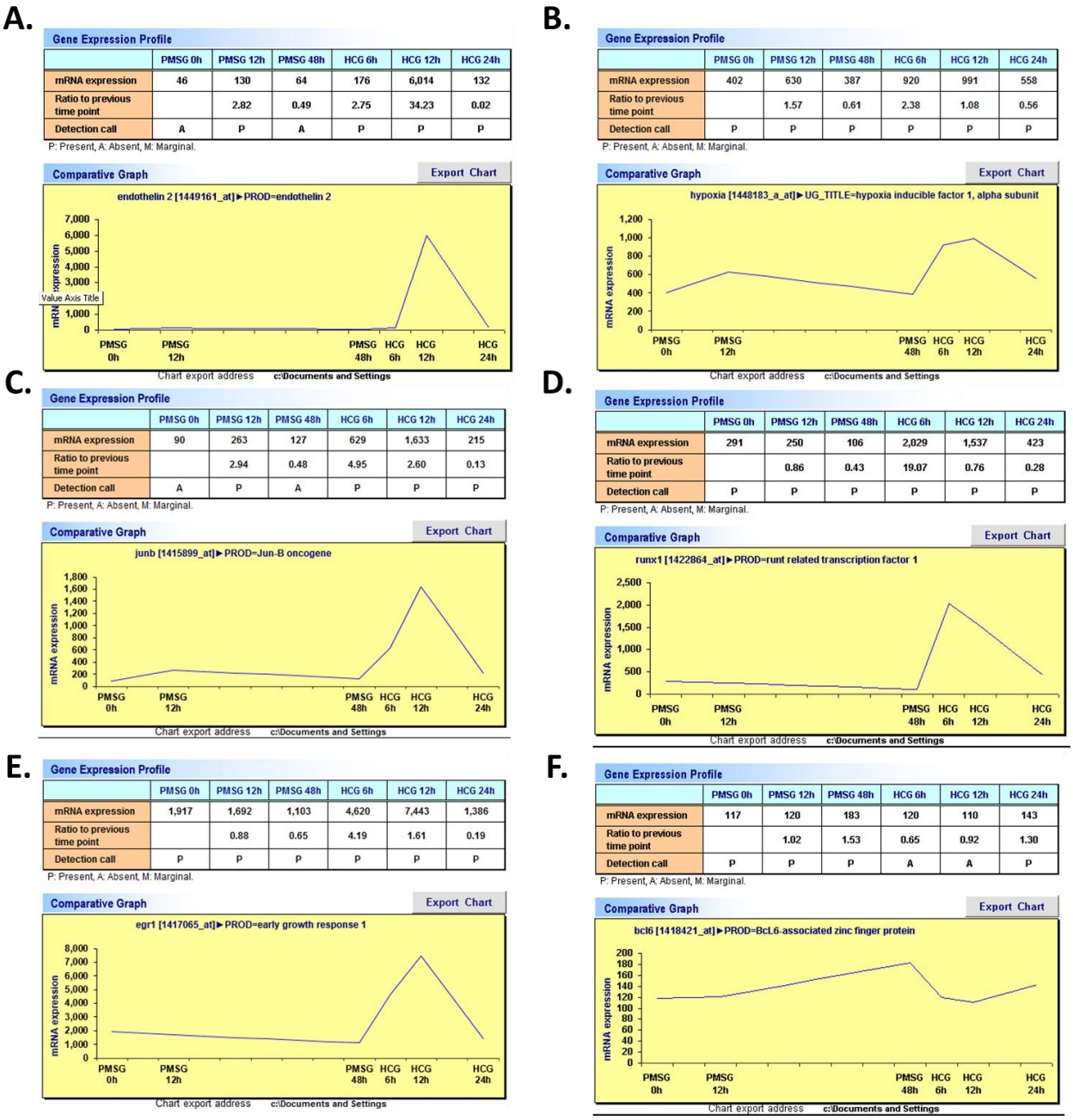

Figure 8.3. Mouse ovarian expression of *Edn2*, *Hif1α*, *Runx1*, and *Bcl6* during ovulation.
Legend continued on next page.

Figure 8.3. Mouse ovarian expression of *Edn2, Hif1α, Runx1,* and *Bcl6* during ovulation. Continued from previous page. Expression levels of genes of interest were determined from the microchip-based mouse ovarian gene expression database (mOGED). **A.** Endothelin-2 remains low or undetectable at all points assayed, excepting hCG12 hours where it spikes during early ovulation before returning to basal levels. **B.** Hypoxia inducible factor 1-alpha has a moderate increase throughout the ovulatory period with the highest point during hCG12 hours. *Hif1α* has a 50-100% increase from baseline during ovulation. **C.** Jun-B proto-oncogene increases sharply during ovulation with peak transcript levels at hCG12 hours, which is nearly three times as high as expression at hCG6 hours and about 15 times higher than baseline levels. **D.** Runt related transcription factor 1 is present throughout ovulation; expression of *Runx1* increases nearly 10-fold at hCG6 hours, prior to ovulation and the increase in *Edn2* expression; *Runx1* declines to about a 5-fold increase from baseline at hCG12 hours and returns to nearly baseline at hCG24 hours. **E.** Transcripts from early growth response 1 increase at hCG6 hours and are highest at hCG12 hours, approximately four times higher than baseline, before dropping again at hCG24 hours. Expression of *Egr1* increases until ovulation occurs. **F.** B cell leukemia/lymphoma 6 expression increases slightly during early ovulation and is highest at hCG0 hours before dropping to basal levels at hCG6 hours and hCG12 hours. *Bcl6* expression is low during ovulation and has an inverse relationship to *Runx1*. Of these genes, only *Runx1* peaks at hCG6 and *Bcl6* is low at hCG6 and hCG12 hours. The mOGED database was constructed from total RNA isolated from intact mouse ovaries following superovulation and run on Affymetrix Mouse Expression Arrays (n=5 animals/time point). PMSG48 hours is synonymous with hCG0 hours. P=present, A=absent, M=marginal. Chart title above line graph provides Affymetrix gene ID numbers and gene name or alternate name.

A.

Consensus binding sites of RUNX1 in the mouse endothelin-2 gene:

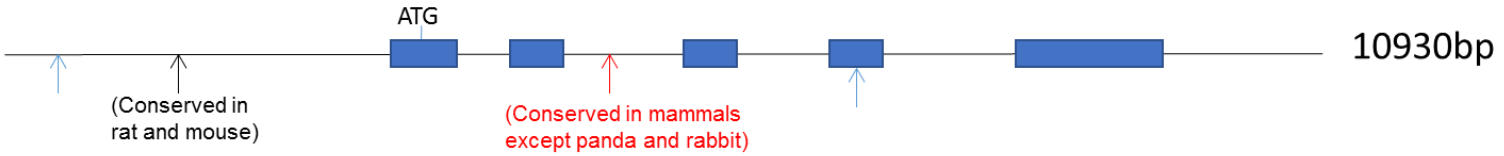

RUNX1: -4014, -2027, +851, 3120
RUNX1 consensus sequences: TGTGGTT (average one site in 16384bp), TGTGGTC (average one site in 16384bp), TGCGGTT (average one site in 16384bp), TGCGGTC (average one site in 16384bp) or their reverse complements

Endothelin-2 Exons: -90/+55, 362/518, 1881/2003, 3111/3209, 5125/5854

B.

Consensus binding sites of BCL6 in the mouse endothelin-2 gene:

BCL6: -3488, -2101, -1255, +1154
BCL6 consensus sequence: TTTNNNGNNAT

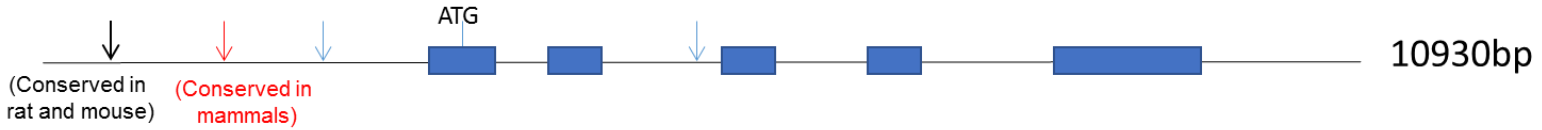

Figure 8.4. Consensus binding sites of RUNX1 and BCL6 in the mouse endothelin-2 gene. The consensus binding sequences of RUNX1 and BCL6 were compared to the mouse endothelin-2 gene sequence and 5000 basepairs upstream and downstream of the first and fifth exon, respectively, using freeware made available by the University of Guelph. Matching binding sequences are indicated with vertical arrows. Blue arrows indicate mouse-specific binding sites, black arrows indicate sites conserved in mice and rats, and red arrows indicate sites conserved amongst mammals including humans (unless otherwise indicated). The five exons are indicated by blue boxes; the DNA runs 5' to 3' from left to right. **A.** Four binding sites were determined for RUNX1. One binding site, 851 base downstream of the ATG start codon and in intron 2, is conserved amongst mammals except for the panda and rabbit. The sequence in this section was either TGCGGTT or TGCGGTC in all animals (red). **B.** Four binding sites were also determined for BCL6. One site that was 2101 base pairs upstream of the start codon was conserved throughout mammals; this sequences was TTTNNNGNNAT.

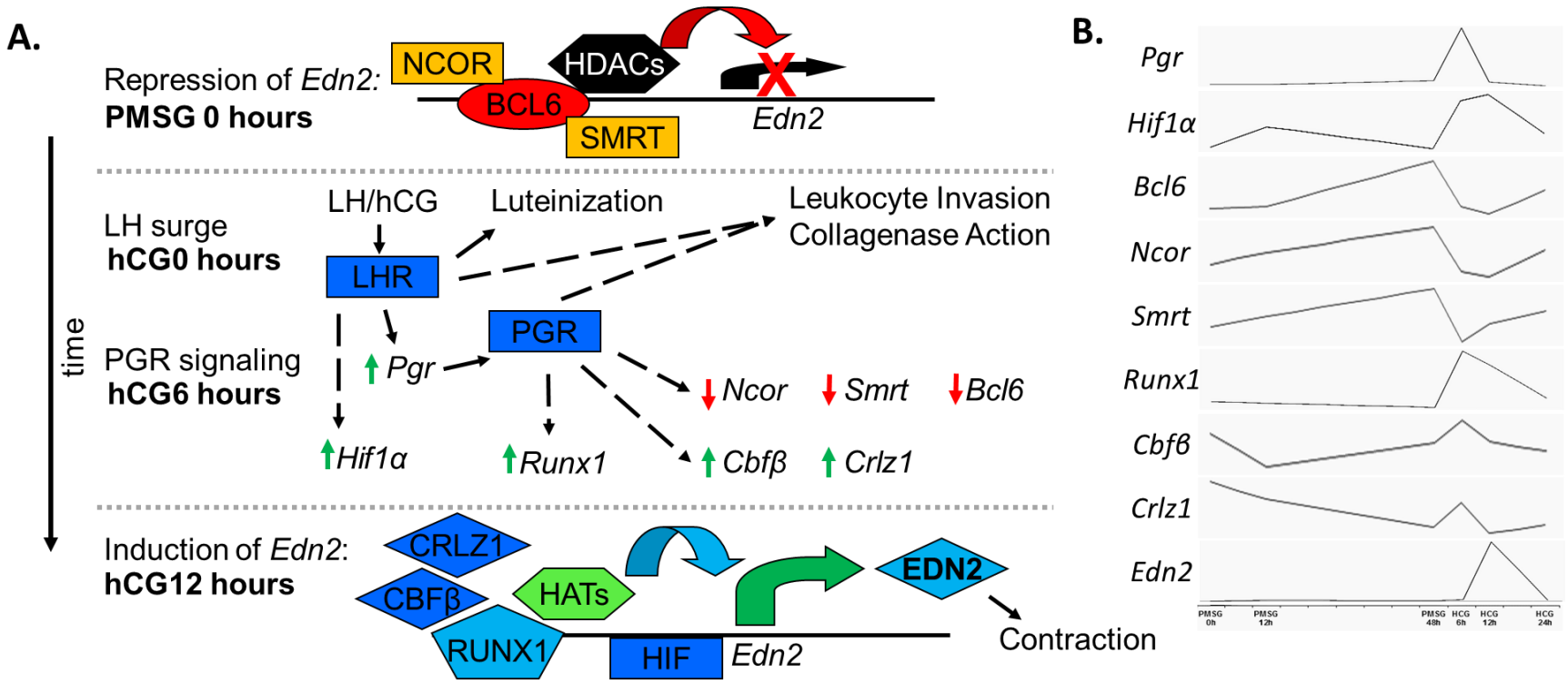

Figure 8.5. Postulated molecular mechanism for ovarian regulation of endothelin-2 during ovulation. A hypothetical mechanism was generated from previous publications examining RUNX1 and BCL6 protein interactions. **A.** Prior to ovulation and during the majority of the cycle in the mouse granulosa cells, the repressor BCL6 is bound about the *Edn2* gene with the corepressors NCOR and SMRT. These corepressors recruit HDACs which deacetylate histones to cause tight DNA binding and prevent transcription. Following the LH surge, via PGR downstream signaling, expression of *Bcl6*, *Ncor*, and *Smrt* all decrease at hCG6 hours. Concurrently, *Runx1*, *Cbfβ*, and *Crlz1* expression levels increase. As *Bcl6* expression is absent at hCG6-hCg12 hours, this then allows the binding of RUNX1 to the *Edn2* gene; this binding is mediated by the heterodimer formed with CBFβ and mediated through CRLZ1 translocation. RUNX1 binding recruits HATs, which acetylate lysine residues to decrease histone-DNA affinity and allow for rapid *Edn2* transcription. This transcription is further enhanced through the presence of the HIF1 complex. After translation, EDN2 causes follicular rupture through a contractile mechanism, and mediates other downstream effects through local endothelin receptors. **B.** Relative expression of relevant genes from the mOGED. Expression is relative to each individual gene in arbitrary units (Y-axes). X-axis describes time during ovulation; each tick mark represents 6 hours. X-axis represents 72 hours in total. Measurements were made at PMSG0, PMSG12, PMSG48 / hCG0, hCG6, hCG12, and hCG24 hours.

CHAPTER 9: CONCLUSIONS AND FUTURE DIRECTIONS

The above work within this dissertation further describes the role for endothelin-2 (EDN2) in ovulation and generates new questions for further research in the molecular mechanisms of ovulation. EDN2, a potent vasoconstrictor, is produced in the granulosa cells of mature follicles just prior to ovulation. Chapter 3 shows that *Edn2* is expressed in multiple tissues throughout the body using a new Edn2-iCre mouse. Areas of expression are particularly interesting, and raise new questions for the role of EDN2 in the cornea and retina of the eye, the villi of the GI tract, and select cells within the kidney. The Edn2-iCre mice may also be used to remove floxed genes within the ovary during ovulation to dissect the roles of individual genes in corpus luteum formation from folliculogenesis.

Through exploration within the ovaries of multiple species, Chapter 4 highlights the discovery that EDN2 induces similar contractile responses in the ovaries of multiple species, even non-mammals, and that this force is associated with the amount of smooth muscle present within the ovary. The location of smooth muscle actin is conserved about the growing follicle in cats and chickens, and is not limited to only the arteries and arterioles within an ovary. Domestic cat and chicken ovaries demonstrate stronger contraction than dog ovaries owing to differential smooth muscle presence. Cat and dog ovaries express the components of the endothelin system, while chickens demonstrate expression of *Ednrb*. Future work may explore the expression and localization of *Edn2* in non-primates and non-rodents throughout the reproductive cycle, such as in fish, lagomorphs, and *Gallus gallus* where ovulation can be easily timed. Conservation of timed ligand expression, or at least potential receptor activation, would be further indicative of a conserved necessary role in ovulation.

Key findings from this dissertation are centered about the role of EDN2 in the ovary, as detailed in Chapter 6. This is the first study to focus on the role of the EDN2 ligand specifically rather than its associated receptors. EDN2 was removed from the ovary using Esr2-iCre mice. The novel Esr2-iCre mice, which are characterized in Chapter 5 with a description of their design and generation, are themselves expected to be useful for numerous future studies in multiple fields. Loss of EDN2 results in reduced fecundity by a deficit in follicle rupture, as previously hypothesized. However, pregnancies of smaller litters are carried to parturition in a normal time span; these mice also retain the ability to produce functional corpora lutea, albeit fewer owing to the lack of follicular rupture. Serum hormone progesterone levels remain normal, and no key genes such as *Mmp2, Mmp9, Timp1, Hifα, Esr1, Esr2, Pgr2,* or *Casp3* are significantly changed

compared to WT mice. Together, this strongly suggests that EDN2 is important, though not required, for follicle rupture and not CL formation, and that the mechanism of action lies through EDNRA signaling in mammals, and potentially through EDNRB in chickens. Stimulation of EDNRA is likely critical for contraction of the theca externa cell layer as a final mechanism for follicular rupture. Future experiments may further confirm this by inducing contraction in the ovary to restore ovulatory function to these conditional knockout mice, though this is complicated by an inverse relationship between follicular pressure and ovulatory ability versus systemic blood pressure and likely necessitates either *ex vivo* or ovary-localized effect. These data may be of clinical relevance for assistance in artificial reproductive technologies.

Using a tamoxifen-inducible alpha-smooth muscle actin Cre system in the next logical area of inquiry, Chapter 7 discusses the removal of EDNRA from contractile cells in mice, either throughout the whole body or the ovary specifically. This did not totally inhibit ovulation. However, tamoxifen acts as an endocrine disrupting chemical (EDC) to antagonize estrogen receptor action and prevent normal ovulation in control mice, making it difficult to tease apart the role of EDNRA from tamoxifen treatment. A final pilot experiment using two different Cre lines that instead ablate genes within granulosa cells suggests that EDNRA may be important there for signaling during ovulation, either in addition to or separately from smooth muscle cells. Mice with granulosa cell loss of *Ednra* demonstrate a phenotype likely to granulosa-cell loss of *Edn2*. Future work may use a different granulosa cell-specific Cre, such as Esr2-iCre, to remove *Ednra*. The resulting phenotype may be compared to results from whole ovary or granulosa cell-specific loss of EDN2. Ovarian cells from those mice may also be used to dissect the ovarian signaling pathway downstream of EDN2 receptor binding. Additionally, when a novel smooth muscle-specific inducible Cre (such as under regulation of tetracycline) becomes available, this may then be used to explore the role of EDNRA in smooth muscle cells during ovulation.

Lastly, the data in Chapter 8 of this dissertation confirm that endothelin-2 is a downstream gene of progesterone receptor (PGR) activity and also demonstrates that acute environmental oxygen deficiency is not sufficient to induce *Edn2* expression in the lungs, kidney, or ovary. New "big-data" tools utilizing global RNA expression profiling at various time points in specific tissues coupled with ChIP-Seq transcription factor analyses allow for generation of the hypothesis that EDN2 action is downstream of RUNX1, which acts through an epigenetic method to modify acetylation. Future work in the endothelin system may utilize ovarian cell cultures from wild type

mice to confirm or reject this proposed mechanistic hypothesis; epigenetic promoter modification via PGR signaling represents a newly developing and exciting topic within reproductive genomics. Such findings may also be extrapolated to endothelin isoform transcriptional regulation in multiple other systems, and may be utilized to develop potential therapies for diseases such as Waardenburg syndrome or Hirschsprung's disease type II which are specific to endothelin ligand or receptor B signaling deficiencies. Overall, the findings from this body of work are useful for understanding the involvement of a complimentary contractile mechanism in ovulation through endothelin-2 and endothelin receptor A signaling. Furthermore, tools and hypotheses developed herein will be of great importance in the field of reproductive biology and steroid hormone signaling within the context of clinical biology research.

REFERENCES

1 Carroll, S. B. *Endless forms most beautiful : the new science of evo devo and the making of the animal kingdom*. 1st edn, (Norton, 2005).
2 Silber, S. J. & Barbey, N. Scientific molecular basis for treatment of reproductive failure in the human: an insight into the future. *Biochimica et biophysica acta* **1822**, 1981-1996, doi:10.1016/j.bbadis.2012.10.004 (2012).
3 Berry, C. W. *et al.* The Euro-Team Early Pregnancy (ETEP) protocol for recurrent miscarriage. *Human reproduction* **10**, 1516-1520 (1995).
4 Carrington, B., Sacks, G. & Regan, L. Recurrent miscarriage: pathophysiology and outcome. *Current opinion in obstetrics & gynecology* **17**, 591-597 (2005).
5 Urman, B. & Yakin, K. Ovulatory disorders and infertility. *The Journal of reproductive medicine* **51**, 267-282 (2006).
6 Ko, C. *et al.* Endothelin-2 in ovarian follicle rupture. *Endocrinology* **147**, 1770-1779, doi:10.1210/en.2005-1228 (2006).
7 Palanisamy, G. S. *et al.* A novel pathway involving progesterone receptor, endothelin-2, and endothelin receptor B controls ovulation in mice. *Molecular endocrinology* **20**, 2784-2795, doi:10.1210/me.2006-0093 (2006).
8 Palanisamy, G. S. *et al.* Endothelin-2, a novel target of progesterone receptor regulation in the mouse ovary, plays a critical role in ovulation. *Biology of Reproduction*, 161-161 (2004).
9 Bradley, B. J. Reconstructing phylogenies and phenotypes: a molecular view of human evolution. *Journal of anatomy* **212**, 337-353, doi:10.1111/j.1469-7580.2007.00840.x (2008).
10 Abbott, A. Mouse genome: The real deal. *Nature* **420**, 456-457, doi:10.1038/420456b (2002).
11 Check, E. Mouse genome: The real deal. *Nature* **420**, 457, doi:10.1038/420457a (2002).
12 Yanagisawa, M. *et al.* Primary structure, synthesis, and biological activity of rat endothelin, an endothelium-derived vasoconstrictor peptide. *Proceedings of the National Academy of Sciences of the United States of America* **85**, 6964-6967 (1988).
13 Bloch, K. D., Eddy, R. L., Shows, T. B. & Quertermous, T. cDNA cloning and chromosomal assignment of the gene encoding endothelin 3. *The Journal of biological chemistry* **264**, 18156-18161 (1989).
14 Choi, D. H. *et al.* Expression pattern of endothelin system components and localization of smooth muscle cells in the human pre-ovulatory follicle. *Human reproduction* **26**, 1171-1180, doi:10.1093/humrep/der066 (2011).
15 A world of 7 billion people. *Lancet* **378**, 1527, doi:10.1016/S0140-6736(11)61658-9 (2011).
16 Philippine Legislators' Committee on, P. & Development, F. Global carrying capacity: how many people? *People Count* **2**, 1-4 (1992).
17 King, M. & Wang, E. Y. The food crisis: is the world exceeding its carrying capacity? *Lancet* **372**, 206, doi:10.1016/S0140-6736(08)61071-5 (2008).
18 Stutz, A. J. Modeling the pre-industrial roots of modern super-exponential population growth. *PloS one* **9**, e105291, doi:10.1371/journal.pone.0105291 (2014).
19 Cohen, J. E. Population growth and earth's human carrying capacity. *Science* **269**, 341-346 (1995).
20 Butler, C. D. Human carrying capacity and human health. *PLoS medicine* **1**, e55, doi:10.1371/journal.pmed.0010055 (2004).

21 Avraam, D., Arnold-Gaille, S., Jones, D. & Vasiev, B. Time-evolution of age-dependent mortality patterns in mathematical model of heterogeneous human population. *Experimental gerontology* **60**, 18-30, doi:10.1016/j.exger.2014.09.006 (2014).
22 McGlade, C. & Ekins, P. The geographical distribution of fossil fuels unused when limiting global warming to 2 degrees C. *Nature* **517**, 187-190, doi:10.1038/nature14016 (2015).
23 Lynas, M. *Six degrees : our future on a hotter planet*. (National Geographic, 2008).
24 Ahlgren, I., Yamada, S. & Wong, A. Rising oceans, climate change, food aid, and human rights in the marshall islands. *Health and human rights* **16**, E69-81 (2014).
25 Kim, K. H., Kabir, E. & Ara Jahan, S. A review of the consequences of global climate change on human health. *Journal of environmental science and health. Part C, Environmental carcinogenesis & ecotoxicology reviews* **32**, 299-318, doi:10.1080/10590501.2014.941279 (2014).
26 Selwood, K. E., McGeoch, M. A. & Mac Nally, R. The effects of climate change and land-use change on demographic rates and population viability. *Biological reviews of the Cambridge Philosophical Society*, doi:10.1111/brv.12136 (2014).
27 McMichael, A. J. Earth as humans' habitat: global climate change and the health of populations. *International journal of health policy and management* **2**, 9-12, doi:10.15171/ijhpm.2014.03 (2014).
28 WorldWildlifeFund. *Half of global wildlife lost, according to new WWF report,* <www.sciencedaily.com/releases/2014/09/140929205312.htm> (2014).
29 Dirzo, R. *et al.* Defaunation in the Anthropocene. *Science* **345**, 401-406, doi:10.1126/science.1251817 (2014).
30 Skakkebaek, N. E. *et al.* Is human fecundity declining? *Int J Androl* **29**, 2-11, doi:DOI 10.1111/j.1365-2605.2005.00573.x (2006).
31 Allen, V. M. *et al.* Pregnancy outcomes after assisted reproductive technology. *Journal of obstetrics and gynaecology Canada : JOGC = Journal d'obstetrique et gynecologie du Canada : JOGC* **28**, 220-250 (2006).
32 Velde, E. T. *et al.* Is human fecundity declining in Western countries? *Human Reproduction* **25**, 1348-1353, doi:DOI 10.1093/humrep/deq085 (2010).
33 Lutz, W., O'Neill, B. C. & Scherbov, S. Demographics: Europe's population at a turning point. *Science* **299**, 1991-1992, doi:DOI 10.1126/science.1080316 (2003).
34 2010 Assisted Reproductive Technology National Summary Report. (US Department of Health and Human Services, Atlanta, GA, 2010).
35 Nybo Andersen, A. M., Wohlfahrt, J., Christens, P., Olsen, J. & Melbye, M. Maternal age and fetal loss: population based register linkage study. *BMJ* **320**, 1708-1712 (2000).
36 Knudsen, U. B., Hansen, V., Juul, S. & Secher, N. J. Prognosis of a new pregnancy following previous spontaneous abortions. *European journal of obstetrics, gynecology, and reproductive biology* **39**, 31-36 (1991).
37 Rai, R. & Regan, L. Recurrent miscarriage. *Lancet* **368**, 601-611, doi:10.1016/S0140-6736(06)69204-0 (2006).
38 Trabert, B. *et al.* Ovulation-inducing drugs and ovarian cancer risk: results from an extended follow-up of a large United States infertility cohort. *Fertility and sterility* **100**, 1660-1666, doi:10.1016/j.fertnstert.2013.08.008 (2013).
39 Rizzuto, I., Behrens, R. F. & Smith, L. A. Risk of ovarian cancer in women treated with ovarian stimulating drugs for infertility. *The Cochrane database of systematic reviews* **8**, CD008215, doi:10.1002/14651858.CD008215.pub2 (2013).

40 Tworoger, S. S., Fairfield, K. M., Colditz, G. A., Rosner, B. A. & Hankinson, S. E. Association of oral contraceptive use, other contraceptive methods, and infertility with ovarian cancer risk. *American journal of epidemiology* **166**, 894-901, doi:10.1093/aje/kwm157 (2007).

41 Prorocic, M. *et al.* Simultaneous dermoid cyst and endometriosis in the same ovary: a case report. *Clinical and experimental obstetrics & gynecology* **40**, 457-459 (2013).

42 Colicchia, M. *et al.* Molecular basis of thyrotropin and thyroid hormone action during implantation and early development. *Human reproduction update* **20**, 884-904, doi:10.1093/humupd/dmu028 (2014).

43 Bluher, S. & Mantzoros, C. S. Leptin in reproduction. *Current opinion in endocrinology, diabetes, and obesity* **14**, 458-464, doi:10.1097/MED.0b013e3282f1cfdc (2007).

44 Alexander, N. B. & Cotanch, P. H. The endocrine basis of infertility in women. *The Nursing clinics of North America* **15**, 511-524 (1980).

45 Artimani, T. *et al.* Estrogen and progesterone receptor subtype expression in granulosa cells from women with polycystic ovary syndrome. *Gynecological endocrinology : the official journal of the International Society of Gynecological Endocrinology*, 1-5, doi:10.3109/09513590.2014.1001733 (2015).

46 Palomba, S., Falbo, A. & La Sala, G. B. Metformin and gonadotropins for ovulation induction in patients with polycystic ovary syndrome: a systematic review with meta-analysis of randomized controlled trials. *Reproductive biology and endocrinology : RB&E* **12**, 3, doi:10.1186/1477-7827-12-3 (2014).

47 Imbar, T. *et al.* Altered endothelin expression in granulosa-lutein cells of women with polycystic ovary syndrome. *Life sciences* **91**, 703-709, doi:10.1016/j.lfs.2012.06.006 (2012).

48 Meirow, D., Laufer, N. & Schenker, J. G. Ovulation induction in polycystic ovary syndrome: a review of conservative and new treatment modalities. *European journal of obstetrics, gynecology, and reproductive biology* **50**, 123-131 (1993).

49 Shi, X., Li, N., Liao, C., Shu, Q. & Zhu, F. Glucocorticoid or androgen for autoimmune premature ovary failure in mice. *Zhong nan da xue xue bao. Yi xue ban = Journal of Central South University. Medical sciences* **34**, 576-581 (2009).

50 Fenichel, P., Gobert, B., Carre, Y., Barbarino-Monnier, P. & Hieronimus, S. Polycystic ovary syndrome in autoimmune disease. *Lancet* **353**, 2210, doi:10.1016/S0140-6736(99)00256-1 (1999).

51 Nandedkar, T. D. & Wadia, P. Autoimmune disorders of the ovary. *Indian journal of experimental biology* **36**, 433-436 (1998).

52 Aoyama, H. & Chapin, R. E. Reproductive toxicities of methoxychlor based on estrogenic properties of the compound and its estrogenic metabolite, hydroxyphenyltrichloroethane. *Vitamins and hormones* **94**, 193-210, doi:10.1016/B978-0-12-800095-3.00007-9 (2014).

53 Patisaul, H. B., Mabrey, N., Adewale, H. B. & Sullivan, A. W. Soy but not bisphenol A (BPA) induces hallmarks of polycystic ovary syndrome (PCOS) and related metabolic co-morbidities in rats. *Reproductive toxicology* **49C**, 209-218, doi:10.1016/j.reprotox.2014.09.003 (2014).

54 Barrett, E. S. & Sobolewski, M. Polycystic ovary syndrome: do endocrine-disrupting chemicals play a role? *Seminars in reproductive medicine* **32**, 166-176, doi:10.1055/s-0034-1371088 (2014).

55 Borgeest, C., Greenfeld, C., Tomic, D. & Flaws, J. A. The effects of endocrine disrupting chemicals on the ovary. *Frontiers in bioscience : a journal and virtual library* **7**, d1941-1948 (2002).
56 Hannon, P. R., Peretz, J. & Flaws, J. A. Daily exposure to Di(2-ethylhexyl) phthalate alters estrous cyclicity and accelerates primordial follicle recruitment potentially via dysregulation of the phosphatidylinositol 3-kinase signaling pathway in adult mice. *Biology of reproduction* **90**, 136, doi:10.1095/biolreprod.114.119032 (2014).
57 Senger, P. L. *Pathways to pregnancy and parturition*. 1st edn, (Current Conceptions, 1997).
58 Oakley, O. R., Frazer, M. L. & Ko, C. Pituitary-ovary-spleen axis in ovulation. *Trends in endocrinology and metabolism: TEM* **22**, 345-352, doi:10.1016/j.tem.2011.04.005 (2011).
59 Senger, P. L. *Pathways to pregnancy & parturition*. 3rd edition. edn.
60 Starup, J. & Visfeldt, J. Ovarian morphology and pituitary gonadotrophins in serum during and after long-term treatment with oral contraceptives. *Acta obstetricia et gynecologica Scandinavica* **53**, 161-167 (1974).
61 Oktay, K., Newton, H., Mullan, J. & Gosden, R. G. Development of human primordial follicles to antral stages in SCID/hpg mice stimulated with follicle stimulating hormone. *Human reproduction* **13**, 1133-1138 (1998).
62 Yoshida, M. *et al.* Morphological characterization of the ovary under normal cycling in rats and its viewpoints of ovarian toxicity detection. *The Journal of toxicological sciences* **34 Suppl 1**, SP189-197 (2009).
63 Trau, H. A., Davis, J. S. & Duffy, D. M. Angiogenesis in the primate ovulatory follicle is stimulated by luteinizing hormone via prostaglandin E2. *Biology of reproduction* **92**, 15, doi:10.1095/biolreprod.114.123711 (2015).
64 Yamashita, H., Murayama, C., Takasugi, R., Miyamoto, A. & Shimizu, T. BMP-4 suppresses progesterone production by inhibiting histone H3 acetylation of StAR in bovine granulosa cells in vitro. *Molecular and cellular biochemistry* **348**, 183-190, doi:10.1007/s11010-010-0653-9 (2011).
65 Qiu, M. *et al.* The influence of ovarian stromal/theca cells during in vitro culture on steroidogenesis, proliferation and apoptosis of granulosa cells derived from the goat ovary. *Reproduction in domestic animals = Zuchthygiene* **49**, 170-176, doi:10.1111/rda.12256 (2014).
66 Espey, L. L. Ovarian contractility and its relationship to ovulation: a review. *Biology of reproduction* **19**, 540-551 (1978).
67 Richards, J. S. & Pangas, S. A. The ovary: basic biology and clinical implications. *The Journal of clinical investigation* **120**, 963-972, doi:10.1172/JCI41350 (2010).
68 Rodgers, R. J., Mitchell, M. D. & Simpson, E. R. Secretion of progesterone and prostaglandins by cells of bovine corpora lutea from three stages of the luteal phase. *The Journal of endocrinology* **118**, 121-126 (1988).
69 Burns, K. H., Yan, C., Kumar, T. R. & Matzuk, M. M. Analysis of ovarian gene expression in follicle-stimulating hormone beta knockout mice. *Endocrinology* **142**, 2742-2751, doi:10.1210/endo.142.7.8279 (2001).
70 Richards, J. S., Russell, D. L., Robker, R. L., Dajee, M. & Alliston, T. N. Molecular mechanisms of ovulation and luteinization. *Molecular and cellular endocrinology* **145**, 47-54 (1998).

71 Chaffin, C. L. & Vandevoort, C. A. Follicle growth, ovulation, and luteal formation in primates and rodents: a comparative perspective. *Experimental biology and medicine* **238**, 539-548, doi:10.1177/1535370213489437 (2013).
72 Merkwitz, C. *et al.* Expression of KIT in the ovary, and the role of somatic precursor cells. *Progress in histochemistry and cytochemistry* **46**, 131-184, doi:10.1016/j.proghi.2011.09.001 (2011).
73 Gilep, A. A., Sushko, T. A. & Usanov, S. A. At the crossroads of steroid hormone biosynthesis: the role, substrate specificity and evolutionary development of CYP17. *Biochimica et biophysica acta* **1814**, 200-209, doi:10.1016/j.bbapap.2010.06.021 (2011).
74 Bakker, J. & Baum, M. J. Neuroendocrine regulation of GnRH release in induced ovulators. *Frontiers in neuroendocrinology* **21**, 220-262, doi:10.1006/frne.2000.0198 (2000).
75 Smith, J. T. The role of kisspeptin and gonadotropin inhibitory hormone in the seasonal regulation of reproduction in sheep. *Domestic animal endocrinology* **43**, 75-84, doi:10.1016/j.domaniend.2011.11.003 (2012).
76 Peng, X. R., Hsueh, A. J., LaPolt, P. S., Bjersing, L. & Ny, T. Localization of luteinizing hormone receptor messenger ribonucleic acid expression in ovarian cell types during follicle development and ovulation. *Endocrinology* **129**, 3200-3207 (1991).
77 Ben-Shlomo, I., Goldman, S. & Shalev, E. Regulation of matrix metalloproteinase-9 (MMP-9), tissue inhibitor of MMP, and progesterone secretion in luteinized granulosa cells from normally ovulating women with polycystic ovary disease. *Fertility and sterility* **79 Suppl 1**, 694-701 (2003).
78 Fraser, H. M. & Wulff, C. Angiogenesis in the primate ovary. *Reproduction, fertility, and development* **13**, 557-566 (2001).
79 Robinson, R. S. *et al.* Angiogenesis and vascular function in the ovary. *Reproduction* **138**, 869-881, doi:10.1530/REP-09-0283 (2009).
80 Conaway, C. H. Ecological adaptation and mammalian reproduction. *Biology of reproduction* **4**, 239-247 (1971).
81 Loewit, K., Kofler, R., Tabarelli, M. & Schwarz, S. Effect of bromocryptine on 20 alpha-hydroxysteroiddehydrogenase regulation in the corpus luteum of the pregnant rat. *Acta endocrinologica* **98**, 133-136 (1981).
82 Garris, D. R. & Curry, T. E., Jr. Ovarian blood flow in the rat: association with body weight, the estrous cycle, and pseudopregnancy. *Proc Soc Exp Biol Med* **174**, 198-204 (1983).
83 Redmer, D. A. *et al.* Characterization and expression of vascular endothelial growth factor (VEGF) in the ovine corpus luteum. *Journal of reproduction and fertility* **108**, 157-165 (1996).
84 Augustin, H. G., Braun, K., Telemenakis, I., Modlich, U. & Kuhn, W. Ovarian angiogenesis. Phenotypic characterization of endothelial cells in a physiological model of blood vessel growth and regression. *The American journal of pathology* **147**, 339-351 (1995).
85 Goligorsky, M. S. *et al.* Nitric oxide modulation of focal adhesions in endothelial cells. *The American journal of physiology* **276**, C1271-1281 (1999).
86 Pauli, S. A. *et al.* The vascular endothelial growth factor (VEGF)/VEGF receptor 2 pathway is critical for blood vessel survival in corpora lutea of pregnancy in the rodent. *Endocrinology* **146**, 1301-1311, doi:10.1210/en.2004-0765 (2005).

87 Miyamoto, A., Shirasuna, K., Shimizu, T., Bollwein, H. & Schams, D. Regulation of corpus luteum development and maintenance: specific roles of angiogenesis and action of prostaglandin F2alpha. *Society of Reproduction and Fertility supplement* **67**, 289-304 (2010).
88 Orre, M. & Rogers, P. A. VEGF, VEGFR-1, VEGFR-2, microvessel density and endothelial cell proliferation in tumours of the ovary. *International journal of cancer. Journal international du cancer* **84**, 101-108 (1999).
89 Wada, Y. *et al.* Role of vascular endothelial growth factor in maintenance of pregnancy in mice. *Endocrinology* **154**, 900-910, doi:10.1210/en.2012-1967 (2013).
90 Duncan, W. C., van den Driesche, S. & Fraser, H. M. Inhibition of vascular endothelial growth factor in the primate ovary up-regulates hypoxia-inducible factor-1alpha in the follicle and corpus luteum. *Endocrinology* **149**, 3313-3320, doi:10.1210/en.2007-1649 (2008).
91 Fantin, A. *et al.* Tissue macrophages act as cellular chaperones for vascular anastomosis downstream of VEGF-mediated endothelial tip cell induction. *Blood* **116**, 829-840, doi:10.1182/blood-2009-12-257832 (2010).
92 Mann, J. S., Kindy, M. S., Edwards, D. R. & Curry, T. E., Jr. Hormonal regulation of matrix metalloproteinase inhibitors in rat granulosa cells and ovaries. *Endocrinology* **128**, 1825-1832 (1991).
93 Curry, T. E., Jr. & Osteen, K. G. The matrix metalloproteinase system: changes, regulation, and impact throughout the ovarian and uterine reproductive cycle. *Endocrine reviews* **24**, 428-465 (2003).
94 Simpson, K. S., Byers, M. J. & Curry, T. E., Jr. Spatiotemporal messenger ribonucleic acid expression of ovarian tissue inhibitors of metalloproteinases throughout the rat estrous cycle. *Endocrinology* **142**, 2058-2069 (2001).
95 Waterhouse, P., Denhardt, D. T. & Khokha, R. Temporal expression of tissue inhibitors of metalloproteinases in mouse reproductive tissues during gestation. *Molecular reproduction and development* **35**, 219-226, doi:10.1002/mrd.1080350302 (1993).
96 Nothnick, W. B., Edwards, D. R., Leco, K. J. & Curry, T. E., Jr. Expression and activity of ovarian tissue inhibitors of metalloproteinases during pseudopregnancy in the rat. *Biology of reproduction* **53**, 684-691 (1995).
97 Goldman, S. & Shalev, E. MMPS and TIMPS in ovarian physiology and pathophysiology. *Frontiers in bioscience : a journal and virtual library* **9**, 2474-2483 (2004).
98 Curry, T. E., Jr., Dean, D. D., Sanders, S. L., Pedigo, N. G. & Jones, P. B. The role of ovarian proteases and their inhibitors in ovulation. *Steroids* **54**, 501-521 (1989).
99 Fedorcsak, P. *et al.* Differential release of matrix metalloproteinases and tissue inhibitors of metalloproteinases by human granulosa-lutein cells and ovarian leukocytes. *Endocrinology* **151**, 1290-1298, doi:10.1210/en.2009-0605 (2010).
100 Matousek, M., Carati, C., Gannon, B. & Brannstrom, M. Novel method for intrafollicular pressure measurements in the rat ovary: increased intrafollicular pressure after hCG stimulation. *Reproduction* **121**, 307-314 (2001).
101 Rondell, P. Follicular Pressure and Distensibility in Ovulation. *The American journal of physiology* **207**, 590-594 (1964).
102 Rondell, P. A. Follicular Fluid Electrolytes in Ovulation. *Proceedings of the Society for Experimental Biology and Medicine. Society for Experimental Biology and Medicine* **116**, 336-339 (1964).

103 Oakley, O. R. *et al.* Periovulatory leukocyte infiltration in the rat ovary. *Endocrinology* **151**, 4551-4559, doi:10.1210/en.2009-1444 (2010).
104 Colgin, D. C. & Murdoch, W. J. Evidence for a role of the ovarian surface epithelium in the ovulatory mechanism of the sheep: secretion of urokinase-type plasminogen activator. *Animal reproduction science* **47**, 197-204 (1997).
105 LeMaire, W. J. Mechanism of mammalian ovulation. *Steroids* **54**, 455-469 (1989).
106 Ny, A. *et al.* Ovulation in plasminogen-deficient mice. *Endocrinology* **140**, 5030-5035, doi:10.1210/endo.140.11.7113 (1999).
107 Ghosh, D., Najwa, A. R., Khan, M. A. & Sengupta, J. IGF2, IGF binding protein 1, and matrix metalloproteinases 2 and 9 in implantation-stage endometrium following immunoneutralization of vascular endothelial growth factor in the rhesus monkey. *Reproduction* **141**, 501-509, doi:10.1530/REP-10-0475 (2011).
108 Robker, R. L. *et al.* Ovulation: a multi-gene, multi-step process. *Steroids* **65**, 559-570 (2000).
109 Peng, J. Y. *et al.* Molecular characterization and hormonal regulation of tissue inhibitor of metalloproteinase 1 in goat ovarian granulosa cells. *Domestic animal endocrinology* **52C**, 1-10, doi:10.1016/j.domaniend.2015.01.001 (2015).
110 Stilley, J. A. & Sharpe-Timms, K. L. TIMP1 contributes to ovarian anomalies in both an MMP-dependent and -independent manner in a rat model. *Biology of reproduction* **86**, 47, doi:10.1095/biolreprod.111.094680 (2012).
111 Cohen-Fredarow, A. *et al.* Ovarian dendritic cells act as a double-edged pro-ovulatory and anti-inflammatory sword. *Molecular endocrinology* **28**, 1039-1054, doi:10.1210/me.2013-1400 (2014).
112 Richards, J. S. Genetics of ovulation. *Seminars in reproductive medicine* **25**, 235-242, doi:10.1055/s-2007-980217 (2007).
113 Bronson, F. H. The reproductive ecology of the house mouse. *The Quarterly review of biology* **54**, 265-299 (1979).
114 Roscoe B. Jackson Memorial Laboratory., Little, C. C., Snell, G. D. & Dingle, J. H. *Biology of the laboratory mouse*. (The Blakiston company, 1941).
115 Roscoe B. Jackson Memorial Laboratory. & Snell, G. D. *Biology of the laboratory mouse*. (Dover Publications, 1956).
116 Gal, A., Lin, P. C., Barger, A. M., MacNeill, A. L. & Ko, C. Vaginal fold histology reduces the variability introduced by vaginal exfoliative cytology in the classification of mouse estrous cycle stages. *Toxicologic pathology* **42**, 1212-1220, doi:10.1177/0192623314526321 (2014).
117 Roscoe B. Jackson Memorial Laboratory. & Green, E. L. *Biology of the laboratory mouse*. 2d edn, (Blakiston Division, 1966).
118 O'Shea, J. D. & Lee, C. S. Shortening of pseudopregnancy and the oestrous cycle following a previous pseudopregnancy in the rat. *Journal of reproduction and fertility* **28**, 281-283 (1972).
119 Roscoe B. Jackson Memorial Laboratory. & Green, E. L. *Biology of the laboratory mouse*. 2d edn, (Dover Publications, 1975).
120 Hantak, A. M., Bagchi, I. C. & Bagchi, M. K. Role of uterine stromal-epithelial crosstalk in embryo implantation. *The International journal of developmental biology* **58**, 139-146, doi:10.1387/ijdb.130348mb (2014).

121 Naik, S. I., Young, L. S., Charlton, H. M. & Clayton, R. N. Pituitary gonadotropin-releasing hormone receptor regulation in mice. II: Females. *Endocrinology* **115**, 114-120, doi:10.1210/endo-115-1-114 (1984).
122 Miller, B. H. *et al.* Circadian clock mutation disrupts estrous cyclicity and maintenance of pregnancy. *Current biology : CB* **14**, 1367-1373, doi:10.1016/j.cub.2004.07.055 (2004).
123 Bachelot, A. *et al.* The permissive role of prolactin as a regulator of luteinizing hormone action in the female mouse ovary and extragonadal tumorigenesis. *American journal of physiology. Endocrinology and metabolism* **305**, E845-852, doi:10.1152/ajpendo.00243.2013 (2013).
124 Grosdemouge, I. *et al.* Effects of deletion of the prolactin receptor on ovarian gene expression. *Reproductive biology and endocrinology : RB&E* **1**, 12 (2003).
125 Bristol, S. K. & Woodruff, T. K. Follicle-restricted compartmentalization of transforming growth factor beta superfamily ligands in the feline ovary. *Biology of reproduction* **70**, 846-859, doi:10.1095/biolreprod.103.021857 (2004).
126 Lohr, C. A., Cox, L. J. & Lepczyk, C. A. Costs and benefits of trap-neuter-release and euthanasia for removal of urban cats in Oahu, Hawaii. *Conservation biology : the journal of the Society for Conservation Biology* **27**, 64-73, doi:10.1111/j.1523-1739.2012.01935.x (2013).
127 Chan, S. Y., Chakraborty, P. K., Bass, E. J. & Wildt, D. E. Ovarian-endocrine-behavioural function in the domestic cat treated with exogenous gonadotrophins during mid-gestation. *Journal of reproduction and fertility* **65**, 395-399 (1982).
128 Fontaine, E. & Fontbonne, A. Clinical use of GnRH agonists in canine and feline species. *Reproduction in domestic animals = Zuchthygiene* **46**, 344-353, doi:10.1111/j.1439-0531.2010.01705.x (2011).
129 Jewgenow, K., Amelkina, O., Painer, J., Goritz, F. & Dehnhard, M. Life cycle of feline Corpora lutea: histological and intraluteal hormone analysis. *Reproduction in domestic animals = Zuchthygiene* **47 Suppl 6**, 25-29, doi:10.1111/rda.12033 (2012).
130 Verstegen, J. P. *et al.* Superovulation and embryo culture in vitro following treatment with ultra-pure follicle-stimulating hormone in cats. *Journal of reproduction and fertility. Supplement* **47**, 209-218 (1993).
131 Tsutsui, T. *et al.* Feline embryo transfer during the non-breeding season. *The Journal of veterinary medical science / the Japanese Society of Veterinary Science* **62**, 1169-1175 (2000).
132 Glover, T. E., Watson, P. F. & Bonney, R. C. Observations on variability in LH release and fertility during oestrus in the domestic cat (Felis catus). *Journal of reproduction and fertility* **75**, 145-152 (1985).
133 Schmidt, P. M., Chakraborty, P. K. & Wildt, D. E. Ovarian activity, circulating hormones and sexual behavior in the cat. II. Relationships during pregnancy, parturition, lactation and the postpartum estrus. *Biology of reproduction* **28**, 657-671 (1983).
134 Tsutsui, T. & Stabenfeldt, G. H. Biology of ovarian cycles, pregnancy and pseudopregnancy in the domestic cat. *Journal of reproduction and fertility. Supplement* **47**, 29-35 (1993).
135 Paape, S. R., Shille, V. M., Seto, H. & Stabenfeldt, G. H. Luteal activity in the pseudopregnant cat. *Biology of reproduction* **13**, 470-474 (1975).

136 Verhage, H. G., Beamer, N. B. & Brenner, R. M. Plasma levels of estradiol and progesterone in the cat during polyestrus, pregnancy and pseudopregnancy. *Biology of reproduction* **14**, 579-585 (1976).
137 Verhage, H. G., Murray, M. K., Boomsma, R. A., Rehfeldt, P. A. & Jaffe, R. C. The postovulatory cat oviduct and uterus: correlation of morphological features with progesterone receptor levels. *The Anatomical record* **208**, 521-531, doi:10.1002/ar.1092080408 (1984).
138 West, N. B., Verhage, H. G. & Brenner, R. M. Suppression of the estradiol receptor system by progesterone in the oviduct and uterus of the cat. *Endocrinology* **99**, 1010-1016, doi:10.1210/endo-99-4-1010 (1976).
139 Chatdarong, K., Axner, E., Manee-In, S., Thuwanut, P. & Linde-Forsberg, C. Pregnancy in the domestic cat after vaginal or transcervical insemination with fresh and frozen semen. *Theriogenology* **68**, 1326-1333, doi:10.1016/j.theriogenology.2007.07.022 (2007).
140 Swanson, W. F. *et al.* Pharmacokinetics and ovarian-stimulatory effects of equine and human chorionic gonadotropins administered singly and in combination in the domestic cat. *Biology of reproduction* **57**, 295-302 (1997).
141 Tsutsui, T. *et al.* Induced ovulation in cats using porcine pituitary gland preparation during the non-breeding season. *Nihon juigaku zasshi. The Japanese journal of veterinary science* **51**, 677-683 (1989).
142 Reynaud, K. *et al.* In vivo canine oocyte maturation, fertilization and early embryogenesis: a review. *Theriogenology* **66**, 1685-1693, doi:10.1016/j.theriogenology.2006.01.049 (2006).
143 Concannon, P. W. Reproductive cycles of the domestic bitch. *Animal reproduction science* **124**, 200-210, doi:10.1016/j.anireprosci.2010.08.028 (2011).
144 Reynaud, K. *et al.* Folliculogenesis, ovulation and endocrine control of oocytes and embryos in the dog. *Reproduction in domestic animals = Zuchthygiene* **47 Suppl 6**, 66-69, doi:10.1111/rda.12055 (2012).
145 Chastant-Maillard, S. *et al.* The canine oocyte: uncommon features of in vivo and in vitro maturation. *Reproduction, fertility, and development* **23**, 391-402, doi:10.1071/RD10064 (2011).
146 Aralla, M., Groppetti, D., Caldarini, L., Cremonesi, F. & Arrighi, S. Morphological evaluation of the placenta and fetal membranes during canine pregnancy from early implantation to term. *Research in veterinary science* **95**, 15-22, doi:10.1016/j.rvsc.2013.02.003 (2013).
147 Burke, T. J. *Small animal reproduction and infertility : a clinical approach to diagnosis and treatment*. (Lea & Febiger, 1986).
148 England, G. C. W., Heimendahl, A. v. & British Small Animal Veterinary Association. *BSAVA manual of canine and feline reproduction and neonatology*. 2nd edn, (British Small Animal Veterinary Association, 2010).
149 Arthur, G. H., Benesch, F. & Wright, J. G. *Veterinary reproduction and obstetrics : formerly Wright's veterinary obstetrics*. 4th edn, (Bailliere Tindall, 1975).
150 Cunningham, F. J., Wilson, S. C., Knight, P. G. & Gladwell, R. T. Chicken ovulation cycle. *The Journal of experimental zoology* **232**, 485-494, doi:10.1002/jez.1402320315 (1984).
151 Bahr, J. M. & Johnson, A. L. Regulation of the follicular hierarchy and ovulation. *The Journal of experimental zoology* **232**, 495-500, doi:10.1002/jez.1402320316 (1984).

152 Dahl, E. Studies of the fine structure of ovarian interstitial tissue. 2. The ultrastructure of the thecal gland of the domestic fowl. *Zeitschrift fur Zellforschung und mikroskopische Anatomie* **109**, 195-211 (1970).
153 Dahl, E. Studies of the fine structure of ovarian interstitial tissue. 3. The innervation of the thecal gland of the domestic fowl. *Zeitschrift fur Zellforschung und mikroskopische Anatomie* **109**, 212-226 (1970).
154 Yao, H. H., Volentine, K. K. & Bahr, J. M. Destruction of the germinal disc region of an immature preovulatory chicken follicle induces atresia and apoptosis. *Biology of reproduction* **59**, 516-521 (1998).
155 Bahr, J. M., Wang, S. C., Huang, M. Y. & Calvo, F. O. Steroid concentrations in isolated theca and granulosa layers of preovulatory follicles during the ovulatory cycle of the domestic hen. *Biology of reproduction* **29**, 326-334 (1983).
156 Johnson, A. L., Johnson, P. A. & van Tienhoven, A. Ovulatory response, and plasma concentrations of luteinizing hormone and progesterone following administration of synthetic mammalian or chicken luteinizing hormone-releasing hormone relative to the first or second ovulation in the sequence of the domestic hen. *Biology of reproduction* **31**, 646-655 (1984).
157 Wang, S. C. & Bahr, J. M. Estradiol secretion by theca cells of the domestic hen during the ovulatory cycle. *Biology of reproduction* **28**, 618-624 (1983).
158 Maia, H., Jr., Barbosa, I. & Coutinho, E. M. Effects of aminophylline, imidazole and indomethacin on spontaneous and prostaglandin induced ovarian contractions in vitro. *International journal of fertility* **20**, 81-86 (1975).
159 Coutinho, E. M. Ovarian contractility and ovulation. *Research in reproduction* **6**, 3-4 (1974).
160 Coutinho, E. M., Maia, H. & Maia, H., Jr. Ovarian contractility. *Basic life sciences* **4**, 127-137 (1974).
161 Burden, H. W. The distribution of smooth muscle in the cat ovary with a note on its adrenergic innervation. *Journal of morphology* **140**, 467-475, doi:10.1002/jmor.1051400407 (1973).
162 Virutamasen, P., Wright, K. H. & Wallach, E. E. Monkey ovarian contractility--its relationship to ovulation. *Fertility and sterility* **24**, 763-771 (1973).
163 Palti, Z. & Freund, M. Spontaneous contractions of the human ovary in vitro. *Journal of reproduction and fertility* **28**, 113-115 (1972).
164 Virutamasen, P., Wright, K. H. & Wallach, E. E. Effects of prostaglandins E 2 and F 2 on ovarian contractility in the rabbit. *Fertility and sterility* **23**, 675-682 (1972).
165 Virutamasen, P., Wright, K. H. & Wallach, E. E. Effects of catecholamines on ovarian contractility in the rabbit. *Obstetrics and gynecology* **39**, 225-236 (1972).
166 Bronson, R. A., Bryant, G., Balk, M. W. & Emanuele, N. Intrafollicular pressure within preovulatory follicles of the pig. *Fertility and sterility* **31**, 205-213 (1979).
167 Virutamasen, P., Smitasiri, Y. & Fuchs, A. R. Intraovarian pressure changes during ovulation in rabbits. *Fertility and sterility* **27**, 188-196 (1976).
168 Blandau, R. J. & Rumery, R. E. Measurements of intrafollicular pressure in ovulatory and preovulatory follicles of the rat. *Fertility and sterility* **14**, 330-341 (1963).
169 Dahm-Kahler, P. *et al.* An intravital microscopy method permitting continuous long-term observations of ovulation in vivo in the rabbit. *Human reproduction* **21**, 624-631, doi:10.1093/humrep/dei394 (2006).

170 Bridges, P. J. *et al.* Production and binding of endothelin-2 (EDN2) in the rat ovary: endothelin receptor subtype A (EDNRA)-mediated contraction. *Reproduction, fertility, and development* **22**, 780-787, doi:10.1071/RD09194 (2010).
171 Cacioppo, J. A. *et al.* Loss of function of endothelin-2 leads to reduced ovulation and CL formation. *PloS one* **9**, e96115, doi:10.1371/journal.pone.0096115 (2014).
172 Shimshek, D. R. *et al.* Codon-improved Cre recombinase (iCre) expression in the mouse. *Genesis* **32**, 19-26 (2002).
173 de Vries, W. N. *et al.* Expression of Cre recombinase in mouse oocytes: a means to study maternal effect genes. *Genesis* **26**, 110-112 (2000).
174 Bouabe, H. & Okkenhaug, K. Gene targeting in mice: a review. *Methods in molecular biology* **1064**, 315-336, doi:10.1007/978-1-62703-601-6_23 (2013).
175 Soriano, P. Generalized lacZ expression with the ROSA26 Cre reporter strain. *Nature genetics* **21**, 70-71, doi:10.1038/5007 (1999).
176 Burn, S. F. Detection of beta-galactosidase activity: X-gal staining. *Methods in molecular biology* **886**, 241-250, doi:10.1007/978-1-61779-851-1_21 (2012).
177 Madisen, L. *et al.* A robust and high-throughput Cre reporting and characterization system for the whole mouse brain. *Nature neuroscience* **13**, 133-140, doi:10.1038/nn.2467 (2010).
178 Su, J., Cao, X. & Wang, K. A novel degradation signal derived from distal C-terminal frameshift mutations of KCNQ2 protein which cause neonatal epilepsy. *The Journal of biological chemistry* **286**, 42949-42958, doi:10.1074/jbc.M111.287268 (2011).
179 Dubach, J. M., Das, S., Rosenzweig, A. & Clark, H. A. Visualizing sodium dynamics in isolated cardiomyocytes using fluorescent nanosensors. *Proceedings of the National Academy of Sciences of the United States of America* **106**, 16145-16150, doi:10.1073/pnas.0905909106 (2009).
180 Maldve, R. E., Chen, X., Zhang, T. A. & Morrisett, R. A. Ethanol selectively inhibits enhanced vesicular release at excitatory synapses: real-time visualization in intact hippocampal slices. *Alcoholism, clinical and experimental research* **28**, 143-152, doi:10.1097/01.ALC.0000106304.39174.AD (2004).
181 Raymond, C. R., Aucouturier, P. & Mabbott, N. A. In vivo depletion of CD11c+ cells impairs scrapie agent neuroinvasion from the intestine. *Journal of immunology* **179**, 7758-7766 (2007).
182 Tian, T., Woodworth, J., Skold, M. & Behar, S. M. In vivo depletion of CD11c+ cells delays the CD4+ T cell response to Mycobacterium tuberculosis and exacerbates the outcome of infection. *Journal of immunology* **175**, 3268-3272 (2005).
183 Dumas, L. *et al.* Multicolor analysis of oligodendrocyte morphology, interactions, and development with Brainbow. *Glia* **63**, 699-717, doi:10.1002/glia.22779 (2015).
184 Cai, D., Cohen, K. B., Luo, T., Lichtman, J. W. & Sanes, J. R. Improved tools for the Brainbow toolbox. *Nature methods* **10**, 540-547 (2013).
185 Livet, J. *et al.* Transgenic strategies for combinatorial expression of fluorescent proteins in the nervous system. *Nature* **450**, 56-62, doi:10.1038/nature06293 (2007).
186 Ringrose, L., Chabanis, S., Angrand, P. O., Woodroofe, C. & Stewart, A. F. Quantitative comparison of DNA looping in vitro and in vivo: chromatin increases effective DNA flexibility at short distances. *The EMBO journal* **18**, 6630-6641, doi:10.1093/emboj/18.23.6630 (1999).

187 Vooijs, M., Jonkers, J. & Berns, A. A highly efficient ligand-regulated Cre recombinase mouse line shows that LoxP recombination is position dependent. *EMBO reports* **2**, 292-297, doi:10.1093/embo-reports/kve064 (2001).
188 Bertolin, K., Gossen, J., Schoonjans, K. & Murphy, B. D. The orphan nuclear receptor Nr5a2 is essential for luteinization in the female mouse ovary. *Endocrinology* **155**, 1931-1943, doi:10.1210/en.2013-1765 (2014).
189 Hammerschmidt, E., Loeffler, I. & Wolf, G. Morg1 heterozygous mice are protected from acute renal ischemia-reperfusion injury. *American journal of physiology. Renal physiology* **297**, F1273-1287, doi:10.1152/ajprenal.00204.2009 (2009).
190 Fenske, T. S. *et al.* Stem cell expression of the AML1/ETO fusion protein induces a myeloproliferative disorder in mice. *Proceedings of the National Academy of Sciences of the United States of America* **101**, 15184-15189, doi:10.1073/pnas.0400751101 (2004).
191 Utomo, A. R., Nikitin, A. Y. & Lee, W. H. Temporal, spatial, and cell type-specific control of Cre-mediated DNA recombination in transgenic mice. *Nature biotechnology* **17**, 1091-1096, doi:10.1038/15073 (1999).
192 Chen, M. R. *et al.* RU486-inducible recombination in the salivary glands of lactoferrin promoter-driven green fluorescent Cre transgenic mice. *Genesis* **48**, 585-595, doi:10.1002/dvg.20666 (2010).
193 Wendling, O., Bornert, J. M., Chambon, P. & Metzger, D. Efficient temporally-controlled targeted mutagenesis in smooth muscle cells of the adult mouse. *Genesis* **47**, 14-18, doi:10.1002/dvg.20448 (2009).
194 Farley, F. W., Soriano, P., Steffen, L. S. & Dymecki, S. M. Widespread recombinase expression using FLPeR (flipper) mice. *Genesis* **28**, 106-110 (2000).
195 Jiang, W., Bikard, D., Cox, D., Zhang, F. & Marraffini, L. A. RNA-guided editing of bacterial genomes using CRISPR-Cas systems. *Nature biotechnology* **31**, 233-239, doi:10.1038/nbt.2508 (2013).
196 Sander, J. D. & Joung, J. K. CRISPR-Cas systems for editing, regulating and targeting genomes. *Nature biotechnology* **32**, 347-355, doi:10.1038/nbt.2842 (2014).
197 Hsu, P. D., Lander, E. S. & Zhang, F. Development and applications of CRISPR-Cas9 for genome engineering. *Cell* **157**, 1262-1278, doi:10.1016/j.cell.2014.05.010 (2014).
198 Hsueh, A. J. & Rauch, R. Ovarian Kaleidoscope database: ten years and beyond. *Biology of reproduction* **86**, 192, doi:10.1095/biolreprod.112.099127 (2012).
199 Jo, M. *et al.* Development and application of a rat ovarian gene expression database. *Endocrinology* **145**, 5384-5396, doi:10.1210/en.2004-0407 (2004).
200 Ko, C., Meidan, R. & Bridges, P. J. Why two endothelins and two receptors for ovulation and luteal regulation? *Life sciences* **91**, 501-506, doi:10.1016/j.lfs.2012.05.010 (2012).
201 Kim, J., Bagchi, I. C. & Bagchi, M. K. Control of ovulation in mice by progesterone receptor-regulated gene networks. *Molecular human reproduction* **15**, 821-828, doi:10.1093/molehr/gap082 (2009).
202 Gardiner, S. M., Compton, A. M. & Bennett, T. Regional hemodynamic effects of endothelin-2 and sarafotoxin-S6b in conscious rats. *The American journal of physiology* **258**, R912-917 (1990).
203 Minkes, R. K. & Kadowitz, P. J. Comparative responses to endothelin 2 and sarafotoxin 6b in systemic vascular bed of cats. *The American journal of physiology* **258**, H1550-1558 (1990).

204 Emoto, N. *et al.* 25 years of endothelin research: the next generation. *Life sciences* **118**, 77-86, doi:10.1016/j.lfs.2014.07.035 (2014).
205 Suzuki, N. *et al.* Sandwich-enzyme immunoassays for endothelin family peptides. *Journal of cardiovascular pharmacology* **17 Suppl 7**, S420-422 (1991).
206 Okishima, N., Hagiwara, Y., Seito, T., Yano, M. & Kido, H. Specific sandwich-type enzyme immunoassays for smooth muscle constricting novel 31-amino acid endothelins. *Biochemical and biophysical research communications* **256**, 1-5, doi:10.1006/bbrc.1999.0277 (1999).
207 Wakisaka, N. *et al.* New EIA technique for tyrosinase in human melanocytes and its application. *Life sciences* **66**, Pl1-Pl6 (2000).
208 Horinouchi, T., Terada, K., Higashi, T. & Miwa, S. Endothelin receptor signaling: new insight into its regulatory mechanisms. *Journal of pharmacological sciences* **123**, 85-101 (2013).
209 Bur, D., Dale, G. E. & Oefner, C. A three-dimensional model of endothelin-converting enzyme (ECE) based on the X-ray structure of neutral endopeptidase 24.11 (NEP). *Protein engineering* **14**, 337-341 (2001).
210 Gupta, A., Fujita, W., Gomes, I., Bobeck, E. & Devi, L. A. Endothelin-converting enzyme 2 differentially regulates opioid receptor activity. *British journal of pharmacology* **172**, 704-719, doi:10.1111/bph.12833 (2015).
211 Emoto, N. & Yanagisawa, M. Endothelin-converting enzyme-2 is a membrane-bound, phosphoramidon-sensitive metalloprotease with acidic pH optimum. *The Journal of biological chemistry* **270**, 15262-15268 (1995).
212 Itoh, Y., Kimura, C., Onda, H. & Fujino, M. Canine endothelin-2: cDNA sequence for the mature peptide. *Nucleic acids research* **17**, 5389 (1989).
213 Devesly, P., Phillips, P. E., Johns, A., Rubanyi, G. & Parker-Botelho, L. H. Receptor kinetics differ for endothelin-1 and endothelin-2 binding to Swiss 3T3 fibroblasts. *Biochemical and biophysical research communications* **172**, 126-134 (1990).
214 Davenport, A. P., Cameron, I. T., Smith, S. K. & Brown, M. J. Binding sites for iodinated endothelin-1, endothelin-2 and endothelin-3 demonstrated on human uterine glandular epithelial cells by quantitative high-resolution autoradiography. *The Journal of endocrinology* **129**, 149-154 (1991).
215 Davenport, A. P. International Union of Pharmacology. XXIX. Update on endothelin receptor nomenclature. *Pharmacological reviews* **54**, 219-226 (2002).
216 Davenport, A. P. & Barton, M. Themed section: endothelin. *British journal of pharmacology* **168**, 279-282, doi:10.1111/bph.12022 (2013).
217 Ling, L., Maguire, J. J. & Davenport, A. P. Endothelin-2, the forgotten isoform: emerging role in the cardiovascular system, ovarian development, immunology and cancer. *British journal of pharmacology* **168**, 283-295, doi:10.1111/j.1476-5381.2011.01786.x (2013).
218 Braasch, I., Volff, J. N. & Schartl, M. The endothelin system: evolution of vertebrate-specific ligand-receptor interactions by three rounds of genome duplication. *Molecular biology and evolution* **26**, 783-799, doi:10.1093/molbev/msp015 (2009).
219 Kohidai, L., Toth, K., Ruskoaho, H. & Csaba, G. Effect of vasoactive peptides on Tetrahymena. chemotactic properties of endothelins (ET-1, ET-2, ET-3, fragment 11-21 of ET-1 and big endothelin-1): a short-term inducible signalling mechanism of chemotaxis. *Cell biology international* **25**, 1173-1177, doi:10.1006/cbir.2001.0783 (2001).

220 Zhang, J., Leontovich, A. & Sarras, M. P., Jr. Molecular and functional evidence for early divergence of an endothelin-like system during metazoan evolution: analysis of the Cnidarian, hydra. *Development* **128**, 1607-1615 (2001).
221 Braasch, I. & Schartl, M. Evolution of endothelin receptors in vertebrates. *General and comparative endocrinology*, doi:10.1016/j.ygcen.2014.06.028 (2014).
222 Kurihara, Y. *et al.* Aortic arch malformations and ventricular septal defect in mice deficient in endothelin-1. *The Journal of clinical investigation* **96**, 293-300, doi:10.1172/JCI118033 (1995).
223 Chang, I. *et al.* Endothelin-2 deficiency causes growth retardation, hypothermia, and emphysema in mice. *The Journal of clinical investigation* **123**, 2643-2653, doi:10.1172/JCI66735 (2013).
224 Baynash, A. G. *et al.* Interaction of endothelin-3 with endothelin-B receptor is essential for development of epidermal melanocytes and enteric neurons. *Cell* **79**, 1277-1285 (1994).
225 Hosoda, K. *et al.* Targeted and natural (piebald-lethal) mutations of endothelin-B receptor gene produce megacolon associated with spotted coat color in mice. *Cell* **79**, 1267-1276 (1994).
226 Henkel, C. V. *et al.* First draft genome sequence of the Japanese eel, Anguilla japonica. *Gene* **511**, 195-201, doi:10.1016/j.gene.2012.09.064 (2012).
227 Clouthier, D. E. *et al.* Cranial and cardiac neural crest defects in endothelin-A receptor-deficient mice. *Development* **125**, 813-824 (1998).
228 Iwai, M. *et al.* Localization of endothelin receptor messenger ribonucleic acid in the rat ovary and fallopian tube by in situ hybridization. *Biology of reproduction* **49**, 675-680 (1993).
229 Otani, H., Yamoto, M., Fujinaga, H. & Nakano, R. Presence and localization of endothelin receptor in the rat ovary and its regulation by pituitary gonadotropins. *European journal of endocrinology / European Federation of Endocrine Societies* **135**, 449-454 (1996).
230 Tedeschi, C. *et al.* Rat ovarian granulosa cell as a site of endothelin reception and action: attenuation of gonadotropin-stimulated steroidogenesis via perturbation of the A-kinase signaling pathway. *Biology of reproduction* **51**, 1058-1065 (1994).
231 Mamluk, R., Levy, N., Rueda, B., Davis, J. S. & Meidan, R. Characterization and regulation of type A endothelin receptor gene expression in bovine luteal cell types. *Endocrinology* **140**, 2110-2116, doi:10.1210/endo.140.5.6690 (1999).
232 Mancina, R. *et al.* Identification, characterization, and biological activity of endothelin receptors in human ovary. *The Journal of clinical endocrinology and metabolism* **82**, 4122-4129 (1997).
233 Cho, J., Kim, H., Kang, D. W., Yanagisawa, M. & Ko, C. Endothelin B receptor is not required but necessary for finite regulation of ovulation. *Life sciences* **91**, 613-617, doi:10.1016/j.lfs.2012.02.016 (2012).
234 Mamluk, R., Wolfenson, D. & Meidan, R. LH receptor mRNA and cytochrome P450 side-chain cleavage expression in bovine theca and granulosa cells luteinized by LH or forskolin. *Domestic animal endocrinology* **15**, 103-114 (1998).
235 LaVoie, H. A. *et al.* Coordinate developmental expression of genes regulating sterol economy and cholesterol side-chain cleavage in the porcine ovary. *Biology of reproduction* **57**, 402-407 (1997).
236 Sasano, H. & Suzuki, T. Localization of steroidogenesis and steroid receptors in human corpus luteum. Classification of human corpus luteum (CL) into estrogen-producing

degenerating CL, and nonsteroid-producing degenerating CL. *Seminars in reproductive endocrinology* **15**, 345-351, doi:10.1055/s-2008-1068372 (1997).
237 Ravindranath, N., Little-Ihrig, L., Benyo, D. F. & Zeleznik, A. J. Role of luteinizing hormone in the expression of cholesterol side-chain cleavage cytochrome P450 and 3 beta-hydroxysteroid dehydrogenase, delta 5-4 isomerase messenger ribonucleic acids in the primate corpus luteum. *Endocrinology* **131**, 2065-2070 (1992).
238 Clozel, M. *et al.* Effects of nonpeptide endothelin receptor antagonists in rats with reduced renal mass. *Journal of cardiovascular pharmacology* **33**, 611-618 (1999).
239 Clozel, M. *et al.* Pharmacology of tezosentan, new endothelin receptor antagonist designed for parenteral use. *The Journal of pharmacology and experimental therapeutics* **290**, 840-846 (1999).
240 Rossetti, E. & De Servi, S. Tezosentan. Actelion/Genentech. *Curr Opin Investig Drugs* **4**, 323-328 (2003).
241 Bruce, N. W. & Moor, R. M. Capillary blood flow to ovarian follicles, stroma and corpora lutea of anaesthetized sheep. *Journal of reproduction and fertility* **46**, 299-304 (1976).
242 Wiltbank, M. C., Dysko, R. C., Gallagher, K. P. & Keyes, P. L. Relationship between blood flow and steroidogenesis in the rabbit corpus luteum. *Journal of reproduction and fertility* **84**, 513-520 (1988).
243 Fernandez-Valdivia, R. *et al.* A mouse model to dissect progesterone signaling in the female reproductive tract and mammary gland. *Genesis* **48**, 106-113, doi:10.1002/dvg.20586 (2010).
244 Robker, R. L. *et al.* Progesterone-regulated genes in the ovulation process: ADAMTS-1 and cathepsin L proteases. *Proceedings of the National Academy of Sciences of the United States of America* **97**, 4689-4694, doi:10.1073/pnas.080073497 (2000).
245 Meidan, R., Klipper, E., Zalman, Y. & Yalu, R. The role of hypoxia-induced genes in ovarian angiogenesis. *Reproduction, fertility, and development* **25**, 343-350, doi:10.1071/RD12139 (2013).
246 Klipper, E. *et al.* Induction of endothelin-2 expression by luteinizing hormone and hypoxia: possible role in bovine corpus luteum formation. *Endocrinology* **151**, 1914-1922, doi:en.2009-0767 [pii]10.1210/en.2009-0767 (2010).
247 Na, G., Bridges, P. J., Koo, Y. & Ko, C. Role of hypoxia in the regulation of periovulatory EDN2 expression in the mouse. *Canadian journal of physiology and pharmacology* **86**, 310-319, doi:10.1139/Y08-025 (2008).
248 Dschietzig, T., Richter, C., Asswad, L., Baumann, G. & Stangl, K. Hypoxic induction of receptor activity-modifying protein 2 alters regulation of pulmonary endothelin-1 by adrenomedullin: induction under normoxia versus inhibition under hypoxia. *The Journal of pharmacology and experimental therapeutics* **321**, 409-419, doi:10.1124/jpet.106.114298 (2007).
249 Grimshaw, M. J. Endothelins and hypoxia-inducible factor in cancer. *Endocr Relat Cancer* **14**, 233-244, doi:10.1677/ERC-07-0057 (2007).
250 Grimshaw, M. J., Naylor, S. & Balkwill, F. R. Endothelin-2 is a hypoxia-induced autocrine survival factor for breast tumor cells. *Molecular cancer therapeutics* **1**, 1273-1281 (2002).
251 Kim, J., Bagchi, I. C. & Bagchi, M. K. Signaling by hypoxia-inducible factors is critical for ovulation in mice. *Endocrinology* **150**, 3392-3400, doi:10.1210/en.2008-0948 (2009).
252 Kotake-Nara, E. & Saida, K. Characterization of CoCl2-induced reactive oxygen species (ROS): Inductions of neurite outgrowth and endothelin-2/vasoactive intestinal contractor

in PC12 cells by CoCl2 are ROS dependent, but those by MnCl2 are not. *Neuroscience letters* **422**, 223-227, doi:10.1016/j.neulet.2007.06.026 (2007).

253 Kotake-Nara, E., Takizawa, S., Quan, J., Wang, H. & Saida, K. Cobalt chloride induces neurite outgrowth in rat pheochromocytoma PC-12 cells through regulation of endothelin-2/vasoactive intestinal contractor. *Journal of neuroscience research* **81**, 563-571, doi:10.1002/jnr.20568 (2005).

254 Yalu, R., Oyesiji, A. E., Eisenberg, I., Imbar, T. & Meidan, R. HIF1A-dependent increase in endothelin 2 levels in granulosa cells: role of hypoxia, LH/cAMP, and reactive oxygen species. *Reproduction* **149**, 11-20, doi:10.1530/REP-14-0409 (2014).

255 Sakata, K., Shigemasa, K., Nagai, N. & Ohama, K. Expression of matrix metalloproteinases (MMP-2, MMP-9, MT1-MMP) and their inhibitors (TIMP-1, TIMP-2) in common epithelial tumors of the ovary. *International journal of oncology* **17**, 673-681 (2000).

256 Reich, R. *et al.* Preovulatory changes in ovarian expression of collagenases and tissue metalloproteinase inhibitor messenger ribonucleic acid: role of eicosanoids. *Endocrinology* **129**, 1869-1875, doi:10.1210/endo-129-4-1869 (1991).

257 Curry Jr., T., Komar C, Burns, PD, Nothnick WB. . Periovulatory changes in ovarian metalloproteinases and tissue inhibitors of metalloproteinases (TIMPs) following indomethacin treatment. *In: Adashi EY, ed.* **Ovulation: evolving scientific and clinical concepts. New York:** (2000).

258 Nothnick, W. B., Keeble, S. C. & Curry, T. E., Jr. Collagenase, gelatinase, and proteoglycanase messenger ribonucleic acid expression and activity during luteal development, maintenance, and regression in the pseudopregnant rat ovary. *Biology of reproduction* **54**, 616-624 (1996).

259 Liu, K., Olofsson, J. I., Wahlberg, P. & Ny, T. Distinct expression of gelatinase A [matrix metalloproteinase (MMP)-2], collagenase-3 (MMP-13), membrane type MMP 1 (MMP-14), and tissue inhibitor of MMPs type 1 mediated by physiological signals during formation and regression of the rat corpus luteum. *Endocrinology* **140**, 5330-5338 (1999).

260 Lind, A. K., Dahm-Kahler, P., Weijdegard, B., Sundfeldt & Brannstrom, M. Gelatinases and their tissue inhibitors during human ovulation: increased expression of tissue inhibitor of matrix metalloproteinase-1. *Molecular human reproduction* **12**, 725-736, doi:10.1093/molehr/gal086 (2006).

261 Garncarczyk, A., Jurzak, M. & Gojniczek, K. [Characteristic of the endogenous peptides--endothelins and their role in the connective tissue fibrosis]. *Wiadomosci lekarskie* **61**, 126-134 (2008).

262 Stilley, J. A. *et al.* Neutralizing TIMP1 restores fecundity in a rat model of endometriosis and treating control rats with TIMP1 causes anomalies in ovarian function and embryo development. *Biology of reproduction* **83**, 185-194, doi:10.1095/biolreprod.109.083287 (2010).

263 Rattner, A., Yu, H., Williams, J., Smallwood, P. M. & Nathans, J. Endothelin-2 signaling in the neural retina promotes the endothelial tip cell state and inhibits angiogenesis. *Proceedings of the National Academy of Sciences of the United States of America* **110**, E3830-3839, doi:10.1073/pnas.1315509110 (2013).

264 Doerr, M. D., Goravanahally, M. P., Rhinehart, J. D., Inskeep, E. K. & Flores, J. A. Effects of endothelin receptor type-A and type-B antagonists on prostaglandin F2alpha-induced

luteolysis of the sheep corpus luteum. *Biology of reproduction* **78**, 688-696, doi:10.1095/biolreprod.107.064105 (2008).

265 Keator, C. S., Schreiber, D. T., Hoagland, T. A., McCracken, J. A. & Milvae, R. A. Intrauterine infusion of BQ-610, an endothelin type A receptor antagonist, delays luteolysis in dairy heifers. *Domestic animal endocrinology* **34**, 411-418, doi:10.1016/j.domaniend.2007.11.002 (2008).

266 Skarzynski, D. J. *et al.* Growth and regression in bovine corpora lutea: regulation by local survival and death pathways. *Reproduction in domestic animals = Zuchthygiene* **48 Suppl 1**, 25-37, doi:10.1111/rda.12203 (2013).

267 Balen, A. Ovarian hyperstimulation syndrome. *Hum Fertil (Camb)* **16**, 143, doi:10.3109/14647273.2013.826044 (2013).

268 Leo, C. P., Vitt, U. A. & Hsueh, A. J. The Ovarian Kaleidoscope database: an online resource for the ovarian research community. *Endocrinology* **141**, 3052-3054, doi:10.1210/endo.141.9.7679 (2000).

269 Takizawa, S. *et al.* Differential expression of endothelin-2 along the mouse intestinal tract. *Journal of molecular endocrinology* **35**, 201-209, doi:10.1677/jme.1.01787 (2005).

270 Grimshaw, M. J., Wilson, J. L. & Balkwill, F. R. Endothelin-2 is a macrophage chemoattractant: implications for macrophage distribution in tumors. *European journal of immunology* **32**, 2393-2400, doi:10.1002/1521-4141(200209)32:9<2393::AID-IMMU2393>3.0.CO;2-4 (2002).

271 Brown, M. J., Sharma, P. & Stevens, P. A. Association between diastolic blood pressure and variants of the endothelin-1 and endothelin-2 genes. *Journal of cardiovascular pharmacology* **35**, S41-43 (2000).

272 Uchide, T. *et al.* Expression of endothelin-1 and vasoactive intestinal contractor genes in mouse organs during the perinatal period. *Clinical science* **103 Suppl 48**, 167S-170S, doi:10.1042/CS103S167S (2002).

273 Uchide, T., Masuda, H., Mitsui, Y. & Saida, K. Gene expression of vasoactive intestinal contractor/endothelin-2 in ovary, uterus and embryo: comprehensive gene expression profiles of the endothelin ligand-receptor system revealed by semi-quantitative reverse transcription-polymerase chain reaction analysis in adult mouse tissues and during late embryonic development. *Journal of molecular endocrinology* **22**, 161-171 (1999).

274 Jahrling, P. B. *et al.* The NIAID Integrated Research Facility at Frederick, Maryland: a unique international resource to facilitate medical countermeasure development for BSL-4 pathogens. *Pathog Dis* **71**, 211-216, doi:Doi 10.1111/2049-632x.12171 (2014).

275 Parkitna, J. R., Engblom, D. & Schutz, G. Generation of Cre recombinase-expressing transgenic mice using bacterial artificial chromosomes. *Methods in molecular biology* **530**, 325-342, doi:10.1007/978-1-59745-471-1_17 (2009).

276 Thomason, L. C., Sawitzke, J. A., Li, X., Costantino, N. & Court, D. L. Recombineering: genetic engineering in bacteria using homologous recombination. *Current protocols in molecular biology / edited by Frederick M. Ausubel ... [et al.]* **106**, 1 16 11-11 16 39, doi:10.1002/0471142727.mb0116s106 (2014).

277 Gebhard, S. *et al.* BAC constructs in transgenic reporter mouse lines control efficient and specific LacZ expression in hypertrophic chondrocytes under the complete Col10a1 promoter. *Histochemistry and cell biology* **127**, 183-194, doi:10.1007/s00418-006-0236-8 (2007).

278 Bridges, P. J. *et al.* Generation of Cyp17iCre transgenic mice and their application to conditionally delete estrogen receptor alpha (Esr1) from the ovary and testis. *Genesis* **46**, 499-505, doi:10.1002/dvg.20428 (2008).
279 Makinoda, S., Hirosaki, N., Waseda, T., Tomizawa, H. & Fujii, R. Granulocyte colony-stimulating factor (G-CSF) in the mechanism of human ovulation and its clinical usefulness. *Curr Med Chem* **15**, 604-613 (2008).
280 Szabo, A. *et al.* Statistical modeling for selecting housekeeper genes. *Genome biology* **5**, R59, doi:10.1186/gb-2004-5-8-r59 (2004).
281 Al-Bader, M. D. & Al-Sarraf, H. A. Housekeeping gene expression during fetal brain development in the rat-validation by semi-quantitative RT-PCR. *Brain research. Developmental brain research* **156**, 38-45, doi:10.1016/j.devbrainres.2005.01.010 (2005).
282 Findlater, G. S., McDougall, R. D. & Kaufman, M. H. Eyelid development, fusion and subsequent reopening in the mouse. *Journal of anatomy* **183 (Pt 1)**, 121-129 (1993).
283 Saida, K., Hashimoto, M., Mitsui, Y., Ishida, N. & Uchide, T. The prepro vasoactive intestinal contractor (VIC)/endothelin-2 gene (EDN2): structure, evolution, production, and embryonic expression. *Genomics* **64**, 51-61, doi:10.1006/geno.1999.6083 (2000).
284 Uchide, T., Adur, J., Fukamachi, T. & Saida, K. Quantitative analysis of endothelin-1 and vasoactive intestinal contractor/endothelin-2 gene expression in rats by real-time reverse transcriptase polymerase chain reaction. *Journal of cardiovascular pharmacology* **36**, S5-8 (2000).
285 Kakinuma, Y. *et al.* Myocardial expression of endothelin-2 is altered reciprocally to that of endothelin-1 during ischemia of cardiomyocytes in vitro and during heart failure in vivo. *Life sciences* **65**, 1671-1683 (1999).
286 Plumpton, C., Champeney, R., Ashby, M. J., Kuc, R. E. & Davenport, A. P. Characterization of endothelin isoforms in human heart: endothelin-2 demonstrated. *Journal of cardiovascular pharmacology* **22 Suppl 8**, S26-28 (1993).
287 Bot, B. M. *et al.* Expression of endothelin 2 and localized clear cell renal cell carcinoma. *Human pathology* **43**, 843-849, doi:10.1016/j.humpath.2011.07.011 (2012).
288 Miyauchi, Y. *et al.* Increased plasma levels of big-endothelin-2 and big-endothelin-3 in patients with end-stage renal disease. *Life sciences* **91**, 729-732, doi:10.1016/j.lfs.2012.08.008 (2012).
289 Chang, C. Y. *et al.* NFIB is a governor of epithelial-melanocyte stem cell behaviour in a shared niche. *Nature* **495**, 98-102, doi:10.1038/nature11847 (2013).
290 Kunieda, T. *et al.* A mutation in endothelin-B receptor gene causes myenteric aganglionosis and coat color spotting in rats. *DNA research : an international journal for rapid publication of reports on genes and genomes* **3**, 101-105 (1996).
291 Odgren, P. R. *et al.* False-positive beta-galactosidase staining in osteoclasts by endogenous enzyme: studies in neonatal and month-old wild-type mice. *Connective tissue research* **47**, 229-234, doi:10.1080/03008200600860086 (2006).
292 Davenport, A. P., Hoskins, S. L., Kuc, R. E. & Plumpton, C. Differential distribution of endothelin peptides and receptors in human adrenal gland. *The Histochemical journal* **28**, 779-789 (1996).
293 Howard, P. G., Plumpton, C. & Davenport, A. P. Anatomical localization and pharmacological activity of mature endothelins and their precursors in human vascular tissue. *Journal of hypertension* **10**, 1379-1386 (1992).

294 O'Reilly, G., Charnock-Jones, D. S., Cameron, I. T., Smith, S. K. & Davenport, A. P. Endothelin-2 mRNA splice variants detected by RT-PCR in cultured human vascular smooth muscle and endothelial cells. *Journal of cardiovascular pharmacology* **22 Suppl 8**, S18-21 (1993).
295 Bacon, C. R. & Davenport, A. P. Endothelin receptors in human coronary artery and aorta. *British journal of pharmacology* **117**, 986-992 (1996).
296 Briggs, P. J., Moran, C. G. & Wood, M. B. Actions of endothelin-1, 2, and 3 in the microvasculature of bone. *Journal of orthopaedic research : official publication of the Orthopaedic Research Society* **16**, 340-347, doi:10.1002/jor.1100160310 (1998).
297 Saida, K., Kometani, N., Uchide, T. & Mitsui, Y. Sequence analysis and expression of the mouse full-length vasoactive intestinal contractor/endothelin-2 gene (EDN2): comparison with the endothelin-1 gene (EDN1). *Clinical science* **103 Suppl 48**, 84S-89S, doi:10.1042/CS103S084S (2002).
298 Masuo, Y. *et al.* Vasoactive intestinal contractor/endothelin-2 gene expression in the murine central nervous system. *Biochemical and biophysical research communications* **300**, 661-668 (2003).
299 McCartney, S. A. *et al.* Endothelin content, expression, and receptor type in normal and diseased human gallbladder. *Digestive diseases and sciences* **47**, 1786-1792 (2002).
300 Wang, R. *et al.* Epigenetic inactivation of endothelin-2 and endothelin-3 in colon cancer. *International journal of cancer. Journal international du cancer* **132**, 1004-1012, doi:10.1002/ijc.27762 (2013).
301 Bianchi, M., Adur, J., Takizawa, S., Saida, K. & Casco, V. H. Endothelin system in intestinal villi: A possible role of endothelin-2/vasoactive intestinal contractor in the maintenance of intestinal architecture. *Biochemical and biophysical research communications* **417**, 1113-1118, doi:10.1016/j.bbrc.2011.12.053 (2012).
302 Braunger, B. M. *et al.* Constitutive overexpression of Norrin activates Wnt/beta-catenin and endothelin-2 signaling to protect photoreceptors from light damage. *Neurobiology of disease* **50**, 1-12, doi:10.1016/j.nbd.2012.09.008 (2013).
303 Bramall, A. N. *et al.* Endothelin-2-mediated protection of mutant photoreceptors in inherited photoreceptor degeneration. *PloS one* **8**, e58023, doi:10.1371/journal.pone.0058023 (2013).
304 O'Reilly, G. *et al.* Alternatively spliced mRNAs for human endothelin-2 and their tissue distribution. *Biochemical and biophysical research communications* **193**, 834-840 (1993).
305 Plumpton, C., Ashby, M. J., Kuc, R. E., O'Reilly, G. & Davenport, A. P. Expression of endothelin peptides and mRNA in the human heart. *Clinical science* **90**, 37-46 (1996).
306 Fu, T. *et al.* Effects of vasoactive intestinal contractor (VIC) and endothelin on intracellular calcium level in neuroblastoma NG108-15 cells. *FEBS letters* **257**, 351-353 (1989).
307 Bloch, K. D., Hong, C. C., Eddy, R. L., Shows, T. B. & Quertermous, T. cDNA cloning and chromosomal assignment of the endothelin 2 gene: vasoactive intestinal contractor peptide is rat endothelin 2. *Genomics* **10**, 236-242 (1991).
308 Karet, F. E. & Davenport, A. P. Localization of endothelin peptides in human kidney. *Kidney international* **49**, 382-387 (1996).
309 Hocher, B. *et al.* Characterization of the renal phenotype of transgenic rats expressing the human endothelin-2 gene. *Hypertension* **28**, 196-201 (1996).

310 Ohkubo, S. *et al.* Specific expression of human endothelin-2 (ET-2) gene in a renal adenocarcinoma cell line. Molecular cloning of cDNA encoding the precursor of ET-2 and its characterization. *FEBS letters* **274**, 136-140 (1990).
311 Battistini, B. *et al.* Characterization of endothelin (ET) receptors in the isolated gall bladder of the guinea-pig: evidence for an additional ET receptor subtype. *British journal of pharmacology* **112**, 1244-1250 (1994).
312 Marciniak, S. J., Plumpton, C., Barker, P. J., Huskisson, N. S. & Davenport, A. P. Localization of immunoreactive endothelin and proendothelin in the human lung. *Pulmonary pharmacology* **5**, 175-182 (1992).
313 Yuen, T. J. *et al.* Identification of endothelin 2 as an inflammatory factor that promotes central nervous system remyelination. *Brain : a journal of neurology* **136**, 1035-1047, doi:10.1093/brain/awt024 (2013).
314 Al-Alem, L. *et al.* Endothelin-2 induces oviductal contraction via endothelin receptor subtype A in rats. *The Journal of endocrinology* **193**, 383-391, doi:10.1677/JOE-07-0089 (2007).
315 Jankovic, S. M., Jankovic, S. V., Lukic, G., Canovic, D. & Folic, M. The contractile effects of endothelins on isolated isthmic segment of human oviduct at the luteal phase of the menstrual cycle. *Methods and findings in experimental and clinical pharmacology* **32**, 91-95, doi:10.1358/mf.2010.32.2.1428740 (2010).
316 Lam, H. C. *et al.* Salivary immunoreactive endothelin in patients with upper gastrointestinal diseases. *Journal of cardiovascular pharmacology* **44 Suppl 1**, S413-417 (2004).
317 Lam, H. C. *et al.* Immunoreactive endothelin in human plasma, urine, milk, and saliva. *Journal of cardiovascular pharmacology* **17 Suppl 7**, S390-393 (1991).
318 Tanese, K., Fukuma, M., Ishiko, A. & Sakamoto, M. Endothelin-2 is upregulated in basal cell carcinoma under control of Hedgehog signaling pathway. *Biochemical and biophysical research communications* **391**, 486-491, doi:10.1016/j.bbrc.2009.11.085 (2010).
319 Ergun, S., Harneit, S., Paust, H. J., Mukhopadhyay, A. K. & Holstein, A. F. Endothelin and endothelin receptors A and B in the human testis. *Anatomy and embryology* **199**, 207-214 (1999).
320 Uchide, T. *et al.* Fluctuating gene expression and localized cellular distribution of vasoactive intestinal contractor (VIC) in mouse uterus. *The journal of histochemistry and cytochemistry : official journal of the Histochemistry Society* **48**, 699-707 (2000).
321 Cameron, I. T. *et al.* Identification of endothelin-1, endothelin-2 and endothelin-3 in human endometrium. *Journal of reproduction and fertility* **98**, 251-255 (1993).
322 Uchide, T. *et al.* cDNA and deduced amino acid sequences of ferret preproendothelin-2 and phylogenetic analysis. *DNA sequence : the journal of DNA sequencing and mapping* **13**, 369-374 (2002).
323 O'Shea, J. D. An ultrastructural study of smooth muscle-like cells in the theca externa of ovarian follicles in the rat. *The Anatomical record* **167**, 127-131, doi:10.1002/ar.1091670202 (1970).
324 Iglarz, M. *et al.* Pharmacology of macitentan, an orally active tissue-targeting dual endothelin receptor antagonist. *The Journal of pharmacology and experimental therapeutics* **327**, 736-745, doi:10.1124/jpet.108.142976 (2008).
325 Shinohara, T. *et al.* Macitentan reverses early obstructive pulmonary vasculopathy in rats: Early intervention in overcoming the survivin-mediated resistance to apoptosis. *American*

journal of physiology. Lung cellular and molecular physiology, ajplung 00129 02014, doi:10.1152/ajplung.00129.2014 (2014).

326 Wooldridge, A. A., Dillon, A. R., Tillson, D. M., Zhong, Q. & Barney, S. R. Isometric responses of isolated intrapulmonary bronchioles from cats with and without adult heartworm infection. *American journal of veterinary research* **73**, 439-446, doi:10.2460/ajvr.73.3.439 (2012).

327 Yuan, T. Y. *et al.* Vasodilatory Effect of a Novel Rho-Kinase Inhibitor, DL0805-2, on the rat Mesenteric Artery and its Potential Mechanisms. *Cardiovascular drugs and therapy / sponsored by the International Society of Cardiovascular Pharmacotherapy*, doi:10.1007/s10557-014-6544-7 (2014).

328 Davis, M. J., Lane, M. M., Scallan, J. P., Gashev, A. A. & Zawieja, D. C. An automated method to control preload by compensation for stress relaxation in spontaneously contracting, isometric rat mesenteric lymphatics. *Microcirculation* **14**, 603-612, doi:10.1080/10739680701436152 (2007).

329 Kang, S. *et al.* Nitric oxide synthase inhibitors that interact with both heme propionate and tetrahydrobiopterin show high isoform selectivity. *Journal of medicinal chemistry* **57**, 4382-4396, doi:10.1021/jm5004182 (2014).

330 Senger, P. L. *Pathways to pregnancy and parturition*. 2nd rev. edn, (Current Conceptions, 2005).

331 Concannon, P. W., McCann, J. P. & Temple, M. Biology and endocrinology of ovulation, pregnancy and parturition in the dog. *Journal of reproduction and fertility. Supplement* **39**, 3-25 (1989).

332 Yoshimura, Y., Tanaka, K. & Koga, O. Studies on the contractility of follicular wall with special reference to the mechanism of ovulation in hens. *British poultry science* **24**, 213-218, doi:10.1080/00071668308416732 (1983).

333 Stefenson, A., Owman, C., Sjoberg, N. O., Sporrong, B. & Walles, B. Comparative study of the autonomic innervation of the mammalian ovary, with particular regard to the follicular system. *Cell and tissue research* **215**, 47-62 (1981).

334 Gilbert, A. B., Evans, A. J., Perry, M. M. & Davidson, M. H. A method for separating the granulosa cells, the basal lamina and the theca of the preovulatory ovarian follicle of the domestic fowl (Gallus domesticus). *Journal of reproduction and fertility* **50**, 179-181 (1977).

335 Kheradmand, A., Roshangar, L., Taati, M. & Sirotkin, A. V. Morphometrical and intracellular changes in rat ovaries following chronic administration of ghrelin. *Tissue & cell* **41**, 311-317, doi:10.1016/j.tice.2009.01.002 (2009).

336 Sudik, R., Chari, S., Pascher, E. & Sturm, G. Human follicular fluid levels of endothelins in relation to oocyte maturity status. *Experimental and clinical endocrinology & diabetes : official journal, German Society of Endocrinology [and] German Diabetes Association* **104**, 78-84, doi:10.1055/s-0029-1211426 (1996).

337 Thun, R., Watson, P. & Jackson, G. L. Induction of estrus and ovulation in the bitch, using exogenous gonadotropins. *American journal of veterinary research* **38**, 483-486 (1977).

338 Santana, M. L., Rego de Paula, T.A., Paulino da Costa, E., and Costa, D.S. Exogenous induction of ovarian activity and ovulation and transfer of fresh embryos of domestic cat (Felis catus). *Revista Ceres* **59**, 499-505 (2012).

339 Roth, T. L., Wolfe, B. A., Long, J. A., Howard, J. G. & Wildt, D. E. Effects of equine chorionic gonadotropin, human chorionic gonadotropin, and laparoscopic artificial

insemination on embryo, endocrine, and luteal characteristics in the domestic cat. *Biology of reproduction* **57**, 165-171 (1997).

340 Howard, J. G., Barone, M. A., Donoghue, A. M. & Wildt, D. E. The effect of pre-ovulatory anaesthesia on ovulation in laparoscopically inseminated domestic cats. *Journal of reproduction and fertility* **96**, 175-186 (1992).

341 Stewart, R. A. *et al.* Oral progestin priming increases ovarian sensitivity to gonadotropin stimulation and improves luteal function in the cat. *Biology of reproduction* **87**, 137, doi:10.1095/biolreprod.112.104190 (2012).

342 Sojka, N. J., Jennings, L. L. & Hamner, C. E. Artificial insemination in the cat (Felis catus L.). *Laboratory animal care* **20**, 198-204 (1970).

343 Rocereto, T., Jacobowitz, D. & Wallach, E. E. Observations of spontaneous contractions of the cat ovary in vitro. *Endocrinology* **84**, 1336-1341, doi:10.1210/endo-84-6-1336 (1969).

344 Richards, J. S. Ovulation: new factors that prepare the oocyte for fertilization. *Molecular and cellular endocrinology* **234**, 75-79, doi:10.1016/j.mce.2005.01.004 (2005).

345 Talbot, P. Intrafollicular pressure promotes partial evacuation of the antrum during hamster ovulation in vitro. *The Journal of experimental zoology* **226**, 129-135, doi:10.1002/jez.1402260115 (1983).

346 Troedsson, M. H., Liu, I. K. & Crabo, B. G. Sperm transport and survival in the mare: a review. *Theriogenology* **50**, 807-818 (1998).

347 Langendijk, P., Soede, N. M. & Kemp, B. Uterine activity, sperm transport, and the role of boar stimuli around insemination in sows. *Theriogenology* **63**, 500-513, doi:10.1016/j.theriogenology.2004.09.027 (2005).

348 England, G. C., Moxon, R. & Freeman, S. L. Stimulation of mating-induced uterine contractions in the bitch and their modification and enhancement of fertility by prostatic fluid. *Reproduction in domestic animals = Zuchthygiene* **47 Suppl 6**, 1-5, doi:10.1111/rda.12019 (2012).

349 Willenburg, K. L., Miller, G. M., Rodriguez-Zas, S. L. & Knox, R. V. Influence of hormone supplementation to extended semen on artificial insemination, uterine contractions, establishment of a sperm reservoir, and fertility in swine. *Journal of animal science* **81**, 821-829 (2003).

350 Khimji, A. K. & Rockey, D. C. Endothelin--biology and disease. *Cellular signalling* **22**, 1615-1625, doi:10.1016/j.cellsig.2010.05.002 (2010).

351 Hernandez-Vertiz, A., Gonzalez del Pliego, M., Velazquez, P. & Pedernera, E. Morphological changes in the thecal layer during the maturation of the preovulatory ovarian follicle of the domestic fowl (Gallus domesticus). *General and comparative endocrinology* **92**, 80-87 (1993).

352 Loss, S. R., Will, T. & Marra, P. P. The impact of free-ranging domestic cats on wildlife of the United States. *Nature communications* **4**, 1396, doi:10.1038/ncomms2380 (2013).

353 Bristol-Gould, S. & Woodruff, T. K. Folliculogenesis in the domestic cat (Felis catus). *Theriogenology* **66**, 5-13, doi:10.1016/j.theriogenology.2006.03.019 (2006).

354 Munks, M. W. Progress in development of immunocontraceptive vaccines for permanent non-surgical sterilization of cats and dogs. *Reproduction in domestic animals = Zuchthygiene* **47 Suppl 4**, 223-227, doi:10.1111/j.1439-0531.2012.02079.x (2012).

355 Jordan, B. J., Vogel, S., Stark, M. R. & Beckstead, R. B. Expression of green fluorescent protein in the chicken using in vivo transfection of the piggyBac transposon. *Journal of biotechnology* **173**, 86-89, doi:10.1016/j.jbiotec.2014.01.016 (2014).
356 Tremblay, G. B. *et al.* Cloning, chromosomal localization, and functional analysis of the murine estrogen receptor beta. *Molecular endocrinology* **11**, 353-365, doi:10.1210/mend.11.3.9902 (1997).
357 Levin, E. R. Plasma membrane estrogen receptors. *Trends in endocrinology and metabolism: TEM* **20**, 477-482, doi:10.1016/j.tem.2009.06.009 (2009).
358 Pedram, A., Razandi, M. & Levin, E. R. Nature of functional estrogen receptors at the plasma membrane. *Molecular endocrinology* **20**, 1996-2009, doi:10.1210/me.2005-0525 (2006).
359 Kuiper, G. G. *et al.* Comparison of the ligand binding specificity and transcript tissue distribution of estrogen receptors alpha and beta. *Endocrinology* **138**, 863-870, doi:10.1210/endo.138.3.4979 (1997).
360 Kuiper, G. G. & Gustafsson, J. A. The novel estrogen receptor-beta subtype: potential role in the cell- and promoter-specific actions of estrogens and anti-estrogens. *FEBS letters* **410**, 87-90 (1997).
361 Karolczak, M. & Beyer, C. Developmental sex differences in estrogen receptor-beta mRNA expression in the mouse hypothalamus/preoptic region. *Neuroendocrinology* **68**, 229-234 (1998).
362 Drummond, A. E. & Fuller, P. J. Ovarian actions of estrogen receptor-beta: an update. *Seminars in reproductive medicine* **30**, 32-38, doi:10.1055/s-0031-1299595 (2012).
363 Yu, K. D. *et al.* A systematic review of the relationship between polymorphic sites in the estrogen receptor-beta (ESR2) gene and breast cancer risk. *Breast cancer research and treatment* **126**, 37-45, doi:10.1007/s10549-010-0891-2 (2011).
364 Dupont, S. *et al.* Effect of single and compound knockouts of estrogen receptors alpha (ERalpha) and beta (ERbeta) on mouse reproductive phenotypes. *Development* **127**, 4277-4291 (2000).
365 Krege, J. H. *et al.* Generation and reproductive phenotypes of mice lacking estrogen receptor beta. *Proceedings of the National Academy of Sciences of the United States of America* **95**, 15677-15682 (1998).
366 Binder, A. K. *et al.* The absence of ER-beta results in altered gene expression in ovarian granulosa cells isolated from in vivo preovulatory follicles. *Endocrinology* **154**, 2174-2187, doi:10.1210/en.2012-2256 (2013).
367 Fan, H. Y. *et al.* Selective expression of KrasG12D in granulosa cells of the mouse ovary causes defects in follicle development and ovulation. *Development* **135**, 2127-2137, doi:10.1242/dev.020560 (2008).
368 Cacioppo, J., Koo, Y., Lin, P. C., Gal, A. & Ko, C. Generation and characterization of an Endothelin-2 iCre mouse. *Genesis*, doi:10.1002/dvg.22845 (2015).
369 Rodriguez, C. I. *et al.* High-efficiency deleter mice show that FLPe is an alternative to Cre-loxP. *Nature genetics* **25**, 139-140, doi:10.1038/75973 (2000).
370 Antal, M. C., Krust, A., Chambon, P. & Mark, M. Sterility and absence of histopathological defects in nonreproductive organs of a mouse ERbeta-null mutant. *Proceedings of the National Academy of Sciences of the United States of America* **105**, 2433-2438, doi:10.1073/pnas.0712029105 (2008).

371 Antal, M. C., Petit-Demouliere, B., Meziane, H., Chambon, P. & Krust, A. Estrogen dependent activation function of ERbeta is essential for the sexual behavior of mouse females. *Proceedings of the National Academy of Sciences of the United States of America* **109**, 19822-19827, doi:10.1073/pnas.1217668109 (2012).
372 Fan, H. Y., Liu, Z., Cahill, N. & Richards, J. S. Targeted disruption of Pten in ovarian granulosa cells enhances ovulation and extends the life span of luteal cells. *Molecular endocrinology* **22**, 2128-2140, doi:10.1210/me.2008-0095 (2008).
373 Drummond, A. E. & Fuller, P. J. The importance of ERbeta signalling in the ovary. *The Journal of endocrinology* **205**, 15-23, doi:10.1677/JOE-09-0379 (2010).
374 Byers, M., Kuiper, G. G., Gustafsson, J. A. & Park-Sarge, O. K. Estrogen receptor-beta mRNA expression in rat ovary: down-regulation by gonadotropins. *Molecular endocrinology* **11**, 172-182, doi:10.1210/mend.11.2.9887 (1997).
375 Shughrue, P. J., Lane, M. V., Scrimo, P. J. & Merchenthaler, I. Comparative distribution of estrogen receptor-alpha (ER-alpha) and beta (ER-beta) mRNA in the rat pituitary, gonad, and reproductive tract. *Steroids* **63**, 498-504 (1998).
376 Jakimiuk, A. J., Weitsman, S. R., Yen, H. W., Bogusiewicz, M. & Magoffin, D. A. Estrogen receptor alpha and beta expression in theca and granulosa cells from women with polycystic ovary syndrome. *The Journal of clinical endocrinology and metabolism* **87**, 5532-5538, doi:10.1210/jc.2002-020323 (2002).
377 Sar, M. & Welsch, F. Differential expression of estrogen receptor-beta and estrogen receptor-alpha in the rat ovary. *Endocrinology* **140**, 963-971, doi:10.1210/endo.140.2.6533 (1999).
378 Cardenas, H. & Pope, W. F. Amounts of an estrogen receptor beta isoform increased in the theca of preovulatory follicles of sheep. *Animal reproduction science* **131**, 143-152, doi:10.1016/j.anireprosci.2012.03.002 (2012).
379 Ulbrich, S. E., Kettler, A. & Einspanier, R. Expression and localization of estrogen receptor alpha, estrogen receptor beta and progesterone receptor in the bovine oviduct in vivo and in vitro. *The Journal of steroid biochemistry and molecular biology* **84**, 279-289 (2003).
380 Weihua, Z. *et al.* Estrogen receptor (ER) beta, a modulator of ERalpha in the uterus. *Proceedings of the National Academy of Sciences of the United States of America* **97**, 5936-5941 (2000).
381 Hiroi, H. *et al.* Differential immunolocalization of estrogen receptor alpha and beta in rat ovary and uterus. *Journal of molecular endocrinology* **22**, 37-44 (1999).
382 Minorics, R., Ducza, E., Marki, A., Paldy, E. & Falkay, G. Investigation of estrogen receptor alpha and beta mRNA expression in the pregnant rat uterus. *Molecular reproduction and development* **68**, 463-468, doi:10.1002/mrd.20106 (2004).
383 van Pelt, A. M. *et al.* Ontogeny of estrogen receptor-beta expression in rat testis. *Endocrinology* **140**, 478-483, doi:10.1210/endo.140.1.6438 (1999).
384 Shapiro, E. *et al.* Immunolocalization of androgen receptor and estrogen receptors alpha and beta in human fetal testis and epididymis. *The Journal of urology* **174**, 1695-1698; discussion 1698 (2005).
385 Hess, R. A. *et al.* Estrogen receptor (alpha and beta) expression in the excurrent ducts of the adult male rat reproductive tract. *Journal of andrology* **18**, 602-611 (1997).
386 Choi, I. *et al.* Human estrogen receptor beta-specific monoclonal antibodies: characterization and use in studies of estrogen receptor beta protein expression in reproductive tissues. *Molecular and cellular endocrinology* **181**, 139-150 (2001).

387 Adjei, S., Houck, A. L., Ma, K. & Wesson, D. W. Age-dependent alterations in the number, volume, and localization of islands of Calleja within the olfactory tubercle. *Neurobiology of aging* **34**, 2676-2682, doi:10.1016/j.neurobiolaging.2013.05.014 (2013).
388 Yamaguchi, N. & Yuri, K. Estrogen-dependent changes in estrogen receptor-beta mRNA expression in middle-aged female rat brain. *Brain research* **1543**, 49-57, doi:10.1016/j.brainres.2013.11.010 (2014).
389 Nishihara, E. *et al.* Ontogenetic changes in the expression of estrogen receptor alpha and beta in rat pituitary gland detected by immunohistochemistry. *Endocrinology* **141**, 615-620, doi:10.1210/endo.141.2.7330 (2000).
390 Castiglione, F. *et al.* Expression of estrogen receptor beta in colon cancer progression. *Diagnostic molecular pathology : the American journal of surgical pathology, part B* **17**, 231-236, doi:10.1097/PDM.0b013e3181656d67 (2008).
391 Lamote, I., Demeyere, K., Notebaert, S., Burvenich, C. & Meyer, E. Flow cytometric assessment of estrogen receptor beta expression in bovine blood neutrophils. *Journal of immunological methods* **323**, 88-92, doi:10.1016/j.jim.2007.03.001 (2007).
392 Kalbe, C., Mau, M., Wollenhaupt, K. & Rehfeldt, C. Evidence for estrogen receptor alpha and beta expression in skeletal muscle of pigs. *Histochemistry and cell biology* **127**, 95-107, doi:10.1007/s00418-006-0224-z (2007).
393 Elicevik, M., Horasanli, S., Okaygun, E., Badur, S. & Celayir, S. Estrogen receptor beta type in the rat urinary bladder. *Archives of andrology* **52**, 407-410, doi:10.1080/01485010600666821 (2006).
394 Pelzer, T. *et al.* Increased mortality and aggravation of heart failure in estrogen receptor-beta knockout mice after myocardial infarction. *Circulation* **111**, 1492-1498, doi:10.1161/01.CIR.0000159262.18512.46 (2005).
395 Wu, C. T., Chang, Y. L., Shih, J. Y. & Lee, Y. C. The significance of estrogen receptor beta in 301 surgically treated non-small cell lung cancers. *The Journal of thoracic and cardiovascular surgery* **130**, 979-986, doi:10.1016/j.jtcvs.2005.06.012 (2005).
396 Vanderhorst, V. G., Gustafsson, J. A. & Ulfhake, B. Estrogen receptor-alpha and -beta immunoreactive neurons in the brainstem and spinal cord of male and female mice: relationships to monoaminergic, cholinergic, and spinal projection systems. *The Journal of comparative neurology* **488**, 152-179, doi:10.1002/cne.20569 (2005).
397 Valimaa, H. *et al.* Estrogen receptor-beta is the predominant estrogen receptor subtype in human oral epithelium and salivary glands. *The Journal of endocrinology* **180**, 55-62 (2004).
398 Gao, H. & Dahlman-Wright, K. Implications of estrogen receptor alpha and estrogen receptor beta for adipose tissue functions and cardiometabolic complications. *Hormone molecular biology and clinical investigation* **15**, 81-90, doi:10.1515/hmbci-2013-0021 (2013).
399 Pedersen, S. B. *et al.* Demonstration of estrogen receptor subtypes alpha and beta in human adipose tissue: influences of adipose cell differentiation and fat depot localization. *Molecular and cellular endocrinology* **182**, 27-37 (2001).
400 Tomicek, N. J., Lancaster, T. S. & Korzick, D. H. Increased estrogen receptor beta in adipose tissue is associated with increased intracellular and reduced circulating adiponectin protein levels in aged female rats. *Gender medicine* **8**, 325-333, doi:10.1016/j.genm.2011.05.010 (2011).

401 Georgiadou, D., Sergentanis, T. N. & Papastratis, G. Estrogen receptor alpha to beta ratio: a counterpart also in adrenal cortical neoplasia? *Medical hypotheses* **70**, 1225, doi:10.1016/j.mehy.2007.12.006 (2008).
402 Khasar, S. G., Dina, O. A., Green, P. G. & Levine, J. D. Estrogen regulates adrenal medullary function producing sexual dimorphism in nociceptive threshold and beta-adrenergic receptor-mediated hyperalgesia in the rat. *The European journal of neuroscience* **21**, 3379-3386, doi:10.1111/j.1460-9568.2005.04158.x (2005).
403 Li, Q. Y. *et al.* Involvement of estrogen receptor-beta in farrerol inhibition of rat thoracic aorta vascular smooth muscle cell proliferation. *Acta pharmacologica Sinica* **32**, 433-440, doi:10.1038/aps.2011.1 (2011).
404 Darblade, B. *et al.* Estradiol alters nitric oxide production in the mouse aorta through the alpha-, but not beta-, estrogen receptor. *Circulation research* **90**, 413-419 (2002).
405 Imamov, O. *et al.* Estrogen receptor beta-deficient female mice develop a bladder phenotype resembling human interstitial cystitis. *Proceedings of the National Academy of Sciences of the United States of America* **104**, 9806-9809, doi:10.1073/pnas.0703410104 (2007).
406 Stygar, D., Masironi, B., Eriksson, H. & Sahlin, L. Studies on estrogen receptor (ER) alpha and beta responses on gene regulation in peripheral blood leukocytes in vivo using selective ER agonists. *The Journal of endocrinology* **194**, 101-119, doi:10.1677/JOE-06-0060 (2007).
407 Moverare, S., Skrtic, S., Lindberg, M. K., Dahlman-Wright, K. & Ohlsson, C. Estrogen increases coagulation factor V mRNA levels via both estrogen receptor-alpha and -beta in murine bone marrow/bone. *European journal of endocrinology / European Federation of Endocrine Societies* **151**, 259-263 (2004).
408 Okazaki, R. *et al.* Estrogen promotes early osteoblast differentiation and inhibits adipocyte differentiation in mouse bone marrow stromal cell lines that express estrogen receptor (ER) alpha or beta. *Endocrinology* **143**, 2349-2356, doi:10.1210/endo.143.6.8854 (2002).
409 Yu, B. *et al.* Estrogen receptor alpha and beta expressions in hypothalamus-pituitary-ovary axis in rats exposed lactationally to soy isoflavones and bisphenol A. *Biomedical and environmental sciences : BES* **23**, 357-362, doi:10.1016/S0895-3988(10)60076-1 (2010).
410 Weiser, M. J., Foradori, C. D. & Handa, R. J. Estrogen receptor beta in the brain: from form to function. *Brain research reviews* **57**, 309-320, doi:10.1016/j.brainresrev.2007.05.013 (2008).
411 Hrabovszky, E. *et al.* Estrogen receptor-beta in oxytocin and vasopressin neurons of the rat and human hypothalamus: Immunocytochemical and in situ hybridization studies. *The Journal of comparative neurology* **473**, 315-333, doi:10.1002/cne.20127 (2004).
412 Isgor, C., Cecchi, M., Kabbaj, M., Akil, H. & Watson, S. J. Estrogen receptor beta in the paraventricular nucleus of hypothalamus regulates the neuroendocrine response to stress and is regulated by corticosterone. *Neuroscience* **121**, 837-845 (2003).
413 Isgor, C., Huang, G. C., Akil, H. & Watson, S. J. Correlation of estrogen beta-receptor messenger RNA with endogenous levels of plasma estradiol and progesterone in the female rat hypothalamus, the bed nucleus of stria terminalis and the medial amygdala. *Brain research. Molecular brain research* **106**, 30-41 (2002).
414 Hasson, R. M. *et al.* Estrogen receptor alpha or beta loss in the colon of Min/+ mice promotes crypt expansion and impairs TGFbeta and HNF3beta signaling. *Carcinogenesis* **35**, 96-102, doi:10.1093/carcin/bgt323 (2014).

415 Atanassova, N. *et al.* Age-, cell- and region-specific immunoexpression of estrogen receptor alpha (but not estrogen receptor beta) during postnatal development of the epididymis and vas deferens of the rat and disruption of this pattern by neonatal treatment with diethylstilbestrol. *Endocrinology* **142**, 874-886, doi:10.1210/endo.142.2.7978 (2001).
416 Kawano, N. *et al.* Identification and localization of estrogen receptor alpha- and beta-positive cells in adult male and female mouse intestine at various estrogen levels. *Histochemistry and cell biology* **121**, 399-405, doi:10.1007/s00418-004-0644-6 (2004).
417 Cooke, P. S., Young, P., Hess, R. A. & Cunha, G. R. Estrogen receptor expression in developing epididymis, efferent ductules, and other male reproductive organs. *Endocrinology* **128**, 2874-2879, doi:10.1210/endo-128-6-2874 (1991).
418 Akgun, H., Lechago, J. & Younes, M. Estrogen receptor-beta is expressed in Barrett's metaplasia and associated adenocarcinoma of the esophagus. *Anticancer research* **22**, 1459-1461 (2002).
419 Flynn, J. M. *et al.* Role of wild-type estrogen receptor-beta in mitochondrial cytoprotection of cultured normal male and female human lens epithelial cells. *American journal of physiology. Endocrinology and metabolism* **295**, E637-647, doi:10.1152/ajpendo.90407.2008 (2008).
420 Cammarata, P. R. *et al.* Differential expression and comparative subcellular localization of estrogen receptor beta isoforms in virally transformed and normal cultured human lens epithelial cells. *Experimental eye research* **81**, 165-175, doi:10.1016/j.exer.2005.01.019 (2005).
421 Kararigas, G. *et al.* Comparative proteomic analysis reveals sex and estrogen receptor beta effects in the pressure overloaded heart. *Journal of proteome research* **13**, 5829-5836, doi:10.1021/pr500749j (2014).
422 Babiker, F. A. *et al.* Estrogen receptor beta protects the murine heart against left ventricular hypertrophy. *Arteriosclerosis, thrombosis, and vascular biology* **26**, 1524-1530, doi:10.1161/01.ATV.0000223344.11128.23 (2006).
423 Yu, C. P. *et al.* Estrogen inhibits renal cell carcinoma cell progression through estrogen receptor-beta activation. *PloS one* **8**, e56667, doi:10.1371/journal.pone.0056667 (2013).
424 Esqueda, M. E., Craig, T. & Hinojosa-Laborde, C. Effect of ovariectomy on renal estrogen receptor-alpha and estrogen receptor-beta in young salt-sensitive and -resistant rats. *Hypertension* **50**, 768-772, doi:10.1161/HYPERTENSIONAHA.107.095265 (2007).
425 Warner, M. & Gustafsson, J. A. Estrogen receptor beta and Liver X receptor beta: biology and therapeutic potential in CNS diseases. *Molecular psychiatry* **20**, 18-22, doi:10.1038/mp.2014.23 (2015).
426 Paquette, A. *et al.* Specific adaptations of estrogen receptor alpha and beta transcripts in liver and heart after endurance training in rats. *Molecular and cellular biochemistry* **306**, 179-187, doi:10.1007/s11010-007-9568-5 (2007).
427 Iavarone, M. *et al.* The clinical and pathogenetic significance of estrogen receptor-beta expression in chronic liver diseases and liver carcinoma. *Cancer* **98**, 529-534, doi:10.1002/cncr.11528 (2003).
428 Rodriguez-Lara, V. *et al.* Estrogen receptor beta and CXCR4/CXCL12 expression: differences by sex and hormonal status in lung adenocarcinoma. *Archives of medical research* **45**, 158-169, doi:10.1016/j.arcmed.2014.01.001 (2014).
429 Song, J. Y. *et al.* Genetic variation in ESR2 and estrogen receptor-beta expression in lung tumors. *Cancer epidemiology* **37**, 518-522, doi:10.1016/j.canep.2013.03.020 (2013).

430 Zhang, G. *et al.* Ligand-independent antiapoptotic function of estrogen receptor-beta in lung cancer cells. *Molecular endocrinology* **24**, 1737-1747, doi:10.1210/me.2010-0125 (2010).
431 Jefferson, W. N., Couse, J. F., Banks, E. P., Korach, K. S. & Newbold, R. R. Expression of estrogen receptor beta is developmentally regulated in reproductive tissues of male and female mice. *Biology of reproduction* **62**, 310-317 (2000).
432 O'Brien, M. L., Park, K., In, Y. & Park-Sarge, O. K. Characterization of estrogen receptor-beta (ERbeta) messenger ribonucleic acid and protein expression in rat granulosa cells. *Endocrinology* **140**, 4530-4541, doi:10.1210/endo.140.10.7032 (1999).
433 Morales, A. *et al.* The beta form of the estrogen receptor is predominantly expressed in the papillary cystic neoplasm of the pancreas. *Pancreas* **26**, 258-263 (2003).
434 Jesmin, S. *et al.* Evidence for a potential role of estrogen in the penis: detection of estrogen receptor-alpha and -beta messenger ribonucleic acid and protein. *Endocrinology* **143**, 4764-4774, doi:10.1210/en.2002-220628 (2002).
435 Richards, J. S. *et al.* Novel signaling pathways that control ovarian follicular development, ovulation, and luteinization. *Recent progress in hormone research* **57**, 195-220 (2002).
436 Wilson, M. E., Price, R. H., Jr. & Handa, R. J. Estrogen receptor-beta messenger ribonucleic acid expression in the pituitary gland. *Endocrinology* **139**, 5151-5156, doi:10.1210/endo.139.12.6354 (1998).
437 Ohshiro, K., Rayala, S. K., Williams, M. D., Kumar, R. & El-Naggar, A. K. Biological role of estrogen receptor beta in salivary gland adenocarcinoma cells. *Clin Cancer Res* **12**, 5994-5999, doi:10.1158/1078-0432.CCR-06-1251 (2006).
438 Velders, M., Schleipen, B., Fritzemeier, K. H., Zierau, O. & Diel, P. Selective estrogen receptor-beta activation stimulates skeletal muscle growth and regeneration. *Faseb J* **26**, 1909-1920, doi:10.1096/fj.11-194779 (2012).
439 Milanesi, L., Vasconsuelo, A., de Boland, A. R. & Boland, R. Expression and subcellular distribution of native estrogen receptor beta in murine C2C12 cells and skeletal muscle tissue. *Steroids* **74**, 489-497, doi:10.1016/j.steroids.2009.01.005 (2009).
440 Glenmark, B. *et al.* Difference in skeletal muscle function in males vs. females: role of estrogen receptor-beta. *American journal of physiology. Endocrinology and metabolism* **287**, E1125-1131, doi:10.1152/ajpendo.00098.2004 (2004).
441 Markiewicz, M. *et al.* A role for estrogen receptor-alpha and estrogen receptor-beta in collagen biosynthesis in mouse skin. *The Journal of investigative dermatology* **133**, 120-127, doi:10.1038/jid.2012.264 (2013).
442 Krahn-Bertil, E., Dos Santos, M., Damour, O., Andre, V. & Bolzinger, M. A. Expression of estrogen-related receptor beta (ERRbeta) in human skin. *European journal of dermatology : EJD* **20**, 719-723, doi:10.1684/ejd.2010.1083 (2010).
443 Ohata, C., Tadokoro, T. & Itami, S. Expression of estrogen receptor beta in normal skin, melanocytic nevi and malignant melanomas. *The Journal of dermatology* **35**, 215-221, doi:10.1111/j.1346-8138.2008.00447.x (2008).
444 Hildebrand, F. *et al.* Are the protective effects of 17beta-estradiol on splenic macrophages and splenocytes after trauma-hemorrhage mediated via estrogen-receptor (ER)-alpha or ER-beta? *Journal of leukocyte biology* **79**, 1173-1180, doi:10.1189/jlb.0106029 (2006).
445 Wakui, S. *et al.* Sex-associated difference in estrogen receptor beta expression in N-methyl-N'-nitro-N-nitrosoguanidine-induced gastric cancers in rats. *Comparative medicine* **61**, 412-418 (2011).

446 Campbell-Thompson, M., Reyher, K. K. & Wilkinson, L. B. Immunolocalization of estrogen receptor alpha and beta in gastric epithelium and enteric neurons. *The Journal of endocrinology* **171**, 65-73 (2001).
447 Pearl, C. A., Mason, H. & Roser, J. F. Immunolocalization of estrogen receptor alpha, estrogen receptor beta and androgen receptor in the pre-, peri- and post-pubertal stallion testis. *Animal reproduction science* **125**, 103-111, doi:10.1016/j.anireprosci.2011.03.007 (2011).
448 Pastore, M. B., Jobe, S. O., Ramadoss, J. & Magness, R. R. Estrogen receptor-alpha and estrogen receptor-beta in the uterine vascular endothelium during pregnancy: functional implications for regulating uterine blood flow. *Seminars in reproductive medicine* **30**, 46-61, doi:10.1055/s-0031-1299597 (2012).
449 Kang, J. S. *et al.* Expression of estrogen receptor alpha and beta in the uterus and vagina of immature rats treated with 17-ethinyl estradiol. *The Journal of veterinary medical science / the Japanese Society of Veterinary Science* **65**, 1293-1297 (2003).
450 Kotake-Nara, E. & Saida, K. Endothelin-2/vasoactive intestinal contractor: regulation of expression via reactive oxygen species induced by CoCl2, and Biological activities including neurite outgrowth in PC12 cells. *TheScientificWorldJournal* **6**, 176-186, doi:10.1100/tsw.2006.37 (2006).
451 Hosoda, K. *et al.* Cloning and expression of human endothelin-1 receptor cDNA. *FEBS letters* **287**, 23-26 (1991).
452 Ogawa, Y. *et al.* Molecular cloning of a non-isopeptide-selective human endothelin receptor. *Biochemical and biophysical research communications* **178**, 248-255 (1991).
453 Warner, T. D., Mitchell, J. A., de Nucci, G. & Vane, J. R. Endothelin-1 and endothelin-3 release EDRF from isolated perfused arterial vessels of the rat and rabbit. *Journal of cardiovascular pharmacology* **13 Suppl 5**, S85-88; discussion S102 (1989).
454 de Nucci, G. *et al.* Pressor effects of circulating endothelin are limited by its removal in the pulmonary circulation and by the release of prostacyclin and endothelium-derived relaxing factor. *Proceedings of the National Academy of Sciences of the United States of America* **85**, 9797-9800 (1988).
455 Fukuroda, T. *et al.* Clearance of circulating endothelin-1 by ETB receptors in rats. *Biochemical and biophysical research communications* **199**, 1461-1465, doi:10.1006/bbrc.1994.1395 (1994).
456 Dupuis, J., Goresky, C. A. & Fournier, A. Pulmonary clearance of circulating endothelin-1 in dogs in vivo: exclusive role of ETB receptors. *Journal of applied physiology* **81**, 1510-1515 (1996).
457 Garg, U. C. & Hassid, A. Nitric oxide-generating vasodilators and 8-bromo-cyclic guanosine monophosphate inhibit mitogenesis and proliferation of cultured rat vascular smooth muscle cells. *The Journal of clinical investigation* **83**, 1774-1777, doi:10.1172/JCI114081 (1989).
458 Cardillo, C., Kilcoyne, C. M., Waclawiw, M., Cannon, R. O., 3rd & Panza, J. A. Role of endothelin in the increased vascular tone of patients with essential hypertension. *Hypertension* **33**, 753-758 (1999).
459 Zhang, Z., Fang, Q. & Wang, J. Involvement of macrophage colony-stimulating factor (M-CSF) in the function of follicular granulosa cells. *Fertility and sterility* **90**, 749-754, doi:10.1016/j.fertnstert.2007.06.098 (2008).

460 Saitoh, H. [The role of macrophage migration inhibitory factor (MIF) in follicle growth and ovulation]. *[Hokkaido igaku zasshi] The Hokkaido journal of medical science* **78**, 329-338 (2003).
461 Matsuura, T. *et al.* Anti-macrophage inhibitory factor antibody inhibits PMSG-hCG-induced follicular growth and ovulation in mice. *Journal of assisted reproduction and genetics* **19**, 591-595 (2002).
462 Rossant, J. & McMahon, A. "Cre"-ating mouse mutants-a meeting review on conditional mouse genetics. *Genes & development* **13**, 142-145 (1999).
463 Soyal, S. M. *et al.* Cre-mediated recombination in cell lineages that express the progesterone receptor. *Genesis* **41**, 58-66, doi:10.1002/gene.20098 (2005).
464 Mueller, S. O., Katzenellenbogen, J. A. & Korach, K. S. Endogenous estrogen receptor beta is transcriptionally active in primary ovarian cells from estrogen receptor knockout mice. *Steroids* **69**, 681-686, doi:10.1016/j.steroids.2004.06.004 (2004).
465 Slomczynska, M. & Wozniak, J. Differential distribution of estrogen receptor-beta and estrogen receptor-alpha in the porcine ovary. *Experimental and clinical endocrinology & diabetes : official journal, German Society of Endocrinology [and] German Diabetes Association* **109**, 238-244 (2001).
466 Boerboom, D. *et al.* Misregulated Wnt/beta-catenin signaling leads to ovarian granulosa cell tumor development. *Cancer research* **65**, 9206-9215, doi:10.1158/0008-5472.CAN-05-1024 (2005).
467 Jansen, H. T., West, C., Lehman, M. N. & Padmanabhan, V. Ovarian estrogen receptor-beta (ERbeta) regulation: I. Changes in ERbeta messenger RNA expression prior to ovulation in the ewe. *Biology of reproduction* **65**, 866-872 (2001).
468 Hickey, G. J., Krasnow, J. S., Beattie, W. G. & Richards, J. S. Aromatase cytochrome P450 in rat ovarian granulosa cells before and after luteinization: adenosine 3',5'-monophosphate-dependent and independent regulation. Cloning and sequencing of rat aromatase cDNA and 5' genomic DNA. *Molecular endocrinology* **4**, 3-12, doi:10.1210/mend-4-1-3 (1990).
469 Krasnow, J. S., Hickey, G. J. & Richards, J. S. Regulation of aromatase mRNA and estradiol biosynthesis in rat ovarian granulosa and luteal cells by prolactin. *Molecular endocrinology* **4**, 13-12, doi:10.1210/mend-4-1-13 (1990).
470 Richards, J. S. & Hedin, L. Molecular aspects of hormone action in ovarian follicular development, ovulation, and luteinization. *Annual review of physiology* **50**, 441-463, doi:10.1146/annurev.ph.50.030188.002301 (1988).
471 Truett, G. E. *et al.* Preparation of PCR-quality mouse genomic DNA with hot sodium hydroxide and tris (HotSHOT). *BioTechniques* **29**, 52, 54 (2000).
472 Schmittgen, T. D. & Livak, K. J. Analyzing real-time PCR data by the comparative C(T) method. *Nature protocols* **3**, 1101-1108 (2008).
473 Chakravarthy, U., Douglas, A. J., Bailie, J. R., McKibben, B. & Archer, D. B. Immunoreactive endothelin distribution in ocular tissues. *Investigative ophthalmology & visual science* **35**, 2448-2454 (1994).
474 Scardina, G. A., Cacioppo, A. & Messina, P. Changes of oral microcirculation in chemotherapy patients: A possible correlation with mucositis? *Clinical anatomy* **27**, 417-422, doi:10.1002/ca.22300 (2014).
475 Morin, L. P. Environment and hamster reproduction: responses to phase-specific starvation during estrous cycle. *The American journal of physiology* **251**, R663-669 (1986).

476 Printz, R. H. & Greenwald, G. S. Effects of starvation on follicular development in the cyclic hamster. *Endocrinology* **86**, 290-295, doi:10.1210/endo-86-2-290 (1970).
477 Park, O. K. & Mayo, K. E. Transient expression of progesterone receptor messenger RNA in ovarian granulosa cells after the preovulatory luteinizing hormone surge. *Molecular endocrinology* **5**, 967-978, doi:10.1210/mend-5-7-967 (1991).
478 Webb, R. *et al.* Molecular mechanisms regulating follicular recruitment and selection. *Journal of reproduction and fertility. Supplement* **54**, 33-48 (1999).
479 Chiang, C. H., Cheng, K. W., Igarashi, S., Nathwani, P. S. & Leung, P. C. Hormonal regulation of estrogen receptor alpha and beta gene expression in human granulosa-luteal cells in vitro. *The Journal of clinical endocrinology and metabolism* **85**, 3828-3839, doi:10.1210/jcem.85.10.6886 (2000).
480 Sekiguchi, T. *et al.* Expression of epiregulin and amphiregulin in the rat ovary. *Journal of molecular endocrinology* **33**, 281-291 (2004).
481 Negishi, H. *et al.* Regulation of amphiregulin, EGFR-like factor expression by hCG in cultured human granulosa cells. *Acta obstetricia et gynecologica Scandinavica* **86**, 706-710, doi:10.1080/00016340701314959 (2007).
482 Puttabyatappa, M., Brogan, R. S., Vandevoort, C. A. & Chaffin, C. L. EGF-like ligands mediate progesterone's anti-apoptotic action on macaque granulosa cells. *Biology of reproduction* **88**, 18, doi:10.1095/biolreprod.112.103002 (2013).
483 Jo, M. & Curry, T. E., Jr. Luteinizing hormone-induced RUNX1 regulates the expression of genes in granulosa cells of rat periovulatory follicles. *Molecular endocrinology* **20**, 2156-2172, doi:10.1210/me.2005-0512 (2006).
484 Kuwabara, Y. *et al.* Gonadotropin regulation and role of ovarian osteopontin in the periovulatory period. *The Journal of endocrinology* **224**, 49-59, doi:10.1530/JOE-14-0203 (2015).
485 Ribatti, D. The discovery of the placental growth factor and its role in angiogenesis: a historical review. *Angiogenesis* **11**, 215-221, doi:10.1007/s10456-008-9114-4 (2008).
486 Ahmed, A., Dunk, C., Ahmad, S. & Khaliq, A. Regulation of placental vascular endothelial growth factor (VEGF) and placenta growth factor (PIGF) and soluble Flt-1 by oxygen--a review. *Placenta* **21 Suppl A**, S16-24 (2000).
487 Volanakis, J. E. & Narayana, S. V. Complement factor D, a novel serine protease. *Protein science : a publication of the Protein Society* **5**, 553-564, doi:10.1002/pro.5560050401 (1996).
488 Hajnik, C. A., Goetz, F. W., Hsu, S. Y. & Sokal, N. Characterization of a ribonucleic acid transcript from the brook trout (Salvelinus fontinalis) ovary with structural similarities to mammalian adipsin/complement factor D and tissue kallikrein, and the effects of kallikrein-like serine proteases on follicle contraction. *Biology of reproduction* **58**, 887-897 (1998).
489 Liu, Z. *et al.* Interleukin-6: an autocrine regulator of the mouse cumulus cell-oocyte complex expansion process. *Endocrinology* **150**, 3360-3368, doi:10.1210/en.2008-1532 (2009).
490 Imai, F., Kishi, H., Nakao, K., Nishimura, T. & Minegishi, T. IL-6 up-regulates the expression of rat LH receptors during granulosa cell differentiation. *Endocrinology* **155**, 1436-1444, doi:10.1210/en.2013-1821 (2014).
491 Satokata, I., Benson, G. & Maas, R. Sexually dimorphic sterility phenotypes in Hoxa10-deficient mice. *Nature* **374**, 460-463, doi:10.1038/374460a0 (1995).

492 Finnson, K. W., Kontogiannea, M., Li, X. & Farookhi, R. Characterization of Wnt2 overexpression in a rat granulosa cell line (DC3): effects on CTNNB1 activation. *Biology of reproduction* **87**, 12, 11-18, doi:10.1095/biolreprod.111.096396 (2012).
493 Matousek, M., Carati, C., Gannon, B., Mitsube, K. & Brannstrom, M. Changes in intrafollicular pressure in the rat ovary by nitric oxide and by alteration of systemic blood pressure. *European journal of obstetrics, gynecology, and reproductive biology* **98**, 46-52 (2001).
494 Wulff, C., Dickson, S. E., Duncan, W. C. & Fraser, H. M. Angiogenesis in the human corpus luteum: simulated early pregnancy by HCG treatment is associated with both angiogenesis and vessel stabilization. *Human reproduction* **16**, 2515-2524 (2001).
495 Fitzpatrick, S. L. & Richards, J. S. Regulation of the rat aromatase gene in ovarian granulosa cells and R2C Leydig cells. *The Journal of steroid biochemistry and molecular biology* **44**, 429-433 (1993).
496 Fitzpatrick, S. L. & Richards, J. S. Regulation of cytochrome P450 aromatase messenger ribonucleic acid and activity by steroids and gonadotropins in rat granulosa cells. *Endocrinology* **129**, 1452-1462, doi:10.1210/endo-129-3-1452 (1991).
497 O'Shea, J. D. Structure-function relationships in the wall of the ovarian follicle. *Australian journal of biological sciences* **34**, 379-394 (1981).
498 Young, J. M. & McNeilly, A. S. Theca: the forgotten cell of the ovarian follicle. *Reproduction* **140**, 489-504, doi:10.1530/REP-10-0094 (2010).
499 Herr, D., Bekes, I. & Wulff, C. Regulation of Endothelial Permeability in the Corpus Luteum: A Review of the Literature. *Geburtshilfe und Frauenheilkunde* **73**, 1107-1111, doi:10.1055/s-0033-1351032 (2013).
500 Buratini, J. & Price, C. A. Follicular somatic cell factors and follicle development. *Reproduction, fertility, and development* **23**, 32-39, doi:10.1071/RD10224 (2011).
501 Osvaldo-Decima, L. Smooth muscle in the ovary of the rat and monkey. *Journal of ultrastructure research* **30**, 218-237 (1970).
502 Fumagalli, Z., Motta, P. & Calvieri, S. The presence of smooth muscular cells in the ovary of several mammals as seen under the electron microscope. *Experientia* **27**, 682-683 (1971).
503 Okamura, H., Virutamasen, P., Wright, K. H. & Wallach, E. E. Ovarian smooth muscle in the human being, rabbit, and cat. Histochemical and electron microscopic study. *American journal of obstetrics and gynecology* **112**, 183-191 (1972).
504 Okamura, H., Yang, S. L., Wright, K. H. & Wallach, E. E. The effect of prostaglandin F 2 on the corpus luteum of the pregnant rat. An ultrastructural study. *Fertility and sterility* **23**, 475-483 (1972).
505 O'Shea, J. D. Smooth muscle-like cells in the walls of ovarian follicles and corpora lutea in sheep. *Journal of reproduction and fertility* **28**, 138-139 (1972).
506 Walles, B. *et al.* Evidence for a neuromuscular mechanism involved in the contractility of the ovarian follicular wall: fluorescence and electron microscopy and effects of tyramine on follicle strips. *Biology of reproduction* **12**, 239-247 (1975).
507 Walles, B., Edvinsson, L., Owman, C., Sjoberg, N. O. & Svensson, K. G. Mechanical response in the wall of ovarian follicles mediated by adrenergic receptors. *The Journal of pharmacology and experimental therapeutics* **193**, 460-473 (1975).
508 Burden, H. W. Adrenergic innervation in ovaries of the rat and guinea pig. *The American journal of anatomy* **133**, 455-461, doi:10.1002/aja.1001330407 (1972).

509 Burden, H. W. Ultrastructural observations on ovarian perifollicular smooth muscle in the cat, guinea pig, and rabbit. *The American journal of anatomy* **133**, 125-142, doi:10.1002/aja.1001330202 (1972).
510 Bjersing, L. & Cajander, S. Ovulation and the mechanism of follicle rupture. I. Light microscopic changes in rabbit ovarian follicles prior to induced ovulation. *Cell and tissue research* **149**, 287-300 (1974).
511 Bjersing, L. & Cajander, S. Ovulation and the mechanism of follicle rupture. III. Transmission electron microscopy of rabbit germinal epithelium prior to induced ovulation. *Cell and tissue research* **149**, 313-327 (1974).
512 Bjersing, L. & Cajander, S. Ovulation and the mechanism of follicle rupture. II. Scanning electron microscopy of rabbit germinal epithelium prior to induced ovulation. *Cell and tissue research* **149**, 301-312 (1974).
513 Bjersing, L. & Cajander, S. Ovulation and the mechanism of follicle rupture. VI. Ultrastructure of theca interna and the inner vascular network surrounding rabbit graafian follicles prior to induced ovulation. *Cell and tissue research* **153**, 31-44 (1974).
514 Bjersing, L. & Cajander, S. Ovulation and the mechanism of follicle rupture. V. Ultrastructure of tunica albuginea and theca externa of rabbit graafian follicles prior to induced ovulation. *Cell and tissue research* **153**, 15-30 (1974).
515 Bjersing, L. & Cajander, S. Ovulation and the mechanism of follicle rupture. IV. Ultrastructure of membrana granulosa of rabbit graafian follicles prior to induced ovulation. *Cell and tissue research* **153**, 1-14 (1974).
516 Wessells, N. K. *et al.* Microfilaments in cellular and developmental processes. *Science* **171**, 135-143 (1971).
517 Gabbiani, G. *et al.* Human smooth muscle autoantibody. Its identification as antiactin antibody and a study of its binding to "nonmuscular" cells. *The American journal of pathology* **72**, 473-488 (1973).
518 Montandon, D., Gabbiani, G., Ryan, G. B. & Majno, G. The contractile fibroblast. Its relevance in plastic surgery. *Plastic and reconstructive surgery* **52**, 286-290 (1973).
519 Ryan, G. B. *et al.* Myofibroblasts in an avascular fibrous tissue. *Laboratory investigation; a journal of technical methods and pathology* **29**, 197-206 (1973).
520 Gimeno, M. F., Borda, E., Sterin-Borda, L., Vidal, J. H. & Gimeno, A. L. Pharmacologic influences on human ovarian contractions. *Obstetrics and gynecology* **47**, 218-222 (1976).
521 Sterin-Borda, L., Borda, E., Gimeno, M. F. & Gimeno, A. L. Spontaneous and prostaglandin- or oxytocin-induced motility of rat ovaries isolated during different stages of the estrous cycle: effects of norepinephrine. *Fertility and sterility* **27**, 319-327 (1976).
522 Talbot, P. Videotape analysis of hamster ovulation in vitro. *The Journal of experimental zoology* **225**, 141-148, doi:10.1002/jez.1402250117 (1983).
523 Coutinho, E. M., Maia, H. S. & Schally, A. V. Changes in intra-ovarian pressure in woman following the administration of luteinizing hormone-releasing hormone LH-FSH). *International journal of fertility* **19**, 889-892 (1974).
524 O'Shea, J. D. & Phillips, R. E. Contractility in vitro of ovarian follicles from sheep, and the effects of drugs. *Biology of reproduction* **10**, 370-379 (1974).
525 O'Shea, J. D. & Phillips, R. E. Proceedings: Contractility of ovarian follicles from sheep in vitro. *Journal of reproduction and fertility* **36**, 457 (1974).
526 de la Cruz, A., Wright, K. H. & Wallach, E. E. The effects of cholinergic agents on ovarian contractility in the rabbit. *Obstetrics and gynecology* **47**, 272-278 (1976).

527 O'Shea, J. D., Cran, D. G., Hay, M. F. & Moor, R. M. Ultrastructure of the theca interna of ovarian follicles in sheep. *Cell and tissue research* **187**, 457-472 (1978).
528 O'Shea, J. D., Hay, M. F. & Cran, D. G. Ultrastructural changes in the theca interna during follicular atresia in sheep. *Journal of reproduction and fertility* **54**, 183-187 (1978).
529 Poli, E., Casoli, C., Spaggiari, I., Starcich, R. & Bertaccini, G. Contractile effect of endothelin-2 on the isolated human saphenous vein. *Archives internationales de pharmacodynamie et de therapie* **313**, 108-119 (1991).
530 Kohzuki, M. *et al.* Localization and characterization of endothelin receptor binding sites in the rat brain visualized by in vitro autoradiography. *Neuroscience* **42**, 245-260 (1991).
531 Agapitov, A. V. & Haynes, W. G. Role of endothelin in cardiovascular disease. *Journal of the renin-angiotensin-aldosterone system : JRAAS* **3**, 1-15, doi:10.3317/jraas.2002.001 (2002).
532 Kawanabe, Y. & Nauli, S. M. Endothelin. *Cellular and molecular life sciences : CMLS* **68**, 195-203, doi:10.1007/s00018-010-0518-0 (2011).
533 Flores, J. A. & Sasway, H. M. Gene expression of endothelin-1 in the porcine ovary: follicular development. *Biology of reproduction* **63**, 1377-1382 (2000).
534 Hinckley, S. T. & Milvae, R. A. Endothelin-1 mediates prostaglandin F(2alpha)-induced luteal regression in the ewe. *Biology of reproduction* **64**, 1619-1623 (2001).
535 Meidan, R., Milvae, R. A., Weiss, S., Levy, N. & Friedman, A. Intraovarian regulation of luteolysis. *Journal of reproduction and fertility. Supplement* **54**, 217-228 (1999).
536 Meidan, R. & Levy, N. The ovarian endothelin network: an evolving story. *Trends in endocrinology and metabolism: TEM* **18**, 379-385, doi:10.1016/j.tem.2007.09.002 (2007).
537 Kawamura, K. *et al.* Paracrine regulation of the resumption of oocyte meiosis by endothelin-1. *Developmental biology* **327**, 62-70, doi:10.1016/j.ydbio.2008.11.033 (2009).
538 Sprogar, S., Meh, A., Vaupotic, T., Drevensek, G. & Drevensek, M. Expression levels of endothelin-1, endothelin-2, and endothelin-3 vary during the initial, lag, and late phase of orthodontic tooth movement in rats. *European journal of orthodontics* **32**, 324-328, doi:10.1093/ejo/cjp091 (2010).
539 Oksche, A. *et al.* Late endosomal/lysosomal targeting and lack of recycling of the ligand-occupied endothelin B receptor. *Molecular pharmacology* **57**, 1104-1113 (2000).
540 Shraga-Levine, Z. & Sokolovsky, M. Functional coupling of G proteins to endothelin receptors is ligand and receptor subtype specific. *Cellular and molecular neurobiology* **20**, 305-317 (2000).
541 Pollock, D. M., Keith, T. L. & Highsmith, R. F. Endothelin receptors and calcium signaling. *Faseb J* **9**, 1196-1204 (1995).
542 Irving, R. J., Noon, J. P., Watt, G. C., Webb, D. J. & Walker, B. R. Activation of the endothelin system in insulin resistance. *QJM : monthly journal of the Association of Physicians* **94**, 321-326 (2001).
543 Miwa, S., Kawanabe, Y., Okamoto, Y. & Masaki, T. Ca2+ entry channels involved in endothelin-1-induced contractions of vascular smooth muscle cells. *Journal of smooth muscle research = Nihon Heikatsukin Gakkai kikanshi* **41**, 61-75 (2005).
544 Horinouchi, T. *et al.* Endothelin-1 decreases [Ca2+]i via Na+/Ca2+ exchanger in CHO cells stably expressing endothelin ETA receptor. *European journal of pharmacology* **566**, 28-33, doi:10.1016/j.ejphar.2007.03.019 (2007).

545 Miwa, M. *et al.* Endothelin receptor B2 (EDNRB2) is associated with the panda plumage colour mutation in Japanese quail. *Animal genetics* **38**, 103-108, doi:10.1111/j.1365-2052.2007.01568.x (2007).
546 Ivey, M. E., Osman, N. & Little, P. J. Endothelin-1 signalling in vascular smooth muscle: pathways controlling cellular functions associated with atherosclerosis. *Atherosclerosis* **199**, 237-247, doi:10.1016/j.atherosclerosis.2008.03.006 (2008).
547 Gentili, M., Obermuller, N., Schleich, H. G., Melchert, F. & Weigel, M. Distinct expression of endothelin receptor subtypes A and B in luteinized human granulosa cells. *Hormone and metabolic research = Hormon- und Stoffwechselforschung = Hormones et metabolisme* **33**, 573-576, doi:10.1055/s-2001-17902 (2001).
548 Douglas, S. A. & Hiley, C. R. Endothelium-dependent vascular activities of endothelin-like peptides in the isolated superior mesenteric arterial bed of the rat. *British journal of pharmacology* **101**, 81-88 (1990).
549 Clozel, M., Gray, G. A., Breu, V., Loffler, B. M. & Osterwalder, R. The endothelin ETB receptor mediates both vasodilation and vasoconstriction in vivo. *Biochemical and biophysical research communications* **186**, 867-873 (1992).
550 Gulati, A., Sharma, A. C., Robbie, G. & Saxena, P. R. Endothelin ETA receptor antagonist, BQ-123, blocks the vasoconstriction induced by sarafotoxin 6b in the heart but not in other vascular beds. *General pharmacology* **26**, 183-193 (1995).
551 Schneider, M. P., Inscho, E. W. & Pollock, D. M. Attenuated vasoconstrictor responses to endothelin in afferent arterioles during a high-salt diet. *American journal of physiology. Renal physiology* **292**, F1208-1214, doi:10.1152/ajprenal.00280.2006 (2007).
552 Schneider, M. P., Boesen, E. I. & Pollock, D. M. Contrasting actions of endothelin ET(A) and ET(B) receptors in cardiovascular disease. *Annual review of pharmacology and toxicology* **47**, 731-759, doi:10.1146/annurev.pharmtox.47.120505.105134 (2007).
553 Nelson, J., Bagnato, A., Battistini, B. & Nisen, P. The endothelin axis: emerging role in cancer. *Nature reviews. Cancer* **3**, 110-116, doi:10.1038/nrc990 (2003).
554 Kuhbandner, S. *et al.* Temporally controlled somatic mutagenesis in smooth muscle. *Genesis* **28**, 15-22 (2000).
555 Kedzierski, R. M. *et al.* Cardiomyocyte-specific endothelin A receptor knockout mice have normal cardiac function and an unaltered hypertrophic response to angiotensin II and isoproterenol. *Molecular and cellular biology* **23**, 8226-8232 (2003).
556 Sohal, D. S. *et al.* Temporally regulated and tissue-specific gene manipulations in the adult and embryonic heart using a tamoxifen-inducible Cre protein. *Circulation research* **89**, 20-25 (2001).
557 Arango, N. A. *et al.* A mesenchymal perspective of Mullerian duct differentiation and regression in Amhr2-lacZ mice. *Molecular reproduction and development* **75**, 1154-1162, doi:10.1002/mrd.20858 (2008).
558 Boyer, A. *et al.* WNT4 is required for normal ovarian follicle development and female fertility. *Faseb J* **24**, 3010-3025, doi:10.1096/fj.09-145789 (2010).
559 Hernandez Gifford, J. A., Hunzicker-Dunn, M. E. & Nilson, J. H. Conditional deletion of beta-catenin mediated by Amhr2cre in mice causes female infertility. *Biology of reproduction* **80**, 1282-1292, doi:10.1095/biolreprod.108.072280 (2009).
560 Jorgez, C. J., Klysik, M., Jamin, S. P., Behringer, R. R. & Matzuk, M. M. Granulosa cell-specific inactivation of follistatin causes female fertility defects. *Molecular endocrinology* **18**, 953-967, doi:10.1210/me.2003-0301 (2004).

561 Jamin, S. P., Arango, N. A., Mishina, Y., Hanks, M. C. & Behringer, R. R. Requirement of Bmpr1a for Mullerian duct regression during male sexual development. *Nature genetics* **32**, 408-410, doi:10.1038/ng1003 (2002).
562 Donato, A. J. *et al.* Smooth muscle specific disruption of the endothelin-A receptor in mice reduces arterial pressure, and vascular reactivity and affects vascular development. *Life sciences*, doi:10.1016/j.lfs.2013.12.209 (2014).
563 Jordan, V. C. New insights into the metabolism of tamoxifen and its role in the treatment and prevention of breast cancer. *Steroids* **72**, 829-842, doi:10.1016/j.steroids.2007.07.009 (2007).
564 Lien, E. A., Solheim, E. & Ueland, P. M. Distribution of tamoxifen and its metabolites in rat and human tissues during steady-state treatment. *Cancer research* **51**, 4837-4844 (1991).
565 Jensen, E. V. *et al.* A two-step mechanism for the interaction of estradiol with rat uterus. *Proceedings of the National Academy of Sciences of the United States of America* **59**, 632-638 (1968).
566 Shyamala, G. & Gorski, J. Estrogen receptors in the rat uterus. Studies on the interaction of cytosol and nuclear binding sites. *The Journal of biological chemistry* **244**, 1097-1103 (1969).
567 Gorski, J., Shyamala, G. & Toft, D. Interrelationships of nuclear and cytoplasmic estrogen receptors. *Current topics in developmental biology* **4**, 149-167 (1969).
568 Jordan, V. C. & Dowse, L. J. Tamoxifen as an anti-tumour agent: effect on oestrogen binding. *The Journal of endocrinology* **68**, 297-303 (1976).
569 Jordan, V. C. Antiestrogenic and antitumor properties of tamoxifen in laboratory animals. *Cancer treatment reports* **60**, 1409-1419 (1976).
570 Emmens, C. W. Compounds exhibiting prolonged antioestrogenic and antifertility activity in mice and rats. *Journal of reproduction and fertility* **26**, 175-182 (1971).
571 Jordan, V. C. Prolonged antioestrogenic activity of ICI 46, 474 in the ovariectomized mouse. *Journal of reproduction and fertility* **42**, 251-258 (1975).
572 Furr, B. J. & Jordan, V. C. The pharmacology and clinical uses of tamoxifen. *Pharmacology & therapeutics* **25**, 127-205 (1984).
573 Borgna, J. L. & Rochefort, H. [In vivo occupation of estrogen receptors by hydroxylated metabolites of tamoxifen]. *Comptes rendus des seances de l'Academie des sciences. Serie D, Sciences naturelles* **289**, 1141-1144 (1979).
574 Harper, M. J. & Walpole, A. L. Contrasting endocrine activities of cis and trans isomers in a series of substituted triphenylethylenes. *Nature* **212**, 87 (1966).
575 Emmens, C. W. Prolonged anti-oestrogenic and anti-fertility actions of sometriarylalkenes. *Journal of reproduction and fertility* **24**, 143 (1971).
576 Emmens, C. W. & Carr, W. L. Further studies of compounds exhibiting prolonged antioestrogenic and antifertility activity in the mouse. *Journal of reproduction and fertility* **34**, 29-40 (1973).
577 Jordan, V. C. & Koerner, S. Tamoxifen (ICI 46,474) and the human carcinoma 8S oestrogen receptor. *European journal of cancer* **11**, 205-206 (1975).
578 Miller, W. L. & Huang, E. S. Antiestrogens and ovine gonadotrophs: antagonism of estrogen-induced changes in gonadotropin secretions. *Endocrinology* **108**, 96-102, doi:10.1210/endo-108-1-96 (1981).

579 Harper, M. J. Effects of androstenedione on pre-implantation stages of pregnancy in rats. *Endocrinology* **81**, 1091-1098, doi:10.1210/endo-81-5-1091 (1967).
580 Harper, M. J. Prevention of implantation in rats by I.C.I. 46,474: role of histamine. *The Journal of endocrinology* **38**, 115-120 (1967).
581 Harper, M. J. & Walpole, A. L. Mode of action of I.C.I. 46,474 in preventing implantation in rats. *The Journal of endocrinology* **37**, 83-92 (1967).
582 Garuti, G. *et al.* Histopathologic behavior of endometrial hyperplasia during tamoxifen therapy for breast cancer. *Gynecologic oncology* **101**, 269-273, doi:10.1016/j.ygyno.2005.10.010 (2006).
583 Kimya, Y., Cengiz, C. & Tolunay, S. Endometrial polyps, cystic glandular hyperplasia and atypical leiomyoma associated with tamoxifen therapy. *International journal of gynaecology and obstetrics: the official organ of the International Federation of Gynaecology and Obstetrics* **46**, 69-70 (1994).
584 Ata, B. & Tulandi, T. Ultrasound automated volume calculation in reproduction and in pregnancy. *Fertility and sterility* **95**, 2163-2170, doi:10.1016/j.fertnstert.2011.04.007 (2011).
585 Jiang, B. *et al.* Study of Luan-Pao-Prescription on ovarian dysfunction in rats. *Journal of ethnopharmacology* **141**, 653-658, doi:10.1016/j.jep.2011.08.082 (2012).
586 Sato, J., Hashimoto, S., Doi, T., Yamada, N. & Tsuchitani, M. Histological characteristics of the regression of corpora lutea in wistar hannover rats: the comparisons with sprague-dawley rats. *Journal of toxicologic pathology* **27**, 107-113, doi:10.1293/tox.2013-0054 (2014).
587 Jankovic, S. M. *et al.* Contractile effects of endothelins on isolated ampullar segment of human oviduct in luteal phase of menstrual cycle. *Pharmacological research : the official journal of the Italian Pharmacological Society* **59**, 69-73, doi:10.1016/j.phrs.2008.10.001 (2009).
588 Labadia, A., Costa, G., Jimenez, E., Triguero, D. & Garcia-Pascual, A. Endothelin receptor-mediated Ca2+ mobilization and contraction in bovine oviductal arteries: comparison with noradrenaline and potassium. *General pharmacology* **29**, 611-619 (1997).
589 Nicholson, H. S. & Byrne, J. Fertility and pregnancy after treatment for cancer during childhood or adolescence. *Cancer* **71**, 3392-3399 (1993).
590 Sanders, J. E. *et al.* Ovarian function following marrow transplantation for aplastic anemia or leukemia. *Journal of clinical oncology : official journal of the American Society of Clinical Oncology* **6**, 813-818 (1988).
591 Aubard, Y. Ovarian tissue xenografting. *European journal of obstetrics, gynecology, and reproductive biology* **108**, 14-18 (2003).
592 Kim, S. S., Battaglia, D. E. & Soules, M. R. The future of human ovarian cryopreservation and transplantation: fertility and beyond. *Fertility and sterility* **75**, 1049-1056 (2001).
593 Nisolle, M., Casanas-Roux, F., Qu, J., Motta, P. & Donnez, J. Histologic and ultrastructural evaluation of fresh and frozen-thawed human ovarian xenografts in nude mice. *Fertility and sterility* **74**, 122-129 (2000).
594 Oktay, K., Newton, H., Aubard, Y., Salha, O. & Gosden, R. G. Cryopreservation of immature human oocytes and ovarian tissue: an emerging technology? *Fertility and sterility* **69**, 1-7 (1998).
595 Dissen, G. A., Lara, H. E., Fahrenbach, W. H., Costa, M. E. & Ojeda, S. R. Immature rat ovaries become revascularized rapidly after autotransplantation and show a gonadotropin-

dependent increase in angiogenic factor gene expression. *Endocrinology* **134**, 1146-1154, doi:10.1210/endo.134.3.8119153 (1994).

596 Rone, J. D., Halvorson, L. M. & Goodman, A. L. Ovarian angiogenesis in rabbits: endotheliotrophic chemoattractant activity from isolated follicles and dispersed granulosa cells. *Journal of reproduction and fertility* **97**, 359-365 (1993).

597 Yang, H., Lee, H. H., Lee, H. C., Ko, D. S. & Kim, S. S. Assessment of vascular endothelial growth factor expression and apoptosis in the ovarian graft: can exogenous gonadotropin promote angiogenesis after ovarian transplantation? *Fertility and sterility* **90**, 1550-1558, doi:10.1016/j.fertnstert.2007.08.086 (2008).

598 Terazono, T. *et al.* Assessment of canine ovaries autografted to various body sites. *Theriogenology* **77**, 131-138, doi:10.1016/j.theriogenology.2011.07.026 (2012).

599 Soleimani, R. *et al.* Back muscle as a promising site for ovarian tissue transplantation, an animal model. *Human reproduction* **23**, 619-626, doi:10.1093/humrep/dem405 (2008).

600 Green, C. J. Experimental transplantation. *Progress in allergy* **38**, 123-158 (1986).

601 Spanel-Borowski, K. Vascularization of ovaries from golden hamsters following implantation into the chick chorioallantoic membrane. *Experimental cell biology* **57**, 219-227 (1989).

602 Barnabas, O., Wang, H. & Gao, X. M. Role of estrogen in angiogenesis in cardiovascular diseases. *Journal of geriatric cardiology : JGC* **10**, 377-382, doi:10.3969/j.issn.1671-5411.2013.04.008 (2013).

603 Kyriakides, Z. S., Kremastinos, D. T. & Karayannakos, P. Estrogen stimulates angiogenesis in normoperfused skeletal muscle in rabbits. *Circulation* **103**, E107-108 (2001).

604 Lamping, K. G., Christensen, L. P. & Tomanek, R. J. Estrogen therapy induces collateral and microvascular remodeling. *American journal of physiology. Heart and circulatory physiology* **285**, H2039-2044, doi:10.1152/ajpheart.00405.2003 (2003).

605 Rubanyi, G. M., Johns, A. & Kauser, K. Effect of estrogen on endothelial function and angiogenesis. *Vascular pharmacology* **38**, 89-98 (2002).

606 Wagner, E. M., Gallagher, S. J., Reddy, S. & Mitzner, W. Effects of tamoxifen on ischemia-induced angiogenesis in the mouse lung. *Angiogenesis* **6**, 65-71 (2003).

607 Zhang, J., Yang, W., Hu, B., Wu, W. & Fallon, M. B. Endothelin-1 activation of the endothelin B receptor modulates pulmonary endothelial CX3CL1 and contributes to pulmonary angiogenesis in experimental hepatopulmonary syndrome. *The American journal of pathology* **184**, 1706-1714, doi:10.1016/j.ajpath.2014.02.027 (2014).

608 Leonard, M. G., Briyal, S. & Gulati, A. Endothelin B receptor agonist, IRL-1620, reduces neurological damage following permanent middle cerebral artery occlusion in rats. *Brain research* **1420**, 48-58, doi:10.1016/j.brainres.2011.08.075 (2011).

609 Leonard, M. G. & Gulati, A. Endothelin B receptor agonist, IRL-1620, enhances angiogenesis and neurogenesis following cerebral ischemia in rats. *Brain research* **1528**, 28-41, doi:10.1016/j.brainres.2013.07.002 (2013).

610 Bek, E. L. & McMillen, M. A. Endothelins are angiogenic. *Journal of cardiovascular pharmacology* **36**, S135-139 (2000).

611 Hu, D. E., Hiley, C. R. & Fan, T. P. Comparative studies of the angiogenic activity of vasoactive intestinal peptide, endothelins-1 and -3 and angiotensin II in a rat sponge model. *British journal of pharmacology* **117**, 545-551 (1996).

612 Qiu, Y. *et al.* Ovarian VEGF(165)b expression regulates follicular development, corpus luteum function and fertility. *Reproduction* **143**, 501-511, doi:10.1530/REP-11-0091 (2012).
613 Iijima, K., Jiang, J. Y., Shimizu, T., Sasada, H. & Sato, E. Acceleration of follicular development by administration of vascular endothelial growth factor in cycling female rats. *The Journal of reproduction and development* **51**, 161-168 (2005).
614 Brand, M., Kempf, H., Paul, M., Corvol, P. & Gasc, J. M. Expression of endothelins in human cardiogenesis. *Journal of molecular medicine* **80**, 715-723, doi:10.1007/s00109-002-0379-6 (2002).
615 Liefeldt, L. *et al.* Effects of transgenic endothelin-2 overexpression on diabetic cardiomyopathy in rats. *European journal of clinical investigation* **40**, 203-210, doi:10.1111/j.1365-2362.2009.02251.x (2010).
616 Cho, J. J. *et al.* An oral endothelin-A receptor antagonist blocks collagen synthesis and deposition in advanced rat liver fibrosis. *Gastroenterology* **118**, 1169-1178 (2000).
617 Abe, M., Ruest, L. B. & Clouthier, D. E. Fate of cranial neural crest cells during craniofacial development in endothelin-A receptor-deficient mice. *The International journal of developmental biology* **51**, 97-105, doi:10.1387/ijdb.062237ma (2007).
618 Turner, A. J. & Murphy, L. J. Molecular pharmacology of endothelin converting enzymes. *Biochemical pharmacology* **51**, 91-102 (1996).
619 Lambert, G. L., Barker, S., Lees, D. M. & Corder, R. Endothelin-2 synthesis is stimulated by the type-1 tumour necrosis factor receptor and cAMP: comparison with endothelin-converting enzyme-1 expression. *Journal of molecular endocrinology* **24**, 273-283 (2000).
620 Lambert, G. L., Barker, S. & Corder, R. Comparison of the regulation of endothelin-2 and endothelin-converting enzyme-1 b [correction of beta] by forskolin and TNF-alpha in ACHN cells. *Journal of cardiovascular pharmacology* **31 Suppl 1**, S49-51 (1998).
621 Schug, J. Using TESS to predict transcription factor binding sites in DNA sequence. *Current protocols in bioinformatics / editoral board, Andreas D. Baxevanis ... [et al.]* **Chapter 2**, Unit 2 6, doi:10.1002/0471250953.bi0206s21 (2008).
622 Ntunde, B. N., Hacker, R. R. & Brown, R. G. Aqueous porcine pineal extract: inhibition of ovulation induced with PMSG and HCG in immature mice. *Journal of animal science* **48**, 1422-1428 (1979).
623 Yamaguchi, T., Katsuyama, M., Suzuki, W., Saito, T. R. & Takahashi, K. W. [Comparison of the amounts of hCG and PMSG to induce ovulation in 50% of the animals, mice, Syrian hamsters and rats]. *Jikken dobutsu. Experimental animals* **41**, 153-159 (1992).
624 Kanayama, K., Sankai, T., Nariai, K., Endo, T. & Sakuma, Y. Effects of anti-progesterone compound RU486 on ovulation in immature mice treated with PMSG/hCG. *Research in experimental medicine. Zeitschrift fur die gesamte experimentelle Medizin einschliesslich experimenteller Chirurgie* **194**, 217-220 (1994).
625 Richards, J. S. *et al.* Regulated expression of ADAMTS family members in follicles and cumulus oocyte complexes: evidence for specific and redundant patterns during ovulation. *Biology of reproduction* **72**, 1241-1255, doi:10.1095/biolreprod.104.038083 (2005).
626 Zhang, J. *et al.* Regulatory effect of hypoxia-inducible factor-1alpha on hCG-stimulated endothelin-2 expression in granulosa cells from the PMSG-treated rat ovary. *The Journal of reproduction and development* **58**, 678-684 (2012).
627 Zheng, J., Devalaraja-Narashimha, K., Singaravelu, K. & Padanilam, B. J. Poly(ADP-ribose) polymerase-1 gene ablation protects mice from ischemic renal injury. *American*

journal of physiology. Renal physiology **288**, F387-398, doi:10.1152/ajprenal.00436.2003 (2005).

628 Persy, V. P., Verhulst, A., Ysebaert, D. K., De Greef, K. E. & De Broe, M. E. Reduced postischemic macrophage infiltration and interstitial fibrosis in osteopontin knockout mice. *Kidney international* **63**, 543-553, doi:10.1046/j.1523-1755.2003.00767.x (2003).

629 Yuan, H. T., Li, X. Z., Pitera, J. E., Long, D. A. & Woolf, A. S. Peritubular capillary loss after mouse acute nephrotoxicity correlates with down-regulation of vascular endothelial growth factor-A and hypoxia-inducible factor-1 alpha. *The American journal of pathology* **163**, 2289-2301 (2003).

630 Sabaa, N. *et al.* Endothelin receptor antagonism prevents hypoxia-induced mortality and morbidity in a mouse model of sickle-cell disease. *The Journal of clinical investigation* **118**, 1924-1933, doi:10.1172/JCI33308 (2008).

631 Consortium, E. P. A user's guide to the encyclopedia of DNA elements (ENCODE). *PLoS biology* **9**, e1001046, doi:10.1371/journal.pbio.1001046 (2011).

632 Blatti, C. & Sinha, S. Motif enrichment tool. *Nucleic acids research* **42**, W20-25, doi:10.1093/nar/gku456 (2014).

633 Ben-Shlomo, I., Vitt, U. A. & Hsueh, A. J. Perspective: the ovarian kaleidoscope database-II. Functional genomic analysis of an organ-specific database. *Endocrinology* **143**, 2041-2044, doi:10.1210/endo.143.6.8851 (2002).

634 Wasson, K. M. & Hsueh, A. J. Ovarian gene database. *Journal of the Society for Gynecologic Investigation* **8**, S37-39 (2001).

635 Ma, Y. *et al.* Renal tissue thawed for 30 minutes is still suitable for gene expression analysis. *PloS one* **9**, e93175, doi:10.1371/journal.pone.0093175 (2014).

636 Wollen, E. J. *et al.* Hypoxia-reoxygenation affects whole-genome expression in the newborn eye. *Investigative ophthalmology & visual science* **55**, 1393-1401, doi:10.1167/iovs.13-13159 (2014).

637 Wang, J. *et al.* The novel porcine gene early growth response 4 (Egr4) is differentially expressed in the ovaries of Erhualian and Pietrain pigs. *Reproduction, fertility, and development* **26**, 587-598, doi:10.1071/RD12380 (2014).

638 Swiderski, R. E. *et al.* Gene expression analysis of photoreceptor cell loss in bbs4-knockout mice reveals an early stress gene response and photoreceptor cell damage. *Investigative ophthalmology & visual science* **48**, 3329-3340, doi:10.1167/iovs.06-1477 (2007).

639 Wingender, E. TRANSFAC, TRANSPATH and CYTOMER as starting points for an ontology of regulatory networks. *In silico biology* **4**, 55-61 (2004).

640 Wingender, E., Dietze, P., Karas, H. & Knuppel, R. TRANSFAC: a database on transcription factors and their DNA binding sites. *Nucleic acids research* **24**, 238-241 (1996).

641 Mathelier, A. *et al.* JASPAR 2014: an extensively expanded and updated open-access database of transcription factor binding profiles. *Nucleic acids research* **42**, D142-147, doi:10.1093/nar/gkt997 (2014).

642 Sandelin, A., Alkema, W., Engstrom, P., Wasserman, W. W. & Lenhard, B. JASPAR: an open-access database for eukaryotic transcription factor binding profiles. *Nucleic acids research* **32**, D91-94, doi:10.1093/nar/gkh012 (2004).

643 Chen, Q. K., Hertz, G. Z. & Stormo, G. D. PromFD 1.0: a computer program that predicts eukaryotic pol II promoters using strings and IMD matrices. *Computer applications in the biosciences : CABIOS* **13**, 29-35 (1997).

644 Schug, J. & Overton, G. C. Modeling transcription factor binding sites with Gibbs Sampling and Minimum Description Length encoding. *Proceedings / ... International Conference on Intelligent Systems for Molecular Biology ; ISMB. International Conference on Intelligent Systems for Molecular Biology* **5**, 268-271 (1997).
645 Mayor, C. *et al.* VISTA : visualizing global DNA sequence alignments of arbitrary length. *Bioinformatics* **16**, 1046-1047 (2000).
646 Gu, J. *et al.* Dexmedetomidine provides renoprotection against ischemia-reperfusion injury in mice. *Critical care* **15**, R153, doi:10.1186/cc10283 (2011).
647 Hellwig-Burgel, T., Stiehl, D. P., Wagner, A. E., Metzen, E. & Jelkmann, W. Review: hypoxia-inducible factor-1 (HIF-1): a novel transcription factor in immune reactions. *Journal of interferon & cytokine research : the official journal of the International Society for Interferon and Cytokine Research* **25**, 297-310, doi:10.1089/jir.2005.25.297 (2005).
648 Shaulian, E. AP-1--The Jun proteins: Oncogenes or tumor suppressors in disguise? *Cellular signalling* **22**, 894-899, doi:10.1016/j.cellsig.2009.12.008 (2010).
649 Shaulian, E. & Karin, M. AP-1 as a regulator of cell life and death. *Nature cell biology* **4**, E131-136, doi:10.1038/ncb0502-e131 (2002).
650 Passegue, E. & Wagner, E. F. JunB suppresses cell proliferation by transcriptional activation of p16(INK4a) expression. *The EMBO journal* **19**, 2969-2979, doi:10.1093/emboj/19.12.2969 (2000).
651 Bakiri, L., Lallemand, D., Bossy-Wetzel, E. & Yaniv, M. Cell cycle-dependent variations in c-Jun and JunB phosphorylation: a role in the control of cyclin D1 expression. *The EMBO journal* **19**, 2056-2068, doi:10.1093/emboj/19.9.2056 (2000).
652 Andrecht, S., Kolbus, A., Hartenstein, B., Angel, P. & Schorpp-Kistner, M. Cell cycle promoting activity of JunB through cyclin A activation. *The Journal of biological chemistry* **277**, 35961-35968, doi:10.1074/jbc.M202847200 (2002).
653 Mizuno, T. M., Funabashi, T., Kleopoulos, S. P. & Mobbs, C. V. Specific preservation of biosynthetic responses to insulin in adipose tissue may contribute to hyperleptinemia in insulin-resistant obese mice. *The Journal of nutrition* **134**, 1045-1050 (2004).
654 Pinent, M. *et al.* Adipose triglyceride lipase and hormone-sensitive lipase are involved in fat loss in JunB-deficient mice. *Endocrinology* **152**, 2678-2689, doi:10.1210/en.2010-1477 (2011).
655 Fijneman, R. J. *et al.* Runx1 is a tumor suppressor gene in the mouse gastrointestinal tract. *Cancer science* **103**, 593-599, doi:10.1111/j.1349-7006.2011.02189.x (2012).
656 Linggi, B. E., Brandt, S. J., Sun, Z. W. & Hiebert, S. W. Translating the histone code into leukemia. *Journal of cellular biochemistry* **96**, 938-950, doi:10.1002/jcb.20604 (2005).
657 Watson, J. D. *Molecular biology of the gene*. 6th edn, (Pearson/Benjamin Cummings ; Cold Spring Harbor Laboratory Press, 2008).
658 Amann, J. M. *et al.* ETO, a target of t(8;21) in acute leukemia, makes distinct contacts with multiple histone deacetylases and binds mSin3A through its oligomerization domain. *Molecular and cellular biology* **21**, 6470-6483 (2001).
659 Bresciani, E. *et al.* CBFbeta and RUNX1 are required at 2 different steps during the development of hematopoietic stem cells in zebrafish. *Blood* **124**, 70-78, doi:10.1182/blood-2013-10-531988 (2014).
660 Taniuchi, I. *et al.* Differential requirements for Runx proteins in CD4 repression and epigenetic silencing during T lymphocyte development. *Cell* **111**, 621-633 (2002).

661 Liu, J., Park, E. S. & Jo, M. Runt-related transcription factor 1 regulates luteinized hormone-induced prostaglandin-endoperoxide synthase 2 expression in rat periovulatory granulosa cells. *Endocrinology* **150**, 3291-3300, doi:10.1210/en.2008-1527 (2009).
662 Lee, S. L., Tourtellotte, L. C., Wesselschmidt, R. L. & Milbrandt, J. Growth and differentiation proceeds normally in cells deficient in the immediate early gene NGFI-A. *The Journal of biological chemistry* **270**, 9971-9977 (1995).
663 Perez-Castillo, A., Pipaon, C., Garcia, I. & Alemany, S. NGFI-A gene expression is necessary for T lymphocyte proliferation. *The Journal of biological chemistry* **268**, 19445-19450 (1993).
664 Nguyen, H. Q., Hoffman-Liebermann, B. & Liebermann, D. A. The zinc finger transcription factor Egr-1 is essential for and restricts differentiation along the macrophage lineage. *Cell* **72**, 197-209 (1993).
665 Chevallier, N. *et al.* ETO protein of t(8;21) AML is a corepressor for Bcl-6 B-cell lymphoma oncoprotein. *Blood* **103**, 1454-1463, doi:10.1182/blood-2003-06-2081 (2004).
666 Park, S. K., Lim, J. H. & Kang, C. J. Crlz1 activates transcription by mobilizing cytoplasmic CBFbeta into the nucleus. *Biochimica et biophysica acta* **1789**, 702-708, doi:10.1016/j.bbagrm.2009.08.011 (2009).